



---

# Handbook of Optical Constants of Solids

edited by  
Edward D. Palik

**Handbook of Thermo-Optic  
Coefficients of Optical Materials  
with Applications**

This page intentionally left blank

# **Handbook of Thermo-Optic Coefficients of Optical Materials with Applications**

GORACHAND GHOSH

Electrotechnical Laboratory  
Tsukuba, Japan



Academic Press  
San Diego London Boston  
New York Sydney Tokyo Toronto

*To my beloved Sujata, Rubik, and Ronik*

This book is printed on acid-free paper. 

Copyright © 1998 by Academic Press

All rights reserved.

No part of this publication may be reproduced or transmitted in any form or by any means, electronic or mechanical, including photocopy, recording, or any information storage and retrieval system, without permission in writing from the publisher.

ACADEMIC PRESS  
525 B Street, Suite 1900, San Diego, CA 92101-4495, USA  
1300 Boylston Street, Chestnut Hill, MA 02167, USA  
<http://www.apnet.com>

Academic Press Limited  
24–28 Oval Road, London NW1 7DX, UK  
<http://www.hbuk.co.uk/ap/>

**Library of Congress Cataloging-in-Publication Data**

Ghosh, Gorachand.

Handbook of thermo-optic coefficients of optical materials with applications / Gorachand Ghosh.

p. cm.

Includes bibliographical references and index.

ISBN 0-12-281855-5

1. Optical materials—Tables—Handbooks, manuals, etc.

2. Refractive index—Tables—Handbooks, manuals, etc. I. Title.

QC374.G46 1997

97-33342

621.36—DC21

CIP

Printed in the United States of America

97 98 99 00 01 IC 9 8 7 6 5 4 3 2 1

# Contents

Preface	vii
<b>Chapter 1 Introduction</b>	1
<b>Chapter 2 Refractive Index</b>	5
2.1 Introduction	5
2.2 Measurement	6
2.3 Dispersion Relations for Refractive Index	9
2.4 Derivation of the Sellmeier Coefficients	12
2.5 Sellmeier Coefficients	14
2.6 Comparison of Refractive Indices	34
2.7 References	110
<b>Chapter 3 Thermo-Optic Coefficients</b>	115
3.1 Definition	115
3.2 Measurement	115
3.3 Dispersion Relations	117
3.4 Derivation of Sellmeier Coefficients	127
3.4.1 Nonlinear Crystals	140
3.4.2 Other Oxide and Laser Crystals	190
3.4.3 Halide Crystals/Glasses	202
3.4.4 Semiconductors	226
3.4.5 Optical Fiber/Optical Glasses	233
3.5 References	255
<b>Chapter 4 Applications</b>	263
4.1 Nonlinear Optical Laser Devices	263
4.1.1 Noncritically Phase-Matched Second Harmonic Generations	265
4.1.2 Noncritical Optical Parametric Oscillators	283
4.1.3 Sum Frequency Generation	294
4.2 Optical-Fiber Communication Systems	297
4.2.1 Chromatic Dispersion and Zero-Dispersion Wavelength	299

4.3	Thermo-Optic Switch	305
4.4	Optical-Fiber Temperature Sensor	308
4.5	Thermo-Optic Modulators	310
4.6	References	312
 Chapter 5 Future Technology		
 Subject Index		319

# Preface

The refractive index and its variation with temperature, i.e., the thermo-optic coefficient, are the basic optical parameters of optical materials (including glasses) and are the backbone of both the linear, nonlinear, optical, and opto-electronic devices or systems. Shortly after the invention of ruby laser by Maiman in 1960, Franken and his co-workers observed its second harmonic in a quartz crystal as early as 1961. However, the conversion efficiency was very low due to phase mismatch between the waves at the fundamental and its second harmonic, propagating through the quartz crystal. In 1962, Giordmaine and Maker *et al.* simultaneously proposed and demonstrated a judicious method of phase matching between these two waves. This phase-matching method used the difference between the refractive indices of the waves with different polarizations in an optically anisotropic (uniaxial or biaxial) nonlinear crystal, and the conversion efficiency was enhanced to several ten percents. Also, the refractive index of the optical materials can be varied by changing the ambient temperature, and this leads to the temperature-tuned, phase-matching nonlinear optical devices. There was no proper physical explanation to account for the change of refractive indices with temperature variations of the optical materials.

This book grew out of my 19 years of research experience in the field of nonlinear optics and fiber optics. I found this problem just 19 years ago when I was a research scholar at Burdwan University, India. I faced a lot of problems searching through literature trying to find the values of refractive indices and its variation with temperature in order to characterize nonlinear optical laser devices. I did characterizations for the thermo-optic coefficients of some nonlinear crystals during that period to obtain my Ph.D. degree. In 1993, when I was an STA Fellow at the Electrotechnical Laboratory, I found that the same problem was prevalent in the field of fiber optics, nonlinear optics, opto-electronics, and in ordinary optics. I have single-handedly applied my physical model in these fields with great satisfaction. There are a few Handbooks on Optics, but there is very little value of these optical constants without applications. The purpose of this book is as a reference handbook for the refractive index, thermo-optic coefficients, and their applications. Rather than citing many empirical relations of refractive indices and

thermo-optic coefficients of different optical materials (such as optical glasses, optical fiber glasses, nonlinear crystals, and semiconductors), I have formulated a unique dispersion equation for both the fundamental parameters. These can be used to design new devices or to satisfactorily explain the existing devices or systems.

This book is divided into five chapters. Chapter 1 introduces some philosophical explanations and comparisons of the existing optical systems. Chapter 2 describes different dispersion relations of refractive indices of optical materials at room temperature. Sellmeier coefficients are formulated in a unique dispersion relation and are cited for each optical material to interpolate or extrapolate refractive indices within the transmission region. Some experimental values are tabulated for comparison with the computed values. Chapter 3 deals with the derivation of a physically meaningful dispersion relations for thermo-optic coefficients. The measured values of thermo-optic coefficients are then analyzed with this new model to account for the same satisfactorily. Chapter 4 explains the currently available temperature-dependent nonlinear optical devices and the effect of temperature on optical fiber communication systems. Thermo-optic switches, optical fiber sensors, and thermo-optic modulators are also examined based on the evaluation of thermo-optic coefficients of the optical materials. Chapter 5 focuses on the future technology based on thermo-optic coefficients.

I would like to thank G. C. Bhar, Yoichi Fujii, Fujio Saito, C. J. R. Shepard, Hidemi Tsuchida, and Hiroyoshi Yajima for a fruitful collaboration and numerous discussions. Thanks are also due to Pranay Chaudhuri, M. Endo, P. Fons, G. Ganguly, R. Kaji, K. Komori, Noni McIntosh, N. Ohnishi, and A. Yoshizawa for some suggestions during the preparation of the manuscript. This book would not have been completed without the inspiration and encouragement of Hiroyoshi Yajima. I must acknowledge Sukriti Ghosh and Swati Ghosh for their critical reading of the manuscript. I also received many constructive comments from the anonymous reviewers and some encouragement from the editors of the American journals where most of my research papers have been published. A constant reminder, "time is of the essence for your book, we need it as soon as possible" from Zvi Ruder of Academic Press was also appreciated. I am indebted to ETL, where I am assigned from the Femtosecond Technology Research Association (FESTA) and supported by the New Energy and Industrial Technology Development Organization (NEDO). The academic encouragement from FESTA and support for this book from NEDO is gratefully acknowledged.

Finally, my greatest debt and heartfelt gratitude is to my wife, Sujata, and my sons, Rubik and Ronik, for their patience, understanding, and unwavering support of me from Sydney to Tsukuba.

*Electrotechnical Laboratory  
Tsukuba, Japan  
March, 1997*

**GORACHAND GHOSH**

**Handbook of Thermo-Optic  
Coefficients of Optical Materials  
with Applications**

This page intentionally left blank

# Chapter 1

## Introduction

Glasses are fascinating materials that have been used in our daily life since the begining of human civilization. Recently, optical fiber communication systems (OFCS), designed from silica glass [?] with the two other wonderful inventions in the later half of this century, the light amplification by stimulated emission of radiation (LASER) [2] and the computer [3] have revolutionized scientific ideas for multi-media communication systems of the 21st century. Optical and opto-electronic materials are the backbones in the development of these amazing tools. In OFCS, there are two main parts, systems and fibers. In the systems part, there is the electronic circuitry, computer, source, and detector. The transmission medium is a fiber cable. A good example of this is the blood circulation system in the human body. Blood is the laser, the brain is the computer, the lungs are electronic circuitry and other systems parts, the heart is the laser generating device, and the arteries are the optical fibers. Nerves are the fiber to the home. Eyes, ears, nose, mouth, and skins are detectors. The fluctuation of ambient and body temperature affects our biological and nervous system. Similarly, the variation of the ambient temperature of the optical materials used in optical systems have some effects which must be taken into account.

According to Hindu mythology, Lord Krishna came to know about the happenings of the world through his Abhisaricas. Similarly, the OFCS with information science, computers, and human interface can be compared to Abhisaricas who are capable of efficiently engineering the multi-media communication systems. The number seven also has great significance. The seven colors, the seven seas, the seven continents, the seven stars, etc.

have been fascinating to mankind from the advent of human civilization. Similarly, the *seven letters* of the English alphabet making Abhisaricas have special characteristics [4] to the OFCS and optical materials. The seven letters are characterized by A-attenuation, absorption, amplification, auto-correlation, etc.; B-band gap, bandwidth, broadband communication, bit-rate, Bragg reflector, etc.; H-high-reliability, human interface, etc.; I-ISDN, internet, immunity to electromagnetic interference, isentropic band gap, interconnection, etc.; S-silica glass, single-mode fiber, spectral width, source, system, splicing, signal, soliton communication, etc.; R-refractive index, reliability, reflection, refraction, etc.; and C-computer, core, cladding, connectors, chips, coupler, conduction band, coherence, chromatic dispersion, etc.

The refractive index and its variation with temperature, (i.e., the thermo-optic coefficient,  $dn/dT$ ) are the basic optical parameters of all optical materials and are of practical importance in many optical and opto-electronic applications such as focussing, coupling, and modulation of radiation in OFCS. When the optical materials are used in laser applications, a part of the laser power is absorbed by it, the materials are heated, and consequently, the refractive index of the medium is changed. Also, by changing the ambient temperature, the refractive index is varied.

It is necessary to investigate the origin of the variation of the refractive index and to analyze it in a physically meaningful model to more accurately account for these properties. The linear refractive index, its dispersion, and its chromatic dispersions are important characteristics of the optical materials. These are necessary not only for the evaluation of OFCS designs but also for many other optical devices. The refractive index and its variation with temperature have been accurately measured at discrete wavelengths in the optical transmission regions of the optical materials, i.e., nonlinear crystals, optical crystals, semiconductors, optical glasses, and optical fiber glasses. There are many dispersion relations to account for the room temperature refractive indices of optical materials.

Here, we have analyzed the room temperature refractive indices in a unique dispersion relation for all optical materials so that there is no need to change the dispersion equation to estimate refractive indices. Similarly, we have accounted for the thermo-optic coefficients of all optical materials in another physically meaningful Sellmeier equation. These basic parameters are necessary to characterize the nonlinear optical devices, opto-electronic

applications and femtosecond technology. This book will help scientists in the 21st century to design an environmentally stable, i.e., temperature immune terabit OFCS, or, a more efficient, temperature-tuned, nonlinear optical device, temperature sensor, thermo-optic switch, thermo-optic modulator, and the like.

## REFERENCES

1. K. C. Kao and G. A. Hockman, Proc. IEE **113**, 1151 (1966).
2. T. H. Maiman, Nature **187**, 493 (1960).
3. N. Metropolis *et al.*, Eds., *A History of Computing in the Twentieth Century* (Academic Press, 1980).
4. G. Ghosh, M. Endo, and T. Iwasaki, IEEE J. Lightwave Technol. **LT-12**, 1338 (1994).

This page intentionally left blank

# Chapter 2

## Refractive Index

### 2.1 Introduction

The refractive index is a fundamental parameter of any optical material. Normally, Maxwell's wave equations [1] are the basic source for the derivation of important optical properties, definitions, formulas, and basic concepts of the materials. But for a transparent optical material, the refractive index,  $n$ , is simply defined as the ratio of the velocity,  $c$ , of the electromagnetic wave in vacuum to the phase velocity,  $v$ , of the same wave in the material, i.e.,

$$n = \frac{c}{v}. \quad (2.1)$$

Since the refractive index of air is only 1.0003,  $n$  is conventionally measured with respect to air instead of in vacuum, and normally no correction is required.

In practice, the optical materials are not purely a non-absorbing medium, and it is frequently convenient to define a complex refractive index  $\bar{n}$  as

$$\bar{n} = n + ik, \quad (2.2)$$

where  $k$  is the extinction coefficient or the index of absorption (or imaginary part of the complex refractive index). Both  $n$  and  $k$  are frequency i.e., wavelength dependent. The real and imaginary parts of the square of the complex refractive index are the real and imaginary parts of the complex dielectric constant of the material, i.e.,

$$\epsilon = \epsilon_1 + i\epsilon_2 = \bar{n}^2 = (n^2 - k^2) + i2nk. \quad (2.3)$$

The meanings of  $n$  and  $k$  are clear;  $n$  contributes to phase effects (time delay or variable velocity) and  $k$  contributes to attenuation by absorption.

The three basic physical processes: electronic transitions, lattice vibrations, and free-carrier effects [2-6] are used to define the intrinsic optical properties of a material. Among these physical processes, some are dominant over the others depending on the material and spectral region of interest. All materials have contributions to the complex index of refraction from electronic transitions. The characterization of the long wavelengths lattice vibrations (or phonons) are required to fully understand the optical properties of insulators (glasses and crystals) and semiconductors. Transparency of semiconductors, particularly those with small band gaps, are additionally influenced by free-carrier effects. Detailed discussions of these properties are beyond the scope of this book. In the next section, a brief review on the measurement of the refractive index is given.

## 2.2 Measurement

Several techniques have been used to measure the refractive indices of optical materials. The method of determining minimum deviation [7-8] by using two precision spectrometers has been conducted in many laboratories throughout the world. Schematic diagrams of both spectrometers are shown in Fig. 2.1. The first spectrometer, which contains glass optics, is capable of measuring  $n$  in the visible and in the near infrared to an accuracy of several parts in  $10^6$ . The second spectrometer, which contains mirror optics, is capable of measuring  $n$  from  $0.2 \mu\text{m}$  in the ultraviolet to  $50 \mu\text{m}$  in the infrared to an accuracy of several parts in  $10^5$ . The accuracy depends on specimen quality and size. Normally, all values of the refractive index are measured relative to the refractive index of air.

Measurements are performed at various discrete wavelengths. These wavelengths are selected from the emission spectra of Hg, Cd, He, Cs, and from calibrated absorption bands of  $\text{H}_2\text{O}$ , polystyrene, methylcyclohexane, and 1, 2, 4 trichlorobenzene, and some laser sources. A series of calibrated narrow-band filters is also used in the infrared region.

Sometimes measurements beyond  $0.7 \mu\text{m}$  were determined with the aid of an infrared-detecting viewer mounted to the spectrometer eyepiece. The viewer is a wide angle, monocular, infrared converter with a focal range from 15 cm to infinity. Infrared spectral lines are focussed by objective

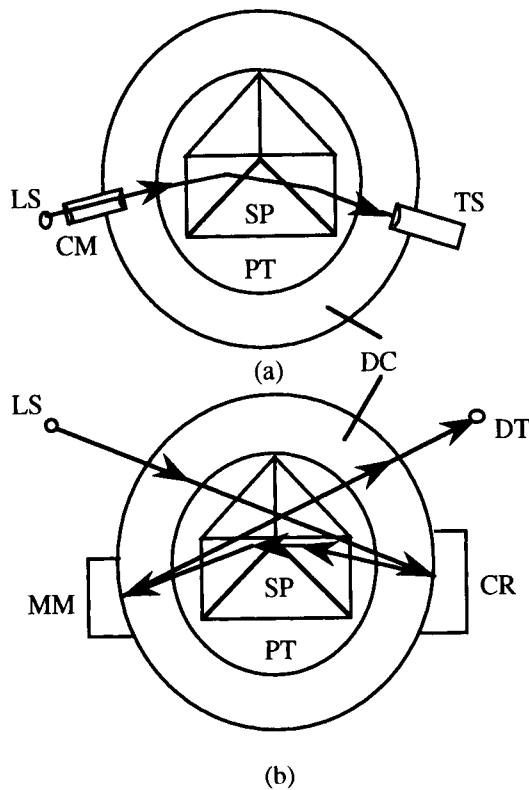


Figure 2.1: The schematic of spectrometers to measure refractive index: (a) Visible region refractometry; (b) Non-visible region refractometry. Symbols: LS = light source, DC = divided circle, PT = prism table, CM = collimator, TS = telescope, CR = collimating mirror, MM = movable mirror, SP = sample prism, and DT = detector.

lens onto an image-converter tube that, in turn, displayed a visual image on a P-20 phosphor screen. This image is then viewed through the instrument eyepiece. The range of maximum sensitivity is from 0.7 to 0.9  $\mu\text{m}$ .

To avoid variations in the refractive index caused by temperature fluctuations during the measurements, a small resistance-type heating element was inserted into a close-fitting cavity bored into the sample stage, particularly for measuring the refractive indices of potassium dihydrogen phosphate (KDP) crystal and its isomorphs group [9]. This stabilized the prism temperature to  $\pm 0.5^\circ\text{C}$  over 8 hours. The temperature was measured by a thermo-couple attached to the top of the prism. To eliminate absorbed water on the crystal faces owing to the hygroscopic nature of the KDP isomorphs, the prism temperature was maintained at  $33^\circ\text{C}$ . A room dehumidifier also was used to keep the ambient environment free of moisture. In each non-centrosymmetric crystals prism, the optic axis was oriented parallel to the prism apex edge. By observing the light polarized *parallel* to the prism apex edge, the extraordinary index of refraction was determined. Observing the light polarized *perpendicular* to the edge determined the ordinary index.

When determining the refractive index by the minimum deviation technique, the collimated radiation is passed through a specimen. The specimen is in the form of a triangular prism. The prism is rotated about an axis parallel to the prism apex until a position is found where the angular deviation of the beam at a chosen wavelength is at a minimum. In terms of the minimum deviation angle  $D_m$ , the angle between the emergent beam and an undeviated beam, and the prism angle  $P_a$ , the refractive index is given by

$$n = \frac{\sin(D_m + P_a)/2}{\sin P_a/2}. \quad (2.4)$$

Therefore, by measuring the two angles  $D_m$  and  $P_a$  and the polarization of the incident light on the prism, the ordinary and extraordinary indices of refraction can be calculated from the above Eq.(2.4). The experimental accuracy is varied from  $\pm 0.00003$  to  $\pm 0.0001$  for nonlinear crystals and optical glasses.

The refractive indices of the semiconductors are measured by using a scanning ellipsometric technique, polarization modulation ellipsometry (PME) [10-12]. Normal incidence reflectivity measurements are carried out using any sophisticated spectrophotometer equipped with a V-W configuration attachment for measuring absolute reflectance. The detailed ex-

perimental procedure is beyond the scope of this book. Only refractive index values have been used here for analyses and to derive some optical constants. The experimental accuracy is from  $\pm 0.0001$  to  $\pm 0.001$  for semiconductor materials.

## 2.3 Dispersion Relations for Refractive Index

The dielectric constant and the refractive index are functions of wavelength, hence frequency. The wavelength or frequency variation of the refractive index is called dispersion. The formation of a rainbow or a beautiful spectrum created by a white light source and a glass prism is due to dispersion of the materials through which light is propagated. Dispersion is an important optical design parameter for correcting chromatic aberration. The recent discovery of the control of dispersion in optical fibers, optical glasses, and semiconductors is of immense importance for ultrafast optical fiber communication systems and other high-technology arenas.

Refractive indices are measured at discrete wavelengths within the transmission region of the optical materials with sufficient accuracy. It is desirable to have a functional form for the dispersion of the refractive index to have interpolated or extrapolated values. There are many formulae used for representing the refractive index. Maxwell's theory gives the relationship

$$n^2 = \varepsilon = 1 + P = 1 + 4\pi(\chi_e + \chi_l), \quad (2.5)$$

where  $n$  is the refractive index,  $\varepsilon$  is the dielectric constant,  $P$  is the polarizability,  $\chi_e$  is the electronic susceptibility, and  $\chi_l$  is the lattice susceptibility. If one treats the material as equivalent to a collection of  $m$  harmonic oscillators resonant to a radiation of various wavelengths  $\lambda_i$ , one can derive [13] the equation

$$n^2(\lambda) = 1 + \sum_{i=1}^m \frac{a_i \lambda^2}{(\lambda^2 - \lambda_i^2)}, \quad (2.6)$$

where  $\lambda$  is the wavelength of the incident radiation, and  $a_i$  is a constant that depends on the number of oscillators per unit volume and is called the *oscillator strength* of the oscillators resonant at wavelength  $\lambda_i$ . Equation (2.6) is generally called the Sellmeier formula, since Sellmeier proposed the above dispersion formula in 1871. By denoting  $\lambda_i$  with the wavelengths

of the various absorption bands of the material, it can be derived by modern quantum theory from more sophisticated models of the solid.

It was traditionally believed that the dispersion formula of the Sellmeier type best fit the refractive indices of the alkali halide crystals in their transmission region. As a result, most of the early experimental workers adopted Eq. (2.6) with the  $\lambda_i$ 's and  $a_i$ 's as adjustable empirical constants chosen only to fit the data, without having any other experimental and theoretical basis or explanation. Nevertheless, this equation, if used correctly, gives a good deal of information concerning the position of absorption band, oscillator strength, and the dielectric constant for static field.

Equation (2.6) can be rewritten for the transparent region as

$$\varepsilon = n^2(\lambda) = 1 + \sum_{i=1} \frac{b_i \lambda^2}{(\lambda^2 - \lambda_i^2)} + \sum_{j=1} \frac{c_j \lambda^2}{(\lambda^2 - \lambda_j^2)}. \quad (2.7)$$

The first summations are contributions from the ultraviolet absorption bands and the second summations are due to the infrared absorption bands. An often-used slight modification of this formula puts the wavelength of the shortest wavelength resonance at zero ( $\lambda_1=0$ ), i.e., the first term is a constant. This constant term represents contributions to the refractive index from electronic transitions at energies far above the band gap. Sellmeier terms with small  $\lambda_i$  (representing electronic transitions) can be expanded as a power series,

$$\frac{a_i \lambda^2}{(\lambda^2 - \lambda_i^2)} = a_i \sum_{j=0}^{\infty} \left( \frac{\lambda_i^2}{\lambda^2} \right)^j = a_i + \frac{a_i \lambda_i^2}{\lambda^2} + \frac{a_i \lambda_i^4}{\lambda^4} + \dots \quad (2.8)$$

and the terms with large  $\lambda_i$  (representing vibrational transitions) are expanded as

$$\frac{a_i \lambda^2}{(\lambda^2 - \lambda_i^2)} = -a_i \sum_{j=1}^{\infty} \left( \frac{\lambda^2}{\lambda_i^2} \right)^j = -a_i \frac{\lambda^2}{\lambda_i^2} - a_i \frac{\lambda^4}{\lambda_i^4} + \dots \quad (2.9)$$

The Eqs. (2.8, 2.9) were used to represent the index of refraction for Schott and Ohara optical glasses as the power-series approximations to the Sellmeier equation, and are expressed in many forms. One common form was the Schott/ Ohara glass formula used for glasses, which is given by

$$n^2 = A_0 + A_1 \lambda^2 + A_2 \lambda^{-2} + A_3 \lambda^{-4} + A_4 \lambda^{-6} + A_5 \lambda^{-8}. \quad (2.10)$$

A comparison of the Schott power-series formula with a three-term Sellmeier formula showed equivalent accuracy of the range of the Schott fit, but that the Sellmeier model was accurate over a much wider wavelength range [14]. Recently, there was shown to be three-oscillators fit of these glasses [14].

A generalized form of the short-wavelength approximation to the Sellmeier equation is the Cauchy formula, developed in 1836. This equation is given by

$$n = A_0 + \sum_{i=1} \frac{A_i}{\lambda_i^2} \text{ or, } n^2 = A'_0 + \sum_{i=1} \frac{A'_i}{\lambda_i^2}. \quad (2.11)$$

This was the first successful attempt to represent dispersion by an empirical equation.

Sometimes, Sellmeier terms are written differently, such as this form used by Li [15]

$$\frac{A_i}{(\lambda^2 - \lambda_i^2)} = \frac{A_i(\lambda^2/\lambda_i^2)}{(\lambda^2 - \lambda_i^2)} - \frac{A_i}{\lambda_i^2}, \quad (2.12)$$

which is the combination of two Sellmeier terms, one located at zero wavelength and the other at  $\lambda_i$ . Zernike [16] also used a term in this form.

The Hartmann formula is also commonly used for the index of refraction. This formula is related to the Sellmeier equation for a limited spectral region as

$$n = A + \frac{B}{(\lambda - \lambda_0)}. \quad (2.13)$$

Sometimes, a combination of Sellmeier and power-series terms are used, and one formula is the Herzberger equation, first introduced in glasses [17] and later applied to infrared crystalline materials [18] as

$$n = A + \frac{B}{(\lambda^2 - \lambda_0^2)} + \frac{C}{(\lambda^2 - \lambda_0^2)^2} + D\lambda^2 + E\lambda^4. \quad (2.14)$$

Among all these dispersion equations, Eq. (2.7) is most significant and can be transformed to

$$\varepsilon = \varepsilon_{uv} + \sum \frac{c_j \lambda^2}{(\lambda^2 - \lambda_j^2)}, \quad (2.15)$$

where  $\varepsilon_{uv} = 1 + \sum b_i = \varepsilon_s - \sum c_j$  is the high-frequency dielectric constant. In the transparent wavelength region, the damping effects are negligibly small, and in an ideal application of Eq. (2.7), one would need to know the wavelength of all of the absorption peaks. However, in practice, it is very difficult to know precisely all the absorption peaks. It is scientifically useful and physically acceptable to use an average electronic absorption band gap and also an average lattice absorption band gap. Then, the above equation can be written as [19]

$$n^2 = A + \frac{B\lambda^2}{(\lambda^2 - C)} + \frac{D\lambda^2}{(\lambda^2 - E)}, \quad (2.16)$$

where  $\lambda$  is the wavelength in micrometers. The first and second terms represent, respectively, the contribution to refractive indices due to higher-energy and lower-energy band gaps of electronic absorption, and the last term accounts for a decrease in refractive indices due to lattice absorption. The optical constants  $A$ ,  $B$ ,  $C$ ,  $D$ , and  $E$  are called Sellmeier coefficients of the optical materials. We have analyzed the refractive indices of all the optical materials with this equation. We have come to the conclusion that this Eq. (2.16) is sufficient to explain the refractive indices of the optical materials, and in particular, there is no problem from UV to near-IR region. This optical region is of great importance for communication, switching, and other optical systems. On the other hand, this equation estimates the average electronic absorption band gap effectively.

Figure 2.2 shows the characteristics of refractive indices versus wavelength for various optical materials. The above five Sellmeier coefficients are capable of explaining these nice curves. Therefore, the first, second, and even third-order dispersions can be estimated with sufficient accuracy.

## 2.4 Derivation of the Sellmeier Coefficients

The refractive indices are the *fundamental parameters* of the optical materials. These values have been measured in the UV, visible and near-infrared (IR) region for nonlinear crystals, ordinary optical crystals, semiconductors, optical glasses, and optical fiber glasses. The measurement accuracy is within four-to-five decimal places. There are many dispersion relations accounting for the refractive indices, as we have shown in the previous section. Normally, the measured refractive indices are fitted with the desired

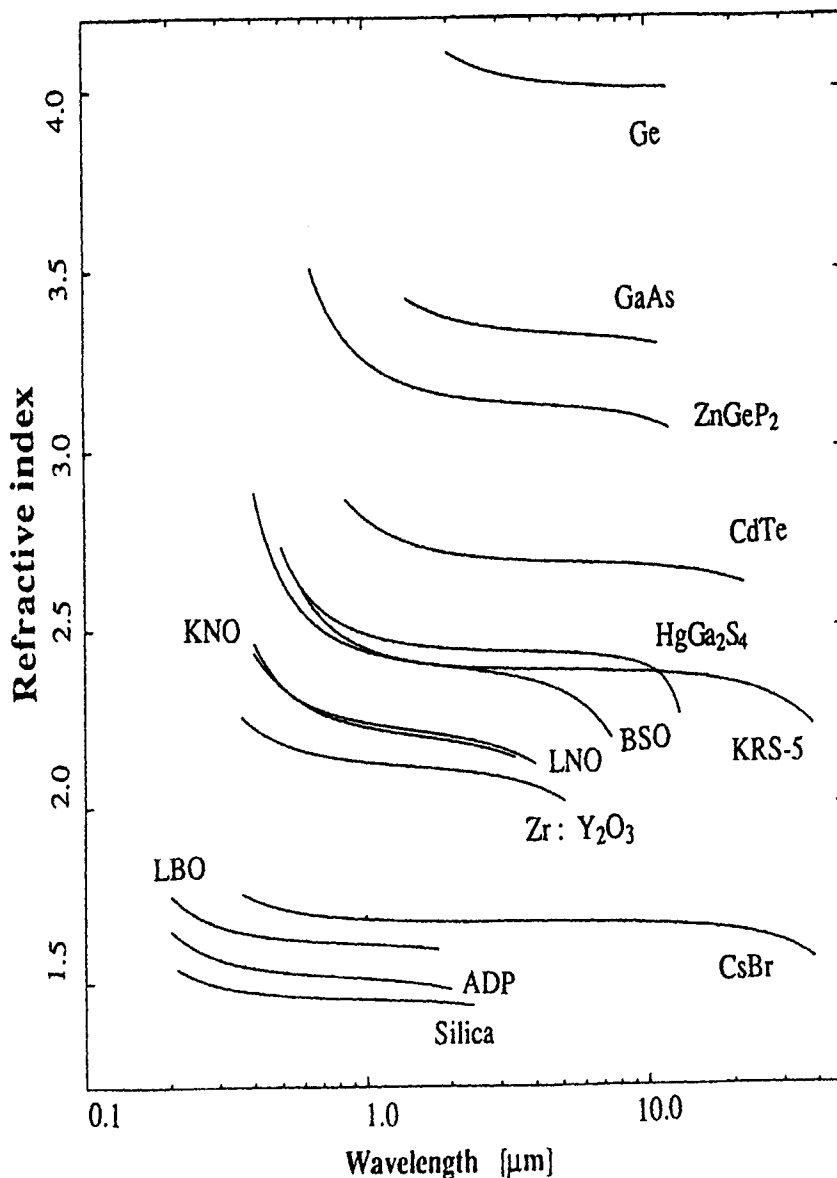


Figure 2.2: Refractive index versus wavelength for some important optical materials.

dispersion relation. However, *the fitting accuracy* should be the dominant consideration in *choosing* a dispersion formula having *fewer optical parameters*. As we have analyzed the refractive indices of the various optical materials, the two-pole Sellmeier dispersion formula, Eq. (2.16) is the most accurate of the dispersion formulas, and can fit index data to an accuracy consistent with the measurements and the accuracy needed for most opto-electronic applications.

The normal approach for calculating the Sellmeier coefficients is to first find the initial values of the parameters and then to add corrections by an iterative process so as to minimize the deviation between the measured and the computed values. We are able to evaluate the Sellmeier coefficients by fitting the measured data obtained from the quoted values (and sometimes from the other form of dispersion relations) to an accuracy better or consistent with, the experimental accuracy. The Sellmeier coefficients  $A$ ,  $B$ ,  $C$ , and  $D$  are evaluated by first taking a reasonably estimated value for  $E$ , the lattice absorption frequency. The choice of the value for  $E$  is not critical since the materials stop transmitting long before the onset of lattice absorption frequency. The average electronic absorption band gaps ( $E_{\text{ag}}$ ) are calculated from the Sellmeier coefficients  $C$  by the following equation

$$E_{\text{ag}} = \frac{1.2398}{\sqrt{C}}. \quad (2.17)$$

The estimated band gaps are also shown in Tables 2.1-2.3. These values are within the measured values of the electronic absorption gaps. The values of these evaluated band gaps are required to estimate the excitonic band gaps, which will be described in the next chapter to characterize the thermo-optic coefficients of the optical materials.

The conversion of wavelength and energy of any electromagnetic wave is required in many opto-electronic applications. This equation is given by

$$\lambda = \frac{1.2398}{E}, \quad (2.18)$$

where  $\lambda$  is the wavelength in  $\mu\text{m}$  and  $E$  is the energy in eV.

## 2.5 Sellmeier Coefficients

The room temperature values of refractive indices are used to evaluate the Sellmeier coefficients  $A$ ,  $B$ ,  $C$ ,  $D$ , and  $E$  for mostly all optical materials.

Sometimes, other forms of Sellmeier equations are used to evaluate the Sellmeier coefficients in the present form. The computed Sellmeier coefficients are shown in Tables 2.1, 2.2, and 2.3 at room temperature for crystals (linear and nonlinear), semiconductors, glasses (fiber glass and optical glasses), and tellurite-based high index glasses, respectively. As we have noticed, the band edge data of refractive indices differ in the third decimal place for nonlinear crystals and in the fourth decimal place for higher index glasses. The refractive index changes in a third decimal place for a change of 1°C ambient temperature at the band-edge region of some optical materials.

The five evaluated Sellmeier coefficients are used to calculate the refractive index for any wavelength lying within the normal transmission region of the optical materials. In Chapter 3, thermo-optic coefficients of several optical materials have been analyzed. The values of thermo-optic coefficients for several wavelengths are available without having the room temperature refractive index values for some materials. Therefore, the corresponding room temperature values of the refractive index are calculated from the Sellmeier coefficients for analyzing thermo-optic coefficients.

**Table 2.1: Sellmeier Coefficients for Some Crystals and Semiconductors; [ $n^2 = A + B/(1-C/\lambda^2) + D/(1-E/\lambda^2)$ ,  $\lambda$  is in  $\mu\text{m}$ ]**

Materials (Crystal/ Semiconductor)	Temp. (°C)	Polar- ization	Sellmeier Coefficients				Range ( $\mu\text{m}$ )	Absorp- tion band gap (eV)	Refs. Eqn.
			A	B	C ( $\times 10^{-2}$ )	D	E		
ADA	33.0	o	1.49117717	0.95173751	1.77351582	1.22764415	36	0.4–1.1	9.31 [9, *]
[ $\text{NH}_4\text{H}_2\text{AsO}_4$ ]		e	1.48811668	0.78810870	1.79381654	0.44890395	36		9.26
AD*A	33.0	o	1.60831944	0.81273393	1.98983870	0.79297224	36	0.4–1.1	8.79 [9, *]
[ $\text{ND}_4\text{D}_2\text{AsO}_4$ ]		e	1.42043624	0.84365085	1.67385409	0.27903481	36		9.58
ADP	33.0	o	1.18918067	1.10385100	1.10453338	1.30107754	49	0.4–1.1	11.8 [9, *]
[ $\text{NH}_4\text{H}_2\text{PO}_4$ ]		e	1.33838706	0.82412401	1.18225569	0.69630836	49		11.4
ADP	24.8	o	1.45233409	0.84995622	1.31484546	1.30189736	36	0.21–1.2	10.8 [16, *]
		e	1.41882936	0.74447222	1.29423990	0.51068171	36		10.9
AD*P	33.0	o	1.38701774	0.89209958	1.21960960	1.01112621	49	0.4–1.1	11.2 [9, *]
[ $\text{NH}_4\text{D}_2\text{PO}_4$ ]		e	1.20368487	0.94636494	1.04697126	0.41558974	49		12.1
$\text{Ag}_3\text{AsS}_3$	25.0	o	3.96061147	3.52626894	12.6344855	1.54935351	900	0.6–7.5	3.49 [20, *]
		e	3.63610700	2.71084707	11.9169211	0.59005174	900		3.59
$\text{Ag}_3\text{AsS}_3$	25.0	o	2.19843460	5.28411478	8.97904251	1.64807314	900	0.63–4.6	4.14 [21, *]
		e	2.53564322	3.81009590	8.98318525	0.95414797	900	0.59–4.6	4.14
AgBr	20.0		3.48460089	1.21022462	8.63304669	0.35646114	16	0.49–0.67	4.22 [22, *]
AgCl	23.9		2.31173639	1.69645766	4.64845739	4.28025210	5000	0.57–20.6	5.75 [23, *]
AgGaS <sub>2</sub>	25.0	o	3.6280	2.1686	10.03	2.1753	950	0.49–12	3.92 [24, 19]
		e	4.0172	1.527	13.10	2.1699	950		3.43

**Table 2.1: (Continued)**

Materials (Crystal/ Semiconductor)	Temp. (°C)	Polar- ization	Sellmeier Coefficients					Range (μm)	Absorp- tion band n and gap (eV)	Refs. Eqn.
			A	B	C (X 10 <sup>2</sup> )	D	E			
AgGaSe <sub>2</sub>	25.0	o	4.6453	2.2057	18.79	1.8377	1600	0.75–13.5	2.86	[25, 19]
		e	5.2912	1.3970	28.45	1.9282	1600		2.32	
AgInSe <sub>2</sub>	25.0	o	5.5429671	1.4313841	45.43274	0.7054795	900	1.05–12.0	1.84	[25, 19]
		e	5.7110545	1.2818184	55.74472	0.7787102	900		1.66	
Ag <sub>3</sub> SbS <sub>3</sub>	25.0	o	1.0	6.585	16.0	0.1133	225	0.7–14	3.10	[26]
		e	1.0	5.845	16.0	0.0202	225		3.10	
AlAs	27.0		2.61642419	5.56711249	8.45071456	0.49251725	100	0.56–2.2	4.27	[27, *]
AlN	20.0	o	3.1399	1.3786	2.941225	3.861	226	0.22–5.0	7.23	[28]
		e	3.0729	1.6173	3.048516	4.139	226		7.10	
Al <sub>2</sub> O <sub>3</sub>	25.0	o	1.62575845	1.45722100	1.13346735	6.67604154	400	0.2–12	11.7	[29, *]
		e	1.58088139	1.47383661	1.10434074	6.54393251	400		11.8	
ALON	24.0		0.43326577	2.70323089	0.84755936	1.22596398	100	0.4–2.3	13.5	[30, *]
AlPO <sub>4</sub>	25.0	o	1.21197074	1.08747601	0.89258225	3.11474175	300	0.4–2.6	13.1	[31, *]
		e	0.32062333	2.00479583	0.52715200	3.22350075	300		17.1	
BBO	20.0	o	1.7018379	1.0357554	1.8003440	1.2479989	91	0.2–2.0	9.24	[32, 33]
[β-BaB <sub>2</sub> O <sub>4</sub> ]		e	1.5920433	0.7816893	1.6067891	0.8403893	91		9.78	
Ba(COOH) <sub>2</sub>	25.0	x	2.16515385	0.45384615	3.90	----	----	0.245–3	6.28	[34, *]
		y	1.96528571	0.52571429	3.50	----	----		6.63	
		z	2.04004762	0.38095238	4.20	----	----		6.05	

**Table 2.1: (Continued)**

Materials (Crystal/ Semiconductor)	Temp. (°C)	Polar- ization	Sellmeier Coefficients					Range (μm)	Absorp- tion band n and gap (eV)	Refs. Eqn.
			A	B	C (X 10 <sup>2</sup> )	D	E			
BaF <sub>2</sub>	25.0		1.31559305	0.83446690	0.98967192	3.54488931	2000	0.27–10.3	12.5	[35, *]
BNN	25.0	x	2.54970167	2.45296585	5.63028676	2.83117205	100	0.37–5	5.22	[36, *]
(Ba <sub>2</sub> NaNb <sub>3</sub> O <sub>15</sub> )		y	2.51568369	2.47680535	5.59403831	2.48705308	100		5.24	
		z	2.40250738	2.23483587	4.58287172	1.98103784	100		5.79	
BaTiO <sub>3</sub>	25.0	o	3.2471665	2.0574813	8.0251842	21.8336219	900	0.42–7.1	4.38	[37, *]
		e	1.1876811	3.8807047	4.6421080	20.5549611	900		5.76	
BeO	25.0	o	2.8689932	0.0605452	9.8531369	1.3803723	100	0.44–7.0	3.95	[38, *]
		e	2.8490135	0.1281764	6.9466268	1.9301310	120		4.70	
BeSO	25.0	o	1.0	1.127884	1.1509	----	----	0.19–1.37	11.6	[39]
(BeSO <sub>4</sub> . 4H <sub>2</sub> O)		e	1.0	1.025413	0.8925	----	----		13.1	
Bi <sub>1.2</sub> SiO <sub>20</sub> (BSO)	20.0		2.75488	2.96265	7.484	2.56788	210	0.4–7.5	4.53	[40, 41]
Bi <sub>1.2</sub> GeO <sub>20</sub> (BGO)	20.0		2.94694	2.77444	7.926	2.62094	210	0.4–7.5	4.40	[42, 41]
BP	20.0		1.0	6.841	7.1289	----	----	0.45–0.63	4.64	[43]
C(diamond)	25.0		2.30982863	3.35656148	1.73019053	3.25669602	2500	0.225–∞	9.43	[44, *]
CaCO <sub>3</sub>	25.0	o	1.75955881	0.93938204	1.97428233	1.53787264	100	0.2–2.2	8.83	[45, *]
(Calcite)		e	1.36499516	0.81788226	1.07385188	0.11805945	100	0.2–3.3	12.0	
CaCO <sub>3</sub>	25.0	o	1.72378731	0.97381251	1.96233175	1.50363785	100	0.2–2.2	8.85	[46, *]
(Calcite)		e	1.43231135	0.75232698	1.14220114	0.24367801	100	0.2–3.3	11.6	
CaF <sub>2</sub>	24.0		1.32182138	0.71686679	0.86079635	3.84678001	1200	0.23–9.7	13.4	[47, *]

**Table 2.1: (Continued)**

Materials (Crystal/ Semiconductor)	Temp. (°C)	Polar- ization	Sellmeier Coefficients					Range (μm)	Absorp- tion band <i>n</i> and gap (eV)	Refs. Eqn.
			A	B	C (X 10 <sup>-2</sup> )	D	E			
CaF <sub>2</sub>	21.7		1.35122586	0.68762632	0.89076710	4.18561863	1300	0.25–8.5	13.1	[48, *]
CaMoO <sub>4</sub>	25.0	o	2.44228105	1.34795307	4.05786102	2.54997955	250	0.45–3.8	6.16	[31, *]
		e	2.46139631	1.35080725	4.36448494	2.57978300	250		5.93	
CaWO <sub>4</sub>	25.0	o	2.21157835	1.34200290	3.16651281	2.17665399	250	0.45–4.0	6.97	[31, *]
		e	0.30134987	3.30128017	1.53505540	2.17625731	250		10.0	
CaWO <sub>4</sub>	20.0	o	2.40741686	1.14657832	3.51454412	2.25359710	250	0.47–1.5	6.61	[49, *]
		e	2.32686755	1.27867147	3.44200063	2.44998186	250		6.68	
CDA (CsH <sub>2</sub> AsO <sub>4</sub> )	33.0	o	1.50448591	0.91580586	1.78065319	1.18195864	49	0.4–1.1	9.30	[9, *]
		e	1.28128675	1.06884369	1.46685543	0.25560232	49		10.2	
CD*A (CsD <sub>2</sub> AsO <sub>4</sub> )	33.0	o	1.55720340	0.85051153	1.84801371	0.82624525	49	0.4–1.1	9.12	[9, *]
		e	1.45487371	0.89097252	1.69727044	0.24944405	49		9.52	
CdF <sub>2</sub>	20.0		2.57160562	-0.2737584	-74.089614	-1.4353088	300	0.4–3.4	---	[48, *]
CdGeAs <sub>2</sub>	20.0	o	10.1064	2.2988	108.72	1.6247	1370	2.4–11.5	1.19	[50, 19]
		e	11.8018	1.2152	269.71	1.6922	1370		0.78	
CdGeP <sub>2</sub>	20.0	o	5.9677	4.2286	20.21	1.6351	671.33		2.76	[50, 51]
		e	6.1573	4.0970	23.30	1.4925	671.33		2.57	
CdS	25.0	o	4.77857305	0.61455005	20.7230850	4.33466894	50	0.51–1.4	2.72	[14, *]
		e	4.82429144	0.64777214	20.3484908	4.44981048	40		2.75	
CdS	25.0	o	4.81271978	0.67544047	19.7475219	5.00692931	50	0.51–1.4	2.79	[52, *]

**Table 2.1: (Continued)**

Materials (Crystal/ Semiconductor)	Temp. (°C)	Polar- ization	<i>A</i>	<i>B</i>	Sellmeier Coefficients	<i>C</i> (X 10 <sup>-2</sup> )	<i>D</i>	<i>E</i>	Range (μm)	Absorp- tion band <i>n</i> and gap (eV)	Refs. Eqn.
CdS		e	4.88329386	0.56078121		20.8828127	5.72253409	50		2.71	
CdSe	25.0	o	4.2243	1.7680		22.70	3.1200	3380	1–22	2.6	[31, 19]
		e	4.2009	1.8875		21.71	3.6461	3629		2.7	
CdTe	27.0		0.9927800	6.2048904		10.044814	3.0942950	5000	0.85–22	3.91	[53, *]
CO(NH <sub>4</sub> ) <sub>2</sub>	20.0	o	1.7656333	0.4166667		3.0000000	----	----	0.3–1.06	7.16	[54, *]
Urea		e	1.6761742	0.8262065		2.9467413	-0.0517576	16		7.22	
CsBr	27.0		1.45663604	1.32697393		2.34246569	2.06490146	10400	0.36–39	8.10	[55, *]
CsCl	25.0		1.62848128	0.99482451		2.19243096	4.50047339	10500	0.18–40	8.37	[56, *]
CsI	24.0		1.62544423	1.41177552		3.45954616	3.23973192	25000	0.29–50	6.67	[57, *]
CuAlSe <sub>2</sub>	25.0	o	3.4941781	2.6278601		9.461934	0.7952733	400	0.5–5.0	4.0	[25, *]
		e	3.7871627	2.2793912		10.679146	0.9246976	400		3.8	
CuCl	20.0		2.6356013	0.9978742		7.4732872	0.4012856	100	0.43–2.5	4.54	[58, *]
CuGaS <sub>2</sub>	25.0	o	3.9064	2.3065		11.49	1.5479	738.43	0.55–11.5	3.66	[24, 51]
		e	4.3165	1.8692		13.64	1.7575	738.43		3.36	
CuGaSe <sub>2</sub>	25.0	o	5.3169114	2.0750143		23.88630	0.9558453	900	0.78–12.0	2.54	[25, *]
		e	5.8665533	1.5688514		30.53616	1.1202028	900		2.24	
CuInS <sub>2</sub>	25.0	o	5.40938697	1.23115001		38.8352077	4.01963679	2000	0.9–12.5	1.99	[24, *]
		e	5.42000634	1.17674877		38.6040791	4.59606517	2000		2.0	
C <sub>12</sub> H <sub>22</sub> O <sub>11</sub>	20.0	x	1.87053852	0.46711960		2.13813927	0.38546818	36	0.19–1.35	8.48	[59, *]

**Table 2.1: (Continued)**

Materials (Crystal/ Semiconductor)	Temp. (°C)	Polar- ization	Sellmeier Coefficients					Range (μm)	Absorp- tion band <i>n</i> and gap (eV)	Refs. Eqn.
			A	B	C (X 10 <sup>2</sup> )	D	E			
DLAP (Deuterated L- Arginine Phosphate)	25.0	y	1.96937278	0.45091898	2.37884165	0.34472179	36	0.25–1.35	10.3	[60, *]
		z	2.05112076	0.39200228	2.51806693	0.63845298	36			
GaAs	25.0	x	1.41859292	0.81635259	1.44978445	0.23019106	36	1.4–11	3.04	[61]
		y	1.71820457	0.71259363	2.12775193	0.48252292	36			
GaN	25.0	z	1.69216712	0.75583480	2.28197845	0.38814926	36	<10	4.84	[62]
		x	3.5	7.4969	16.663	1.9347	1382			
GaP	20.0	y	3.3346794	5.7610532	9.7650944	4.4062455	1500	0.8–10	3.97	[63, *]
		z	3.09558131	5.99865272	9.44041466	0.8387802	300			
GaSb	25.0	x	13.095068	0.7546437	160.70651	0.6824531	100	0.54–4.0	4.04	[31, *]
		y	2.40622747	5.04000694	7.79448739	4.48612725	3000			
GaSe	23.0	o	5.04419996	0.73385456	2.64903269	3.55416460	3000	1.8–2.5	0.98	[64, *]
		e	2.40622747	5.04000694	7.79448739	4.48612725	3000			
Ge	25.0	o	9.28156	6.72880	44.105	0.21307	3870	2–12	1.87	[66]
		e	3.44829864	2.47671447	9.56864600	0.28313910	225			
HgGa <sub>2</sub> S <sub>4</sub>	20.0	o	3.39565649	2.33212283	9.21463300	0.28124737	225	0.5–13	4.0	[67, *]
		e	4.1506	2.7896	13.28	1.1378	705			
HgS	25.0	o	4.0101	4.3736	12.84	1.5604	705	0.6–11	3.4	[19]
		e	2.55425206	0.71628581	5.48091354	0.42016876	25			
$\alpha$ -HIO <sub>3</sub>	25.0	x	2.46046031	1.21369374	5.02832424	0.33429415	25	0.35–1.6	5.30	[68, *]
		y	2.55425206	0.71628581	5.48091354	0.42016876	25			

**Table 2.1: (Continued)**

Materials (Crystal/ Semiconductor)	Temp. (°C)	Polar- ization	Sellmeier Coefficients					Range (μm)	Absorp- tion band <i>n</i> and gap (eV)	Refs. Eqn.
			A	B	C ( X 10 <sup>2</sup> )	D	E			
HfO <sub>2</sub> : 9.8% Y <sub>2</sub> O <sub>3</sub>	25.0	z	2.64260136	1.14790234	5.16574323	0.89755840	25	0.35–1.5	5.46	[69, *]
InAs	25.0		1.6909118	2.6076507	2.0475498	4.0527399	300	0.365–5	8.67	[70]
InP	25.0		11.1	0.71	650.76	2.75	2085	3.7–31.3	0.49	[71]
InSb	25.0		7.255	2.316	39.225	2.765	1085	0.95–10	1.98	[72, *]
KBO	25.0	x	15.399444	0.104253	5118.49479	3.474754	2000	7.8–22	0.17	[73, *]
(KB <sub>3</sub> O <sub>8</sub> .4H <sub>2</sub> O)		y	0.99994323	1.17913677	0.8781	----	----	0.165–1.4	13.2	[74, *]
		z	0.99994082	1.03003918	0.9188	----	----		12.9	[75, *]
			1.00005664	0.99185336	0.9329	----	----		12.8	
KB*O	25.0	x	1.0	1.17845316	0.88888365	----	----	0.16–3.5	13.2	[56, *]
(KB <sub>3</sub> O <sub>8</sub> .4D <sub>2</sub> O)		z	1.0	0.98784945	0.94217129	----	----		12.8	[56, *]
KBr	20.0		1.62554954	0.73710540	2.94034268	2.02684016	6400	0.2–40	7.23	[56, *]
KCl	20.0		1.51943848	0.65597754	2.21072774	2.64871825	5000	0.18–35	8.34	[56, *]
KCl	19.9		1.40336784	0.77086200	1.96710497	5.20427775	10000	0.25–14	8.84	[48, *]
KCl:KI (1.5%)	19.9		1.41761111	0.75856556	1.99820114	4.21512335	8000	0.25–16	8.77	[48, *]
KF	25.0		1.55083	0.29162	1.58760	3.60001	2657.4	0.15–22	9.84	[56]
KDA	33.0	o	1.54838795	0.86600472	1.83570954	1.86055285	64	0.4–1.1	9.15	[9, *]
(KH <sub>2</sub> AsO <sub>4</sub> )		e	1.65314204	0.61106301	2.10214390	0.45514484	64		8.55	
KDP	33.0	o	1.44173237	0.81553628	1.12576306	1.47865442	49	0.4–1.1	11.1	[9, *]
(KH <sub>2</sub> PO <sub>4</sub> )		e	1.37998836	0.75177750	1.16731678	0.36120079	49		14.5	

**Table 2.1: (Continued)**

Materials (Crystal/ Semiconductor)	Temp. (°C)	Polar- ization	Sellmeier Coefficients					Range (μm)	Absorp- tion band n and gap (eV)	Refs. Eqn.
			A	B	C ( X 10 <sup>2</sup> )	D	E			
KDP	24.8	o	1.46289336	0.79550715	1.27782716	1.10560172	36	0.2–1.4	11.0	[16, *]
		e	1.42190536	0.71047582	1.21984109	0.27051559	36		11.2	
(KD <sub>2</sub> PO <sub>4</sub> )	33.0	o	1.59068702	0.65000325	1.49871678	1.11286794	64	0.4–1.1	10.1	[9, *]
		e	1.43418215	0.69205653	1.23182859	0.41594387	64		11.2	
KD*P	25.0	o	0.98363343	1.26014242	0.81911791	0.68954938	36	0.40–0.69	13.7	[76, *]
		e	1.58774984	0.54292865	1.48828489	0.39228493	36		10.2	
KDPRb	33.0	o	0.81960177	1.43173192	0.80682241	1.37946279	49	0.4–1.1	13.8	[9, *]
		e	1.00383613	1.13065110	0.81234817	0.32442632	49		13.8	
KI	20.0		1.66617420	0.98625098	3.81692057	1.86575318	7000	0.25–50	6.35	[56, *]
KLN (K <sub>3</sub> Li <sub>2</sub> Nb <sub>5</sub> O <sub>15</sub> )	24.0	o	1.0	3.708	4.601	---	---	0.4–5	5.78	[77]
		e	1.0	3.349	3.564	---	---		6.57	
KM (COOK-CHOH-CH <sub>2</sub>	20.0	x	1.542	0.8299	2.013561	---	---	0.24–1.4	8.74	[78]
		y	1.470	0.7473	1.803649	---	---		9.23	
COOK.1.5H <sub>2</sub> O)		z	1.339	0.8519	1.428025	---	---		10.4	
KNO (KNbO <sub>3</sub> )	22.0	x	2.54088371	2.29332835	5.62190899	7.30699101	300	0.4–3.4	5.23	[79, 80]
		y	2.62583723	2.36053534	6.42922649	8.29653561	300		4.89	
		z	2.55261698	1.86721183	5.40028525	5.64155101	300		5.34	
KTA (KTiOAsO <sub>4</sub> )	20.0	x	2.3039444	0.8472855	4.8326702	3.0688893	250	0.35–4	5.64	[81, *]
		y	2.3880145	0.7878492	5.5830324	3.3986856	250		5.25	

**Table 2.1: (Continued)**

Materials (Crystal/ Semiconductor)	Temp. (°C)	Polar- ization	Sellmeier Coefficients					Range (μm)	Absorp- tion band n and gap (eV)	Refs. Eqn.
			A	B	C (X 10 <sup>-2</sup> )	D	E			
KTaO <sub>3</sub>	20.0	z	2.3548285	1.0920291	5.8457976	3.8746096	250		5.13	
KTP	20.0	x	2.0009584	1.0011186	4.0294037	1.7740435	20	0.4–1.06	6.42	[82, *]
(KTiOPO <sub>4</sub> )		y	2.0411662	0.9874869	4.3432843	1.8828437	150	0.2–10.6	6.18	[83, 84]
		z	2.2541202	1.0539416	5.5303637	2.2516434	150		5.95	
									5.27	
LaF <sub>3</sub>	20.0	o	1.0	1.537600	0.776161	----	----	0.35–0.70	14.1	[85]
		e	1.0	1.514900	0.770884	----	----		14.1	
LAP	20.0	x	1.57994331	0.66350234	1.77268882	0.37256988	36	0.25–1.4	9.31	[60, *]
(L-Arginine Phosphate)		y	1.59917136	0.84010856	1.89167472	0.71647713	36		9.02	
		z	1.66879020	0.78967786	2.24949793	0.54785154	36		8.27	
LBO	20.0	x	1.4426279	1.0109932	1.1210197	1.2363218	91	0.29–1.7	11.7	[86, 33]
(LiB <sub>3</sub> O <sub>5</sub> )		y	1.5014015	1.0388217	1.2157100	1.7567133	91		11.2	
		z	1.4489240	1.1365228	1.1676746	1.5830069	91		11.5	
LFM	25.0	x	1.43733506	0.40475012	1.69196273	0.01695506	36	0.23–1.3	9.5	[87, *]
(LiCOOH.H <sub>2</sub> O)		y	1.65545000	0.50339981	2.33456179	0.43120589	36		8.1	
		z	1.66828005	0.59550781	2.52926288	0.51969132	36		7.8	
LiF	20.0		1.01369880	0.91190354	0.55023818	7.14251615	1100	0.1–10	16.7	[56, *]
LIO	23.0	o	2.0730090	1.3420521	3.5155686	1.5915063	190	0.5–5	6.61	[88, 89]
(LiIO <sub>3</sub> )		e	1.6658390	1.2525669	2.8115791	0.6580167	190		7.4	

**Table 2.1: (Continued)**

Materials (Crystal/ Semiconductor)	Temp. (°C)	Polar- ization	Sellmeier Coefficients					Range (μm)	Absorp- tion band n and gap (eV)	Refs. Eqn.
			A	B	C (X 10 <sup>2</sup> )	D	E			
LIO (Li <sub>2</sub> O <sub>3</sub> )	25.0	o	2.03132	1.37623	3.50823	1.06745	169	0.5–5	6.62	[90]
		e	1.83086	1.08807	3.13810	0.554582	158.76		7.0	
LNO (LiNbO <sub>3</sub> ) (pure)	25.0	o	2.30868466	2.59943258	4.53622670	7.85093573	300	0.42–4	5.82	[91, *]
		e	2.17136846	2.40239261	4.12238100	6.35196621	300		6.11	
	25.0	o	2.27819911	2.64261396	4.51938833	7.77870589	300	0.42–4	5.83	[92, *]
		e	2.25826059	2.31529513	4.25064669	6.24472815	300		6.01	
(congruently melt)	24.5	o	2.38952126	2.51367167	4.70532927	7.88014969	300	0.40–3.1	5.72	[93, *]
		e	2.31555508	2.26509259	4.39945088	6.36660092	300		5.91	
LNO:MgO (7%MgO:LiNbO <sub>3</sub> )	25.0	o	2.00386576	2.85969043	4.20429003	6.47078590	250	0.4–4	6.05	[94, *]
		e	2.40205217	2.14162463	4.47232281	6.28571221	250		5.86	
LTO (LiTaO <sub>3</sub> )	25.0	o	1.98794841	2.51909534	3.48752303	6.74867738	300	0.45–4	6.64	[31, *]
		e	2.15687934	2.36800178	3.69273851	6.71815687	300		6.45	
LiYF <sub>4</sub>	25.0	o	1.38757	0.70757	0.931	0.18849	51	0.23–2.6	12.9	[95]
		e	1.31021	0.84903	0.876	0.53697	135		13.2	
MAP (C <sub>10</sub> H <sub>11</sub> N <sub>3</sub> O <sub>6</sub> )	20.0	x	2.16757084	0.10542484	16.8505230	0.99126222	64	0.5–2	3.0	[96, *]
		y	2.30650608	0.22784362	17.9514184	1.12305937	64		2.9	
		z	2.73830634	0.61735732	15.9882765	3.18448050	64		3.1	
MDB	23.0	x	2.16007371	0.72471419	6.37947255	0.18117133	36	0.43–1.2	4.91	[97, *]

**Table 2.1: (Continued)**

Materials (Crystal/ Semiconductor)	Temp. (°C)	Polar- ization	Sellmeier Coefficients					Range (μm)	Absorp- tion band <i>n</i> and gap (eV)	Refs. Eqn.
			<i>A</i>	<i>B</i>	<i>C</i> (X 10 <sup>2</sup> )	<i>D</i>	<i>E</i>			
(Meta-di- nitrobenzene)		y	2.02036204	0.68508036	5.91484437	0.22989248	36		5.1	
		z	1.95937253	0.20285306	6.76086193	0.32565318	36		4.77	
mNA	20.0	x	2.46752274	0.18691228	15.9965171	1.19780255	64	0.42–2	3.1	[98, *]
		y	2.66462581	0.16286509	17.1893347	1.27902389	64		3.0	
		z	2.80751576	0.15347567	17.4861506	1.76534933	64		2.96	
MgAl <sub>2</sub> O <sub>4</sub>	25.0		1.93704783	0.95795641	1.83214061	3.76543269	300	0.35–5.5	9.16	[99, *]
MgBaF <sub>4</sub>	25.0	x	1.11497468	0.96202532	0.79	---	---	0.185–12	14.0	[100, *]
		y	2.13246088	-0.0000172	9.60889563	-0.0003404	100			
		z	1.32842222	0.81777778	0.90	---	---		13.1	
MgF <sub>2</sub>	19.0	o	1.30618931	0.58007346	0.77355208	2.24075551	550	0.2–7.0	14.1	[101, *]
		e	1.29108974	0.62728316	0.75322929	2.41840547	550		14.3	
MgO	20.0		1.53180538	1.42502805	1.52465664	6.98416419	650	0.36–5.6	10.0	[102, *]
NaBr	20.0		1.59778665	0.99998568	2.81766115	3.74557330	5500	0.21–34	7.39	[56, *]
NaCl	20.0		1.47469012	0.85594247	2.03004560	3.75408845	4000	0.2–20	8.7	[45, *]
			1.44354608	0.88670071	1.98488774	3.76346189	4000	0.2–20	8.8	[56, *]
NaCOOH	25.0	x	1.25793545	0.64465461	1.20293934	0.06407803	64	0.24–2.3	11.3	[103, *]
		y	1.25686750	0.84428339	1.44481248	0.02913995	64		10.3	
		z	1.24795357	1.07632137	1.72301349	0.07580585	64		9.45	
NaF	20.0		1.41572	0.32785	1.3689	3.18248	1646	0.15–17	10.6	[56]

**Table 2.1: (Continued)**

Materials (Crystal/ Semiconductor)	Temp. (°C)	Polar- ization	Sellmeier Coefficients					Range (μm)	Absorp- tion band <i>n</i> and gap (eV)	Refs. Eqn.
			A	B	C (X 10 <sup>2</sup> )	D	E			
NaI	20.0		1.478	1.532	2.89	4.27	7432	0.25–40	7.29	[56]
NaNO <sub>3</sub>	20.0	o	1.59308418	0.82617497	3.36964254	-0.0672546	8	0.43–0.67	6.76	[45, *]
		e	1.80519648	0.00005263	30.3948024	0.45661747	8			
PbF <sub>2</sub>	20.0		2.09306602	0.90416734	4.08164901	20.1725555	6400	0.3–11.9	6.14	[104, *]
PbMoO <sub>4</sub>	20.0	o	3.31789001	1.86140800	8.79777777	0.44986321	16	0.44–1.08	4.18	[105, *]
		e	2.64112802	2.10847245	5.95220598	0.13386036	16		5.08	
PbS	20.0		9.40992387	8.02618811	20.113303	21.6436590	1600	0.77–10	2.76	[106, *]
PbSe	20.0		24.1893580	0.30084592	3608.56902	28.0282537	2200	3.8–13.5	0.2	[107, *]
PbTe	20.0		33.4027989	0.62478499	1293.87844	52.2010221	2000	3.8–12.8	0.34	[108, *]
POM	20.0	x	2.4529	0.1641	12.8	---	---		3.47	[98]
		y	2.42537085	0.35919999	12.7376916	16.8156613	300	0.4–3	3.47	[109, *]
		z	2.54247743	0.80174478	12.8750995	27.3304994	300		3.46	
RDA (RbH <sub>2</sub> AsO <sub>4</sub> )	33.0	o	1.50606328	0.88415270	1.76568589	1.31351957	49	0.4–1.1	9.33	[9, *]
		e	1.61511634	0.66209986	2.00025850	0.32661854	49		8.77	
RD*A (RbD <sub>2</sub> AsO <sub>4</sub> )	33.0	o	1.33583395	1.03686649	1.50236618	0.53504393	36	0.4–1.1	10.1	[9, *]
		e	1.40197441	0.86871957	1.56890123	0.16618676	36		9.9	
RDP (RbH <sub>2</sub> PO <sub>4</sub> )	33.0	o	0.46887920	1.78028444	0.60468401	1.37656471	49	0.4–1.1	16.0	[9, *]
		e	0.77570462	1.38378378	0.69797980	0.35986808	49		14.8	
RD*P	33.0	o	1.40975881	0.82816019	1.20032692	0.70839664	36	0.4–1.1	11.3	[9, *]

**Table 2.1: (Continued)**

Materials (Crystal/ Semiconductor)	Temp. (°C)	Polar- ization	Sellmeier Coefficients				Range (μm)	Absorp- tion band <i>n</i> and gap (eV)	Refs. Eqn.
			<i>A</i>	<i>B</i>	<i>C</i> (X 10 <sup>-2</sup> )	<i>D</i>	<i>E</i>		
(RbD <sub>2</sub> PO <sub>4</sub> ) RTP		e	1.95174985	0.20821402	3.48645486	0.36467178	36	6.64	
	25.0	x	2.55394111	0.54963261	6.31675331	6.37560225	400	0.35–4.5	4.93 [110, *]
(RbTiOPO <sub>4</sub> )		y	2.32406026	0.80211190	5.36954608	8.07214470	400	5.35	
		z	2.76506945	0.64609710	8.12649480	8.56631709	400	4.35	
Ruby	22.0	o	2.29369544	0.79270179	1.93353194	0.15249716	8	0.43–0.71	8.92 [111, *]
		e	0.21068676	2.84112240	0.60377295	0.09851843	8		
Se	23.0	o	6.72405013	0.30138425	80.4896316	3.54312711	1600	1.06–10.6	1.38 [112, *]
		e	10.3912809	1.54560920	46.3106277	4.17305674	1600		1.82
Si	27.0		3.12896495	8.54278728	11.337073	0.00527631	1500	1.36–11	3.68 [14, *]
Si	25.0		4.92719645	7.27691471	11.5786091	42.7173925	100	0.4–0.78	3.64 [113, *]
β-SiC	20.0		1.0	5.5705	2.673225	----	----	0.47–0.69	7.58 [114]
α-SiC	20.0	o	1.0	5.5515	2.640625	----	----	0.49–1.06	6.15 [115]
		e	1.0	5.7382	2.855086	----	----		7.34
α-SiO <sub>2</sub> (Quartz)	25.0	o	1.29605832	1.06065833	1.01235868	2.25605819	200	0.185–2.1	12.3 [116, *]
		e	1.39617770	0.98848948	1.10298606	2.41678691	200	0.185–2.1	11.8
α-SiO <sub>2</sub>	25.0	o	1.40905664	0.94887690	1.10800934	1.28256514	100	0.18–0.75	11.8 [117, *]
		e	1.41805074	0.96717725	1.12715045	0.88589739	100		11.7
SrF <sub>2</sub>	20.0		1.35310542	0.69638061	0.92797488	3.36565804	1600	0.25–11.5	12.9 [48, *]
SrMoO <sub>4</sub>	25.0	o	2.13633823	1.35522958	3.49855079	2.27020622	300	0.45–2.4	6.62 [31, *]

**Table 2.1: (Continued)**

Materials (Crystal/ Semiconductor)	Temp. (°C)	Polar- ization	Sellmeier Coefficients					Range (μm)	Absorp- tion band n and gap (eV)	Refs. Eqn.
			A	B	C (X 10 <sup>2</sup> )	D	E			
SrTiO <sub>3</sub>	25.0	e	2.29721810	1.20510636	4.03047127	2.52723226	300	0.43–3.8	4.67 [45, *]	[45, *]
			2.86912089	2.34233183	7.06002312	10.9753287	300			
Te	25.0		2.42187038	2.76968545	6.28759701	7.53814810	300	0.45–3.8	4.95 [31, *]	[31, *]
		o	18.5346	4.3289	398.10	3.7800	11813			
TeO <sub>2</sub>	20.0	e	29.5222	9.3068	257.66	9.2350	13521	4–14	0.62 [19]	0.77
		o	2.71688346	2.0362633	5.95328147	0.11344622	16			
TiO <sub>2</sub>	25.0	e	2.88752546	2.49103113	6.06531999	0.12676676	16	0.4–1	5.08 [118, *]	5.03
		o	2.84860910	3.06181302	8.00134067	-0.03198089	25			
TiO <sub>2</sub>	25.0	e	3.17419736	4.01135254	8.36350921	-0.09750392	25	0.43–1.53	4.38 [45, *]	4.29
		o	3.23385217	2.72670030	8.39522371	3.38150919	100			
Tl <sub>3</sub> AsSe <sub>3</sub> [TAS]	25.0	e	4.51423711	2.77391366	9.79744383	5.31788562	100	0.45–2.4	4.28 [31, *]	3.96
		o	6.03737957	5.19399305	34.6307307	2.90084653	2500			
TlBr	25.0		8.40171923	1.62283661	82.3603918	2.05812267	2500	2–12	2.1 [119, *]	1.4
			3.83190858	1.44039164	11.266023	1.30884878	16			
Tl[Br: Cl] KRS-6	25.0		0.45587304	4.36355477	4.45018360	7.90340049	9500	0.58–24	5.88 [120, *]	
Tl[Br: I] KRS-5	19.0		2.84207150	2.82918542	10.1422791	14.3405647	31000	0.58–39	3.89 [121, *]	
TlCl	25.0		3.74680347	1.02028243	9.73387282	1.98890646	16	0.43–0.66	3.97 [22, *]	
Y <sub>3</sub> Al <sub>5</sub> O <sub>12</sub> (YAG)	25.0		1.80034564	1.49343976	1.77099120	3.50903401	300	0.4–4	9.32 [31, *]	
Y <sub>2</sub> O <sub>3</sub>	20.0		0.99859062	2.57931374	1.92329098	3.72479973	500	0.2–12	8.94 [122, *]	

**Table 2.1: (Continued)**

Materials (Crystal/ Semiconductor)	Temp. (°C)	Polar- ization	Sellmeier Coefficients					Range (μm)	Absorp- tion band <i>n</i> and gap (eV)	Refs. Eqn.
			<i>A</i>	<i>B</i>	<i>C</i> (X 10 <sup>-2</sup> )	<i>D</i>	<i>E</i>			
ZnGeP <sub>2</sub>	20.0	o	4.47330	5.26576	13.381	1.49085	662.55	0.64–12	3.39	[50, 51]
		e	4.63318	5.34215	14.255	1.45785	662.55		3.28	
ZnO	25.0	o	2.85349562	0.84269535	9.46396061	2.17891980	300	0.45–4.0	4.03	[31, *]
		e	2.80512169	0.94272630	9.03655516	2.09919541	300		4.12	
β-ZnS	21.6		2.23696722	2.86316280	5.18497733	2.86977560	1200	0.55–10.5	5.4	[48, *]
Zns	25.0		2.57477308	2.53722297	5.70100072	0.411111677	100	0.45–2.4	5.2	[31, *]
α-Zns	25.0	o	3.41601054	1.74084980	7.16458591	-0.0023589	20	0.36–1.4	4.63	[123, *]
		e	3.46184666	1.72082603	7.19323780	0.11687750	20		4.62	
ZnSe	20.3		3.34955729	2.57689896	9.38826749	2.88904268	2200	0.55–18	4.05	[48, *]
ZnSiAs <sub>2</sub>	25.0	o	4.6066	5.6912	14.37	1.1316	700	0.7–11.5	3.27	[50, 19]
		e	4.9091	5.5565	15.78	1.1287	700		3.12	
ZnTe	25.0		4.29515331	2.98859685	14.2458772	2.45419969	3000	0.57–25	3.29	[15, *]
ZnWO <sub>4</sub>	25.0	x	2.72421908	1.73800676	4.75449530	3.98567817	300	0.42–4.0	5.69	[31, *]
		y	2.40450786	2.11263371	4.29666836	4.02381019	300	0.42–3.6	5.98	
		z	2.65345900	2.43455523	4.83248161	5.58536560	300	0.42–3.6	5.64	
ZrO <sub>2</sub> : 12%Y <sub>2</sub> O <sub>3</sub>	25.0		2.05122399	2.41401832	2.64827500	11.2670449	700	0.36–5.1	7.67	[124, *]

\* – My fit

**Table 2.2: Sellmeier Coefficients for Some Optical and Fiber Glasses; [ $n^2 = A + B/(1 - C/\lambda^2) + D/(1 - E/\lambda^2)$ ,  $\lambda$  is in  $\mu\text{m}$ ]**

Glasses		Temp. (°C)	Sellmeier Coefficients					Range ( $\mu\text{m}$ )	Absorp. band gap (eV)	Ref. for $n$ and Eqn.
Schott	Ohara		A	B	C ( $\times 10^{-2}$ )	D	E			
---	BAH32	20	1.89298845	0.82387607	2.88317368	1.85495930	200	0.36–2.33	7.3	[125, *]
BaLF4	BAL4	20	1.64229267	0.80996963	1.84821497	1.32867267	150	0.33–2.33	9.1	[126, 127]
BaK1	BAL11	20	1.53163489	0.90159230	1.55142286	1.25742434	150	0.31–2.33	10.0	[126, 127]
PSK3	BAL23	20	1.45898859	0.91813830	1.30700097	1.53653204	150	0.31–2.33	10.8	[126, 127]
SK4	BSM4	20	1.53418270	1.02432620	1.47483619	0.97315045	100	0.33–2.33	10.2	[126, 127]
---	BSM9	20	1.61343315	0.94601273	1.69493728	1.36313318	150	0.36–2.33	9.5	[125, *]
---	BSM22	20	1.66142576	0.92219278	1.82037106	1.35578530	150	0.36–2.33	9.2	[125, *]
SSK4A	BSM24	20	1.60142499	0.96932959	1.66620095	1.17740089	130	0.33–2.33	9.6	[126, 127]
K5	NSL5	20	1.50879617	0.77615273	1.52773045	1.26816265	150	0.31–2.33	10.0	[126, 127]
---	PBM3	20	1.81718900	0.71735619	3.06533130	1.73341223	200	0.36–2.33	7.1	[125, *]
SF6	PBH6	20	2.07890466	1.03775076	4.23019093	1.39213190	150	0.36–2.33	6.0	[126, 127]
---	PBL26	20	1.74817094	0.65645522	2.65692509	1.68327025	200	0.36–2.33	7.6	[125, *]
---	S-BAL2	20	1.69375672	0.72988760	2.09938544	1.27069569	150	0.36–2.33	8.6	[125, *]
---	S-BAL14	20	1.59915353	0.82264667	1.69901106	1.37033083	150	0.36–2.33	9.5	[125, *]
BK7	S-BSL7	20	1.43131380	0.84014624	1.28897582	0.97506873	100	0.31–2.33	10.9	[126, 127]
---	S-FPL51	20	1.33782101	0.87986171	0.96071215	0.80365148	150	0.36–2.33	12.7	[125, *]
---	S-FPL52	20	1.33336620	0.76802212	0.88491995	0.71925847	150	0.36–2.33	13.2	[125, *]
---	S-FPL53	20	1.24672804	0.80625247	0.77204904	0.61817308	150	0.36–2.33	14.1	[125, *]
FK5	S-FSL5	20	1.36459305	0.82393169	1.10838681	0.93306279	100	0.28–2.33	11.8	[126, 127]

**Table 2.2: (Continued)**

Glasses		Temp. (°C)	Sellmeier Coefficients					Range (μm)	Absorp. band gap (eV)	Ref. for $n$ and Eqn.
Schott	Ohara		A	B	C ( $\times 10^{-2}$ )	D	E			
LaF2	S-LAM2	20	1.90798862	1.05969452	2.35627833	1.65229731	150	0.36–2.33	8.1	[126, 127]
---	S-LAM51	20	1.79270360	1.03443101	2.08695053	1.61986479	150	0.36–2.33	8.6	[125, *]
LaK10	S-LAL10	20	1.77798367	1.11987423	1.90728779	1.28954539	90	0.36–2.33	9.0	[126, 127]
---	S-NSL36	20	1.65681095	0.60902200	2.11054490	1.28405587	150	0.36–2.33	8.5	[125, *]
---	SSL6	20	1.63685176	0.65644946	2.04645940	1.00701091	100	0.31–2.32	8.7	[125, 127]
ZK1	ZSL1	20	1.53023177	0.78537672	1.58905079	1.03208380	120	0.31–2.33	9.8	[126, 127]
KzFS6	---	20	1.70910663	0.77858837	2.12286099	0.88503243	70	0.36–2.33	8.5	[126, 127]
FS (Corning 7940)		26	1.31563132	0.78910058	1.10325933	0.91298262	100	0.23–2.26	11.8	[128, 129]
FS (Corning 7940)		471	1.33514985	0.78426280	1.15873913	0.92097109	100	0.23–2.26	11.5	[128, 129]
Fused silica		20	1.30912262	0.79514557	1.09439467	0.92107106	100	0.21–2.33	11.9	[130, 129]
SiO <sub>2</sub>		20.5	1.31138256	0.79429689	1.09514652	0.99952574	100	0.24–0.55	11.9	[131, 129]
AS (Corning 1723)		28	1.40919164	0.95486678	1.31952169	0.90459781	100	0.36–2.26	10.8	[128, 129]
AS (Corning 1723)		526	1.49368555	0.88229977	1.48132649	0.90324053	100	0.36–2.26	10.2	[128, 129]
V (Corning 7913)		28	1.28802423	0.81471590	1.07852766	0.94473185	100	0.26–2.26	11.9	[128, 129]
V (Corning 7913)		526	1.35308250	0.76529922	1.19368978	0.94868688	100	0.26–2.26	11.4	[128, 129]
BGZA(4) (Fluoride)		25	1.91829737	0.35130064	2.61388311	0.50447475	150	0.40–4.9	7.67	[135, *]

FS – Fused silica, AS – Alumino silicate, and V – Vycor glasses; and \* – My fit.

**Table 2.3: Sellmeier Coefficients for Binary Tellurite  $xM_mO_n - (100-x)TeO_2$  glasses\* at 23°C;  
[ $n^2 = A + B/(1 - C/\lambda^2) + D/(1 - E/\lambda^2)$ ,  $\lambda$  is in  $\mu\text{m}$ ]**

Modifier $xM_mO_n$	Sellmeier Coefficients					Range ( $\mu\text{m}$ )	Absorp- tion band gap (eV)	Refs. for $n$ and Eqn.
	A	B	C ( $X 10^{-2}$ )	D	E			
20 Na <sub>2</sub> O	2.1810511	1.5538234	5.0408437	1.9356580	225	0.40–1.71	5.522	[132, 133]
10Al <sub>2</sub> O <sub>3</sub>	2.2777923	1.6538030	4.7884340	2.3782506	225	0.40–1.71	5.667	[132, 133]
25ZnO	2.4843245	1.6174321	5.3715551	2.4765135	225	0.40–1.71	5.350	[132, 133]
20BaO	2.3771962	1.7305093	5.2136822	2.2568767	225	0.40–1.71	5.430	[132, 133]
15BaO	2.5047737	1.6413512	5.5021797	2.4738861	225	0.40–1.71	5.286	[132, 133]
10Sb <sub>2</sub> S <sub>3</sub>	2.4365621	1.8695097	5.3694094	2.6890812	225	0.40–1.71	5.351	[132, 133]
20MoO <sub>3</sub>	2.4716292	1.9138763	5.9416834	2.5412795	225	0.55–1.71	5.088	[132, 133]
20WO <sub>3</sub>	2.4909866	1.9515037	5.6740339	3.0212592	225	0.44–1.71	5.206	[132, 133]
10Nb <sub>2</sub> O <sub>5</sub>	2.5952567	1.8697504	5.8576383	3.5414649	225	0.40–1.71	5.123	[132, 133]
20Tl <sub>2</sub> O	2.5804773	1.8635211	6.3945516	2.4311168	225	0.40–1.71	4.904	[132, 133]
TeO <sub>2</sub>	3.5483034	0.9783726	8.2669346	6.6510879	225	0.49–1.00	4.312	[134, 133]

\* Glass compositions are expressed by molar fraction and type of modifier.

## 2.6 Comparison of Refractive Indices

It is helpful to have available a reference of the experimental and estimated values of refractive indices for various optical materials. The comparison of experimental and calculated values of refractive indices are shown alphabetically in Tables 2.4 to 2.76 for various optical materials. The experimental accuracy, where applicable, fit average, and root mean square (RMS) errors are also mentioned in the tables.

**Table 2.4: The Experimental [9] and Computed Refractive Index Values of ADA Crystal at 33°C**

Polarization	Wavelength (μm)	Observed [9]	Computed (This work)	Difference	Av. RMS Dev. Dev.
Ordinary	0.404656	1.59779	1.597782	0.000008	1.9 2.4
	0.435833	1.59199	1.591985	0.000005	[10 <sup>-5</sup> ]
	0.467815	1.58722	1.587241	-0.000021	
	0.479991	1.58567	1.585680	-0.000010	Expt.
	0.508582	1.58243	1.582432	-0.000002	accuracy is
	0.546074	1.57885	1.578874	-0.000024	± 0.00003
	0.589300	1.57553	1.575493	0.000037	
	0.643847	1.57204	1.571990	0.000050	
	0.780027	1.56537	1.565370	0.000000	
	0.794760	1.56472	1.564764	-0.000044	
	0.852113	1.56250	1.562521	-0.000021	
	0.894346	1.56097	1.560961	0.000009	
	1.064000	1.55507	1.555057	0.000013	
Extra-ordinary	0.404656	1.53984	1.539848	-0.000008	1.9 2.2
	0.435833	1.53489	1.534937	-0.000047	[10 <sup>-5</sup> ]
	0.467815	1.53098	1.530962	0.000018	
	0.479991	1.52968	1.529666	0.000014	
	0.508582	1.52700	1.526993	0.000007	Expt.
	0.546074	1.52413	1.524113	0.000017	accuracy is
	0.589300	1.52147	1.521440	0.000030	± 0.00003
	0.643847	1.51878	1.518763	0.000017	
	0.780027	1.51406	1.514084	-0.000024	
	0.794760	1.51366	1.513686	-0.000026	
	0.852113	1.51225	1.512266	-0.000016	
	0.894346	1.51131	1.511326	-0.000016	
	1.064000	1.50812	1.508091	0.000029	

**Table 2.5: The Experimental [9] and Computed Refractive Index Values of AD\*A Crystal at 33°C**

Polarization	Wavelength (μm)	Observed [9]	Computed (This work)	Difference	Av. RMS Dev.	Dev. Dev.
Ordinary	0.404656	1.59056	1.590552	0.000008	2.7	3.7
	0.435833	1.58487	1.584913	-0.000043	[10 <sup>-5</sup> ]	
	0.467815	1.58036	1.580345	0.000015		
	0.479991	1.57889	1.578853	0.000037		
	0.508582	1.57580	1.575769	0.000031		
	0.546074	1.57242	1.572432	-0.000012	Expt.	
	0.589300	1.56921	1.569308	-0.000098	accuracy	
	0.643847	1.56619	1.566140	0.000050	±0.00003	
	0.780027	1.56045	1.560416	0.000034		
	0.794760	1.55991	1.559913	-0.000003		
	0.852113	1.55808	1.558086	-0.000006		
	0.894346	1.55683	1.556846	-0.000016		
Extra-ordinary	1.064000	1.55237	1.552368	0.000002		
	0.404656	1.53586	1.535862	-0.000002	2.6	3.7
	0.435833	1.53102	1.531057	-0.000037	[10 <sup>-5</sup> ]	
	0.467815	1.52722	1.527171	0.000049		
	0.479991	1.52593	1.525905	0.000025		
	0.508582	1.52331	1.523299	0.000011	Expt.	
	0.546074	1.52050	1.520503	-0.000003	accuracy	
	0.589300	1.51784	1.517924	-0.000084	±0.00003	
	0.643847	1.51538	1.515366	0.000014		
	0.780027	1.51103	1.511012	0.000018		
	0.794760	1.51063	1.510652	-0.000022		
	0.852113	1.50944	1.509387	0.000053		
	0.894346	1.50856	1.508569	-0.000009		
	1.064000	1.50587	1.505885	-0.000015		

**Table 2.6: The Experimental [9] and Computed Refractive Index Values of ADP Crystal at 33°C**

Polarization	Wavelength (μm)	Observed [9]	Computed (This work)	Difference	Av. Dev.	RMS Dev.
Ordinary	0.404656	1.53885	1.538614	0.000236	2.2	2.6
	0.435833	1.53497	1.535069	-0.000099	[10 <sup>-4</sup> ]	
	0.467815	1.53171	1.531916	-0.000206		
	0.479991	1.53065	1.530828	-0.000178		
	0.508582	1.52835	1.528485	-0.000135		
	0.546074	1.52588	1.525802	0.000078	Expt.	
	0.589300	1.52331	1.523160	0.000150	accuracy	
	0.643847	1.52076	1.520368	0.000392	± 0.00003	
	0.780027	1.51534	1.515181	0.000159		
	0.794760	1.51490	1.514728	0.000172		
	0.852113	1.51285	1.513103	-0.000253		
	0.894346	1.51143	1.512026	-0.000596		
Extra-ordinary	1.064000	1.50866	1.508380	0.000280		
	0.404656	1.49141	1.491412	-0.000002	2.6	3.3
	0.435833	1.48810	1.488119	-0.000019	[10 <sup>-5</sup> ]	
	0.467815	1.48540	1.485412	-0.000012		
	0.479991	1.48452	1.484520	0.000000		
	0.508582	1.48268	1.482663	0.000017	Expt.	
	0.546074	1.48062	1.480632	-0.000012	accuracy	
	0.589300	1.47875	1.478711	0.000039	± 0.00003	
	0.643847	1.47678	1.476741	0.000039		
	0.780027	1.47316	1.473122	0.000038		
	0.794760	1.47278	1.472799	-0.000019		
	0.852113	1.47155	1.471624	-0.000074		
	0.894346	1.47078	1.470823	-0.000043		
	1.064000	1.46795	1.467903	0.000047		

**Table 2.7: The Experimental and Computed Refractive Index Values of ADP Crystal at 24.8°C**

Polari-zation	Wavelength ( $\mu\text{m}$ )	Observed [16]	Computed (This work)	Difference	Av RMS Dev. Dev.
Ordinary	0.2138560	1.62598	1.625913	0.000067	3.4    4.1
	0.2288018	1.60785	1.607941	-0.000091	$[10^{-5}]$
	0.2536519	1.58688	1.586906	-0.000026	
	0.2967278	1.56462	1.564707	-0.000087	Expt.
	0.3021499	1.56270	1.562687	0.000013	accuracy
	0.3125663	1.55917	1.559143	0.000027	$\pm 0.00003$
	0.3131545	1.55897	1.558955	0.000015	
	0.3341478	1.55300	1.552962	0.000038	
	0.3650146	1.54615	1.546130	0.000020	
	0.3654833	1.54608	1.546040	0.000040	
	0.3662878	1.54592	1.545887	0.000033	
	0.3906410	1.54174	1.541716	0.000024	
	0.4046561	1.53969	1.539659	0.000031	
	0.4077811	1.53925	1.539229	0.000021	
	0.4358350	1.53578	1.535771	0.000009	
	0.5460740	1.52662	1.526638	-0.000018	
	0.5769590	1.52478	1.524825	-0.000045	
	0.5790654	1.52466	1.524709	-0.000049	
	0.6328160	1.52195	1.522005	-0.000055	
Extra-ordinary	1.0139750	1.50835	1.508319	0.000031	
	1.1287040	1.50446	1.504457	0.000003	
	1.1522760	1.50364	1.503641	-0.000001	
	0.2138560	1.56738	1.567317	0.000063	2.3    3.1
	0.2288018	1.55138	1.551470	-0.000090	$[10^{-5}]$
	0.2536519	1.53289	1.532924	-0.000034	
	0.2967278	1.51339	1.513387	0.000003	
	0.3021499	1.51163	1.511614	0.000016	Expt.
	0.3125663	1.50853	1.508508	0.000022	accuracy
	0.3131545	1.50832	1.508343	-0.000023	$\pm 0.00003$
	0.3341478	1.50313	1.503104	0.000026	
	0.3650146	1.49720	1.497165	0.000035	
	0.3654833	1.49712	1.497087	0.000033	
	0.3662878	1.49698	1.496955	0.000025	
	0.4046561	1.49159	1.491597	-0.000007	
	0.4077811	1.49123	1.491230	0.000000	
	0.4358350	1.48831	1.488296	0.000014	
	0.4916036	1.48390	1.483905	-0.000005	
	0.5460740	1.48079	1.480815	-0.000025	
	0.5769590	1.47939	1.479409	-0.000019	
	0.5790654	1.47930	1.479320	-0.000020	
	0.6328160	1.47727	1.477302	-0.000032	
	1.0139750	1.46895	1.468938	0.000012	
	1.1287040	1.46704	1.467040	0.000000	
	1.1522760	1.46666	1.466654	0.000006	

**Table 2.8: The Experimental [9] and Computed Refractive Index Values of AD\*P Crystal at 33°C**

Polarization	Wavelength (μm)	Observed [9]	Computed (This work)	Difference	Av. RMS Dev.	Dev. Dev.
Ordinary	0.404656	1.53216	1.532162	-0.000002	4.4	6.1
	0.435833	1.52858	1.528526	0.000054	[10 <sup>-5</sup> ]	
	0.467815	1.52546	1.525526	-0.000066		
	0.479991	1.52450	1.524534	-0.000034		
	0.508582	1.52241	1.522464	-0.000054		
	0.546074	1.52027	1.520187	0.000083	Expt.	
	0.579066	1.51862	1.518493	0.000127	accuracy	
	0.643847	1.51564	1.515761	-0.000121	± 0.00003	
	0.780027	1.51152	1.511506	0.000014		
	0.794760	1.51112	1.511118	0.000002		
	0.852113	1.50969	1.509685	0.000005		
	0.894346	1.50868	1.508692	-0.000012		
	1.064000	1.50497	1.504965	0.000005		
Extra-ordinary	0.404656	1.48738	1.487716	-0.000336	12.6	22
	0.435833	1.48519	1.484465	0.000725	[10 <sup>-5</sup> ]	
	0.467815	1.48162	1.481801	-0.000181		
	0.479991	1.48080	1.480925	-0.000125		
	0.508582	1.47898	1.479110	-0.000130		
	0.546074	1.47713	1.477140	-0.000010	Expt.	
	0.579066	1.47575	1.475699	0.000051	accuracy	
	0.643847	1.47337	1.473440	-0.000070	± 0.00003	
	0.780027	1.47019	1.470168	0.000022		
	0.794760	1.46992	1.469889	0.000031		
	0.852113	1.46894	1.468892	0.000048		
	0.894346	1.46824	1.468232	0.000008		
	1.064000	1.46593	1.465966	-0.000036		

**Table 2.9: The Experimental [23] and Computed Refractive Index Values of AgCl Crystal at 23.9°C**

Wavelength ( $\mu\text{m}$ )	Observed [23]	Computed (This work)	Difference	Av. Dev.	RMS Dev.
0.5780	2.06932	2.069325	-0.000005	1.5	1.8
0.6438	2.05479	2.054783	0.000007	[ $10^{-5}$ ]	
1.0142	2.02179	2.021783	0.000007		
1.129	2.01776	2.017749	0.000011		
1.37	2.01238	2.012379	0.000001	Expt. accuracy	
1.70	2.00833	2.008345	-0.000015	was not	
2.02	2.00603	2.006053	-0.000023	mentioned	
2.43	2.00412	2.004144	-0.000024		
3.39	2.00129	2.001305	-0.000015		
4.24	1.99927	1.999287	-0.000017		
4.62	1.99837	1.998386	-0.000016		
4.87	1.99777	1.997780	-0.000010		
6.26	1.99409	1.994091	-0.000001		
6.44	1.99357	1.993564	0.000006		
6.62	1.99303	1.993025	0.000005		
8.22	1.98766	1.987644	0.000016		
10.34	1.97877	1.978739	0.000031		
11.03	1.97541	1.975373	0.000037		
11.47	1.97313	1.973101	0.000029		
11.86	1.97104	1.971004	0.000036		
13.22	1.96303	1.963063	-0.000033		
14.32	1.95591	1.955896	0.000014		
14.98	1.95127	1.951261	0.000009		
16.90	1.93627	1.936275	-0.000005		
17.38	1.93215	1.932161	-0.000011		
17.80	1.92842	1.928435	-0.000015		
18.16	1.92513	1.925145	-0.000015		
19.80	1.90898	1.908988	-0.000008		
20.56	1.90082	1.900815	0.000005		

**Table 2.10: The Experimental [25] and Computed Refractive Index Values of AgInSe<sub>2</sub> Crystal at 25°C**

Polarization	Wavelength ( μm)	Observed [25]	Computed (This work)	Difference	Av. Dev.	RMS Dev.
Ordinary	1.05	2.8265	2.82432	0.00218	7.2	9.7
	1.10	2.7971	2.79893	-0.00183	[10 <sup>-4</sup> ]	
	1.20	2.7608	2.76279	-0.00199		
	1.30	2.7376	2.73849	-0.00089		
	1.40	2.7211	2.72116	-0.00006		
	1.60	2.6992	2.69837	0.00083		
	1.80	2.6856	2.68426	0.00134		
	2.00	2.6761	2.67481	0.00129		
	2.20	2.6694	2.66811	0.00129	No expt.	
	2.40	2.6643	2.66315	0.00115	accuracy	
	2.60	2.6601	2.65935	0.00075		
	2.80	2.6568	2.65635	0.00045		
	3.00	2.6542	2.65393	0.00027		
	3.20	2.6521	2.65192	0.00018		
	3.40	2.6503	2.65023	0.00007		
	3.60	2.6488	2.64878	0.00002		
	3.80	2.6474	2.64752	-0.00012		
	4.00	2.6463	2.64640	-0.00010		
	4.50	2.6436	2.64404	-0.00044		
	5.50	2.6399	2.64039	-0.00049		
	6.00	2.6381	2.63880	-0.00070		
	6.50	2.6366	2.63726	-0.00066		
	7.00	2.6352	2.63574	-0.00054		
	7.50	2.6335	2.63419	-0.00069		
	8.00	2.6318	2.63260	-0.00080		
	8.50	2.6302	2.63094	-0.00074		
	9.00	2.6286	2.62919	-0.00059		
	9.50	2.6266	2.62735	-0.00075		
	10.00	2.6251	2.62540	-0.00030		
	10.50	2.6233	2.62332	-0.00002		
	11.00	2.6210	2.62110	-0.00010		
	11.50	2.6187	2.61873	-0.00003		
	12.00	2.6187	2.61620	0.00250		

**Table 2.10: (Continued)**

Polarization	Wavelength ( $\mu\text{m}$ )	Observed [25]	Computed (This work)	Difference	Av. Dev.	RMS Dev.
Extra-ordinary	1.10	2.8453	2.84373	0.00157	7.0	8.4
	1.20	2.7906	2.79307	-0.00247	[ $10^{-4}$ ]	
	1.30	2.7595	2.76086	-0.00136		
	1.40	2.7385	2.73873	-0.00023		
	1.60	2.7116	2.71062	0.00098		
	1.80	2.6949	2.69378	0.00112		
	2.00	2.6838	2.68271	0.00109		
	2.20	2.6758	2.67498	0.00082		
	2.40	2.6702	2.66931	0.00089	No expt.	
	2.60	2.6658	2.66499	0.00081	accuracy	
	2.80	2.6623	2.66161	0.00069		
	3.00	2.6592	2.65888	0.00032		
	3.20	2.6570	2.65663	0.00037		
	3.40	2.6551	2.65475	0.00035		
	3.60	2.6533	2.65313	0.00017		
	3.80	2.6516	2.65173	-0.00013		
	4.00	2.6504	2.65048	-0.00008		
	4.50	2.6475	2.64787	-0.00037		
	5.00	2.6451	2.64572	-0.00062		
	5.50	2.6431	2.64383	-0.00073		
	6.00	2.6414	2.64208	-0.00068		
	6.50	2.6398	2.64039	-0.00059		
	7.00	2.6379	2.63871	-0.00081		
	7.50	2.6361	2.63700	-0.00090		
	8.00	2.6343	2.63525	-0.00095		
	8.50	2.6327	2.63341	-0.00071		
	9.00	2.6310	2.63149	-0.00049		
	9.50	2.6290	2.62946	-0.00046		
	10.00	2.6274	2.62730	0.00010		
	10.50	2.6254	2.62501	0.00039		
	11.00	2.6229	2.62257	0.00033		
	11.50	2.6204	2.61995	0.00045		
	12.00	2.6183	2.61716	0.00114		

**Table 2.11: The Experimental [27] and Computed Refractive Index Values of AlAs at 27°C**

Wavelength ( $\mu\text{m}$ )	Observed [27]	Computed (This work)	Difference	Av. Dev.	RMS Dev.
0.55906	3.201	3.200794	0.000206	5.91	7.64
0.56699	3.189	3.188622	0.000378	[ $10^{-4}$ ]	
0.60400	3.139	3.140075	-0.001075		
0.64116	3.102	3.101942	0.000058		
0.67723	3.072	3.072249	-0.000249	No expt.	
0.71223	3.049	3.048574	0.000426	accuracy	
0.74699	3.029	3.028923	0.000077		
0.78332	3.012	3.011593	0.000407		
0.78830	3.009	3.009434	-0.000434		
0.80000	3.005	3.004545	0.000455		
0.81740	2.999	2.997719	0.001281		
0.82337	2.995	2.995491	-0.000491		
0.85694	2.983	2.983935	-0.000935		
0.90248	2.970	2.970526	-0.000526		
0.94512	2.960	2.959872	0.000128		
0.98726	2.951	2.950801	0.000199		
1.0	2.948	2.948302	-0.000302		
1.04027	2.942	2.941046	0.000954		
1.20039	2.919	2.919451	-0.000451		
1.6	2.892	2.891467	0.000533		
2.0	2.876	2.878039	-0.002039		
2.19858	2.875	2.873604	0.001396		

**Table 2.12: The Experimental [31] and Computed Refractive Index Values of AlPO<sub>4</sub> Crystal at 25°C**

Polarization	Wavelength ( $\mu\text{m}$ )	Observed	Computed	Difference	Av. RMS	
		[31]	(This work)		Dev.	Dev.
Ordinary	0.40	1.5369	1.53689	0.00001	0.8	1.0
	0.50	1.5287	1.52876	-0.00006	$[10^{-5}]$	
	0.60	1.5243	1.52425	0.00005		
	0.70	1.5215	1.52136	0.00014	No expt.	
	0.80	1.5192	1.51927	-0.00007	accuracy	
	1.00	1.5161	1.51619	-0.00009		
	1.20	1.5136	1.51367	-0.00007		
	1.40	1.5112	1.51127	-0.00007		
	1.60	1.5088	1.50879	0.00001		
	1.80	1.5062	1.50614	0.00006		
	2.00	1.5034	1.50326	0.00014		
	2.20	1.5001	1.50013	-0.00003		
	2.40	1.4969	1.49672	0.00018		
	2.60	1.4928	1.49301	-0.00021		
Extra-ordinary	0.40	1.5465	1.54661	-0.00011	1.5	1.9
	0.50	1.5385	1.53815	0.00035	$[10^{-4}]$	
	0.60	1.5334	1.53341	-0.00001		
	0.70	1.5301	1.53034	-0.00024		
	0.80	1.5281	1.52813	-0.00003		
	1.00	1.5245	1.52488	-0.00038		
	1.20	1.5223	1.52225	0.00005		
	1.40	1.5198	1.51975	0.00005		
	1.60	1.5174	1.51717	0.00023		
	1.80	1.5145	1.51443	0.00007		
	2.00	1.5116	1.51146	0.00014		
	2.20	1.5083	1.50823	0.00007		
	2.40	1.5048	1.50471	0.00009		
	2.60	1.5006	1.50089	-0.00029		

**Table 2.13:** The Experimental [36] and Computed Refractive Index Values of BNN Crystal at 25°C

Polarization	Wavelength (μm)	Observed [36]	Computed (This work)	Difference	Avg. Dev.	RMS Dev.
<i>x</i> -axis	0.4579	2.4284	2.42842	-0.00002	2.5	3.2
	0.4765	2.4094	2.40937	0.00003	[10 <sup>-5</sup> ]	
	0.4880	2.3991	2.39904	0.00006	Expt.	
	0.4965	2.3920	2.39202	-0.00002	accuracy	
	0.5017	2.3879	2.38795	-0.00005	was not	
	0.5145	2.3786	2.37862	-0.00002	mentioned	
	0.5321	2.3672	2.36717	0.00003		
	0.6328	2.3222	2.32220	0.00000		
	1.0642	2.2580	2.25800	0.00000		
<i>y</i> -axis	0.4579	2.4266	2.42663	-0.00003	4.8	7.5
	0.4765	2.4076	2.40760	0.00000	[10 <sup>-5</sup> ]	
	0.4880	2.3974	2.39729	0.00011		
	0.4965	2.3903	2.39027	0.00003		
	0.5017	2.3862	2.38621	-0.00001		
	0.5145	2.3767	2.37688	-0.00018		
	0.5321	2.3655	2.36544	0.00006		
	0.6328	2.3205	2.32049	0.00001		
	1.0642	2.2567	2.25670	0.00000		
<i>z</i> -axis	0.4579	2.2931	2.29310	0.00000	1.0	1.3
	0.4765	2.2799	2.27991	-0.00001	[10 <sup>-5</sup> ]	
	0.4880	2.2727	2.27270	0.00000		
	0.4965	2.2678	2.26777	0.00003		
	0.5017	2.2649	2.26491	-0.00001		
	0.5145	2.2583	2.25832	-0.00002		
	0.5321	2.2502	2.25018	0.00002		
	0.6328	2.2177	2.21770	0.00000		
	1.0642	2.1700	2.17000	0.00000		

**Table 2.14: The Experimental [37] and Computed Refractive Index Values of BaTiO<sub>3</sub> Crystal at 25°C**

Polarization	Wavelength (μm)	Observed [37]	Computed (This work)	Difference	Avg. Dev.	RMS Dev.
Ordinary	0.422	2.645	2.643498	0.001502	3.52	5.41
	0.450	2.578	2.578837	-0.000837	[10 <sup>-3</sup> ]	
	0.475	2.534	2.536727	-0.002727		
	0.496	2.510	2.509058	0.000942		
	0.500	2.500	2.504256	-0.004256		
	0.525	2.478	2.478527	-0.000527	Expt. accuracy	
	0.550	2.459	2.457691	0.001309	± [0.002 ~	
	0.575	2.442	2.440514	0.001486	0.0045]	
	0.600	2.430	2.426138	0.003862		
	0.620	2.420	2.416283	0.003717		
	0.625	2.416	2.413951	0.002049		
	0.650	2.405	2.403506	0.001494		
	0.675	2.396	2.394465	0.001535		
	0.690	2.390	2.389605	0.000395		
	0.750	2.372	2.373475	-0.001475		
	0.800	2.361	2.363069	-0.002069		
	0.850	2.352	2.354612	-0.002612		
	0.900	2.344	2.347604	-0.003604		
	1.000	2.332	2.336640	-0.004640		
	1.200	2.317	2.321872	-0.004872		
	1.400	2.308	2.311890	-0.003890		
	1.653	2.310	2.302263	0.007737		
	1.900	2.297	2.294231	0.002769		
	2.480	2.300	2.276316	0.023684		
	2.500	2.270	2.275682	-0.005682		
	3.030	2.250	2.257824	-0.007824		
	3.570	2.230	2.236975	-0.006975		
	4.000	2.220	2.218071	0.001929		
	5.000	2.160	2.165053	-0.005053		
	5.560	2.130	2.129173	0.000827		
	6.250	2.080	2.078039	0.001961		
	7.140	2.000	1.999222	0.000778		

**Table 2.14: (Continued)**

Polarization	Wavelength ( $\mu\text{m}$ )	Observed [37]	Computed (This work)	Difference	Av. Dev.	RMS Dev.
Extra-ordinary	0.422	2.541	2.536249	0.004751	5.55	7.54
	0.450	2.492	2.493584	-0.001584	[ $10^{-3}$ ]	
	0.475	2.461	2.463431	-0.002431		
	0.500	2.436	2.438765	-0.002765		
	0.525	2.416	2.418275	-0.002275		
	0.550	2.400	2.401032	-0.001032		
	0.575	2.385	2.386356	-0.001356		
	0.600	2.372	2.373741	-0.001741		
	0.625	2.362	2.362802	-0.000802	Note:	
	0.650	2.352	2.353241	-0.001241	The experimental	
	0.675	2.344	2.344826	-0.000826	values are from	
	0.690	2.340	2.340249	-0.000249	melt-grown and	
	0.750	2.327	2.324779	0.002221	from flux-grown	
	0.800	2.317	2.314574	0.002426	samples. The expt.	
	0.850	2.309	2.306150	0.002850	accuracy and the	
	0.900	2.302	2.299085	0.002915	measured ambient	
	1.000	2.292	2.287889	0.004111	temperature are	
	1.200	2.279	2.272601	0.006399	different at	
	1.400	2.271	2.262226	0.008774	different labora-	
	1.600	2.266	2.254201	0.011799	tories; and also	
	1.900	2.262	2.244138	0.017862	differ from	
	2.500	2.210	2.225687	-0.015687	sample to sample.	
	3.030	2.190	2.208227	-0.018227		
	3.570	2.180	2.187993	-0.007993		
	4.000	2.160	2.169710	-0.009710		
	5.000	2.110	2.118566	-0.008566		
	5.560	2.080	2.084005	-0.004005		
	6.250	2.040	2.034793	0.005207		
	7.140	1.970	1.959004	0.010996		

**Table 2.15:** The Experimental [45] and Computed Refractive Index Values of CaCO<sub>3</sub> Crystal at 25°C

Polarization	Wavelength (μm)	Observed [45]	Computed (This work)	Difference	Av. Dev.	RMS Dev.
Ordinary	0.200	1.90284	1.901014	0.001826	3.26	4.56
	0.204	1.88242	1.883133	-0.000713	[10 <sup>-4</sup> ]	
	0.208	1.86733	1.867286	0.000044		
	0.211	1.85692	1.856540	0.000380		
	0.214	1.84558	1.846643	-0.001063	The experimental	
	0.219	1.83075	1.831786	-0.001036	values are	
	0.226	1.81309	1.813850	-0.000760	obtained from	
	0.231	1.80233	1.802717	-0.000387	different sources	
	0.242	1.78111	1.782069	-0.000959	and for different	
	0.257	1.76038	1.760237	0.000143	wavelength	
	0.263	1.75343	1.753027	0.000403	regions. The expt.	
	0.267	1.74864	1.748610	0.000030	accuracy and the	
	0.274	1.74139	1.741538	-0.000148	ambient	
	0.291	1.72774	1.727204	0.000536	temperature are	
	0.303	1.71959	1.718975	0.000615	different for	
	0.312	1.71425	1.713603	0.000647	different sources.	
	0.330	1.70515	1.704488	0.000662	Therefore, the	
	0.340	1.70078	1.700187	0.000593	present fitting	
	0.346	1.69833	1.697824	0.000506	accuracy is	
	0.361	1.69316	1.692529	0.000631	sufficient.	
	0.394	1.68374	1.683279	0.000461		
	0.410	1.68014	1.679691	0.000449		
	0.434	1.67552	1.675121	0.000399		
	0.441	1.67423	1.673942	0.000288		
	0.508	1.66527	1.665167	0.000103		
	0.533	1.66277	1.662744	0.000026		
	0.560	1.66046	1.660487	-0.000027		
	0.589	1.65835	1.658394	-0.000044		
	0.643	1.65504	1.655193	-0.000153		
	0.656	1.65437	1.654528	-0.000158		

**Table 2.15:** (*Continued*)

Polarization	Wavelength ( $\mu\text{m}$ )	Observed [45]	Computed (This work)	Difference	Avg. Dev.	RMS Dev.
Ordinary	0.670	1.65367	1.653850	-0.000180		
	0.700	1.65207	1.652515	-0.000445	3.26	4.56
	0.768	1.64974	1.649954	-0.000214		$[10^{-4}]$
	0.795	1.64886	1.649075	-0.000215		
	0.801	1.64869	1.648889	-0.000199		
	0.833	1.64772	1.647940	-0.000220		
	0.867	1.64676	1.647007	-0.000247		
	0.905	1.64578	1.646039	-0.000259		
	0.946	1.64480	1.645067	-0.000267		
	0.991	1.64380	1.644068	-0.000268		
	1.042	1.64276	1.643003	-0.000243		
	1.097	1.64167	1.641913	-0.000243		
	1.159	1.64051	1.640736	-0.000226		
	1.229	1.63926	1.639450	-0.000190		
	1.273	1.63849	1.638656	-0.000166		
	1.307	1.63789	1.638047	-0.000157		
	1.320	1.63767	1.637814	-0.000144		
	1.369	1.63681	1.636939	-0.000129		
	1.396	1.63637	1.636456	-0.000086		
	1.422	1.63590	1.635990	-0.000090		
	1.479	1.63490	1.634963	-0.000063		
	1.497	1.63457	1.634636	-0.000066		
	1.541	1.63381	1.633832	-0.000022		
	1.609	1.63261	1.632571	0.000039		
	1.682	1.63127	1.631186	0.000084		
	1.761	1.62974	1.629645	0.000095		
	1.849	1.62800	1.627869	0.000131		
	1.946	1.62602	1.625833	0.000187		
	2.053	1.62372	1.623481	0.000239		
	2.172	1.62099	1.620724	0.000266		

**Table 2.15: (Continued)**

Polarization	Wavelength ( $\mu\text{m}$ )	Observed [45]	Computed (This work)	Difference	Av. Dev.	RMS Dev.
Extra-ordinary	0.198	1.57796	1.578409	-0.000449	2.83	3.94
	0.200	1.57649	1.575748	0.000742	[ $10^{-4}$ ]	
	0.204	1.57081	1.570755	0.000055		
	0.208	1.56640	1.566160	0.000240		
	0.211	1.56327	1.562948	0.000322		
	0.214	1.55976	1.559920	-0.000160		
	0.219	1.55496	1.555241	-0.000281		
	0.226	1.54921	1.549371	-0.000161		
	0.231	1.54541	1.545599	-0.000189		
	0.242	1.53782	1.538328	-0.000508		
	0.257	1.53005	1.530226	-0.000176		
	0.263	1.52736	1.527452	-0.000092		
	0.267	1.52547	1.525727	-0.000257		
	0.274	1.52261	1.522925	-0.000315		
	0.291	1.51705	1.517088	-0.000038		
	0.303	1.51365	1.513640	0.000010		
	0.312	1.51140	1.511349	0.000051		
	0.330	1.50746	1.507389	0.000071		
	0.340	1.50562	1.505489	0.000131		
	0.346	1.50450	1.504436	0.000064		
	0.361	1.50224	1.502055	0.000185		
	0.394	1.49810	1.497824	0.000276		
	0.410	1.49640	1.496159	0.000241		
	0.434	1.49430	1.494022	0.000278		
	0.441	1.49373	1.493468	0.000262		
	0.508	1.48956	1.489323	0.000237		
	0.533	1.48841	1.488177	0.000233		
	0.560	1.48736	1.487113	0.000247		
	0.589	1.48640	1.486133	0.000267		
	0.643	1.48490	1.484654	0.000246		
	0.656	1.48459	1.484351	0.000239		

**Table 2.15: (*Continued*)**

Polarization	Wavelength ( $\mu\text{m}$ )	Observed [45]	Computed (This work)	Difference	Av. Dev.	RMS Dev.
Extra-ordinary	0.670	1.48426	1.484045	0.000215		
	0.700	1.48353	1.483449	0.000081		
	0.768	1.48259	1.482344	0.000246	2.83	3.94
	0.795	1.48216	1.481979	0.000181	[ $10^{-4}$ ]	
	0.801	1.48216	1.481903	0.000257		
	0.833	1.48176	1.481522	0.000238		
	0.867	1.48137	1.481161	0.000209		
	0.905	1.48098	1.480800	0.000180		
	0.946	1.48060	1.480454	0.000146		
	0.991	1.48022	1.480118	0.000102		
	1.042	1.47985	1.479781	0.000069		
	1.097	1.47948	1.479460	0.000020		
	1.159	1.47910	1.479142	-0.000042		
	1.229	1.47870	1.478825	-0.000125		
	1.307	1.47831	1.478513	-0.000203		
	1.396	1.47789	1.478196	-0.000306		
	1.497	1.47744	1.477873	-0.000433		
	1.615	1.47695	1.477531	-0.000581		
	1.749	1.47638	1.477171	-0.000791		
	1.909	1.47573	1.476763	-0.001033		
	2.100	1.47492	1.476288	-0.001368		
	3.324	1.47392	1.472755	0.001165		

**Table 2.16:** The Experimental [48] and Computed Refractive Index Values of CaF<sub>2</sub> Crystal at 21.7°C

Wavelength ( $\mu\text{m}$ )	Observed [48]	Computed (This work)	Difference	Av. Dev.	RMS Dev.
0.25	1.46728	1.467291	-0.000011	1.8	2.4
0.30	1.45401	1.453993	0.000017	[10 <sup>-5</sup> ]	
0.35	1.44652	1.446506	0.000014		
0.40	1.44184	1.441831	0.000009		
0.45	1.43870	1.438694	0.000006		
0.50	1.43647	1.436472	-0.000002	No expt.	
0.55	1.43483	1.434831	-0.000001	accuracy	
0.60	1.43357	1.433576	-0.000006		
0.65	1.43257	1.432585	-0.000015		
0.70	1.43177	1.431784	-0.000014		
0.75	1.43111	1.431120	-0.000010		
0.80	1.43054	1.430558	-0.000018		
0.85	1.43006	1.430073	-0.000013		
0.90	1.42963	1.429646	-0.000016		
0.95	1.42925	1.429265	-0.000015		
1.00	1.42890	1.428919	-0.000019		
1.50	1.42628	1.426299	-0.000019		
2.00	1.42388	1.423892	-0.000012		
2.50	1.42112	1.421131	-0.000011		
3.00	1.41787	1.417870	0.000000		
3.50	1.41406	1.414050	0.000010		
4.00	1.40966	1.409638	0.000022		
4.50	1.40464	1.404608	0.000032		
5.00	1.39897	1.398938	0.000032		
5.50	1.39264	1.392601	0.000039		
6.00	1.38561	1.385573	0.000037		
6.50	1.37786	1.377823	0.000037		
7.00	1.36934	1.369318	0.000022		
7.50	1.36003	1.360023	0.000007		
8.00	1.34987	1.349895	-0.000025		
8.50	1.33881	1.338889	-0.000079		

**Table 2.17: The Experimental [31] and Computed Refractive Index Values of CaMoO<sub>4</sub> Crystal at 25°C**

Polari-zation	Wavelength ( $\mu\text{m}$ )	Observed [31]	Computed (This work)	Difference	Av. Dev.	RMS Dev.
Ordinary	0.45	1.9497	1.949503	0.000197	1.5	2.1
	0.50	1.9351	1.935467	-0.000367	$[ 10^{-4} ]$	
	0.60	1.9181	1.918298	-0.000198		
	0.70	1.9089	1.908408	0.000492		
	0.80	1.9023	1.902064	0.000236		
	0.90	1.8977	1.897657	0.000043		
	1.0	1.8944	1.894393	0.000007		
	1.2	1.8892	1.889747	-0.000547		
	1.4	1.8863	1.886377	-0.000077		
	1.6	1.8835	1.883579	-0.000079	No expt. accuracy	
	1.8	1.8811	1.881023	0.000077		
	2.0	1.8787	1.878536	0.000164		
	2.2	1.8760	1.876019	-0.000019		
	2.4	1.8733	1.873410	-0.000110		
	2.6	1.8706	1.870669	-0.000069		
	2.8	1.8679	1.867767	0.000133		
	3.0	1.8648	1.864680	0.000120		
	3.2	1.8615	1.861392	0.000108		
	3.4	1.8579	1.857885	0.000015		
	3.6	1.8542	1.854147	0.000053		
	3.8	1.8502	1.850162	0.000038		
	4.0	1.8457	1.845917	-0.000217		
Extra-ordinary	0.45	2.0448	2.044808	-0.000008		
	0.50	2.0239	2.023690	0.000210		
	0.60	1.9983	1.998710	-0.000410		
	0.70	1.9843	1.984747	-0.000447		
	0.80	1.9761	1.975966	0.000134		
	0.90	1.9705	1.969961	0.000539		
	1.0	1.9658	1.965576	0.000224		
	1.1	1.9625	1.962194	0.000306		
	1.2	1.9588	1.959459	-0.000659		
	1.4	1.9563	1.955143	0.001157		
	1.6	1.9518	1.951651	0.000149		
	1.8	1.9483	1.948532	-0.000232		
	2.0	1.9457	1.945548	0.000152		
	2.2	1.9420	1.942567	-0.000567		
	2.4	1.9390	1.939504	-0.000504		
	2.6	1.9360	1.936307	-0.000307		
	2.8	1.9327	1.932937	-0.000237		
	3.0	1.9294	1.929364	0.000036		
	3.2	1.9255	1.925566	-0.000066		

**Table 2.17: (*Continued*)**

Polarization	Wavelength ( $\mu\text{m}$ )	Observed [31]	Computed (This work)	Difference	Av. Dev.	RMS Dev.
	3.4	1.9215	1.921523	-0.000023		
	3.6	1.9174	1.917217	0.000183		
	3.8	1.9130	1.912631	0.000369		

**Table 2.18: The Experimental and Computed Refractive Index Values of  $\text{CaWO}_4$  Crystal at 25°C**

Polarization	Wavelength ( $\mu\text{m}$ )	Observed [31]	Computed (This work)	Difference	Av. Dev.	RMS Dev.
Ordinary	0.45	1.9497	1.949503	0.000197	1.5	2.1
	0.50	1.9351	1.935467	-0.000367	[ $10^{-4}$ ]	
	0.60	1.9181	1.918298	-0.000198		
	0.70	1.9089	1.908408	0.000492		
	0.80	1.9023	1.902064	0.000236	No expt. accuracy	
	0.90	1.8977	1.897657	0.000043		
	1.0	1.8944	1.894393	0.000007		
	1.2	1.8892	1.889747	-0.000547		
	1.4	1.8863	1.886377	-0.000077		
	1.6	1.8835	1.883579	-0.000079		
	1.8	1.8811	1.881023	0.000077		
	2.0	1.8787	1.878536	0.000164		
	2.2	1.8760	1.876019	-0.000019		
	2.4	1.8733	1.873410	-0.000110		
	2.6	1.8706	1.870669	-0.000069		
	2.8	1.8679	1.867767	0.000133		
	3.0	1.8648	1.864680	0.000120		
	3.2	1.8615	1.861392	0.000108		
	3.4	1.8579	1.857885	0.000015		
	3.6	1.8542	1.854147	0.000053		
	3.8	1.8502	1.850162	0.000038		
	4.0	1.8457	1.845917	-0.000217		
Extra- ordinary	0.45	1.9684	1.967650	0.000750	5.0	8.9
	0.50	1.9523	1.953566	-0.001260	[ $10^{-4}$ ]	
	0.60	1.9343	1.935595	-0.001234		
	0.7	1.9283	1.924869	0.003431		
	0.8	1.9173	1.917856	-0.000556		
	0.9	1.9123	1.912937	-0.000637		
	1.0	1.9089	1.909282	-0.000382		

**Table 2.18: (Continued)**

Polarization	Wavelength ( $\mu\text{m}$ )	Observed [31]	Computed (This work)	Difference	Av. Dev.	RMS Dev.
	1.2	1.9040	1.904099	-0.000099		
	1.4	1.9004	1.900393	0.000007		
	1.6	1.8975	1.897374	0.000126		
	1.8	1.8948	1.894669	0.000131		
	2.0	1.8924	1.892079	0.000321		
	2.2	1.8896	1.889489	0.000111		
	2.4	1.8862	1.886830	-0.000630		
	2.6	1.8834	1.884055	-0.000655		
	2.8	1.8813	1.881130	0.000170		
	3.0	1.8783	1.878031	0.000269		
	3.2	1.8749	1.874737	0.000163		
	3.4	1.8713	1.871232	0.000068		
	3.6	1.8675	1.867501	-0.000001		
	3.8	1.8635	1.863528	-0.000028		
	4.0	1.8593	1.859300	0.000000		

**Table 2.19: The Experimental [49] and Computed Refractive Index Values of  $\text{CaWO}_4$  Crystal at 20°C**

Polarization	Wavelength ( $\mu\text{m}$ )	Observed [49]	Computed (This work)	Difference	Av. Dev.	RMS Dev.
Ordinary	0.4678	1.9421	1.942008	0.000092	1.6	1.9
	0.5086	1.9315	1.931822	-0.000322	[10 <sup>-4</sup> ]	
	0.5461	1.9249	1.924702	0.000198	Expt.	
	0.5896	1.9184	1.918284	0.000116	accuracy is	
	0.6438	1.9122	1.912193	0.000007	± 0.0002 ~	
	0.8521	1.8986	1.898882	-0.000282	± 0.0004	
	1.0140	1.8937	1.893480	0.000220		
	1.4695	1.8850	1.885028	-0.000028		
Extra- ordinary	0.4678	1.9602	1.960114	0.000086	1.7	2.2
	0.4800	1.9564	1.956490	-0.000090	[10 <sup>-4</sup> ]	
	0.5086	1.9490	1.949169	-0.000169		
	0.5461	1.9417	1.941507	0.000193	Expt.	
	0.5896	1.9347	1.934592	0.000108	accuracy is	
	0.6438	1.9280	1.928023	-0.000023	± 0.0002 ~	
	0.8521	1.9132	1.913645	-0.000445	± 0.0004	
	1.0140	1.9082	1.907802	0.000398		
	1.4695	1.8986	1.898658	-0.000058		

**Table 2.20: The Experimental [9] and Computed Refractive Index Values of CDA Crystal at 33°C**

Polari-zation	Wavelength ( $\mu\text{m}$ )	Observed [9]	Computed (This work)	Difference	Av. RMS
					Dev. Dev.
Ordinary	0.404656	1.59003	1.589990	0.000040	3.4    4.0
	0.435833	1.58440	1.584431	-0.000031	[ $10^{-5}$ ]
	0.467815	1.57987	1.579906	-0.000036	
	0.479991	1.57837	1.578423	-0.000053	
	0.508582	1.57535	1.575350	0.000000	Expt.
	0.546074	1.57206	1.572010	0.000050	accuracy
	0.589300	1.56894	1.568869	0.000071	$\pm 0.00003$
	0.643847	1.56568	1.565666	0.000014	
	0.780027	1.55981	1.559821	-0.000011	
	0.794760	1.55931	1.559302	0.000008	
	0.852113	1.55735	1.557414	-0.000064	
	0.894346	1.55610	1.556127	-0.000027	
	1.064000	1.55148	1.551442	0.000038	
Extra-ordinary	0.404656	1.56669	1.566666	0.000024	3.2    3.7
	0.435833	1.56159	1.561596	-0.000006	[ $10^{-5}$ ]
	0.467815	1.55744	1.557488	-0.000048	
	0.479991	1.55612	1.556149	-0.000029	
	0.508582	1.55338	1.553394	-0.000014	
	0.546074	1.55052	1.550440	0.000080	Expt.
	0.589300	1.54776	1.547722	0.000038	accuracy
	0.643847	1.54502	1.545043	-0.000023	$\pm 0.00003$
	0.780027	1.54060	1.540559	0.000041	
	0.794760	1.54016	1.540196	-0.000036	
	0.852113	1.53892	1.538936	-0.000016	
	0.894346	1.53810	1.538134	-0.000034	
	1.064000	1.53564	1.535616	0.000024	

**Table 2.21: The Experimental [9] and Computed Refractive Index Values of CD\*A Crystal at 33°C**

Polarization	Wavelength (μm)	Observed [9]	Computed (This work)	Difference	Av. Dev.	RMS Dev.
Ordinary	0.404656	1.58529	1.585289	0.000001	3.2	4.2
	0.435833	1.57990	1.579925	-0.000025	[10 <sup>-5</sup> ]	
	0.467815	1.57562	1.575579	0.000041		
	0.479991	1.57419	1.574161	0.000029		
	0.508582	1.57122	1.571233	-0.000013	Expt.	
	0.546074	1.56801	1.568071	-0.000061	accuracy	
	0.589300	1.56512	1.565127	-0.000007	±0.00003	
	0.643847	1.56218	1.562162	0.000018		
	0.780027	1.55701	1.556910	0.000100		
	0.794760	1.55646	1.556457	0.000003		
	0.852113	1.55476	1.554831	-0.000071		
	0.894346	1.55371	1.553744	-0.000034		
	1.064000	1.54995	1.549932	0.000018		
Extra-ordinary	0.404656	1.56464	1.564622	0.000018	2.0	2.4
	0.435833	1.55954	1.559583	-0.000043	[10 <sup>-5</sup> ]	
	0.467815	1.55553	1.555518	0.000012		
	0.479991	1.55421	1.554196	0.000014		
	0.508582	1.55148	1.551481	-0.000001	Expt.	
	0.546074	1.54856	1.548577	-0.000017	accuracy	
	0.589300	1.54593	1.545914	0.000016	±0.00003	
	0.643847	1.54330	1.543293	0.000007		
	0.780027	1.53896	1.538921	0.000039		
	0.794760	1.53854	1.538568	-0.000028		
	0.852113	1.53735	1.537342	0.000008		
	0.894346	1.53652	1.536562	-0.000042		
	1.064000	1.53413	1.534115	0.000015		

**Table 2.22:** The Experimental [25] and Computed Refractive Index Values of CuAlSe<sub>2</sub> Crystal at 25°C

Polarization	Wavelength Observed ( $\mu\text{m}$ )	Computed (This work)	Difference	Av. Dev.	RMS Dev.
Ordinary	0.50	2.7797	2.77881	0.00089	5.2
	0.55	2.7038	2.70509	-0.00129	[ $10^{-4}$ ]
	0.60	2.6560	2.65674	-0.00074	
	0.65	2.6230	2.62289	0.00011	
	0.70	2.5973	2.59806	-0.00076	
	0.75	2.5789	2.57921	-0.00031	
	0.80	2.5650	2.56450	0.00050	
	0.85	2.5536	2.55276	0.00084	Expt.
	0.90	2.5437	2.54323	0.00047	accuracy
	0.95	2.5364	2.53535	0.00105	was not
	1.00	2.5293	2.52877	0.00053	mentioned
	1.10	2.5189	2.51844	0.00046	
	1.20	2.5113	2.51077	0.00053	
	1.30	2.5053	2.50490	0.00040	
	1.40	2.5007	2.50028	0.00042	
	1.50	2.4969	2.49658	0.00032	
	1.60	2.4938	2.49355	0.00025	
	1.70	2.4913	2.49102	0.00028	
	1.80	2.4892	2.48889	0.00031	
	1.90	2.4872	2.48707	0.00013	
	2.00	2.4851	2.48549	-0.00039	
	2.10	2.4832	2.48411	-0.00091	
	2.20	2.4820	2.48288	-0.00088	
	2.30	2.4807	2.48178	-0.00108	
	2.40	2.4802	2.48079	-0.00059	
	2.50	2.4795	2.47988	-0.00038	
	2.60	2.4786	2.47905	-0.00045	
	2.80	2.4771	2.47755	-0.00045	
	3.00	2.4759	2.47622	-0.00032	
	3.50	2.4733	2.47333	-0.00003	
	4.00	2.4712	2.47074	0.00046	
	4.50	2.4685	2.46819	0.00031	
	5.00	2.4659	2.46556	0.00034	

**Table 2.22: (Continued)**

Polarization	Wavelength Observed ( $\mu\text{m}$ )	Computed (This work)	Difference	Av. Dev.	RMS Dev.
Extra-ordinary	0.50	2.7886	2.78671	0.00189	7.5
	0.55	2.7005	2.70363	-0.00313	[ $10^{-4}$ ]
	0.60	2.6489	2.65086	-0.00196	
	0.65	2.6145	2.61469	-0.00019	
	0.70	2.5886	2.58856	0.00004	
	0.75	2.5699	2.56893	0.00097	
	0.80	2.5556	2.55374	0.00186	
	0.85	2.5428	2.54170	0.00110	Expt.
	0.90	2.5327	2.53196	0.00074	accuracy
	0.95	2.5252	2.52396	0.00124	was not
	1.00	2.5179	2.51729	0.00061	mentioned
	1.10	2.5075	2.50687	0.00063	
	1.20	2.4997	2.49916	0.00054	
	1.30	2.4937	2.49327	0.00043	
	1.40	2.4889	2.48864	0.00026	
	1.50	2.4852	2.48493	0.00027	
	1.60	2.4821	2.48190	0.00020	
	1.70	2.4794	2.47937	0.00003	
	1.80	2.4773	2.47724	0.00006	
	1.90	2.4753	2.47540	-0.00010	
	2.00	2.4734	2.47381	-0.00041	
	2.10	2.4714	2.47241	-0.00101	
	2.20	2.4700	2.47116	-0.00116	
	2.30	2.4689	2.47005	-0.00115	
	2.40	2.4683	2.46903	-0.00073	
	2.50	2.4676	2.46810	-0.00050	
	2.60	2.4665	2.46723	-0.00073	
	2.80	2.4651	2.46567	-0.00057	
	3.00	2.4638	2.46427	-0.00047	
	3.50	2.4609	2.46118	-0.00028	
	4.00	2.4586	2.45832	0.00028	
	4.50	2.4559	2.45547	0.00043	
	5.00	2.4533	2.45249	0.00081	

**Table 2.23: The Experimental [25] and Computed Refractive Index Values of CuGaSe<sub>2</sub> Crystal at 25°C**

Polari-zation	Wavelength ( $\mu\text{m}$ )	Observed [25]	Computed (This work)	Difference	Av.	RMS
					Dev.	Dev.
Ordinary	0.78	2.9580	2.95509	0.00291	8.0	10
	0.80	2.9365	2.93715	-0.00065	[ $10^{-4}$ ]	
	0.85	2.8984	2.90103	-0.00263		
	0.90	2.8716	2.87383	-0.00223		
	0.95	2.8513	2.85269	-0.00139		
	1.00	2.8358	2.83585	-0.00005	Expt.	
	1.10	2.8115	2.81087	0.00063	accuracy	
	1.20	2.7951	2.79339	0.00171	was not	
	1.30	2.7823	2.78059	0.00171	mentioned	
	1.40	2.7725	2.77089	0.00161		
	1.60	2.7587	2.75731	0.00139		
	1.80	2.7496	2.74839	0.00121		
	2.00	2.7430	2.74216	0.00084		
	2.20	2.7377	2.73760	0.00010		
	2.40	2.7344	2.73414	0.00026		
	2.60	2.7315	2.73143	0.00007		
	2.80	2.7293	2.72924	0.00006		
	3.00	2.7273	2.72742	-0.00012		
	3.20	2.7256	2.72589	-0.00029		
	3.40	2.7242	2.72457	-0.00037		
	4.00	2.7211	2.72141	-0.00031		
	4.50	2.7188	2.71932	-0.00052		
	5.00	2.7170	2.71747	-0.00047		
	5.50	2.7152	2.71573	-0.00053		
	6.00	2.7133	2.71403	-0.00073		
	6.50	2.7116	2.71231	-0.00071		
	7.00	2.7101	2.71054	-0.00044		
	7.50	2.7082	2.70870	-0.00050		
	8.00	2.7060	2.70676	-0.00076		
	8.50	2.7042	2.70470	-0.00050		
	9.00	2.7021	2.70250	-0.00040		
	10.00	2.6974	2.69767	-0.00027		
	11.00	2.6926	2.69213	0.00047		
	12.00	2.6872	2.68576	0.00144		

**Table 2.23: (*Continued*)**

Polarization	Wavelength ( $\mu\text{m}$ )	Observed [25]	Computed (This work)	Difference	Av. Dev.	RMS Dev.
Extra-ordinary	0.78	3.0093	3.00259	0.00671	18	26
	0.80	2.9759	2.97762	-0.00172	[ $10^{-4}$ ]	
	0.85	2.9197	2.92967	-0.00997		
	0.90	2.8925	2.89547	-0.00297		
	0.95	2.8690	2.86994	-0.00094		
	1.00	2.8513	2.85023	0.00107		
	1.10	2.8245	2.82196	0.00254		
	1.20	2.8066	2.80283	0.00377		
	1.30	2.7928	2.78914	0.00366	Expt.	
	1.40	2.7825	2.77894	0.00356	accuracy	
	1.60	2.7677	2.76490	0.00280	was not	
	1.80	2.7579	2.75583	0.00207	mentioned	
	2.20	2.7456	2.74499	0.00061		
	2.40	2.7419	2.74154	0.00036		
	2.60	2.7388	2.73882	-0.00002		
	2.80	2.7363	2.73663	-0.00033		
	3.00	2.7344	2.73481	-0.00041		
	3.20	2.7328	2.73326	-0.00046		
	3.40	2.7311	2.73192	-0.00082		
	3.60	2.7300	2.73073	-0.00073		
	4.50	2.7252	2.72647	-0.00127		
	5.00	2.7232	2.72448	-0.00128		
	5.50	2.7212	2.72258	-0.00138		
	6.00	2.7192	2.72069	-0.00149		
	6.50	2.7174	2.71876	-0.00136		
	7.00	2.7158	2.71675	-0.00095		
	7.50	2.7136	2.71464	-0.00104		
	8.00	2.7111	2.71241	-0.00131		
	8.50	2.7089	2.71003	-0.00113		
	9.00	2.7065	2.70750	-0.00100		
	10.00	2.7014	2.70189	-0.00049		
	11.00	2.6981	2.69544	0.00266		
	12.00	2.6898	2.68800	0.00180		

**Table 2.24:** The Experimental [24] and Computed Refractive Index Values of CuInS<sub>2</sub> Crystal at 25°C

Polarization	Wavelength (μm)	Observed [24]	Computed (This work)	Difference	Av. Dev.	RMS Dev.
Ordinary	0.90	2.7907	2.78798	0.00272	7.5	9.3
	0.92	2.7718	2.77176	0.00004	[10 <sup>-4</sup> ]	
	0.94	2.7567	2.75757	-0.00087		
	0.96	2.7437	2.74505	-0.00135		
	0.98	2.7324	2.73394	-0.00154		
	1.00	2.7225	2.72401	-0.00151	Expt.	
	1.10	2.6861	2.68701	-0.00091	accuracy	
	1.20	2.6638	2.66313	0.00067	was not	
	1.30	2.6478	2.64659	0.00121	mentioned	
	1.40	2.6359	2.63454	0.00136		
	1.50	2.6267	2.62542	0.00128		
	1.60	2.6195	2.61831	0.00119		
	1.80	2.6089	2.60800	0.00090		
	2.00	2.6020	2.60094	0.00106		
	2.20	2.5961	2.59580	0.00030		
	2.40	2.5915	2.59190	-0.00040		
	2.60	2.5886	2.58881	-0.00021		
	2.80	2.5860	2.58629	-0.00029		
	3.00	2.5838	2.58416	-0.00036		
	3.50	2.5802	2.57994	0.00026		
	4.00	2.5760	2.57658	-0.00058		
	4.50	2.5729	2.57362	-0.00072		
	5.00	2.5699	2.57081	-0.00091		
	5.50	2.5673	2.56804	-0.00074		
	6.00	2.5645	2.56521	-0.00071		
	7.00	2.5587	2.55918	-0.00048		
	8.00	2.5522	2.55248	-0.00028		
	9.00	2.5448	2.54496	-0.00016		
	10.00	2.5366	2.53649	0.00011		
	11.00	2.5274	2.52698	0.00042		
	12.00	2.5166	2.51635	0.00025		
	12.50	2.5108	2.51057	0.00023		

**Table 2.24: (Continued)**

Polarization	Wavelength ( $\mu\text{m}$ )	Observed [24]	Computed (This work)	Difference	Av. Dev.	RMS Dev.
Extra-ordinary	0.90	2.7713	2.76883	0.00247	6.9	8.6
	0.92	2.7536	2.75347	0.00013	[ $10^{-4}$ ]	
	0.94	2.7392	2.74002	-0.00082		
	0.96	2.7268	2.72816	-0.00136		
	0.98	2.7162	2.71762	-0.00142		
	1.00	2.7067	2.70820	-0.00150	Expt.	
	1.10	2.6727	2.67307	-0.00037	accuracy	
	1.20	2.6510	2.65037	0.00063	was not	
	1.30	2.6357	2.63462	0.00108	mentioned	
	1.40	2.6243	2.62314	0.00116		
	1.50	2.6156	2.61444	0.00116		
	1.60	2.6087	2.60765	0.00105		
	1.80	2.5985	2.59778	0.00072		
	2.00	2.5918	2.59099	0.00081		
	2.20	2.5860	2.58604	-0.00004		
	2.40	2.5821	2.58225	-0.00015		
	2.60	2.5789	2.57923	-0.00033		
	2.80	2.5765	2.57674	-0.00024		
	3.00	2.5741	2.57463	-0.00053		
	3.50	2.5707	2.57035	0.00035		
	4.00	2.5663	2.56686	-0.00056		
	4.50	2.5630	2.56371	-0.00071		
	5.00	2.5598	2.56067	-0.00087		
	5.50	2.5571	2.55761	-0.00051		
	6.00	2.5539	2.55446	-0.00056		
	7.00	2.5474	2.54768	-0.00028		
	8.00	2.5401	2.54007	0.00003		
	9.00	2.5311	2.53148	-0.00038		
	10.00	2.5225	2.52179	0.00071		
	11.00	2.5112	2.51089	0.00031		
	12.00	2.4987	2.49867	0.00003		

**Table 2.25:** The Experimental [31] and Computed Refractive Index Values of GaP Crystal at 25°C

Wavelength ( $\mu\text{m}$ )	Observed [31]	Computed (This work)	Difference	Av. Dev.	RMS Dev.
0.54	3.4595	3.45907	0.00043	4.2	6.5
0.60	3.3495	3.35043	-0.00093	[ $10^{-4}$ ]	
0.70	3.2442	3.24413	0.00007		
0.80	3.1830	3.18283	0.00017		
0.90	3.1430	3.14378	-0.00078		
1.00	3.1192	3.11717	0.00203	Expt.	
1.10	3.0981	3.09814	-0.00004	accuracy	
1.20	3.0844	3.08400	0.00040	was not	
1.40	3.0646	3.06468	-0.00008	mentioned	
1.60	3.0509	3.05233	-0.00143		
1.80	3.0439	3.04386	0.00004		
2.00	3.0379	3.03775	0.00015		
2.20	3.0331	3.03312	-0.00002		
2.40	3.0296	3.02948	0.00012		
2.60	3.0271	3.02653	0.00057		
2.80	3.0236	3.02404	-0.00044		
3.00	3.0215	3.02190	-0.00040		
3.20	3.0197	3.02000	-0.00030		
3.40	3.0181	3.01828	-0.00018		
3.60	3.0166	3.01668	-0.00008		
3.80	3.0159	3.01518	0.00072		
4.00	3.0137	3.01373	-0.00003		

**Table 2.26:** The Experimental [68] and Computed Refractive Index Values of  $\alpha$ -HIO<sub>3</sub> Crystal at 20°C

Polarization	Wavelength ( $\mu\text{m}$ )	Observed [68]	Computed (This work)	Difference	Av. Dev.	RMS Dev.
<i>x</i> -axis	0.35	1.9612	1.96175	-0.00055	5.5	6.8
	0.36	1.9474	1.94763	-0.00023	[ $10^{-4}$ ]	
	0.37	1.9360	1.93558	0.00042		
	0.38	1.9257	1.92518	0.00052	Expt.	
	0.39	1.9154	1.91611	-0.00071	accuracy is	
	0.40	1.9086	1.90815	0.00045	$\pm 0.0005$	
	0.41	1.9020	1.90111	0.00089		
	0.42	1.8952	1.89484	0.00036		
	0.44	1.8847	1.88418	0.00052		
	0.46	1.8753	1.87546	-0.00016		

Table 2.26: (Continued)

Polarization	Wavelength ( $\mu\text{m}$ )	Observed [68]	Computed (This work)	Difference	Av. Dev.	RMS Dev.
y-axis	0.48	1.8685	1.86821	0.00029		
	0.50	1.8624	1.86210	0.00030		
	0.52	1.8562	1.85689	-0.00069		
	0.54	1.8522	1.85240	-0.00020		
	0.56	1.8476	1.84849	-0.00089		
	0.58	1.8436	1.84505	-0.00145		
	0.60	1.8405	1.84202	-0.00152		
	0.62	1.8388	1.83932	-0.00052		
	0.64	1.8368	1.83690	-0.00010		
	0.66	1.8348	1.83472	0.00008		
	0.68	1.8328	1.83274	0.00006		
	0.70	1.8311	1.83094	0.00016		
	0.80	1.8248	1.82389	0.00091		
	0.85	1.8222	1.82122	0.00098		
	0.90	1.8202	1.81892	0.00128		
	0.95	1.8184	1.81690	0.00150		
	1.00	1.8150	1.81509	-0.00009		
	1.10	1.8114	1.81195	-0.00055		
	1.20	1.8088	1.80920	-0.00040		
	1.30	1.8063	1.80668	-0.00038		
	1.40	1.8038	1.80427	-0.00047		
	1.50	1.8018	1.80191	-0.00011		
	1.60	1.7998	1.79952	0.00028		
	0.35	2.1265	2.12546	0.00104	5.9	7.9
	0.36	2.1077	2.10757	0.00013	$[10^{-4}]$	
	0.37	2.0917	2.09210	-0.00040		
	0.38	2.0782	2.07862	-0.00042		
	0.39	2.0662	2.06676	-0.00056	Expt. accuracy is $\pm 0.0005$	
	0.40	2.0545	2.05627	-0.00177		
	0.41	2.0465	2.04692	-0.00042		
	0.42	2.0394	2.03855	0.00085		
	0.44	2.0246	2.02420	0.00040		
	0.46	2.0119	2.01237	-0.00047		
	0.48	2.0026	2.00247	0.00013		
	0.50	1.9926	1.99408	-0.00148		
	0.52	1.9883	1.98690	0.00140		
	0.54	1.9829	1.98068	0.00222		
	0.56	1.9763	1.97527	0.00103		
	0.58	1.9712	1.97051	0.00069		
	0.60	1.9665	1.96630	0.00020		
	0.62	1.9632	1.96255	0.00065		
	0.64	1.9589	1.95919	-0.00029		
	0.66	1.9560	1.95617	-0.00017		
	0.68	1.9529	1.95344	-0.00054		
	0.70	1.9506	1.95096	-0.00036		

Table 2.26: (*Continued*)

Polarization	Wavelength ( $\mu\text{m}$ )	Observed [68]	Computed (This work)	Difference	Av. Dev.	RMS Dev.
z-axis	0.80	1.9409	1.94135	-0.00045		
	0.85	1.9377	1.93778	-0.00008		
	0.90	1.9346	1.93476	-0.00016		
	0.95	1.9314	1.93216	-0.00076		
	1.00	1.9286	1.92989	-0.00129		
	1.10	1.9260	1.92608	-0.00008		
	1.20	1.9229	1.92292	-0.00002		
	1.30	1.9206	1.92019	0.00041		
	1.40	1.9180	1.91773	0.00027		
	1.50	1.9157	1.91542	0.00028		
	1.60	1.9132	1.91320	0.00000		
	0.35	2.1485	2.15014	-0.00164	5.3	6.7
	0.36	2.1330	2.13228	0.00072	$[10^{-4}]$	
	0.37	2.1171	2.11688	0.00022	Expt.	
	0.38	2.1053	2.10349	0.00181	accuracy is	
	0.39	2.0929	2.09174	0.00116	$\pm 0.0005$	
	0.40	2.0808	2.08136	-0.00056		
	0.41	2.0715	2.07212	-0.00062		
	0.42	2.0637	2.06385	-0.00015		
	0.44	2.0494	2.04970	-0.00030		
	0.46	2.0378	2.03803	-0.00023		
	0.48	2.0292	2.02828	0.00092		
	0.50	2.0194	2.02000	-0.00060		
	0.52	2.0126	2.01290	-0.00030		
	0.54	2.0065	2.00675	-0.00025		
	0.56	2.0010	2.00137	-0.00037		
	0.58	1.9960	1.99663	-0.00063		
	0.60	1.9918	1.99241	-0.00061		
	0.62	1.9884	1.98864	-0.00024		
	0.64	1.9854	1.98525	0.00015		
	0.66	1.9821	1.98218	-0.00008		
	0.68	1.9791	1.97938	-0.00028		
	0.70	1.9763	1.97682	-0.00052		
	0.80	1.9668	1.96665	0.00015		
	0.85	1.9634	1.96270	0.00070		
	0.90	1.9602	1.95925	0.00095		
	0.95	1.9569	1.95616	0.00074		
	1.00	1.9541	1.95336	0.00074		
	1.10	1.9486	1.94834	0.00026		
	1.20	1.9436	1.94380	-0.00020		
	1.30	1.9390	1.93949	-0.00049		
	1.40	1.9348	1.93526	-0.00046		
	1.50	1.9310	1.93099	0.00001		

**Table 2.27: The Experimental [72] and Computed Refractive Index Values of InSb Crystal at 25°C**

Wavelength ( $\mu\text{m}$ )	Observed [72]	Computed (This work)	Difference	Av. Dev.	RMS Dev.
7.87	4.00	3.986	0.014	0.009	0.011
8.00	3.99	3.976	0.014		
9.01	3.96	3.941	0.019	Expt.	
10.06	3.95	3.927	0.023	accuracy	
11.01	3.93	3.919	0.011	was not	
12.06	3.92	3.910	0.010	mentioned	
12.98	3.91	3.903	0.007		
13.90	3.90	3.895	0.005		
15.13	3.88	3.884	-0.004		
15.79	3.87	3.878	-0.008		
16.96	3.86	3.866	-0.006		
17.85	3.85	3.856	-0.006		
18.85	3.84	3.843	-0.003		
19.98	3.82	3.828	-0.008		
21.15	3.81	3.810	0.000		
22.20	3.80	3.792	0.008		

**Table 2.28: The Experimental [48] and Computed Refractive Index Values of KCl Crystal at 19.9°C**

Wavelength ( $\mu\text{m}$ )	Observed [48]	Computed (This work)	Difference	Av. Dev.	RMS Dev.
0.25	1.59010	1.590047	0.000053	2.6	3.6
0.30	1.54574	1.545896	-0.000156	[ $10^{-5}$ ]	
0.35	1.52365	1.523690	-0.000040		
0.40	1.51072	1.510697	0.000023		
0.45	1.50240	1.502353	0.000047		
0.50	1.49670	1.496641	0.000059	Expt.	
0.55	1.49260	1.492544	0.000056	accuracy	
0.60	1.48955	1.489496	0.000054	was not	
0.65	1.48721	1.487163	0.000047	mentioned	
0.70	1.48537	1.485333	0.000037		
0.75	1.48390	1.483871	0.000029		
0.80	1.48271	1.482680	0.000030		
0.85	1.48172	1.481698	0.000022		
0.90	1.48089	1.480876	0.000014		
0.95	1.48019	1.480181	0.000009		

**Table 2.28: (Continued)**

Wavelength ( $\mu\text{m}$ )	Observed [48]	Computed (This work)	Difference	Av. Dev.	RMS Dev.
1.00	1.47959	1.479587	0.000003		
1.50	1.47642	1.476434	-0.000014		
2.00	1.47508	1.475113	-0.000033		
2.50	1.47422	1.474249	-0.000029		
3.00	1.47348	1.473510	-0.000030		
3.50	1.47275	1.472782	-0.000032		
4.00	1.47199	1.472019	-0.000029		
4.50	1.47117	1.471197	-0.000027		
5.00	1.47028	1.470304	-0.000024		
5.50	1.46931	1.469333	-0.000023		
6.00	1.46826	1.468281	-0.000021		
6.50	1.46712	1.467143	-0.000023		
7.00	1.46590	1.465917	-0.000017		
7.50	1.46459	1.464602	-0.000012		
8.00	1.46319	1.463197	-0.000007		
8.50	1.46169	1.461699	-0.000009		
9.00	1.46010	1.460109	-0.000009		
9.50	1.45842	1.458424	-0.000004		
10.00	1.45664	1.456644	-0.000004		
10.50	1.45477	1.454768	0.000002		
11.00	1.45280	1.452795	0.000005		
11.50	1.45073	1.450722	0.000008		
12.00	1.44856	1.448550	0.000010		
12.50	1.44629	1.446278	0.000012		
13.00	1.44391	1.443903	0.000007		
13.50	1.44143	1.441424	0.000006		
14.00	1.43885	1.438841	0.000009		

**Table 2.29: The Experimental [48] and Computed Refractive Index Values of KCl:KI Crystal at 19.9°C**

Wavelength ( $\mu\text{m}$ )	Observed [48]	Computed (This work)	Difference	Av. Dev.	RMS Dev.
0.25	1.59146	1.591428	0.000032	6.3	7.7
0.30	1.54669	1.546807	-0.000117	[ $10^{-5}$ ]	
0.35	1.52445	1.524456	-0.000006		
0.40	1.51146	1.511406	0.000054		
0.45	1.50310	1.503036	0.000064		

**Table 2.29: (Continued)**

Wavelength ( $\mu\text{m}$ )	Observed [48]	Computed (This work)	Difference	Av. Dev.	RMS Dev.
0.50	1.49737	1.497312	0.000058		
0.55	1.49326	1.493208	0.000052		
0.60	1.49019	1.490156	0.000034		
0.65	1.48784	1.487821	0.000019		
0.70	1.48599	1.485990	0.000000		
0.75	1.48452	1.484527	-0.000007	Expt. accuracy was not mentioned	
0.80	1.48332	1.483336	-0.000016		
0.85	1.48232	1.482354	-0.000034		
0.90	1.48149	1.481532	-0.000042		
0.95	1.48079	1.480836	-0.000046		
1.00	1.48019	1.480242	-0.000052		
1.50	1.47700	1.477088	-0.000088		
2.00	1.47567	1.475763	-0.000093		
2.50	1.47480	1.474895	-0.000095		
3.00	1.47406	1.474150	-0.000090		
3.50	1.47334	1.473415	-0.000075		
4.00	1.47258	1.472643	-0.000063		
4.50	1.47176	1.471812	-0.000052		
5.00	1.47087	1.470908	-0.000038		
5.50	1.46991	1.469925	-0.000015		
6.00	1.46886	1.468858	0.000002		
6.50	1.46772	1.467704	0.000016		
7.00	1.46649	1.466462	0.000028		
7.50	1.46518	1.465128	0.000052		
8.00	1.46377	1.463701	0.000069		
8.50	1.46226	1.462180	0.000080		
9.00	1.46066	1.460565	0.000095		
9.50	1.45895	1.458852	0.000098		
10.00	1.45715	1.457042	0.000108		
10.50	1.45524	1.455133	0.000107		
11.00	1.45323	1.453124	0.000106		
11.50	1.45112	1.451013	0.000107		
12.00	1.44889	1.448799	0.000091		
12.50	1.44656	1.446481	0.000079		
13.00	1.44411	1.444057	0.000053		
13.50	1.44154	1.441525	0.000015		
14.00	1.43886	1.438885	-0.000025		
14.50	1.43605	1.436134	-0.000084		
15.00	1.43312	1.433270	-0.000150		
15.50	1.43006	1.430292	-0.000232		

**Table 2.30: The Experimental [9] and Computed Refractive Index Values of KDA Crystal at 33°C**

Polarization	Wavelength (μm)	Observed [9]	Computed (This work)	Difference	Av. RMS Dev.	Dev.
Ordinary	0.404656	1.58714	1.587124	0.000016	3.1	3.8
	0.435833	1.58163	1.581613	0.000017	$[10^{-5}]$	
	0.467815	1.57708	1.577117	-0.000037		
	0.479991	1.57559	1.575641	-0.000051		
	0.508582	1.57257	1.572577	-0.000007		
	0.546074	1.56923	1.569233	-0.000003	Expt.	
	0.579066	1.56685	1.566764	0.000086	accuracy	
	0.643847	1.56284	1.562814	0.000026		
	0.780027	1.55677	1.556752	0.000018	$\pm 0.00003$	
	0.794760	1.55619	1.556203	-0.000013		
	0.852113	1.55416	1.554189	-0.000029		
	0.894346	1.55274	1.552800	-0.000060		
	1.064000	1.54767	1.547631	0.000039		
Extra-ordinary	0.404656	1.53391	1.533962	-0.000052	4.0	5.0
	0.435833	1.52931	1.529343	-0.000033	$[10^{-5}]$	
	0.467815	1.52561	1.525639	-0.000029		
	0.479991	1.52448	1.524439	0.000041		
	0.508582	1.52204	1.521977	0.000063		
	0.546074	1.51935	1.519348	0.000002	Expt.	
	0.579066	1.51756	1.517458	0.000102	accuracy	
	0.643847	1.51454	1.514556	-0.000016		
	0.780027	1.51053	1.510531	-0.000001	$\pm 0.00003$	
	0.794760	1.51016	1.510200	-0.000040		
	0.852113	1.50895	1.509040	-0.000090		
	0.894346	1.50827	1.508290	-0.000020		
	1.064000	1.50591	1.505845	0.000065		

**Table 2.31: The Experimental [9] and Computed Refractive Index Values of KDP Crystal at 33°C**

Polarization	Wavelength (μm)	Observed [9]	Computed (This work)	Difference	Av. RMS Dev.	Dev.
Ordinary	0.404656	1.52322	1.523206	0.000014	3.9	5.1
	0.435833	1.51963	1.519651	-0.000021	$[10^{-5}]$	
	0.455526	1.51779	1.517761	0.000029		
	0.467815	1.51665	1.516693	-0.000043		
	0.479991	1.51570	1.515708	-0.000008		

**Table 2.31: (Continued)**

Polarization	Wavelength (μm)	Observed [9]	Computed (This work)	Difference	Av. RMS Dev. Dev.
Extra-ordinary	0.508592	1.51365	1.513638	0.000012	
	0.535046	1.51195	1.511970	-0.000020	
	0.546074	1.51137	1.511332	0.000038	
	0.579066	1.50970	1.509589	0.000111	
	0.589300	1.50897	1.509092	-0.000122	
	0.643847	1.50671	1.506708	0.000002	Expt.
	0.780027	1.50201	1.501962	0.000048	accuracy
	0.794760	1.50154	1.501508	0.000032	
	0.852113	1.49975	1.499801	-0.000051	± 0.00003
	0.894346	1.49854	1.498586	-0.000046	
	1.064000	1.49383	1.493807	0.000023	
	0.404656	1.47925	1.479277	-0.000027	4.9 6.3
	0.435833	1.47635	1.476342	0.000008	[10 <sup>-5</sup> ]
	0.455526	1.47486	1.474802	0.000058	
	0.467815	1.47386	1.473941	-0.000081	
	0.479991	1.47314	1.473154	-0.000014	
	0.508592	1.47150	1.471523	-0.000023	Expt.
	0.535046	1.47019	1.470238	-0.000048	accuracy
	0.546074	1.46983	1.469756	0.000074	
	0.579066	1.46862	1.468466	0.000154	± 0.00003
	0.589300	1.46808	1.468107	-0.000027	
	0.643847	1.46644	1.466447	-0.000007	
	0.780027	1.46358	1.463533	0.000047	
	0.794760	1.46328	1.463285	-0.000005	
	0.852113	1.46230	1.462401	-0.000101	
	0.894346	1.46173	1.461816	-0.000086	
	1.064000	1.45989	1.459814	0.000076	

**Table 2.32: The Experimental [16] and Computed Refractive Index Values of KDP Crystal at 24.8°C**

Polarization	Wavelength (μm)	Observed [16]	Computed (This work)	Difference	Av. RMS Dev. Dev.
Ordinary	0.2138560	1.60177	1.601699	0.000071	8.8 13.7
	0.2288018	1.58546	1.585456	0.000004	[10 <sup>-5</sup> ]
	0.2446905	1.57228	1.572388	-0.000108	
	0.2464068	1.57105	1.571172	0.000122	
	0.2536519	1.56631	1.566388	-0.000078	
	0.2800869	1.55263	1.552668	-0.000038	

**Table 2.32: (Continued)**

Polarization	Wavelength ( $\mu\text{m}$ )	Observed [16]	Computed (This work)	Difference	Av. RMS Dev. Dev.
Extra-ordinary	0.2980628	1.54618	1.545738	0.000442	
	0.3021499	1.54433	1.544363	-0.000033	Expt.
	0.3125663	1.54117	1.541135	0.000035	accuracy
	0.3131545	1.54098	1.540963	0.000017	
	0.3650146	1.52932	1.529275	0.000045	$\pm 0.00003$
	0.3654833	1.52923	1.529193	0.000037	
	0.3662878	1.52909	1.529054	0.000036	
	0.4046561	1.52301	1.523378	-0.000368	
	0.4358350	1.51990	1.519839	0.000061	
	0.5460740	1.51152	1.511549	-0.000029	
	0.5769580	1.50987	1.509913	-0.000043	
	0.5790654	1.50977	1.509809	-0.000039	
	0.6328160	1.50737	1.507377	-0.000007	
	1.0139750	1.49535	1.495295	0.000055	
	1.1287040	1.49205	1.491945	0.000105	
	1.1522760	1.49135	1.491239	0.000111	
	1.3570700	1.48455	1.484706	-0.000156	
	0.2138560	1.54615	1.546113	0.000037	3.0
	0.2536519	1.51586	1.515953	-0.000093	$[10^{-5}]$
	0.2800869	1.50416	1.504197	-0.000037	
	0.2980628	1.49824	1.498262	-0.000022	Expt.
	0.3021499	1.49708	1.497085	-0.000005	accuracy
	0.3035781	1.49667	1.496687	-0.000017	
	0.3125663	1.49434	1.494326	0.000014	$\pm 0.00003$
	0.3131545	1.49419	1.494180	0.000010	
	0.3341478	1.48954	1.489523	0.000017	
	0.3650146	1.48432	1.484244	0.000076	
	0.3654833	1.48423	1.484175	0.000055	
	0.3662878	1.48409	1.484057	0.000033	
	0.3906410	1.48089	1.480864	0.000026	
	0.4046561	1.47927	1.479301	-0.000031	
	0.4077811	1.47898	1.478976	0.000004	
	0.4358350	1.47640	1.476382	0.000018	
	0.4916036	1.47254	1.472522	0.000018	
	0.5460740	1.46982	1.469838	-0.000018	
	0.5790654	1.46856	1.468557	0.000003	
	0.6328160	1.46685	1.466854	-0.000004	
	1.0139750	1.46041	1.460465	-0.000055	
	1.1287040	1.45917	1.459221	-0.000051	
	1.1522760	1.45893	1.458976	-0.000046	
	1.5231000	1.45521	1.455165	0.000045	
	1.5295250	1.45512	1.455096	0.000024	

**Table 2.33: The Experimental [9] and Computed Refractive Index Values of KD\*P Crystal at 33°C**

Polarization	Wavelength (μm)	Observed [9]	Computed (This work)	Difference	Av. RMS Dev.	Dev. Dev.
Ordinary	0.404656	1.51770	1.517670	0.000030	3.2	3.9
	0.435833	1.51427	1.514284	-0.000014	[10 <sup>-5</sup> ]	
	0.467815	1.51147	1.511508	-0.000038		
	0.479991	1.51055	1.510594	-0.000044		
	0.508582	1.50870	1.508693	0.000007	Expt.	
	0.546074	1.50662	1.506612	0.000008	accuracy	
	0.589300	1.50472	1.504638	0.000082	±0.00003	
	0.643847	1.50263	1.502603	0.000027		
	0.780027	1.49882	1.498808	0.000012		
	0.794760	1.49840	1.498464	-0.000064		
	0.852113	1.49721	1.497204	0.000006		
	0.894346	1.49629	1.496335	-0.000045		
	1.064000	1.49314	1.493108	0.000032		
	0.404656	1.47696	1.476980	-0.000020	4.1	6.2
Extra-ordinary	0.435833	1.47412	1.474107	0.000013	[10 <sup>-5</sup> ]	
	0.467815	1.47174	1.471764	-0.000024		
	0.479991	1.47099	1.470996	-0.000006		
	0.508582	1.46945	1.469407	0.000043		
	0.546074	1.46774	1.467689	0.000051	Expt.	
	0.589300	1.46610	1.466090	0.000010	accuracy	
	0.643847	1.46449	1.464487	0.000003	±0.00003	
	0.780027	1.46162	1.461693	-0.000073		
	0.794760	1.46146	1.461457	0.000003		
	0.852113	1.46059	1.460619	-0.000029		
	0.894346	1.46007	1.460068	0.000002		
	1.064000	1.45824	1.458205	0.000035		

**Table 2.34: The Experimental [76] and Computed Refractive Index Values of KD\*P Crystal at 25°C**

Polarization	Wavelength (μm)	Observed [76]	Computed (This work)	Difference	Av. RMS Dev.	Dev. Dev.
Ordinary	0.4047	1.5189	1.518870	0.000030	3.5	3.9
	0.4078	1.5185	1.518506	-0.000006	[10 <sup>-5</sup> ]	
	0.4358	1.5155	1.515558	-0.000058		

**Table 2.34: (Continued)**

Polarization	Wavelength ( $\mu\text{m}$ )	Observed [76]	Computed (This work)	Difference	Av. RMS
				Dev.	Dev.
Extra-ordinary	0.4916	1.5111	1.511068	0.000032	Expt. accuracy
	0.5461	1.5079	1.507848	0.000052	$\pm 0.0001$
	0.5779	1.5063	1.506321	-0.000021	
	0.6234	1.5044	1.504454	-0.000054	
	0.6907	1.5022	1.502175	0.000025	
	0.4047	1.47760	1.477550	0.000050	5.1 [10 <sup>-5</sup> ] 6.4
	0.4078	1.47720	1.477235	-0.000035	
	0.4358	1.47470	1.474707	-0.000007	
	0.4916	1.47100	1.470937	0.000063	Expt. accuracy
	0.5461	1.46830	1.468305	-0.000005	
	0.5779	1.46700	1.467082	-0.000082	$\pm 0.0001$
	0.6234	1.46560	1.465612	-0.000012	
	0.6907	1.46390	1.463862	0.000038	

**Table 2.35: The Experimental [9] and Computed Refractive Index Values of KDP:Rb Crystal at 33°C**

Polarization	Wavelength ( $\mu\text{m}$ )	Observed [9]	Computed (This work)	Difference	Av. RMS
				Dev.	Dev.
Extra-ordinary	0.404656	1.48070	1.480682	0.000018	2.1 2.7
	0.435833	1.47772	1.477748	-0.000028	[10 <sup>-5</sup> ]
	0.467815	1.47534	1.475337	0.000003	
	0.479991	1.47454	1.474543	-0.000003	Expt. accuracy
	0.546074	1.47107	1.471110	-0.000040	
	0.579066	1.46985	1.469804	0.000046	$\pm 0.00003$
	0.643847	1.46780	1.467760	0.000040	
	0.780027	1.46482	1.464824	-0.000004	
	0.794760	1.46453	1.464575	-0.000045	
	0.852113	1.46370	1.463694	0.000006	
	0.894346	1.46311	1.463115	-0.000005	
	1.064000	1.46117	1.461159	0.000011	

**Table 2.36: The Experimental [79] and Computed Refractive Index Values of KNbO<sub>3</sub> (KNO) Crystal at 22°C**

Polarization	Wavelength (μm)	Observed [79]	Computed (This work)	Difference	Av. Dev.	RMS Dev.
x-axis	0.4050	2.4553	2.45482	0.00046	2.3	2.8
	0.4300	2.4145	2.41488	-0.00038	[10 <sup>-4</sup> ]	
	0.4500	2.3895	2.38970	-0.00021		
	0.4880	2.3527	2.35310	-0.00040		
	0.5000	2.3437	2.34381	-0.00012	Expt. accuracy is	
	0.5145	2.3337	2.33370	0.00000	± 0.00025	
	0.5300	2.3240	2.32405	-0.00002		
	0.5400	2.3184	2.31837	0.00002		
	0.5800	2.2993	2.29917	0.00013		
	0.6000	2.2914	2.29125	0.00018		
	0.6330	2.2801	2.28007	0.00003		
	0.7000	2.2629	2.26263	0.00028		
	0.7500	2.2531	2.25281	0.00029		
	0.8000	2.2452	2.24487	0.00029		
	0.8600	2.2372	2.23714	0.00006		
	0.9000	2.2331	2.23282	0.00025		
	1.0640	2.2195	2.21954	-0.00004		
	1.5000	2.1992	2.19949	-0.00029		
y-axis	2.0000	2.1832	2.18361	-0.00041		
	2.5000	2.1674	2.16785	-0.00045		
	3.0000	2.1498	2.15003	-0.00023		
	3.4000	2.1342	2.13368	0.00056		
	0.4050	2.5508	2.55020	0.00061	3.2	3.8
	0.4300	2.4974	2.49792	-0.00052	[10 <sup>-4</sup> ]	
	0.4500	2.4652	2.46553	-0.00034		
	0.4880	2.4187	2.41924	-0.00054		
	0.5000	2.4075	2.40763	-0.00017		
	0.5145	2.3951	2.39505	0.00005		
	0.5300	2.3831	2.38312	-0.00001	Expt. accuracy is	
	0.5400	2.3762	2.37612	0.00005		
	0.5800	2.3528	2.35261	0.00021		
	0.6000	2.3433	2.34300	0.00026	± 0.00025	
	0.6330	2.3296	2.32947	0.00013		
	0.7000	2.3089	2.30853	0.00037		
	0.7500	2.2972	2.29683	0.00037		
	0.8000	2.2878	2.28741	0.00035		
	0.8600	2.2784	2.27829	0.00011		
	0.9000	2.2735	2.27320	0.00027		
z-axis	1.0640	2.2576	2.25767	-0.00007		
	1.5000	2.2341	2.23453	-0.00043		
	2.0000	2.2159	2.21649	-0.00059		
	2.5000	2.1981	2.19872	-0.00062		
	3.0000	2.1785	2.17871	-0.00021		
	3.4000	2.1610	2.16034	0.00071		
	0.4050	2.3098	2.30938	0.00040	1.9	2.4
	0.4300	2.2771	2.27743	-0.00033	[10 <sup>-4</sup> ]	
	0.4500	2.2571	2.25722	-0.00016		
	0.4880	2.2274	2.22777	-0.00037		

**Table 2.36: (Continued)**

Polarization	Wavelength (μm)	Observed [79]	Computed (This work)	Difference	Avg. Dev.	RMS Dev.
	0.5000	2.2202	2.22027	-0.00010		
	0.5145	2.2121	2.21210	0.00000		
	0.5300	2.2043	2.20430	-0.00001	Expt. accuracy is ± 0.00025	
	0.5400	2.1997	2.19971	0.00002		
	0.5800	2.1843	2.18416	0.00011		
	0.6000	2.1779	2.17775	0.00014		
	0.6330	2.1687	2.16867	0.00003		
	0.7000	2.1547	2.15450	0.00024		
	0.7500	2.1468	2.14652	0.00025		
	0.8000	2.1403	2.14006	0.00024		
	0.8600	2.1338	2.13377	0.00003		
	0.9000	2.1305	2.13024	0.00022		
	1.0640	2.1194	2.11943	-0.00003		
	1.5000	2.1029	2.10312	-0.00022		
	2.0000	2.0899	2.09025	-0.00035		
	2.5000	2.0771	2.07752	-0.00042		
	3.0000	2.0630	2.06316	-0.00016		
	3.4000	2.0505	2.05000	0.00046		

**Table 2.37: The Experimental [86] and Computed Refractive Index Values of LiB<sub>3</sub>O<sub>5</sub> (LBO) Crystal at 20°C**

Wavelength	Expt. (x)	Com-	Expt. (y)	Com-	Expt. (z)	Com-
		puted		puted		puted
0.365	1.59523	1.59521	1.62518	1.62541	1.64025	1.64083
0.400	1.58995	1.58985	1.61918	1.61943	NM	1.63467
0.450	1.58449	1.58433	1.61301	1.61327	1.62793	1.62833
0.500	1.58059	1.58040	1.60862	1.60888	1.62348	1.62381
0.525	1.57906	1.57884	1.60686	1.60712	NM	1.62201
0.532	1.57868	1.57844	1.60642	1.60666	1.62122	1.62155
0.550	1.57772	1.57747	1.60535	1.60557	1.62014	1.62043
0.600	1.57541	1.57518	1.60276	1.60298	1.61753	1.61779
0.700	NM	1.57181	1.59893	1.59911	1.61363	1.61388
0.800	1.56959	1.56836	1.59615	1.59621	1.61078	1.61101
0.900	1.56764	1.56739	1.59386	1.59382	1.60843	1.60868
1.000	1.56586	1.56568	1.59187	1.59169	1.60637	1.60664
1.064	1.56487	1.56466	1.59072	1.59040	1.60515	1.60541
1.100	1.56432	1.56410	1.59005	1.58968	1.60449	1.60474

Wavelength is in μm, NM = not measured

**Table 2.38: The Experimental [91] and Computed Refractive Index Values of LiNbO<sub>3</sub> (LNO) Crystal at 25°C**

Polarization	Wavelength (μm)	Observed [91]	Computed (This work)	Difference	Av. Dev.	RMS Dev.
Ordinary	0.42	2.4089	2.40902	-0.00012	5.1 [10 <sup>-4</sup> ] Expt. accuracy was not mentioned	6.3
	0.45	2.3780	2.37765	0.00035		
	0.50	2.3410	2.34047	0.00053		
	0.55	2.3132	2.31490	-0.00170		
	0.60	2.2967	2.29640	0.00030		
	0.70	2.2716	2.27167	-0.00007		
	0.80	2.2571	2.25602	0.00108		
	0.90	2.2448	2.24523	-0.00043		
	1.00	2.2370	2.23727	-0.00027		
	1.20	2.2269	2.22594	0.00096		
	1.40	2.2184	2.21767	0.00073		
	1.60	2.2113	2.21076	0.00054		
	1.80	2.2049	2.20438	0.00052		
	2.00	2.1974	2.19814	-0.00074		
	2.20	2.1909	2.19180	-0.00090		
	2.40	2.1850	2.18519	-0.00019		
	2.60	2.1778	2.17823	-0.00043		
	2.80	2.1703	2.17085	-0.00055		
	3.00	2.1625	2.16298	-0.00048		
	3.20	2.1543	2.15458	-0.00028		
	3.40	2.1456	2.14563	-0.00003		
	3.60	2.1363	2.13607	0.00023		
	3.80	2.1263	2.12587	0.00043		
	4.00	2.1155	2.11499	0.00051		
Extra-ordinary	0.42	2.3025	2.30275	-0.00025	4.9 [10 <sup>-4</sup> ] 5.6	
	0.45	2.2772	2.27674	0.00046		
	0.50	2.2457	2.24562	0.00008		
	0.55	2.2237	2.22405	-0.00035		
	0.60	2.2082	2.20835	-0.00015		
	0.70	2.1874	2.18725	0.00015		
	0.80	2.1745	2.17384	0.00066		
	0.90	2.1641	2.16458	-0.00048		
	1.00	2.1567	2.15773	-0.00103		
	1.20	2.1478	2.14801	-0.00021		
	1.40	2.1417	2.14093	0.00077		
	1.60	2.1361	2.13504	0.00106		
	1.80	2.1306	2.12964	0.00096		
	2.00	2.1250	2.12437	0.00063		
	2.20	2.1183	2.11902	-0.00072		
	2.40	2.1129	2.11346	-0.00056		
	2.60	2.1071	2.10762	-0.00052		
	2.80	2.1009	2.10143	-0.00053		
	3.00	2.0945	2.09484	-0.00034		
	3.20	2.0871	2.08782	-0.00072		
	3.40	2.0804	2.08033	0.00007		
	3.60	2.0725	2.07235	0.00015		
	3.80	2.0642	2.06384	0.00036		

**Table 2.39: The Experimental [92] and Computed Refractive Index Values of LiNbO<sub>3</sub> (LNO) Crystal at 25°C**

Polari-zation	Wavelength ( μm)	Observed [92]	Computed (This work)	Difference	Av. Dev.	RMS Dev.
Ordinary	0.42	2.4144	2.41381	0.00059	2.0 [10 <sup>-4</sup> ]	2.7
	0.45	2.3814	2.38218	-0.00078		
	0.50	2.3444	2.34467	-0.00027		
	0.55	2.3188	2.31886	-0.00006		
	0.60	2.3002	2.30018	0.00002		
	0.65	2.2862	2.28613	0.00007		
	0.70	2.2756	2.27521	0.00039		
	0.90	2.2487	2.24854	0.00016		
	1.00	2.2407	2.24051	0.00019		
	1.20	2.2291	2.22911	-0.00001		
	1.40	2.2208	2.22082	-0.00002		
	1.60	2.2139	2.21390	0.00000		
	1.80	2.2074	2.20755	-0.00015		
	2.00	2.2015	2.20134	0.00016		
	2.20	2.1948	2.19503	-0.00023		
	2.40	2.1882	2.18848	-0.00028		
	2.60	2.1814	2.18158	-0.00018		
	2.80	2.1741	2.17426	-0.00016		
	3.00	2.1663	2.16647	-0.00017		
	3.20	2.1580	2.15815	-0.00015		
	3.40	2.1493	2.14929	0.00001		
	3.60	2.1398	2.13982	-0.00002		
	3.80	2.1299	2.12973	0.00017		
	4.00	2.1193	2.11898	0.00032		
Extra-ordinary	0.42	2.3038	2.30324	0.00056	2.3 [10 <sup>-4</sup> ]	3.2
	0.45	2.2765	2.27694	-0.00044		
	0.50	2.2446	2.24558	-0.00098		
	0.55	2.2241	2.22391	0.00019		
	0.60	2.2083	2.20817	0.00013		
	0.65	2.1964	2.19630	0.00010		
	0.80	2.1741	2.17369	0.00041		
	0.90	2.1647	2.16446	0.00024		
	1.00	2.1580	2.15765	0.00035		
	1.20	2.1481	2.14799	0.00011		
	1.40	2.1410	2.14098	0.00002		
	1.60	2.1351	2.13516	-0.00006		
	1.80	2.1297	2.12983	-0.00013		
	2.00	2.1244	2.12463	-0.00023		
	2.20	2.1187	2.11936	-0.00066		
	2.40	2.1138	2.11389	-0.00009		
	2.60	2.1080	2.10814	-0.00014		
	2.80	2.1020	2.10205	-0.00005		
	3.00	2.0955	2.09557	-0.00007		
	3.20	2.0886	2.08866	-0.00006		
	3.40	2.0814	2.08130	0.00010		
	3.60	2.0735	2.07346	0.00004		
	3.80	2.0652	2.06509	0.00011		
	4.00	2.0564	2.05619	0.0002		

**Table 2.40: The Experimental and Computed Refractive Index Values of Cong. Melt LiNbO<sub>3</sub> (LNO) Crystal at 24.5°C**

Polarization	Wavelength (μm)	Observed [93]	Computed (This work)	Difference	Av. RMS Dev.	Dev.
Ordinary	0.40463	2.4317	2.43159	0.00011	0.9	1.1
	0.43584	2.3928	2.39288	-0.00008	[10 <sup>-4</sup> ]	
	0.46782	2.3634	2.36345	-0.00005		
	0.47999	2.3541	2.35420	-0.00010		
	0.50858	2.3356	2.33567	-0.00007		
	0.54607	2.3165	2.31653	-0.00003		
	0.57696	2.3040	2.30396	0.00004		
	0.57897	2.3032	2.30322	-0.00002		
	0.58756	2.3002	2.30017	0.00003	Expt.	
	0.64385	2.2835	2.28345	0.00005	accuracy	
	0.66782	2.2778	2.27771	0.00009	is	
	0.70652	2.2699	2.26973	0.00017	± 0.0002	
	0.80926	2.2541	2.25400	0.00010		
	0.87168	2.2471	2.24703	0.00007		
	0.93564	2.2412	2.24119	0.00001		
	0.95998	2.2393	2.23923	0.00007		
	1.01400	2.2351	2.23532	-0.00022		
	1.09214	2.2304	2.23046	-0.00006		
	1.15392	2.2271	2.22714	-0.00004		
	1.15794	2.2269	2.22693	-0.00003		
	1.28770	2.2211	2.22099	0.00011		
	1.43997	2.2151	2.21511	-0.00001		
	1.63821	2.2083	2.20838	-0.00008		
	1.91125	2.1994	2.19974	-0.00034		
	2.18428	2.1912	2.19109	0.00011		
	2.39995	2.1840	2.18395	0.00005		
	2.61504	2.1765	2.17642	0.00008		
	2.73035	2.1724	2.17218	0.00022		
	2.89733	2.1657	2.16576	-0.00006		
	3.05148	2.1594	2.15952	-0.00012		
Extra-ordinary	0.40463	2.3260	2.32583	0.00017	0.9	1.2
	0.43584	2.2932	2.29332	-0.00012	[10 <sup>-4</sup> ]	
	0.46782	2.2683	2.26846	-0.00016		
	0.47999	2.2605	2.26061	-0.00011		
	0.50858	2.2448	2.24486	-0.00006		
	0.54607	2.2285	2.22853	-0.00003	Expt.	
	0.57696	2.2178	2.21777	0.00003	accuracy	
	0.57897	2.2171	2.21714	-0.00004	± 0.0002	

**Table 2.40: (Continued)**

Polarization	Wavelength (μm)	Observed [93]	Computed (This work)	Difference	Av. RMS Dev. Dev.
	0.58756	2.2147	2.21453	0.00017	
	0.64385	2.2002	2.20017	0.00003	
	0.66782	2.1953	2.19524	0.00006	
	0.70652	2.1886	2.18837	0.00023	
	0.80926	2.1749	2.17482	0.00008	
	0.87168	2.1688	2.16880	0.00000	
	0.93564	2.1639	2.16376	0.00014	
	0.95998	2.1622	2.16208	0.00012	
	1.01400	2.1584	2.15870	-0.00030	
	1.09214	2.1545	2.15453	-0.00003	
	1.15392	2.1517	2.15166	0.00004	
	1.15794	2.1515	2.15149	0.00001	
	1.28770	2.1464	2.14639	0.00001	
	1.43997	2.1413	2.14136	-0.00006	
	1.63821	2.1356	2.13563	-0.00003	
	1.91125	2.1280	2.12833	-0.00033	
	2.18428	2.1211	2.12105	0.00005	
	2.39995	2.1151	2.11505	0.00005	
	2.61504	2.1087	2.10874	-0.00004	
	2.73035	2.1053	2.10520	0.00010	
	2.89733	2.0999	2.09983	0.00007	
	3.05148	2.0946	2.09463	-0.00003	

**Table 2.41: The Experimental [31] and Computed Refractive Index Values of LiTaO<sub>3</sub> (LTO) Crystal at 25°C**

Polarization	Wavelength (μm)	Observed [31]	Computed (This work)	Difference	Av. Dev.	RMS Dev.
Ordinary	0.45	2.2420	2.24201	-0.00001	1.93	2.53
	0.50	2.2160	2.21581	0.00019	[10 <sup>-4</sup> ]	
	0.60	2.1834	2.18384	-0.00044		
	0.70	2.1652	2.16542	-0.00022		
	0.80	2.1538	2.15355	0.00025	Expt.	
	0.90	2.1454	2.14525	0.00015	accuracy	
	1.00	2.1391	2.13904	0.00006	was not	
	1.20	2.1305	2.13003	0.00047	'mentioned	
	1.40	2.1236	2.12328	0.00032		

**Table 2.41: (Continued)**

Polarization	Wavelength ( $\mu\text{m}$ )	Observed [31]	Computed (This work)	Difference	Av. Dev.	RMS Dev.
	1.60	2.1174	2.11749	-0.00009		
	1.80	2.1120	2.11205	-0.00005		
	2.00	2.1066	2.10666	-0.00006		
	2.20	2.1009	2.10111	-0.00021		
	2.40	2.0951	2.09530	-0.00020		
	2.60	2.0891	2.08915	-0.00005		
	2.80	2.0825	2.08259	-0.00009		
	3.00	2.0755	2.07560	-0.00010		
	3.20	2.0680	2.06813	-0.00013		
	3.40	2.0601	2.06014	-0.00004		
	3.60	2.0513	2.05162	-0.00032		
	3.80	2.0424	2.04252	-0.00012		
	4.00	2.0335	2.03282	0.00068		
Extra-ordinary	0.45	2.2468	2.24688	-0.00008	1.8	2.5
	0.50	2.2205	2.22029	0.00021	$[10^{-4}]$	
	0.60	2.1878	2.18803	-0.00023		
	0.70	2.1696	2.16954	0.00006		
	0.80	2.1578	2.15766	0.00014		
	0.90	2.1493	2.14937	-0.00007	Expt.	
	1.00	2.1432	2.14318	0.00002	accuracy	
	1.20	2.1341	2.13420	-0.00010	was not	
	1.40	2.1273	2.12748	-0.00018	mentioned	
	1.60	2.1213	2.12173	-0.00043		
	1.80	2.1170	2.11633	0.00067		
	2.00	2.1115	2.11096	0.00054		
	2.20	2.1053	2.10545	-0.00015		
	2.40	2.0993	2.09968	-0.00038		
	2.60	2.0936	2.09357	0.00003		
	2.80	2.0871	2.08706	0.00004		
	3.20	2.0727	2.07269	0.00001		
	3.40	2.0649	2.06476	0.00014		
	3.60	2.0561	2.05629	-0.00019		
	3.80	2.0473	2.04725	0.00005		
	4.00	2.0377	2.03761	0.00009		

**Table 2.42:** The Experimental [97] and Computed Refractive Index Values of MDB Crystal at 23°C

Polari-zation	Wavelength ( $\mu\text{m}$ )	Observed [97]	Computed (This work)	Difference	Av. Dev.	RMS Dev.
<i>x</i> -axis	0.436	1.8027	1.80274	-0.000042	1.52	2.04
	0.492	1.7731	1.77282	0.000276	[10 <sup>-4</sup> ]	
	0.532	1.7586	1.75905	-0.000445		
	0.546	1.7554	1.75516	0.000242	Expt.	
	0.576	1.7480	1.74804	-0.000035	accuracy	
	0.579	1.7472	1.74740	-0.000200	is	
	0.589	1.7454	1.74537	0.000029	$\pm 0.0005$ .	
	0.633	1.7380	1.73781	0.000191		
	1.064	1.7094	1.70944	-0.000039		
	1.152	1.7072	1.70718	0.000024		
<i>y</i> -axis	0.436	1.7360	1.73599	0.000008	1.15	1.47
	0.492	1.7104	1.71039	0.000015	[10 <sup>-4</sup> ]	
	0.532	1.6984	1.69842	-0.000017		
	0.546	1.6950	1.69502	-0.000020		
	0.576	1.6889	1.68877	0.000132		
	0.579	1.6880	1.68821	-0.000209		
	0.589	1.6863	1.68642	-0.000121		
	0.633	1.6800	1.67973	0.000269		
	1.064	1.6538	1.65401	-0.000209		
	1.152	1.6520	1.65185	0.000152		
<i>z</i> -axis	0.436	1.5075	1.50747	0.000030	1.34	1.60
	0.492	1.4960	1.49621	-0.000207	[10 <sup>-4</sup> ]	
	0.532	1.4912	1.49108	0.000123		
	0.546	1.4897	1.48963	0.000068		
	0.576	1.4871	1.48698	0.000119		
	0.579	1.4868	1.48674	0.000056		
	0.589	1.4861	1.48599	0.000113		
	0.633	1.4828	1.48315	-0.000350		
	1.064	1.4714	1.47124	0.000164		
	1.152	1.4698	1.46992	-0.000115		

**Table 2.43: The Experimental [45] and Computed Refractive Index Values of NaNO<sub>3</sub> Crystal at 20°C**

Polarization	Wavelength (μm)	Observed [45]	Computed (This work)	Difference	Avg. Dev.	RMS Dev.
Ordinary	0.434	1.6126	1.612725	-0.000125	1.79 [10 <sup>-4</sup> ]	2.56
	0.436	1.6121	1.612109	-0.000009		
	0.486	1.5998	1.599620	0.000180		
	0.501	1.5968	1.596731	0.000069		
	0.546	1.5899	1.589700	0.000200		
	0.578	1.5860	1.585833	0.000167		
	0.589	1.5840	1.584673	-0.000673		
	0.656	1.5791	1.579009	0.000091		
	0.668	1.5783	1.578200	0.000100		
	0.434	1.340	1.33944	0.00056		
Extra-ordinary	0.436	1.340	1.33940	0.00060	3.72 [10 <sup>-4</sup> ]	4.77
	0.486	1.338	1.33833	-0.00033		
	0.501	1.337	1.33797	-0.00097		
	0.546	1.336	1.33598	0.00002		
	0.578	1.336	1.33637	-0.00037		
	0.589	1.336	1.33601	-0.00001		
	0.656	1.334	1.33395	0.00005		
	0.668	1.334	1.33356	0.00044		

**Table 2.44: The Experimental [108] and Computed Refractive Index Values of PbTe Semiconductor at 20°C**

Wavelength (μm)	Observed [108]	Computed (This work)	Difference	Avg. Dev.	RMS Dev.
3.850	6.16	6.159	0.001	1.3 [10 <sup>-2</sup> ]	1.9
4.000	6.02	6.021	-0.001		
4.133	5.95	5.961	-0.011		
4.428	5.90	5.893	0.007		
4.592	5.88	5.871	0.009		
4.769	5.85	5.852	-0.002		
4.959	5.84	5.837	0.003		
5.276	5.82	5.817	0.003		
5.636	5.80	5.798	0.002		
5.904	5.78	5.785	-0.005		
6.199	5.77	5.773	-0.003		
6.702	5.76	5.752	0.008		
6.888	5.72	5.744	-0.024		
8.856	5.68	5.659	0.021		
10.00	5.66	5.601	0.059		
10.20	5.55	5.590	-0.040		
10.64	5.54	5.566	-0.026		
11.11	5.52	5.538	-0.018		
11.90	5.48	5.488	-0.008		
12.50	5.45	5.446	0.004		
12.82	5.44	5.423	0.017		

**Table 2.45: The Experimental [9] and Computed Refractive Index Values of RDA Crystal at 33°C**

Polarization	Wavelength (μm)	Observed [9]	Computed (This work)	Difference	Av. RMS Dev. Dev.
Ordinary	0.404656	1.57882	1.578820	0.000000	1.3 [10 <sup>-5</sup> ] 1.7
	0.435833	1.57344	1.573440	0.000000	
	0.467815	1.56906	1.569050	0.000010	
	0.479991	1.56761	1.567608	0.000002	
	0.508582	1.56460	1.564616	-0.000016	Expt.
	0.546074	1.56134	1.561352	-0.000012	accuracy
	0.589300	1.55827	1.558269	0.000001	is
	0.643847	1.55512	1.555102	0.000018	±0.00003
	0.780027	1.54926	1.549234	0.000026	
	0.794760	1.54872	1.548706	0.000014	
	0.852113	1.54674	1.546769	-0.000029	
	0.894346	1.54541	1.545438	-0.000028	
	1.064000	1.54052	1.540506	0.000014	
	0.404656	1.53880	1.538914	-0.000114	3.5 [10 <sup>-5</sup> ] 4.3
	0.435833	1.53421	1.534234	-0.000024	
	0.467815	1.53052	1.530475	0.000045	
	0.479991	1.52932	1.529255	0.000065	Expt.
Extra-ordinary	0.508582	1.52678	1.526754	0.000026	accuracy
	0.546074	1.52410	1.524081	0.000019	is
	0.589300	1.52162	1.521628	-0.000008	±0.00003
	0.643847	1.51923	1.519209	0.000021	
	0.780027	1.51511	1.515129	-0.000019	
	0.794760	1.51476	1.514795	-0.000035	
	0.852113	1.51360	1.513625	-0.000025	
	0.894346	1.51285	1.512871	-0.000021	
	1.064000	1.51047	1.510431	0.000039	

**Table 2.46: The Experimental [9] and Computed Refractive Index Values of RD\*A Crystal at 33°C**

Polarization	Wavelength (μm)	Observed [9]	Computed (This work)	Difference	Av. RMS Dev. Dev.
Ordinary	0.404656	1.57325	1.573213	0.000037	4.2 [10 <sup>-5</sup> ] 5.0
	0.435833	1.56806	1.568092	-0.000032	
	0.467815	1.56388	1.563922	-0.000042	
	0.479991	1.56252	1.562557	-0.000037	Expt.
	0.508582	1.55977	1.559733	0.000037	accuracy
	0.546074	1.55663	1.556677	-0.000047	is
	0.579066	1.55457	1.554447	0.000123	±0.00003
	0.643847	1.55097	1.550954	0.000016	
	0.780027	1.54591	1.545882	0.000028	
	0.794760	1.54538	1.545447	-0.000067	
	0.852113	1.54384	1.543889	-0.000049	
	0.894346	1.54286	1.542852	0.000008	

**Table 2.46: (Continued)**

Polarization	Wavelength (μm)	Observed [9]	Computed (This work)	Difference	Av. RMS Dev. Dev.
Extra-ordinary	1.064000	1.53927	1.539244	0.000026	
	0.404656	1.53690	1.536876	0.000024	2.6 [ $10^{-5}$ ]
	0.435833	1.53231	1.532327	-0.000017	
	0.467815	1.52861	1.528648	-0.000038	
	0.479991	1.52745	1.527450	0.000000	Expt.
	0.508582	1.52498	1.524987	-0.000007	accuracy
	0.546074	1.52232	1.522350	-0.000030	$\pm 0.00003$
	0.579066	1.52054	1.520452	0.000088	
	0.643847	1.51756	1.517541	0.000019	
	0.780027	1.51356	1.513549	0.000011	
	0.794760	1.51320	1.513226	-0.000026	
	0.852113	1.51210	1.512104	-0.000004	
	0.894346	1.51134	1.511390	-0.000050	
	1.064000	1.50917	1.509141	0.000029	

**Table 2.47: The Experimental [9] and Computed Refractive Index Values of RDP Crystal at 33°C**

Polarization	Wavelength (μm)	Observed [9]	Computed (This work)	Difference	Av. RMS Dev. Dev.
Ordinary	0.404656	1.52078	1.520793	-0.000013	4.5 [ $10^{-5}$ ]
	0.435833	1.51741	1.517347	0.000063	
	0.467815	1.51447	1.514455	0.000015	
	0.479991	1.51343	1.513488	-0.000058	Expt.
	0.508582	1.51138	1.511448	-0.000068	accuracy
	0.546074	1.50915	1.509166	-0.000016	is
	0.589300	1.50697	1.506946	0.000024	$\pm 0.00003$
	0.643847	1.50469	1.504584	0.000106	
	0.780027	1.49995	1.499909	0.000041	
	0.794760	1.49946	1.499465	-0.000005	
	0.852113	1.49774	1.497801	-0.000061	
	0.894346	1.49655	1.496623	-0.000073	
	1.064000	1.49208	1.492035	0.000045	
Extra-ordinary	0.404656	1.48995	1.489930	0.000020	2.5 [ $10^{-5}$ ]
	0.435833	1.48689	1.486901	-0.000011	
	0.467815	1.48439	1.484406	-0.000016	
	0.479991	1.48356	1.483584	-0.000024	Expt.
	0.508582	1.48187	1.481876	-0.000006	accuracy
	0.546074	1.48002	1.480017	0.000003	is
	0.589300	1.47830	1.478277	0.000023	$\pm 0.00003$
	0.643847	1.47658	1.476522	0.000058	
	0.780027	1.47339	1.473439	-0.000049	
	0.794760	1.47321	1.473177	0.000033	
	0.852113	1.47222	1.472245	-0.000025	
	0.894346	1.47160	1.471631	-0.000031	
	1.064000	1.46957	1.469545	0.000025	

**Table 2.48: The Experimental [9] and Computed Refractive Index Values of RD\*P Crystal at 33°C**

Polarization	Wavelength (μm)	Observed [9]	Computed (This work)	Difference	Av. RMS Dev.	Dev. Dev.
Ordinary	0.404656	1.51655	1.516638	-0.000088	6.4	7.1
	0.435833	1.51325	1.513283	-0.000033	[ 10 <sup>-5</sup> ]	
	0.467815	1.51058	1.510511	0.000069		
	0.479991	1.50963	1.509594	0.000036		
	0.508582	1.50772	1.507679	0.000041		
	0.546074	1.50555	1.505568	-0.000018	Expt.	
	0.579066	1.50410	1.503996	0.000104	accuracy	
	0.643847	1.50150	1.501453	0.000047	± 0.00003	
	0.780027	1.49742	1.497467	-0.000047		
	0.794760	1.49705	1.497101	-0.000051		
	0.852113	1.49565	1.495746	-0.000096		
	0.894346	1.49472	1.494804	-0.000084		
	1.064000	1.49136	1.491239	0.000121		
	0.404656	1.48780	1.487770	0.000030	3.1	3.5
	0.435833	1.48486	1.484873	-0.000013	[ 10 <sup>-5</sup> ]	
	0.467815	1.48240	1.482454	-0.000054		
	0.479991	1.48162	1.481652	-0.000032	Expt.	
Extra-ordinary	0.508582	1.48001	1.479976	0.000034	accuracy	
	0.546074	1.47814	1.478143	-0.000003	± 0.00003	
	0.579066	1.47683	1.476797	0.000033		
	0.643847	1.47474	1.474687	0.000053		
	0.780027	1.47166	1.471684	-0.000024		
	0.794760	1.47146	1.471435	0.000025		
	0.852113	1.47050	1.470558	-0.000058		
	0.894346	1.46997	1.469991	-0.000021		
	1.064000	1.46818	1.468151	0.000029		

**Table 2.49: The Experimental [111] and Computed Refractive Index Values of Ruby Crystal at 22°C**

Polarization	Wavelength (μm)	Observed [111]	Computed (This work)	Difference	Av. Dev.	RMS Dev.
Ordinary	0.4358	1.78115	1.781162	-0.000012	1.25	1.27
	0.5461	1.77071	1.770720	-0.000010	[ 10 <sup>-5</sup> ]	
	0.5876	1.76822	1.768203	0.000017		
	0.6678	1.76445	1.764461	-0.000011	No expt.	
	0.7065	1.76302	1.763007	0.000013	accuracy	

**Table 2.49: (Continued)**

Polarization	Wavelength ( $\mu\text{m}$ )	Observed [111]	Computed (This work)	Difference	Av. Dev.	RMS Dev.
Extra-ordinary	0.4358	1.77276	1.772766	-0.000006	0.49	0.51
	0.5461	1.76258	1.762584	-0.000004	$[10^{-5}]$	
	0.5876	1.76010	1.760094	0.000006		
	0.6678	1.75641	1.756413	-0.000003		
	0.7065	1.75501	1.755005	0.000005		

**Table 2.50: The Experimental [9] and Computed Refractive Index Values of Se Crystal at  $23(\pm 2)^\circ\text{C}$** 

Polarization	Wavelength ( $\mu\text{m}$ )	Observed [9]	Computed (This work)	Difference	Av. Dev.	RMS Dev.
Ordinary	1.06	2.790	2.7900	0.0000	7.2	8.8
	1.15	2.737	2.7370	0.0000	$[10^{-8}]$	
	3.39	2.650	2.6500	0.0000	Expt. accuracy	
	10.60	2.600	2.6000	0.0000	$\pm 0.008 \sim$	$\pm 0.001$
Extra-ordinary	1.06	3.608	3.6080	0.0000	5.2	5.6
	1.15	3.573	3.5730	0.0000	$[10^{-8}]$	
	3.39	3.460	3.4600	0.0000		
	10.6	3.410	3.4100	0.0000		

**Table 2.51: The Experimental [113] and Computed Refractive Index Values of Si Semiconductor at  $25^\circ\text{C}$** 

Wavelength ( $\mu\text{m}$ )	Observed [113]	Computed (This work)	Difference	Av. Dev.	RMS Dev.
0.40	5.585	5.585	0.0000	0.00	0.00
0.49	4.345	4.345	0.0000		
0.63	3.877	3.877	0.0000		
0.78	3.695	3.695	0.0000		

**Table 2.52: The Experimental [116] and Computed Refractive Index Values of Quartz ( $\alpha\text{-SiO}_2$ ) Crystal at 25°C**

Polari-zation	Wavelength ( $\mu\text{m}$ )	Observed [116]	Computed (This work)	Difference	Av. RMS Dev. Dev.
Ordinary	0.1980	1.65087	1.650913	-0.000043	3.11 4.12
	0.2310	1.61395	1.613833	0.000117	[ $10^{-5}$ ]
	0.3400	1.56747	1.567550	-0.000080	
	0.3940	1.55846	1.558512	-0.000052	
	0.4340	1.55396	1.553974	-0.000014	
	0.5893	1.54424	1.544228	0.000012	
	0.7680	1.53903	1.539015	0.000015	
	0.8325	1.53773	1.537724	0.000006	
	0.9914	1.53514	1.535126	0.000014	Note:
	1.1592	1.53283	1.532810	0.000020	There is no
	1.3070	1.53090	1.530884	0.000016	experimental
	1.4792	1.52865	1.528624	0.000026	accuracy. But
	1.5414	1.52781	1.527787	0.000023	this fitting
	1.6815	1.52583	1.525836	-0.000006	accuracy is
	1.7614	1.52468	1.524677	0.000003	sufficient to
Extra-ordinary	1.9457	1.52184	1.521852	-0.000012	use this
	2.0531	1.52005	1.520098	-0.000048	Sellmeier.
	0.1850	1.68988	1.689469	0.000411	11.9 21.0
	0.1980	1.66394	1.664685	-0.000745	[ $10^{-5}$ ]
	0.2310	1.62555	1.625295	0.000255	
	0.3940	1.56805	1.567927	0.000123	
	0.4340	1.56339	1.563289	0.000101	
	0.5080	1.55746	1.557459	0.000001	
	0.5893	1.55335	1.553348	0.000002	
	0.7680	1.54794	1.548017	-0.000077	
	0.8325	1.54661	1.546690	-0.000080	
	0.9914	1.54392	1.544005	-0.000085	
	1.1592	1.54152	1.541590	-0.000070	
	1.3070	1.53951	1.539568	-0.000058	
	1.4792	1.53716	1.537187	-0.000027	
	1.5414	1.53630	1.536301	-0.000001	
	1.7614	1.53301	1.533008	0.000002	
	1.9457	1.53004	1.530009	0.000031	
	2.0531	1.52823	1.528145	0.000085	

**Table 2.53: The Experimental [48] and Computed Refractive Index Values of SrF<sub>2</sub> Crystal at 20°C**

Wavelength ( μm)	Observed [48]	Computed (This work)	Difference	Av. Dev.	RMS Dev.
0.25	1.47336	1.473356	0.000004	0.4	0.5
0.30	1.45922	1.459231	-0.000011	[10 <sup>-5</sup> ]	
0.35	1.45131	1.451311	-0.000001		
0.40	1.44639	1.446383	0.000007		
0.45	1.44309	1.443089	0.000001	Expt.	
0.50	1.44077	1.440766	0.000004	accuracy	
0.55	1.43906	1.439058	0.000002	was not	
0.65	1.43675	1.436745	0.000005	mentioned	
0.70	1.43593	1.435931	-0.000001		
0.75	1.43527	1.435264	0.000006		
0.85	1.43423	1.434234	-0.000004		
0.90	1.43382	1.433824	-0.000004		
1.00	1.43314	1.433145	-0.000005		
1.50	1.43095	1.430954	-0.000004		
2.00	1.42922	1.429220	0.000000		
2.50	1.42734	1.427348	-0.000008		
3.00	1.42519	1.425190	0.000000		
4.00	1.41982	1.419822	-0.000002		
5.00	1.41291	1.412912	-0.000002		
5.50	1.40884	1.408844	-0.000004		
6.00	1.40435	1.404349	0.000001		
6.50	1.39941	1.399412	-0.000002		
7.00	1.39402	1.394019	0.000001		
7.50	1.38816	1.388152	0.000008		
8.00	1.38180	1.381793	0.000007		
9.00	1.36752	1.367514	0.000006		
9.50	1.35955	1.359546	0.000004		
10.0	1.35099	1.350990	0.000000		

**Table 2.54: The Experimental [31] and Computed Refractive Index Values of SrMoO<sub>4</sub> Crystal at 25°C**

Polarization	Wavelength (μm)	Observed [31]	Computed (This work)	Difference	Av. RMS Dev.	Dev. Dev.
Ordinary	0.45	1.9424	1.94244	-0.00004	8.3	9.1
	0.50	1.9263	1.92618	0.00012	[ 10 <sup>-5</sup> ]	
	0.60	1.9064	1.90649	-0.00009		
	0.70	1.8952	1.89527	-0.00007		
	0.80	1.8881	1.88814	-0.00004		
	0.90	1.8834	1.88324	0.00016		
	1.00	1.8797	1.87966	0.00004		
	1.20	1.8747	1.87466	0.00004		
	1.40	1.8711	1.87117	-0.00007		
	1.60	1.8683	1.86837	-0.00007		
	1.80	1.8660	1.86590	0.00010		
	2.00	1.8635	1.86356	-0.00006		
	2.20	1.8611	1.86124	-0.00014		
	2.40	1.8590	1.85887	0.00013		
Extra-ordinary	0.45	1.9497	1.94938	0.00032	2.3	3.2
	0.50	1.9311	1.93180	-0.00070	[ 10 <sup>-4</sup> ]	
	0.60	1.9110	1.91082	0.00018		
	0.70	1.8993	1.89900	0.00030		
	0.80	1.8917	1.89154	0.00016		
	0.90	1.8864	1.88642	-0.00002		
	1.00	1.8827	1.88268	0.00002		
	1.20	1.8774	1.87745	-0.00005		
	1.40	1.8736	1.87377	-0.00017		
	1.60	1.8708	1.87079	0.00001		
	1.80	1.8683	1.86813	0.00017		
	2.00	1.8649	1.86559	-0.00069		
	2.20	1.8634	1.86306	0.00034		
	2.40	1.8606	1.86047	0.00013		

**Table 2.55: The Experimental and Computed Refractive Index Values of SrTiO<sub>3</sub> Crystal at 25°C**

Wavelength ( $\mu\text{m}$ )	Observed [45]	Computed (This work)	Difference	Av. Dev.	RMS Dev.
0.43583	2.5680	2.567452	0.000548	4.17	5.47
0.48613	2.4897	2.490547	-0.000847	[ $10^{-4}$ ]	
0.54607	2.4346	2.435129	-0.000529		
0.57696	2.4149	2.415121	-0.000221		
0.57907	2.4137	2.413907	-0.000207	Expt.	
0.58926	2.4081	2.408260	-0.000160	accuracy	
0.65628	2.3790	2.378834	0.000166	was not	
0.66782	2.3750	2.374815	0.000185	mentioned	
0.70652	2.3634	2.362965	0.000435		
0.76786	2.3488	2.348165	0.000635		
0.85212	2.3337	2.333189	0.000511		
0.89440	2.3276	2.327272	0.000328		
1.01398	2.3147	2.314275	0.000425		
1.12866	2.3055	2.305173	0.000327		
1.36220	2.2921	2.291930	0.000170		
1.51700	2.2859	2.285187	0.000713		
1.52952	2.2848	2.284682	0.000118		
1.70120	2.2783	2.278165	0.000135		
1.81307	2.2744	2.274186	0.000214		
1.87100	2.2710	2.272172	-0.001172		
1.91800	2.2704	2.270553	-0.000153		
2.15260	2.2624	2.262535	-0.000135		
2.31260	2.2564	2.257001	-0.000601		
2.43740	2.2525	2.252589	-0.000089		
2.56280	2.2466	2.248040	-0.001440		
2.67070	2.2438	2.244016	-0.000216		
2.72480	2.2404	2.241957	-0.001557		
3.24340	2.2211	2.220550	0.000550		
3.30260	2.2181	2.217893	0.000207		
3.42260	2.2124	2.212361	0.000039		
3.50700	2.2088	2.208349	0.000451		
3.55640	2.2063	2.205953	0.000347		

**Table 2.56:** The Experimental and Computed Refractive Index Values of  $\text{TiO}_2$  Crystal at 25°C

Polarization	Wavelength ( $\mu\text{m}$ )	Observed [45]	Computed (This work)	Difference	Av. Dev.	RMS Dev.
Ordinary	0.4358	2.853	2.853011	-0.000011	0.66	0.90
	0.4916	2.725	2.725106	-0.000106	[ $10^{-4}$ ]	
	0.4960	2.718	2.717818	0.000182		
	0.5461	2.652	2.652076	-0.000076	No expt.	
	0.5770	2.623	2.622880	0.000120	accuracy	
	0.5791	2.621	2.621125	-0.000125		
	0.6907	2.555	2.555006	-0.000006		
	0.7082	2.548	2.547990	0.000010		
	1.0140	2.484	2.483982	0.000018		
	1.5296	2.454	2.454005	-0.000005		
Extra-ordinary	0.4358	3.216	3.216017	-0.000017	2.06	2.95
	0.4916	3.051	3.051127	-0.000127	[ $10^{-4}$ ]	
	0.4960	3.042	3.041806	0.000194		
	0.5461	2.958	2.958061	-0.000061		
	0.5770	2.921	2.921066	-0.000066	No expt.	
	0.5791	2.919	2.918845	0.000155	accuracy	
	0.6907	2.836	2.835520	0.000480		
	0.7082	2.826	2.826716	-0.000716		
	1.0140	2.747	2.746800	0.000200		
	1.5296	2.710	2.710042	-0.000042		

**Table 2.57:** The Experimental [119] and Computed Refractive Index Values of  $\text{Tl}_3\text{AsSe}_3$  Crystal at 25°C

Polarization	Wavelength ( $\mu\text{m}$ )	Observed [119]	Computed (This work)	Difference	Av. Dev.	RMS Dev.
Ordinary	2.056	3.419	3.419056	-0.000056	5.0	5.8
	3.05	3.380	3.379361	0.000639	[ $10^{-4}$ ]	
	4.060	3.364	3.365053	-0.001053		
	5.035	3.357	3.357617	-0.000617		
	5.856	3.354	3.353210	0.000790		
	6.945	3.349	3.348413	0.000587		

**Table 2.57: (Continued)**

Polarization	Wavelength ( $\mu\text{m}$ )	Observed [119]	Computed (This work)	Difference	Av. Dev.	RMS Dev.
Extra-ordinary	7.854	3.345	3.344744	0.000256		
	9.016	3.340	3.340075	-0.000075		
	9.917	3.336	3.336306	-0.000306		
	10.961	3.331	3.331658	-0.000658		
	12.028	3.327	3.326508	0.000492		
	2.056	3.227	3.227038	-0.000038	3.2	3.8
	3.059	3.190	3.189584	0.000416	[ $10^{-4}$ ]	
	4.060	3.177	3.177459	-0.000459		
	5.035	3.171	3.171429	-0.000429		
	5.856	3.168	3.167944	0.000056		
	6.945	3.164	3.164216	-0.000216		
	7.854	3.162	3.161400	0.000600		
	9.016	3.158	3.157847	0.000153		
	9.917	3.155	3.154993	0.000007		
	10.961	3.152	3.151485	0.000515		
	12.028	3.147	3.147607	-0.000607		

**Table 2.58: The Experimental and Computed Refractive Index Values of KRS-6 Crystal at 25°C**

Wavelength ( $\mu\text{m}$ )	Observed [120]	Computed (This work)	Difference	Av. Dev.	RMS Dev.
Na-D	2.3367	2.336771	-0.000071	6.6	11.25
	0.6	2.3294	2.331227	-0.001827	[ $10^{-4}$ ]
	0.7	2.2982	2.292358	0.005842	
	0.8	2.2660	2.268256	-0.002256	
	1.0	2.2404	2.240943	-0.000543	Note: The composition of KRS-6 used was 44% TlBr and 56% TlCl.
	1.1	2.2321	2.232719	-0.000619	
	1.2	2.2255	2.226518	-0.001018	
	1.3	2.2212	2.221718	-0.000518	
	1.4	2.2176	2.217921	-0.000321	
	1.6	2.2124	2.212350	0.000050	
	1.7	2.2103	2.210264	0.000036	
	1.8	2.2086	2.208506	0.000094	

**Table 2.58: (Continued)**

Wavelength ( $\mu\text{m}$ )	Observed [120]	Computed (This work)	Difference	Av. Dev.	RMS Dev.
1.9	2.2071	2.207008	0.000092	Expt.	
2.2	2.2039	2.203609	0.000291	accuracy	
2.4	2.2024	2.201956	0.000444	was not	
2.6	2.2011	2.200617	0.000483	mentioned	
3.0	2.1990	2.198549	0.000451		
3.5	2.1972	2.196619	0.000581		
4.0	2.1956	2.195055	0.000545		
4.5	2.1942	2.193663	0.000537		
5.0	2.1928	2.192340	0.000460		
7.0	2.1870	2.186874	0.000126		
8.0	2.1830	2.183772	-0.000772		
9.0	2.1805	2.180335	0.000165		
10.0	2.1767	2.176532	0.000168		
12.0	2.1674	2.167749	-0.000349		
14.0	2.1563	2.157295	-0.000995		
16.0	2.1442	2.145067	-0.000867		
17.0	2.1377	2.138253	-0.000553		
19.0	2.1236	2.123152	0.000445		
21.0	2.1067	2.105973	0.000727		
22.0	2.0976	2.096558	0.001042		
24.0	2.0752	2.075967	-0.000767		

**Table 2.59: The Experimental and Computed Refractive Index Values of  $\text{Y}_3\text{Al}_5\text{O}_{12}$  (YAG) Crystal at 25°C**

Wavelength ( $\mu\text{m}$ )	Observed [31]	Computed (This work)	Difference	Av. Dev.	RMS Dev.
0.40	1.8650	1.86488	0.00012	1.5	2.3
0.45	1.8532	1.85325	-0.00005	[ $10^{-4}$ ]	
0.50	1.8450	1.84519	-0.00019		
0.60	1.8347	1.83489	-0.00019		
0.70	1.8285	1.82867	-0.00017		
0.80	1.8245	1.82450	0.00000	Expt.	
0.90	1.8222	1.82145	0.00075	accuracy	
1.00	1.8197	1.81906	0.00064	was not	
1.10	1.8170	1.81707	-0.00007	mentioned	

**Table 2.59: (Continued)**

Wavelength ( $\mu\text{m}$ )	Observed [31]	Computed (This work)	Difference	Av. Dev.	RMS Dev.
1.20	1.8152	1.81534	-0.00014		
1.40	1.8121	1.81227	-0.00017		
1.60	1.8093	1.80942	-0.00012		
1.80	1.8065	1.80657	-0.00007		
2.00	1.8035	1.80361	-0.00011		
2.20	1.8004	1.80048	-0.00008		
2.40	1.7970	1.79714	-0.00014		
2.60	1.7935	1.79355	-0.00005		
2.80	1.7896	1.78969	-0.00009		
3.00	1.7855	1.78555	-0.00005		
3.20	1.7810	1.78111	-0.00011		
3.40	1.7764	1.77636	0.00004		
3.60	1.7713	1.77127	0.00003		
3.80	1.7659	1.76584	0.00006		
4.00	1.7602	1.76004	0.00016		

**Table 2.60: The Experimental [31] and Computed Refractive Index Values of ZnS Crystal at 25°C**

Wavelength ( $\mu\text{m}$ )	Observed [31]	Computed (This work)	Difference	Av. Dev.	RMS Dev.
0.45	2.47090	2.470904	-0.000004	2.4	3.5
0.50	2.42080	2.420841	-0.000041	$[10^{-4}]$	
0.60	2.36400	2.363876	0.000124		
0.70	2.33330	2.333246	0.000054		
0.80	2.31460	2.314619	-0.000019		
0.90	2.30260	2.302333	0.000267		
1.00	2.29320	2.293738	-0.000538		
1.20	2.28220	2.282669	-0.000469		
1.40	2.27620	2.275915	0.000285		
1.60	2.27160	2.271340	0.000260		
1.80	2.26800	2.267967	0.000033		
2.00	2.26530	2.265293	0.000007		
2.20	2.26370	2.263035	0.000665		
2.40	2.26040	2.261024	-0.000624		

**Table 2.61: The Experimental and Computed Refractive Index Values of ZnO Crystal at 25°C**

Polarization	Wavelength (μm)	Observed [31]	Computed (This work)	Difference	Avg. Dev.	RMS Dev.
Ordinary	0.45	2.1058	2.10574	0.00006	4.5	7.2
	0.50	2.0511	2.05127	-0.00017	[ 10 <sup>-4</sup> ]	
	0.60	1.9985	1.99853	-0.00003		
	0.70	1.9735	1.97341	0.00009		
	0.80	1.9597	1.95902	0.00068		
	0.90	1.9493	1.94981	-0.00051		
	1.00	1.9435	1.94345	0.00005		
	1.20	1.9354	1.93519	0.00021		
	1.40	1.9298	1.92993	-0.00013	Expt.	
	1.60	1.9257	1.92608	-0.00038	accuracy	
	1.80	1.9226	1.92296	-0.00036	was not	
	2.00	1.9197	1.92020	-0.00050	mentioned	
	2.20	1.9173	1.91762	-0.00032		
	2.40	1.9152	1.91510	0.00010		
	2.60	1.9128	1.91257	0.00023		
	2.80	1.9100	1.90998	0.00002		
	3.00	1.9075	1.90729	0.00021		
	3.20	1.9049	1.90448	0.00042		
	3.40	1.9022	1.90153	0.00067		
	3.60	1.8994	1.89842	0.00098		
	3.80	1.8964	1.89514	0.00126		
	4.00	1.8891	1.89168	-0.00258		
Extra-ordinary	0.45	2.1231	2.12277	0.00033	4.6	5.7
	0.50	2.0681	2.06876	-0.00066	[ 10 <sup>-4</sup> ]	
	0.60	2.0147	2.01526	-0.00056		
	0.70	1.9897	1.98937	0.00033		
	0.80	1.9752	1.97442	0.00078		
	0.90	1.9654	1.96483	0.00057		
	1.00	1.9589	1.95818	0.00072	No expt.	
	1.20	1.9500	1.94958	0.00042	accuracy	
	1.40	1.9429	1.94412	-0.00122		
	1.60	1.9402	1.94017	0.00003		
	1.80	1.9370	1.93700	0.00000		
	2.00	1.9330	1.93424	-0.00124		
	2.20	1.9313	1.93167	-0.00037		
	2.40	1.9297	1.92919	0.00051		
	2.60	1.9265	1.92671	-0.00021		
	2.80	1.9251	1.92419	0.00091		
	3.00	1.9214	1.92158	-0.00018		
	3.20	1.9186	1.91887	-0.00027		
	3.40	1.9160	1.91602	-0.00002		
	3.60	1.9127	1.91303	-0.00033		
	3.80	1.9101	1.90988	0.00022		
	4.00	1.9068	1.90655	0.00025		

**Table 2.62:** The Experimental and Computed Refractive Index Values of  $\beta$ -ZnS Crystal at 21.6°C

Wavelength ( $\mu\text{m}$ )	Observed [48]	Computed (This work)	Difference	Avg. Dev.	RMS Dev.
0.55	2.38579	2.385725	0.000065	3.4	4.8
0.60	2.36237	2.362420	-0.000050	[10 <sup>-5</sup> ]	
0.65	2.34509	2.345132	-0.000042		
0.70	2.33189	2.331904	-0.000014		
0.75	2.32135	2.321530	-0.000180	Expt.	
0.80	2.31327	2.313225	0.000045	accuracy	
0.85	2.30652	2.306460	0.000060	was not	
0.90	2.30093	2.300870	0.000060	mentioned	
0.95	2.29626	2.296190	0.000070		
1.00	2.29230	2.292228	0.000072		
1.50	2.27209	2.272064	0.000026		
2.00	2.26453	2.264538	-0.000008		
2.50	2.26030	2.260322	-0.000022		
3.00	2.25719	2.257218	-0.000028		
3.50	2.25445	2.254485	-0.000035		
4.00	2.25178	2.251812	-0.000032		
4.50	2.24903	2.249049	-0.000019		
5.00	2.24610	2.246113	-0.000013		
5.50	2.24294	2.242952	-0.000012		
6.00	2.23953	2.239532	-0.000002		
6.50	2.23583	2.235827	0.000003		
7.00	2.23183	2.231814	0.000016		
7.50	2.22749	2.227473	0.000017		
8.00	2.22280	2.222785	0.000015		
8.50	2.21775	2.217731	0.000019		
9.00	2.21231	2.212291	0.000019		
9.50	2.20645	2.206443	0.000007		
10.00	2.20016	2.200165	-0.000005		
10.50	2.19340	2.193432	-0.000032		

**Table 2.63:** The Experimental and Computed Refractive Index Values of  $\alpha$ -ZnS Crystal at 25°C

Polarization	Wavelength ( $\mu\text{m}$ )	Observed [123]	Computed (This work)	Difference	Avg. Dev.	RMS Dev.
Ordinary	0.360	2.705	2.7035	0.0015	0.0013	0.0018
	0.375	2.637	2.6391	-0.0021		
	0.400	2.560	2.5629	-0.0029		
	0.410	2.539	2.5397	-0.0007		
	0.420	2.522	2.5194	0.0026		
	0.425	2.511	2.5103	0.0007		
	0.430	2.502	2.5016	0.0004		
	0.440	2.486	2.4859	0.0001		

**Table 2.63: (Continued)**

Polarization	Wavelength ( $\mu\text{m}$ )	Observed [123]	Computed (This work)	Difference	Av. Dev.	RMS Dev.
Ordinary	0.450	2.473	2.4718	0.0012		
	0.460	2.459	2.4593	-0.0003		
	0.470	2.448	2.4480	0.0000		
	0.475	2.445	2.4427	0.0023	Expt. accuracy was not mentioned	
	0.480	2.438	2.4377	0.0003		
	0.490	2.428	2.4284	-0.0004		
	0.500	2.421	2.4200	0.0010		
	0.525	2.402	2.4017	0.0003		
	0.550	2.386	2.3869	-0.0009		
	0.575	2.375	2.3746	0.0004		
	0.600	2.363	2.3642	-0.0012		
	0.625	2.354	2.3554	-0.0014		
	0.650	2.346	2.3479	-0.0019		
	0.675	2.339	2.3413	-0.0023		
	0.700	2.332	2.3356	-0.0036		
	0.800	2.324	2.3187	0.0053		
	0.900	2.310	2.3078	0.0022		
	1.000	2.301	2.3003	0.0007		
	1.200	2.290	2.2909	-0.0009		
	1.400	2.285	2.2854	-0.0004		
Extra- ordinary	0.360	2.709	2.7071	0.0019	0.0015	0.0018
	0.375	2.640	2.6427	-0.0027		
	0.400	2.564	2.5666	-0.0026		
	0.410	2.544	2.5434	0.0006	Expt. accuracy was not mentioned	
	0.420	2.525	2.5232	0.0018		
	0.425	2.514	2.5140	0.0000		
	0.430	2.505	2.5055	-0.0005		
	0.440	2.488	2.4898	-0.0018		
	0.450	2.477	2.4758	0.0012		
	0.460	2.463	2.4633	-0.0003		
	0.470	2.453	2.4520	0.0010		
	0.475	2.449	2.4468	0.0022		
	0.480	2.443	2.4418	0.0012		
	0.490	2.433	2.4326	0.0004		
	0.500	2.425	2.4241	0.0009		
	0.525	2.407	2.4060	0.0010		
	0.550	2.392	2.3912	0.0008		
	0.575	2.378	2.3789	-0.0009		
	0.600	2.368	2.3686	-0.0006		
	0.625	2.358	2.3598	-0.0018		
	0.650	2.350	2.3523	-0.0023		
	0.675	2.343	2.3458	-0.0028		
	0.700	2.337	2.3400	-0.0030		
	0.800	2.328	2.3231	0.0049		
	0.900	2.315	2.3120	0.0030		
	1.000	2.303	2.3043	-0.0013		
	1.200	2.294	2.2944	-0.0004		
	1.400	2.288	2.2881	-0.0001		

**Table 2.64: The Experimental and Computed Refractive Index Values of ZnSe Crystal at 20.3°C**

Wavelength ( $\mu\text{m}$ )	Observed [48]	Computed (This work)	Difference	Av. Dev.	RMS Dev.
0.55	2.66246	2.661902	0.000558	1.4	2.0
0.60	2.61380	2.614398	-0.000598	[ $10^{-4}$ ]	
0.65	2.58054	2.581104	-0.000564		
0.70	2.55636	2.556669	-0.000309		
0.75	2.53804	2.538104	-0.000064	Expt.	
0.80	2.52373	2.523610	0.000120	accuracy	
0.85	2.51230	2.512043	0.000257	was not	
0.90	2.50298	2.502643	0.000337	mentioned	
0.95	2.49528	2.494886	0.000394		
1.00	2.48882	2.488400	0.000420		
1.50	2.45708	2.456767	0.000313		
2.00	2.44620	2.446043	0.000157		
2.50	2.44087	2.440804	0.000066		
3.00	2.43758	2.437571	0.000009		
3.50	2.43517	2.435196	-0.000026		
4.00	2.43316	2.433208	-0.000048		
4.50	2.43132	2.431382	-0.000062		
5.00	2.42953	2.429601	-0.000071		
5.50	2.42772	2.427797	-0.000077		
6.00	2.42584	2.425929	-0.000089		
6.50	2.42388	2.423969	-0.000089		
7.00	2.42181	2.421898	-0.000088		
7.50	2.41961	2.419702	-0.000092		
8.00	2.41728	2.417370	-0.000090		
8.50	2.41481	2.414893	-0.000083		
9.00	2.41218	2.412263	-0.000083		
9.50	2.40939	2.409472	-0.000082		
10.00	2.40644	2.406513	-0.000073		
10.50	2.40331	2.403380	-0.000070		
11.00	2.40000	2.400065	-0.000065		
11.50	2.39650	2.396562	-0.000062		
12.00	2.39281	2.392863	-0.000053		
12.50	2.38892	2.388960	-0.000040		
13.00	2.38481	2.384846	-0.000036		
13.50	2.38048	2.380512	-0.000032		
14.00	2.37593	2.375948	-0.000018		
14.50	2.37114	2.371146	-0.000006		
15.00	2.36610	2.366094	0.000006		
15.50	2.36080	2.360781	0.000019		
16.00	2.35523	2.355197	0.000033		
16.50	2.34937	2.349326	0.000044		
17.00	2.34322	2.343157	0.000063		
17.50	2.33675	2.336673	0.000077		
18.00	2.32996	2.329859	0.000101		

**Table 2.65: The Experimental and Computed Refractive Index Values of  $\text{ZnWO}_4$  Crystal at 25°C**

Polarization	Wavelength ( $\mu\text{m}$ )	Observed [31]	Computed (This work)	Difference	Av. RMS Dev.	Dev. Dev.
<i>x</i>	0.42	2.2587	2.25858	0.00012	1.9	2.6
	0.45	2.2344	2.23446	-0.00006	[10 <sup>-4</sup> ]	
	0.50	2.2059	2.20614	-0.00024		
	0.55	2.1870	2.18685	0.00015		
	0.60	2.1728	2.17299	-0.00019		
	0.65	2.1626	2.16263	-0.00003		
	0.80	2.1434	2.14317	0.00023		
	0.90	2.1356	2.13537	0.00023		
	1.00	2.1299	2.12971	0.00019		
	1.10	2.1255	2.12536	0.00014		
	1.20	2.1220	2.12187	0.00013	Expt.	
	1.40	2.1165	2.11642	0.00008	accuracy	
	1.60	2.1121	2.11206	0.00004	was not	
	1.80	2.1083	2.10822	0.00008	mentioned	
	2.00	2.1047	2.10458	0.00012		
	2.20	2.1011	2.10098	0.00012		
	2.80	2.0893	2.08947	-0.00017		
	3.00	2.0852	2.08523	-0.00003		
	3.20	2.0807	2.08074	-0.00004		
	3.40	2.0752	2.07597	-0.00077		
	3.60	2.0711	2.07091	0.00019		
	3.80	2.0658	2.06553	0.00027		
	4.00	2.0603	2.05982	0.00048		
<i>y</i>	0.42	2.2788	2.27927	-0.00047	1.5	2.3
	0.45	2.2555	2.25464	0.00086	[10 <sup>-4</sup> ]	
	0.50	2.2253	2.22536	-0.00006		
	0.60	2.1905	2.19058	-0.00008		
	0.80	2.1590	2.15884	0.00016		
	0.90	2.1508	2.15049	0.00031		
	1.00	2.1447	2.14442	0.00028	No expt.	
	1.10	2.1400	2.13977	0.00023	accuracy	
	1.20	2.1363	2.13605	0.00025		
	1.40	2.1305	2.13027	0.00023		
	1.60	2.1260	2.12569	0.00031		

**Table 2.65: (Continued)**

Polari-zation	Wavelength ( $\mu\text{m}$ )	Observed [31]	Computed (This work)	Difference	Av. RMS Dev. Dev.
z	1.80	2.1220	2.12170	0.00030	
	2.00	2.1182	2.11795	0.00025	
	2.20	2.1145	2.11426	0.00024	
	2.40	2.1080	2.11051	-0.00251	
	2.80	2.1027	2.10257	0.00013	
	3.00	2.0984	2.09829	0.00011	
	3.20	2.0939	2.09376	0.00014	
	3.40	2.0892	2.08896	0.00024	
	3.60	2.0841	2.08386	0.00024	
	0.42	2.4497	2.45017	-0.00047	1.7 2.6
z	0.45	2.4191	2.41813	0.00097	$[10^{-4}]$
	0.50	2.3802	2.38049	-0.00029	
	0.65	2.3224	2.32262	-0.00022	
	0.70	2.3118	2.31198	-0.00018	No expt.
	0.80	2.2970	2.29672	0.00028	accuracy
	0.90	2.2865	2.28634	0.00016	
	1.00	2.2790	2.27881	0.00019	
	1.10	2.2731	2.27303	0.00007	
	1.20	2.2684	2.26839	0.00001	
	1.40	2.2612	2.26116	0.00004	
	1.60	2.2554	2.25539	0.00001	
	1.80	2.2503	2.25031	-0.00001	
	2.00	2.2455	2.24551	-0.00001	
	2.20	2.2406	2.24075	-0.00015	
	2.40	2.2359	2.23591	-0.00001	
	2.60	2.2309	2.23087	0.00003	
	2.80	2.2254	2.22559	-0.00019	
	3.00	2.2199	2.22000	-0.00010	
	3.20	2.2140	2.21409	-0.00009	
	3.40	2.2079	2.20780	0.00010	
	3.60	2.2013	2.20112	0.00018	

**Table 2.66: The Experimental and Computed Refractive Index Values of  $\text{ZrO}_2:12\% \text{Y}_2\text{O}_3$  Crystal at 25°C**

Wavelength ( $\mu\text{m}$ )	Observed [124]	Computed (This work)	Difference	Av. RMS Dev. Dev.
0.361051	2.25364	2.253573	0.000067	4.77 7.12
0.365015	2.24990	2.249879	0.000021	$[10^{-5}]$
0.365483	2.24947	2.249453	0.000017	
0.366308	2.24871	2.248706	0.000004	
0.388865	2.23052	2.230547	-0.000027	Expt.
0.404656	2.21986	2.219989	-0.000129	accuracy
0.435833	2.20290	2.203014	-0.000114	$\pm 0.00005$
0.447148	2.19783	2.197859	-0.000029	
0.467815	2.18956	2.189532	0.000028	
0.479991	2.18523	2.185190	0.000040	
0.492193	2.18120	2.181199	0.000001	
0.501567	2.17835	2.178351	-0.000001	
0.508582	2.17639	2.176335	0.000055	
0.546073	2.16694	2.166962	-0.000022	
0.576959	2.16066	2.160678	-0.000018	
0.579066	2.16026	2.160288	-0.000028	
0.587566	2.15878	2.158760	0.000020	
0.601033	2.15649	2.156478	0.000012	
0.621287	2.15334	2.153334	0.000006	
0.643847	2.15026	2.150188	0.000072	
0.658651	2.14833	2.148302	0.000028	
0.662865	2.14781	2.147788	0.000022	
0.667815	2.14723	2.147197	0.000033	
0.672328	2.14669	2.146670	0.000020	
0.687045	2.14503	2.145023	0.000007	
0.697329	2.14394	2.143934	0.000006	
0.706518	2.14303	2.143000	0.000030	
0.722853	2.14144	2.141427	0.000013	
0.727995	2.14097	2.140953	0.000017	
0.728135	2.14098	2.140940	0.000040	
0.760901	2.13812	2.138137	-0.000017	
0.794411	2.13559	2.135606	-0.000016	
0.852110	2.13192	2.131882	0.000038	
0.894350	2.12959	2.129558	0.00003	

**Table 2.66: (Continued)**

Wavelength ( $\mu\text{m}$ )	Observed [124]	Computed (This work)	Difference	Av. RMS Dev. Dev.
0.917224	2.12842	2.128413	0.000007	
1.002439	2.12476	2.124708	0.000052	
1.012360	2.12437	2.124325	0.000045	
1.013975	2.12425	2.124263	-0.000013	
1.039460	2.12338	2.123318	0.000062	
1.083030	2.12184	2.121814	0.000026	
1.128660	2.12038	2.120366	0.000014	
1.148000	2.11967	2.119786	-0.000116	
1.188900	2.11861	2.118617	-0.000007	4.77 7.12
1.197730	2.11817	2.118374	-0.000204	$[10^{-5}]$
1.357021	2.11439	2.114414	-0.000024	
1.358900	2.11435	2.114371	-0.000021	
1.408000	2.11319	2.113274	-0.000084	
1.459500	2.11194	2.112165	-0.000225	
1.529582	2.11072	2.110710	0.000010	
1.688000	2.10747	2.107567	-0.000097	
1.692720	2.10749	2.107476	0.000014	
1.712810	2.10716	2.107086	0.000074	
1.800000	2.10534	2.105408	-0.000068	
1.860000	2.10425	2.104258	-0.000008	
1.965000	2.10219	2.102242	-0.000052	
2.058090	2.10047	2.100437	0.000033	
2.228000	2.09707	2.097074	-0.000004	
2.371000	2.09419	2.094147	0.000043	
2.389000	2.09381	2.093771	0.000039	
3.270000	2.07295	2.072789	0.000161	
3.300000	2.07203	2.071974	0.000056	
3.425000	2.06869	2.068495	0.000195	
3.505000	2.06633	2.066201	0.000129	
4.225000	2.04282	2.043035	-0.000215	
4.271000	2.04127	2.041393	-0.000123	
5.079000	2.00916	2.009135	0.000025	
5.120000	2.00732	2.007318	0.000002	
5.135000	2.00664	2.006649	-0.000009	

**Table 2.67: The Experimental and Computed Refractive Index Values of Alimino-Silicate (Corning code 1723) Glass at 28°C**

Wavelength ( $\mu\text{m}$ )	Observed [128]	Computed (This work)	Difference	Av. RMS Dev. Dev.
0.36502	1.57093	1.570926	0.000004	
0.40466	1.56405	1.564053	-0.000003	2.71 3.66
0.43584	1.56000	1.560006	-0.000006	$[10^{-5}]$
0.54607	1.55100	1.550988	0.000012	
0.57800	1.54928	1.549287	-0.000007	
1.01398	1.53854	1.538530	0.000010	
1.12866	1.53699	1.537004	-0.000014	Expt.
1.36728	1.53419	1.534149	0.000041	accuracy
1.47000	1.53292	1.532953	-0.000033	$\pm 9.6$ to
1.52952	1.53224	1.532255	-0.000015	$\pm 21$
1.66000	1.53078	1.530692	0.000088	$[10^{-5}]$
1.70100	1.53014	1.530189	-0.000049	
1.98100	1.52648	1.526542	-0.000062	
2.26200	1.52245	1.522415	0.000035	

**Table 2.68: The Experimental and Computed Refractive Index Values of BaLF4 (BAL) Glass at 20°C**

Wavelength ( $\mu\text{m}$ )	Observed [126]	Computed (This work)	Difference	Av. Dev.	RMS Dev.
0.33410	1.61618	1.616168	0.000012	0.84	0.97
0.36500	1.60670	1.606719	-0.000019		$[10^{-5}]$
0.40470	1.59807	1.598073	-0.000003		
0.43580	1.59307	1.593078	-0.000008		
0.48000	1.58773	1.587721	0.000009		
0.48610	1.58710	1.587103	-0.000003		
0.54610	1.58214	1.582128	0.000012		
0.58760	1.57957	1.579559	0.000011	Expt.	
0.58930	1.57947	1.579465	0.000005	accuracy	
0.63280	1.57731	1.577308	0.000002	$\pm 0.00003$	
0.64380	1.57683	1.576827	0.000003		
0.65630	1.57631	1.576309	0.000001		
0.70650	1.57447	1.574475	-0.000005		
0.85210	1.57065	1.570655	-0.000005		
1.01400	1.56776	1.567775	-0.000015		
1.06000	1.56708	1.567093	-0.000013		
1.52960	1.56131	1.561300	0.000010		
1.97010	1.55592	1.555906	0.000014		
2.32540	1.55091	1.550919	-0.000009		

**Table 2.69:** The Experimental and Computed Refractive Index Values of BK7 (S-BSL7) Glass at 20°C

Wavelength ( $\mu\text{m}$ )	Observed [126]	Computed (This work)	Difference	Av. Dev.	RMS Dev.
0.31260	1.54862	1.548601	0.000019	0.66	0.83
0.33410	1.54272	1.542742	-0.000022	[ $10^{-5}$ ]	
0.36500	1.53627	1.536278	-0.000008		
0.40470	1.53024	1.530238	0.000002		
0.43580	1.52668	1.526688	-0.000008		
0.48000	1.52283	1.522825	0.000005		
0.48610	1.52238	1.522375	0.000005		
0.54610	1.51872	1.518715	0.000005	Expt.	
0.58760	1.51680	1.516793	0.000007	accuracy is	
0.58930	1.51673	1.516723	0.000007	$\pm 0.00003$	
0.63280	1.51509	1.515085	0.000005		
0.64380	1.51472	1.514717	0.000003		
0.65630	1.51432	1.514318	0.000002		
0.70650	1.51289	1.512891	-0.000001		
0.85210	1.50980	1.509806	-0.000006		
1.01400	1.50731	1.507314	-0.000004		
1.06000	1.50669	1.506695	-0.000005		
1.52960	1.50091	1.500918	-0.000008		
1.97010	1.49495	1.494954	-0.000004		
2.32540	1.48921	1.489203	0.000007		

**Table 2.70:** The Experimental [125] and Computed Refractive Index Values of BSM9 (SK9) Glass at 20°C

Wavelength ( $\mu\text{m}$ )	Observed [125]	Computed (This work)	Difference	Av . RMS Dev. Dev.
0.365015	1.64199	1.641987	0.0000033	0.3 0.3
0.404656	1.63315	1.633152	-0.0000015	[ $10^{-5}$ ]
0.435835	1.62800	1.628005	-0.0000049	
0.441570	1.62718	1.627186	-0.0000060	
0.479990	1.62249	1.622489	0.0000005	Expt.
0.486130	1.62185	1.621847	0.0000033	accuracy
0.546070	1.61671	1.616707	0.0000026	is
0.587560	1.61405	1.614046	0.0000038	$\pm 0.00003$
0.589290	1.61395	1.613947	0.0000028	
0.632800	1.61171	1.611710	0.0000000	

**Table 2.70: (Continued)**

Wavelength ( $\mu\text{m}$ )	Observed [125]	Computed (This work)	Difference	Av . RMS Dev. Dev.
0.643850	1.61121	1.611210	0.0000004	
0.656270	1.61068	1.610675	0.0000045	
0.706520	1.60877	1.608771	-0.0000014	
0.768190	1.60687	1.606872	-0.0000018	
0.852110	1.60481	1.604813	-0.0000035	
1.013980	1.60184	1.601841	-0.0000010	
1.128640	1.60016	1.600165	-0.0000050	
1.529580	1.59523	1.595228	0.0000024	
1.970090	1.58978	1.589776	0.0000042	
2.325420	1.58475	1.584753	-0.0000026	

**Table 2.71: The Experimental and Computed Refractive Index Values of Fused-Silica (Corning code 7940) Glass at 26°C**

Wavelength ( $\mu\text{m}$ )	Observed [128]	Computed (This work)	Difference	Av. Dev.	RMS Dev.
0.23021	1.52034	1.520430	-0.000090		
0.23783	1.51496	1.515066	-0.000106		
0.24070	1.51361	1.513213	0.000397		
0.24650	1.50970	1.509715	-0.000015		
0.24827	1.50865	1.508709	-0.000059	5.60	9.35
0.26520	1.50023	1.500301	-0.000071	[ $10^{-5}$ ]	
0.27528	1.49615	1.496162	-0.000012		
0.28035	1.49425	1.494278	-0.000028		
0.28936	1.49121	1.491215	-0.000005	Expt.	
0.29673	1.48892	1.488948	-0.000028	accuracy is	
0.30215	1.48738	1.487402	-0.000022	$\pm 9.6$ to	
0.31300	1.48462	1.484580	0.000040	$\pm 21 [10^{-5}]$	
0.33415	1.48000	1.479943	0.000057		
0.36502	1.47469	1.474704	-0.000014		
0.40466	1.46978	1.469776	0.000004		
0.43584	1.46685	1.466851	-0.000001		
0.54607	1.46028	1.460246	0.000034		
0.57800	1.45899	1.458979	0.000011		
1.01398	1.45039	1.450451	-0.000061		

**Table 2.71: (Continued)**

Wavelength ( $\mu\text{m}$ )	Observed [128]	Computed (This work)	Difference	Av. Dev.	RMS Dev.
1.12866	1.44903	1.449084	-0.000054		
1.25400	1.44772	1.447661	0.000059		
1.36728	1.44635	1.446383	-0.000033		
1.47000	1.44524	1.445205	0.000035		
1.52952	1.44444	1.444507	-0.000067		
1.66000	1.44307	1.442925	0.000145		
1.70100	1.44230	1.442411	-0.000111		
1.98100	1.43863	1.438633	-0.000003		
2.26200	1.43430	1.434296	0.000004		

**Table 2.72: The Experimental and Computed Refractive Index Values of PBL26 Glass at 20°C**

Wavelength ( $\mu\text{m}$ )	Observed [125]	Computed (This work)	Difference	Av. Dev.	RMS Dev.
0.365015	1.60222	1.602192	0.0000283	1.40	1.67
0.404656	1.59069	1.590721	-0.0000309	[ $10^{-5}$ ]	
0.435835	1.58420	1.584228	-0.0000279		
0.441570	1.58319	1.583208	-0.0000176	Expt.	
0.479990	1.57742	1.577421	-0.0000012	accuracy	
0.486130	1.57664	1.576638	0.0000020	is	
0.546070	1.57047	1.570454	0.0000164		
0.587560	1.56732	1.567307	0.0000134	$\pm 0.00003$	
0.589290	1.56721	1.567190	0.0000198		
0.632800	1.56459	1.564577	0.0000130		
0.643850	1.56401	1.563997	0.0000133		
0.656270	1.56339	1.563379	0.0000114		
0.706520	1.56120	1.561192	0.0000082		
0.768190	1.55904	1.559036	0.0000036		
0.852110	1.55673	1.556736	-0.0000058		
1.013980	1.55347	1.553493	-0.0000235		
1.128640	1.55169	1.551715	-0.0000253		
1.529580	1.54668	1.546688	-0.0000076		
1.970090	1.54138	1.541376	0.0000045		
2.325420	1.53659	1.536584	0.0000059		

**Table 2.73: The Experimental and Computed Refractive Index Values of PSK3 (BAL23) Glass at 20°C**

Wavelength ( $\mu\text{m}$ )	Observed [126]	Computed (This work)	Difference	Av. Dev.	RMS Dev.
0.31260	1.58679	1.586786	0.000004		
0.33410	1.58041	1.580426	-0.000016		
0.36500	1.57342	1.573414	0.000006		
0.40470	1.56688	1.566866	0.000014	0.89	1.16
0.43580	1.56302	1.563020	0.000000	[ $10^{-5}$ ]	
0.48000	1.55885	1.558839	0.000011		
0.48610	1.55835	1.558352	-0.000002	Expt.	
0.54610	1.55440	1.554397	0.000003	accuracy	
0.58760	1.55232	1.552322	-0.000002	is	
0.58930	1.55224	1.552246	-0.000006	$\pm 0.00003$	
0.63280	1.55048	1.550481	-0.000001		
0.64380	1.55008	1.550085	-0.000005		
0.65630	1.54965	1.549656	-0.000006		
0.70650	1.54811	1.548123	-0.000013		
0.85210	1.54482	1.544825	-0.000005		
1.01400	1.54218	1.542188	-0.000008		
1.06000	1.54154	1.541537	0.000003		
1.52960	1.53558	1.535558	0.000022		
1.97010	1.52954	1.529515	0.000025		
2.32540	1.52375	1.523774	-0.000024		

**Table 2.74: The Experimental and Computed Refractive Index Values of SF6 (PBH6) Glass at 20°C**

Wavelength ( $\mu\text{m}$ )	Observed [126]	Computed (This work)	Difference	Av. Dev.	RMS Dev.
0.36501	1.89714	1.896988	0.000152	8.8	10.3
0.40466	1.86436	1.864563	-0.000203	[ $10^{-5}$ ]	
0.43583	1.84706	1.847192	-0.000132		
0.44157	1.84441	1.844521	-0.000111		
0.47999	1.82970	1.829696	0.000004		
0.48613	1.82775	1.827730	0.000020		
0.54607	1.81265	1.812554	0.000096		

**Table 2.74: (Continued)**

Wavelength ( $\mu\text{m}$ )	Observed [126]	Computed (This work)	Difference	Av. RMS Dev. Dev.
0.58756	1.80518	1.805080	0.000100	
0.58929	1.80490	1.804807	0.000093	
0.63280	1.79883	1.798749	0.000081	Expt.
0.64385	1.79750	1.797423	0.000077	accuracy
0.65627	1.79609	1.796019	0.000071	is
0.70652	1.79118	1.791128	0.000052	$\pm 0.0003$
0.76819	1.78647	1.786441	0.000029	[ For
0.85211	1.78162	1.781629	-0.000009	different
1.01398	1.77524	1.775312	-0.000072	glass
1.06000	1.77380	1.773953	-0.000153	samples]
1.52960	1.76444	1.764609	-0.000169	
1.97010	1.75813	1.758166	-0.000036	
2.32540	1.75302	1.752909	0.000111	

**Table 2.75: The Experimental [125] and Computed Refractive Index Values of S-FPL53 Glass at 20°C**

Wavelength ( $\mu\text{m}$ )	Observed [125]	Computed (This work)	Difference	Av. RMS Dev. Dev.
0.365015	1.44984	1.449836	0.0000042	0.5 0.6
0.404656	1.44644	1.446444	-0.0000039	$[10^{-5}]$
0.435835	1.44442	1.444422	-0.0000019	
0.441570	1.44410	1.444097	0.0000031	
0.479990	1.44221	1.442215	-0.0000051	
0.486130	1.44195	1.441955	-0.0000051	
0.546070	1.43985	1.439854	-0.0000038	
0.587560	1.43875	1.438749	0.0000014	
0.589290	1.43871	1.438707	0.0000028	
0.632800	1.43777	1.437768	0.0000023	
0.643850	1.43756	1.437556	0.0000037	
0.656270	1.43733	1.437330	0.0000002	
0.706520	1.43652	1.436517	0.0000025	
0.768190	1.43570	1.435697	0.0000026	
0.852110	1.43480	1.434796	0.0000044	
1.013980	1.43347	1.433462	0.0000077	
1.128640	1.43269	1.432691	-0.0000006	

**Table 2.75:** (*Continued*)

Wavelength ( $\mu\text{m}$ )	Observed [125]	Computed (This work)	Difference	Av. RMS Dev. Dev.
1.529580	1.43032	1.430334	-0.0000140	
1.970090	1.42763	1.427644	-0.0000140	
2.325420	1.42515	1.425137	0.0000133	

**Table 2.76:** The Experimental and Computed Refractive Index Values of Vycor (Corning code 7913) Glass at 28°C

Wavelength ( $\mu\text{m}$ )	Observed [128]	Computed (This work)	Difference	Av. RMS Dev. Dev.
0.26520	1.49988	1.499880	0.000000	
0.28936	1.49074	1.490775	-0.000035	
0.29673	1.48851	1.488501	0.000009	
0.30215	1.48694	1.486949	-0.000009	
0.31300	1.48416	1.484116	0.000044	
0.33415	1.47949	1.479458	0.000032	
0.36502	1.47415	1.474190	-0.000040	2.98 4.07
0.40466	1.46925	1.469229	0.000021	$[10^{-5}]$
0.43584	1.46628	1.466282	-0.000002	
0.54607	1.45960	1.459619	-0.000019	Expt.
0.57800	1.45831	1.458339	-0.000029	accuracy is
1.01398	1.44968	1.449677	0.000003	$\pm 9.6$ to
1.12866	1.44831	1.448277	0.000033	$\pm 21$
1.25400	1.44677	1.446815	-0.000045	$[10^{-5}]$
1.36728	1.44554	1.445500	0.000040	
1.47000	1.44422	1.444286	-0.000066	
1.52952	1.44356	1.443566	-0.000006	
1.66000	1.44206	1.441933	0.000127	
1.70100	1.44137	1.441402	-0.000032	
1.98100	1.43750	1.437497	0.000003	
2.26200	1.43298	1.433009	-0.000029	

## 2.7 References

1. J. D. Jackson, *Classical Electrodynamics* (John Wiley, New York, 1962), Chap. 7.
2. E. D. Palik, Ed. *Handbook of Optical Constants of Solids* (Academic Press, New York, 1985).
3. E. D. Palik, Ed. *Handbook of Optical Constants of Solids, Vol. II.* (Academic Press, New York, 1991).
4. G. D. Cody, in *Semiconductors and Semimetals, Vol. 21, Hydrogenated Amorphous Silicon, Part B, Optical Properties*, J. I. Pankove, Ed. (Academic Press, New York, 1984).
5. T. Skettrup, Phys. Rev. B **18**, 2622 (1978).
6. F. K. Kneubuhl, Infrared Physics **29**, 925 (1989).
7. L. W. Tilton, J. Res. Natl. Bur. Std. (Report 64) (U.S.) **2**, 909 (1929).
8. C. Weir, S. Spinner, I. H. Malitson, and W. J. Rodney, J. Res. Natl. Bur. Std. (Report 2751) (U. S.) **58**, 189 (1957).
9. K. W. Kirby and L. G. DeShazer, J. Opt. Soc. Am. B **4**, 1072 (1987).
10. G. E. Jellison, Jr. and F. A. Modine, J. Appl. Phys. **53**, 3745 (1982).
11. S. N. Jasperson and S. E. Schnatterly, Rev. Sci. Instrum. **40**, 761 (1969).
12. V. M. Bermudez and V. H. Ritz, Appl. Opt. **17**, 542 (1978).
13. G. R. Fowles, *Introduction to Modern Optics* (Holt, Rinehart and Winston, Inc., New York, 1968), p. 304.
14. B. Tatian, Appl. Opt. **23**, 4477 (1984).
15. H. H. Li, J. Phys. Chem. Ref. Data **13**, 103 (1984).
16. F. Zernike, J. Opt. Soc. Am. **54**, 1215 (1964);  
F. Zernike, Errata, J. Opt. Soc. Am. **55**, 210E (1965).
17. M. Herzberger, Opt. Acta **6**, 197 (1959).
18. M. Herzberger and C. D. Salzberg, J Opt. Soc. Am. **52**, 420 (1962).
19. G. C. Bhar, Appl. Opt. **15**, 305 (1976).
20. R. F. Lucy, Appl. Opt. **11**, 1329 (1972).
21. K. F. Hulme, O. Jones, P. H. Davies, and M. V. Hobden, Appl. Phys. Lett. **10**, 133 (1967).
22. H. Schröter, Z. Phys. **67**, 24 (1931).
23. L. W. Tilton, E. K. Plyler, and R. E. Stephens, J. Opt. Soc. Am. **40**, 540 (1950).
24. G. D. Boyd, H. M. Kasper, and J. H. McFee, IEEE J. Quantum Electron. **QE-7**, 563 (1971).
25. G. D. Boyd, H. M. Kasper, J. H. McFee, and F. G. Storz, IEEE J. Quantum Electron. **QE-8**, 900 (1972).
26. J. D. Feichtner, R. Johannes, and G. W. Roland, Appl. Opt. **9**, 1716 (1970).

27. R. E. Fern and A. Onton, *J. Appl. Phys.* **42**, 3499 (1971).
28. J. Pastrnak and L. Roskocova, *Phys. Stat. Sol.* **14**, K5 (1966); D. A. Yaskov and A. N. Pikhtin, *Sov. Phys. Semicond.* **15**, 8 (1981).
29. I. H. Malitson and M. J. Dodge, *J. Opt. Soc. Am.* **62**, 1405A (1972); M. J. Dodge, *Handbook of Laser Science and Technology, IV, Optical Materials, Part 2* (CRC Press, Boca Raton, 1986).
30. W. J. Tropf and M. E. Thomas, in *Handbook of Optical Constants of Solids II*, E. D. Palik, Ed. (Academic Press, New York, 1991), p.775.
31. W. L. Bond, *J. Appl. Phys.* **36**, 1674 (1965).
32. D. Eimerl, L. Davis, and S. Velsko, *J. Appl. Phys.* **62**, 1968 (1987).
33. G. Ghosh, *J. Appl. Phys.* **78**, 6752 (1995).
34. B. S. Bechtold and S. Haussuhl, *Appl. Phys.* **14**, 403 (1977).
35. I. H. Malitson, *J. Opt. Soc. Am.* **54**, 628 (1964).
36. S. Singh, D. A. Draegert, and J. E. Geusic, *Phys. Rev. B* **2**, 2709 (1970).
37. C. Wong, Y. Y. Teng, J. Ashok, and P. L. H. Varaprasad, in *Handbook of Optical Constants of Solids, Vol. II*, E. D. Palik, Ed. (Academic Press, Orlando, 1991), p. 789.
38. H. W. Newkirk, D. K. Smith, and J. S. Kahn, *Am. Mineral.* **51**, 141 (1966); M. Herzberger and C. D. Salzberg, *J. Opt. Soc. Am.* **52**, 420 (1962); M. Herzberger, *Opt. Acta* **6**, 197 (1959).
39. K. Kato, *Appl. Phys. Lett.* **33**, 413 (1978).
40. R. E. Aldrich, S. L. Hou, and M. L. Harvill, *J. Appl. Phys.* **42**, 493 (1971).
41. G. Ghosh and Y. Fujii, *Denshi Tsushin Gakkai, OQE* **83-123**, 69 (1984).
42. E. Burattini, G. Cappuccio, M. Grandolfo, P. Vecchia, and Sh. M. Efendiev, *J. Opt. Soc. Am.* **73**, 495 (1983).
43. W. Wetling and J. Windscheif, *Solid State Commun.* **50**, 33 (1984).
44. F. Peter, *Z. Phys.* **15**, 358 (1923).
45. S. S. Ballard, J. S. Browder, and J. F. Ebersole, in *American Institute of Physics Handbook*, D. E. Gray, Ed. (McGraw-Hill, New York, 1982), p. 6-20.
46. W. J. Tropf, M. E. Thomas, and T. J. Harris, in *Handbook of Optics, Vol. II*, M. Bass, Ed. (McGraw-Hill, New York, 1995) p. 33.62.
47. I. H. Malitson, *Appl. Opt.* **2**, 1103 (1963).
48. A. Feldman, D. Horowitz, R. M. Waxler, and M. J. Dodge, *Nat. Bur. Stand. (U.S.)*, Tech. Note **993**, (Feb. 1979), p.33.
49. T. H. Houston, L. F. Johnson, P. Kisliuk, and D. J. Walsh, *J. Opt. Soc. Am.* **53**, 1286 (1963).
50. G. D. Boyd, E. Buehler, F. G. Storz, and J. H. Wernick, *IEEE J. Quantum Electron.* **QE-8**, 419 (1972).
51. G. C. Bhar and G. Ghosh, *J. Opt. Soc. Am.* **69**, 730 (1979).

52. T. M. Bieniewski and S. J. Czyzak, *J. Opt. Soc. Am.* **53**, 496 (1963).
53. A. G. DeBell, E. L. Dereniak, J. Harvey, J. Nissley, J. Palmer, A. Selvarajan, and W. L. Wolfe, *Appl. Opt.* **18**, 3114 (1979).
54. M. J. Rosker, K. Cheng, and C. L. Tang, *IEEE J. Quantum Electron.* **QE-21**, 1600 (1985).
55. W. S. Rodney and R. J. Spindler, *J. Res. Natl. Bur. Stand.* **51**, 123 (1953).
56. H. H. Li, *J. Phys. Chem. Ref. Data* **5**, 329 (1976).
57. W. S. Rodney, *J. Opt. Soc. Am.* **45**, 987 (1955).
58. A. Feldman and D. Horowitz, *J. Opt. Soc. Am.* **59**, 1406 (1969).
59. J. M. Halbout and C. L. Tang, *IEEE J. Quantum Electron.* **QE-18**, 410 (1982).
60. D. Eimerl, S. Velsko, L. Davis, F. Wang, G. Loiacono, and G. Kennedy, *IEEE J. Quantum Electron.* **QE-25**, 179 (1989).
61. A. H. Kachare, W. G. Spitzer, and J. E. Fredrickson, *J. Appl. Phys.* **47**, 4209 (1976).
62. A. S. Barkar and M. Illegems, *Phys. Rev. B* **7**, 743 (1973).
63. D. F. Parsons and P. D. Coleman, *Appl. Opt.* **10**, 1683 (1971).
64. D. F. Edwards and G. S. Haynes, *J. Opt. Soc. Am.* **59**, 414 (1959).
65. K. L. Vodopyanov and L. A. Kulevskii, *Opt. Commun.* **118**, 375 (1995).
66. N. P. Barnes and M. S. Piltch, *J. Opt. Soc. Am.* **69**, 178 (1979).
67. V. V. Badikov, I. N. Matveev, V. L. Panyutin, S. M. Pshenichnikov, T. M. Repyakhova, O. V. Rychik, A. E. Rozenson, N. K. Trotsenko, and N. D. Ustinov, *Sov. J. Quantum Electron.* **9**, 1068 (1979).
68. H. Naito and H. Inaba, *Opto-electronics* **4**, 335 (1972).
69. D. L. Wood, K. Nassau, T. Y. Kometani, and D. L. Nash, *Appl. Opt.* **29**, 604 (1990).
70. O. G. Lorimer and W. G. Spitzer, *J. Appl. Phys.* **36**, 1841 (1965).
71. G. D. Pettit and W. J. Turner, *J. Appl. Phys.* **36**, 2081 (1965); A. N. Pikhtin and A. D. Yas'kov, *Sov. Phys. Semicond.* **12**, 622 (1978).
72. R. G. Breckenridge, *Phys. Rev.* **96**, 571 (1954).
73. W. R. Cook and Jr. L. H. Hubby, *J. Opt. Soc. Am.* **66**, 72 (1976).
74. F. B. Dunning and R. G. Stickel Jr., *Appl. Opt.* **15**, 3131 (1976); N. Umemura and K. Kato, *Appl. Opt.* **35**, 5332 (1996).
75. J. A. Paisner, M. L. Spaeth, D. C. Gerstenberger, and I. W. Ruderman, *Appl. Phys. Lett.* **32**, 476 (1978).
76. R. A. Phillips, *J. Opt. Soc. Am.* **56**, 629 (1966).
77. S. Singh, in *Handbook of Lasers with Selected Data on Optical Technology*, R. J. Pressley, Ed. (Chemical Rubber Co., Cleveland, OH 1971).
78. L. Schuler, K. Betzler, H. Hesse, and S. Kapphan, *Opt. Commun.* **43**, 157 (1982).

79. B. Zysset, I. Biaggio, and P. Gunter, J. Opt. Soc. Am. B **9**, 380 (1992).
80. G. Ghosh, Appl. Phys. Lett. **65**, 3311 (1994).
81. K. Kato, IEEE J. Quantum Electron. **30**, 881 (1994).
82. Y. Fujii and T. Sakudo, J. Phys. Soc. Japan **41**, 888 (1976).
83. K. Kato, IEEE J. Quantum Electron. **27**, 1137 (1991).
84. G. Ghosh, IEEE Photon. Technol. Lett. **7**, 68 (1995).
85. R. Laiho and M. Lakkisto, Phil. Mag. B **48**, 203 (1983).
86. S. Velsko, M. Webb, L. Davis, and C. Huang, IEEE J. Quantum Electron. **27**, 2182 (1991).
87. H. Naito and H. Inaba, Opto-electronics **5**, 256 (1973).
88. K. Kato, IEEE J. Quantum Electron. **QE-21**, 119 (1985).
89. G. Ghosh and M. Endo, in *Digest of Annual Meeting* (Japan Soc. of Applied Physics, Tokyo, 1995), paper 28p-ZQ-18.
90. M. M. Choy and R. L. Byer, Phys. Rev. B **14**, 1693 (1976).
91. G. D. Boyd, R. C. Miller, K. Nassau, W. L. Bond, and A. Savage, Appl. Phys. Lett. **5**, 234 (1964).
92. G. D. Boyd, W. L. Bond, and H. L. Carter, J. Appl. Phys. **38**, 1941 (1967).
93. D. F. Nelson and R. M. Mikulyak, J. Appl. Phys. **45**, 3688 (1974).
94. S. Lin, Y. Tanaka, S. Takeuchi, and T. Suzuki, IEEE J. Quantum Electron. **32**, 124 (1996).
95. N. P. Barnes and D. J. Gettemy, J. Opt. Soc. Am. **70**, 1244 (1980).
96. J. L. Oudar and R. Hierle, J. Appl. Phys. **48**, 2699 (1977).
97. G. S. Belikova, M. P. Golovey, V. D. Shigorin, and G. P. Shipulo, Opt. Spectrosc. **38**, 441 (1975).
98. S. K. Kurtz, J. Jerphagnon, and M. M. Choy, in *Landolt-Bornstein, Vol. 11* (Springer, Berlin, Heidelberg, 1979) p. 671; J. Jerphagnon, S. K. Kurtz, and J. L. Oudar, in *Landolt-Bornstein, Vol. 18* (Springer, Berlin, Heidelberg, 1984), p. 456.
99. W. J. Tropf and M. E. Thomas, in *Handbook of Optical Constants of Solids, II*, E. D. Palik, Ed. (Academic Press, New York, 1991), p. 881.
100. B. S. Bechtold and S. Haussuhl, Appl. Phys. **14**, 403 (1977).
101. M. J. Dodge, Appl. Opt. **23**, 1980 (1984).
102. R. E. Stephens and I. H. Malitson, J. Nat. Bur. Stand. **49**, 249 (1952).
103. H. Ito, H. Naito, and H. Inaba, IEEE J. Quantum Electron. **QE-10**, 247 (1974).
104. I. H. Malitson and M. J. Dodge, J. Opt. Soc. Am. **59**, 500A (1969); M. J. Dodge, in *Handbook of Laser Science and Technology, Vol. IV, Optical Materials, Part 2* (CRC Press, Boca Raton, 1986), p. 31.
105. I. H. Malitson, in *Handbook of Optics*, W. G. Driscoll, Ed. (McGraw-Hill, New York, 1978).

106. G. Guizzetti and A. Borghesi, in *Handbook of Optical Constants of Solids*, E. D. Palik, Ed. (Academic Press, New York, 1985), p. 525.
107. G. Bauer and H. Krenn, in *Handbook of Optical Constants of Solids*, E. D. Palik, Ed. (Academic Press, New York, 1985), p. 517.
108. *ibid*, p.535.
109. J. Zyss, D. S. Chemla, and J. F. Nicoud, *J. Chem. Phys.* **74**, 4800 (1981).
110. V. G. Dmitriev, G. G. Gurzadyan, and D. N. Nikogosyan, in *Handbook of Nonlinear Optical Crystals* (Springer-Verlag, Berlin, 1991), p. 105.
111. M. J. Dodge, I. H. Malitson, and A. I. Mahan, *Appl. Opt.* **8**, 1703 (1969).
112. L. Gampel and F. M. Johnson, *J. Opt. Soc. Am.* **59**, 72 (1969).
113. G. E. Jellison Jr. and F. A. Modine, *J. Appl. Phys.* **76**, 3758 (1994).
114. P. T. B. Schaffer, *Appl. Opt.* **10**, 1034 (1971).
115. S. Singh, J. R. Potopowicz, L. G. Van Uitert, and S. H. Wemple, *Appl. Phys. Lett.* **19**, 53 (1971).
116. F. J. Micheli, *Ann. Physik* **4**, 7 (1902).
117. T. Radhakrishnan, *Proc. Indian Acad. Sci. A* **33**, 22 (1951).
118. N. Uchida, *Phys. Rev. B* **4**, 3736 (1971).
119. M. D. Ewbank, P. R. Newman, N. L. Mota, S. M. Lee, W. L. Wolfe, A. G. DeBell, and W. A. Harrison, *J. Appl. Phys.* **51**, 3848 (1980).
120. G. Hettner and Leisegang, *Optik* **3**, 305(1948).
121. W. S. Rodney and I. H. Malitson, *J. Opt. Soc. Am.* **46**, 956 (1956).
122. Y. Nigara, *Jpn. J. Appl. Phys.* **7**, 404 (1968).
123. T. M. Bieniewski and S. J. Czyak, *J. Opt. Soc. Am.* **53**, 496 (1963).
124. D. L. Wood and K. Nassau, *Appl. Opt.* **21**, 2978 (1982).
125. *Ohara Optical Glass Catalog* (Ohara Inc., Kanagawa, 1990; 1995).
126. *Schott Optical Glass Catalog* (Schott Glass Technologies Inc., Duryea, 1992).
127. G. Ghosh, *Appl. Opt.* **36**, 1540 (1997).
128. J. H. Wray and J. T. Neu, *J. Opt. Soc. Am.* **59**, 774 (1969).
129. G. Ghosh, M. Endo, and T. Iwasaki, *IEEE J. Lightwave Technol.* **LT-12**, 1338 (1994).
130. I. H. Malitson, *J. Opt. Soc. Am.* **55**, 1205 (1965).
131. J. Matsuoka, N. Kitamura, S. Fujinaga, T. Kitaoka, and H. Yamashita, *J. Non-Cry. Sol.* **135**, 86 (1991).
132. H. Takebe, S. Fujino, and K. Morinaga, *J. Am. Ceram. Soc.* **77**, 2455 (1994); and private communication.
133. G. Ghosh, *J. Am. Ceram. Soc.* **78**, 2828 (1995).
134. S. Kim, T. Yoko, and S. Sakka, *J. Am. Ceram. Soc.* **76**, 2486 (1993).
135. S. Mitachi and T. Miyashita, *Appl. Opt.* **22**, 2419 (1983).

# **Chapter 3**

## **Thermo-Optic Coefficients**

### **3.1 Definition**

The refractive index of the optical materials is not a constant parameter over the temperature region in which the materials, such as crystals, semiconductors, and glasses are used in different optical devices or systems. The variation of the refractive index with the temperature at a constant pressure is called the thermo-optic coefficient. It is denoted as  $dn/dT$ , where  $n$  and  $T$  are the refractive index and temperature, respectively. Its unit is per degree centigrade or Kelvin. Normally, the value of  $dn/dT$  is very small, of the order of  $10^{-3}$  to  $10^{-6}/^{\circ}\text{C}$ . Although the value is quite small, it is possible to measure with sufficient accuracy. The analyses of thermo-optic coefficients are essential to characterize the temperature-dependent nonlinear optical devices, the optical fiber communication systems, semiconductor technology, and the ultrafast femtosecond technology.

### **3.2 Measurement**

Since the begining of this century, measurements of the change in refractive index as a function of temperature for crystals and other optical materials were reported by various groups [1-9]. Micheli [1] measured the thermo-optic coefficients of the crystal Quartz for several wavelengths from 0.202 to 0.643  $\mu\text{m}$ . Hobden and Warner [4] measured the temperature dependence of the refractive indices of pure lithium niobate,  $\text{LiNbO}_3$ , LNO crystal. A prism of LNO was mounted in a small oven on the prism table of

a conventional spectrometer. As usual, the refractive indices were measured by the minimum deviation technique at eight temperatures from 19 to 374°C using seven prominent lines from a helium discharge lamp. At high temperature measurements, the heater is normally made of platinum wire. Phillips [5] used a mixture of solid-liquid chlorobenzene (228 K), solid CO<sub>2</sub> - ethyl alcohol (201 K), and a solid-liquid methyl bromide (154 K) for measuring refractive indices of ammonium dihydrogen phosphate, ADP, potassium dihydrogen phosphate, KDP, and deuterated potassium dihydrogen phosphate, KD\*P crystals. Recently some sophisticated equipments [8] have been used for measuring the same. But the basic principle is the measurement of the angle of minimum deviation with temperature. Nowadays, some lasers are additionally used as a light source, and some efficient detectors are also used both in the UV and the IR region. Also, liquid nitrogen (77 K) and liquid helium (20 K) are used as coolants. The temperature of the dewar or the oven is controlled by a temperature controller. The temperature of the measuring sample is precisely monitored by thermocouples attached above and below the sample. Refractive indices of three Corning glasses were measured by Wray and Neu [6] at several temperatures from 26 to 826°C. In the case of refractive index measurements at low temperatures, the sample prism was kept inside a dewar and the whole assembly was mounted on the turntable of the spectrometer. Fixed temperatures were maintained in the dewar by using different mixtures to keep a selective temperature. Jellison and Modine [9] have measured the refractive indices of silicon at elevated temperatures from room temperature to 490°C in the wavelength region of 0.24 to 0.84 μm by using a two-channel spectroscopic polarization modulation ellipsometer.

A laser interferometric technique has been reported by Lipson *et al.* [10] to measure  $dn/dT$  of some fluoride single crystals over a temperature range from 20 to 80°C. Simultaneously, Harris *et al.* [11] used this technique to determine the thermo-optic coefficients of some polycrystalline ZnSe, ZnS, etc. — optical materials over a temperature range from 25 to 65°C. The following expression was used to calculate  $dn/dT$

$$\frac{dn}{dT} = [\lambda/(2L_c\Delta T)] - n\alpha, \quad (3.1)$$

where  $\lambda$  is the wavelength of the laser used,  $L_c$  is the sample thickness,  $\Delta T$  is the temperature difference between successive maxima or minima of the fringes,  $n$  is the refractive index, and  $\alpha$  is the linear thermal expansion co-

efficient. Each set of measurements gives a statistically large number of  $dn/dT$  values which are then averaged. The accuracy of the  $dn/dT$  values depends largely on the accuracy of the values of  $n$  and  $\alpha$  used in the calculation and on the accuracy of the thermometry in the experiment. If, for example, the value of  $\alpha$  used in the calculations is in error by 5%, the  $dn/dT$  value obtained will be in error by 3%.

Recently, a Fabry-Perot-type interferometer is described by Jewell *et al.* [12] to measure simultaneously the thermal expansion coefficient,  $\alpha$ , and  $dn/dT$  for transparent optical materials. In this apparatus, a He-Ne laser beam is expanded and partially transmitted through a beam splitter. The transmitted beam interacts with the heated sample and mirrors to produce interfering beams, which are reflected back to the beam splitter and deflected onto the screen and silicon detectors. The previous Eq. (3.1) is used to calculate  $dn/dT$ .

### 3.3 Dispersion Relations

The thermo-optic coefficients,  $dn/dT$ , can be estimated from a derivation of the Clausius-Mossotti relationship [13]

$$\frac{(\varepsilon - 1)}{(\varepsilon + 2)} = \left( \frac{4\pi}{3} \right) \left( \frac{\alpha_m}{V} \right), \quad (3.2)$$

where  $\alpha_m$  is the polarizability of a macroscopic, small sphere with a volume,  $V$ . The macroscopic polarizability,  $\alpha_m$ , is proportional to the number of unit cells in the sphere, but it may be a complicated function of the polarizabilities of the particles and the structure of the lattice of the materials. Differentiating Eq. (3.2) with respect to temperature at constant pressure gives [14]

$$\begin{aligned} \frac{1}{(\varepsilon - 1)(\varepsilon + 2)} \left( \frac{d\varepsilon}{dT} \right) &= -\alpha \left[ 1 - \frac{V}{\alpha_m} \left( \frac{d\alpha_m}{dV} \right)_T \right] \\ &\quad + \frac{1}{3\alpha_m} \left( \frac{d\alpha_m}{dT} \right)_V. \end{aligned} \quad (3.3)$$

The first two terms are the principal contributors in ionic materials: a positive thermal expansion coefficient  $\alpha$  exhibits in a negative thermo-optic coefficient. In ionic materials with a low melting point, thermal expansion is high and the thermo-optic coefficient is negative; when thermal expansion

is small for some nonlinear crystals and has a high melting point, hardness, and high elastic moduli optical materials, the thermo-optic coefficient is positive, dominated by the volume change in polarizability.

Thermal expansion has no frequency i.e., it has no wavelength dependence but the polarizability has dependent characteristics. At the edge of transparency, the polarizability rises, and  $dn/dT$  becomes more positive or less negative depending on the values of  $\alpha$ . The above equation was used to analyze the thermo-optic coefficients of some cubic ionic compounds. But this formulation is not sufficient to explain the thermo-optic characteristics of all the optical materials. It is also difficult to measure the change of macroscopic polarizability against temperature.

In 1960, Prod'homme [15] suggested a model to analyze the thermo-optic coefficients of glasses. He accounted for the factors affecting the refractive index. The thermal variation of electronic polarizability and the thermal expansion coefficient are used to explain  $dn/dT$ . The increase in specific volume,  $V$ , causes the refractive index to decrease as a result of greater interatomic spacings in the lattice. On the other hand, the increase in electronic polarization,  $P$ , causes the index to rise gradually as the structure tends to a more dissociated state, which entails a decrease in size of atomic groupings responsible for the greater electronic polarizability. He derived the following formula from the Lorentz and Lorenz relation

$$n^2 = \frac{V + 2S_r}{V - S_r}, \quad (3.4)$$

where  $V$  is the specific volume of the medium and  $S_r$  is a constant defined as the specific refractivity. Differentiating the above Eq. (3.4) we have

$$2n(dn) = \frac{3V(dS_r) - 3S_r(dV)}{(V - S_r)^2} = \frac{3S_r V}{(V - S_r)^2} \left( \frac{dS_r}{S_r} - \frac{dV}{V} \right). \quad (3.5)$$

The first factor is expressed in terms of  $n$  as

$$\frac{3S_r V}{(V - S_r)^2} = \frac{(n^2 - 1)(n^2 + 2)}{3}. \quad (3.6)$$

Differentiating with respect to temperature,  $T$ , it is possible to include the volume expansion coefficient,  $\beta$ , which is defined as

$$\beta = \frac{dV}{V} \frac{1}{dT}, \quad (3.7)$$

and a similar coefficient, called electronic polarizability,  $\phi$ , is defined as

$$\phi = \frac{dS_r}{S_r} \frac{1}{dT} = \frac{dP}{P} \frac{1}{dT}, \quad (3.8)$$

where  $P$  is proportional to  $S_r$ . Now the expression for the thermo-optic coefficient is given by

$$2n \frac{dn}{dT} = \frac{(n^2 - 1)(n^2 + 2)}{3} (\phi - \beta). \quad (3.9)$$

This formula shows that the thermo-optic coefficient is determined by the difference between the polarization coefficient,  $\phi$ , and the thermal expansion coefficient,  $\alpha$ .

Recently, Jewell has measured the thermo-optic coefficients and the thermal expansion coefficient for four National Institute of Standards and Technology (NIST) standard reference material (SRM) glasses[16] and vitreous silica [12]. He attempted to explain the behavior of the thermo-optic coefficient of these glasses by using the above mentioned model, Eq. (3.9). However, he observed that for this model it is not possible to explain the linear behavior of the temperature coefficient of the electronic polarizability for all glasses by correlating it to the activation energy for viscous flow, as proposed by Prod'homme. Therefore, Jewell proposed a modified model [17] by introducing additional factors for the various types of bridging and non-bridging oxygen ions in the glass, which modify the calculation for the temperature coefficient of the electronic polarizability. However, Prod'homme's model [17] is unable to explain the thermo-optic behavior of refractive indices of different optical glasses.

There is no analysis for accounting the thermo-optic coefficients of some basic widely used optical glasses made by Ohara [18], whereas there is a dispersion formula of the Sellmeier type for the temperature coefficients of refractive indices of Schott glasses [19]. The equation is given below

$$2n(\lambda, T_0) \frac{dn_{\text{abs}}(\lambda, T)}{dT} = [n^2(\lambda, T_0) - 1][D_0 + 2.D_1.\Delta T + 3.D_2.\Delta T^2 + \frac{E_0 + 2.E_1.\Delta T}{\lambda^2 - \lambda_{TK}^2}], \quad (3.10)$$

where,  $T_0$  is the reference temperature ( $20^\circ\text{C}$ ),  $T$  is the temperature in  $^\circ\text{C}$ ,  $\Delta T$  is the tempertaure difference with  $T_0$ ,  $\lambda$  is the wavelength of the

electro-magnetic wave in a vacuum (in  $\mu\text{m}$ ),  $\lambda_{TK}$  is the average effective resonance wavelength (in  $\mu\text{m}$ ) for the thermo-optic coefficients. Although the optical constants  $D_0$ ,  $D_1$ ,  $D_2$ ,  $E_0$ ,  $E_1$ , and  $\lambda_{TK}$  are used in analyzing the absolute thermo-optic coefficients, this equation has no physical explanation. Moreover, it is not possible to analyze the thermo-optic coefficients of other optical materials by using this formula.

Tsay *et al.* [20] derived the thermo-optic coefficients for some semiconductors and ionic crystals by considering a two-oscillator model. They did a formulation of  $dn/dT$  based on variation with temperature of the fundamental transitions in crystals, which are the energy gap  $E_g$  and fundamental phonon frequency  $\omega_0$ , and their corresponding oscillator strengths. One obtains the electronic susceptibility at frequency  $\omega$  by neglecting damping effects, as

$$4\pi\chi_e(\omega) = \frac{\omega_{pe}^2}{(\omega_g^2 - \omega^2)} \quad (\omega < \omega_g), \quad (3.11)$$

where  $\omega_{pe}$  is the electronic plasma frequency and  $\omega_g$  is an average optical band gap. Similarly, the lattice susceptibility of a diatomic material can be written as

$$4\pi\chi_l(\omega) = \frac{\omega_{pl}^2}{(\omega_0^2 - \omega^2)} \quad (\omega < \omega_g), \quad (3.12)$$

where  $\omega_{pl}^2 = 4\pi Ne^{*2}/\mu = (\epsilon_0 - \epsilon_\infty)\omega_0^2$ ,  $e^*$  is the transverse effective charge, and the other symbols have their usual meanings. Of course, one requires a sum of susceptibilities of the above form for crystals with more than one infrared-active phonon. We are interested in the transmission region of the optical materials, and therefore, we need just the real part of the dielectric function. It can be written as  $\epsilon = n^2 = 1 + 4\pi(\chi_e + \chi_l)$ . Employing the fact that the square of the plasma frequency,  $\omega_{pe}$  is inversely proportional to the volume, one obtains

$$\frac{dn}{dT} = \left( \frac{dn}{dT} \right)_e + \left( \frac{dn}{dT} \right)_l, \quad (3.13)$$

where

$$2n \left( \frac{dn}{dT} \right)_e = 4\pi\chi_e \left( -3\alpha - \frac{2}{\omega_g} \frac{d\omega_g}{dT} \frac{1}{1 - \omega^2/\omega_g^2} \right), \quad (3.14)$$

and

$$2n \left( \frac{dn}{dT} \right)_l = 4\pi\chi_l \left( -3\alpha + \frac{2}{e^*} \frac{de^*}{dT} - \frac{2}{\omega_0} \frac{d\omega_0}{dT} \frac{1}{1 - \omega^2/\omega_0^2} \right), \quad (3.15)$$

where  $(dn/dT)_e$  and  $(dn/dT)_l$  are the electronic and lattice contributions to  $dn/dT$ , and  $\alpha$  is the linear thermal expansion coefficient. The above two equations were used to explain the thermo-optic behavior of some semiconductors and ionic/halide crystals, but the evaluation is critical for many unknown parameters and the procedure is not straightforward. On the other hand, it is not possible to explain the same for all other optical materials. These equations are also unable to explain the *nonlinear behavior of dn/dT against temperature*, which remained a problem for several decades.

A semiempirical theory was presented by Ramachandran [21] to characterize the thermo-optical effects in crystals, in which the dispersion was fitted to experimental data. A series of oscillator wavelengths and oscillator strengths were used as adjustable parameters. He found a relationship between temperature shifts of various parameters and fundamental oscillator wavelengths, which is shown below as

$$2n \frac{dn}{dT} = M - 3\alpha(n^2 - 1) + \sum_i F(\lambda, \lambda_i) \left( \frac{1}{\lambda_i} \frac{d\lambda_i}{dT} \right), \quad (3.16)$$

where  $M$  is effectively a constant over a limited temperature range and

$$F(\lambda, \lambda_i) = \frac{2k_i \lambda^4}{(\lambda^2 - \lambda_i^2)^2}, \quad (3.17)$$

with  $k_i$  a constant. However, the chosen parameters were rather numerous and often not unique, no general formulation was presented for determining their temperature variation which are necessary for the calculation of  $dn/dT$ . Similarly, Harris *et al.* [11] reported an empirical relation without having any theoretical justification for the dispersion of  $dn/dT$ . It is related to the observed values of  $dn/dT$  and its wavelength  $\lambda$ , and the wavelength corresponding to energy gap  $\lambda_g$  by the expression

$$\frac{dn}{dT} = aR^b, \quad (3.18)$$

where  $a$  and  $b$  are constants and  $R = \lambda^2/(\lambda^2 - \lambda_g^2)$ . Johnston [22] re-examined the above equation in light of some phenomenological calcula-

tions of Tsay *et al.* [20], and he derived the following equation

$$2n \frac{dn}{dT} = K^2(-3\alpha R + \frac{2}{\lambda_g} \frac{d\lambda_g}{dT} R^2). \quad (3.19)$$

In this derivation, the contribution from the lattice was neglected. For practical data interpolation, Eq. (3.19) was simplified by Johnston to

$$2n \frac{dn}{dT} = CR + HR^2. \quad (3.20)$$

It is to be noted that most published works on semiconductors generally assumes that  $dn/dT$  data are nearly constant and independent of temperature over a fairly wide range of temperature and the lattice contribution to  $dn/dT$  are negligible. Therefore, much of the reported  $dn/dT$  data remains nearly constant over a temperature range of a few hundred degrees. But in practice, all these assumptions become inadequate and are not acceptable, since  $dn/dT$ s are not constant [16] even for less than a hundred degrees.

In order to overcome the above mentioned limitations of the existing equations, we have derived a *new physically meaningful dispersion relation* for analyzing the thermo-optic coefficients of all the optical materials, which is explained below.

In any transparent medium, such as optical glass, fiber glass, semiconductors, and nonlinear crystals the normal transmission region is determined by the resonant band-gaps of average electronic absorption and the lattice absorption frequency; lying in the vacuum ultraviolet/ultraviolet (VUV/UV) and infrared (IR) region, respectively. The refractive index is dispersive from the UV to the IR absorption region. Similarly, the variation of the refractive index with temperature, i.e., the thermo-optic coefficient, is dispersive in the transmission region. The dispersions of these two important optical parameters, the refractive index and the thermo-optic coefficient, are not same. The thermo-optic coefficient contains contributions of both electrons and optical phonons. However, the electronic effect, particularly the temperature variation of the excitonic band, which will be defined later on, yields the dominant contribution.

The refractive index of the optical material can be described in the transmission region at room temperature as

$$n^2 = \varepsilon(\omega) = 1 + 4\pi(\chi_e + \chi_l), \quad (3.21)$$

where  $\chi_e$  and  $\chi_l$  are the electronic and lattice susceptibilities of the optical material. Again, by neglecting damping effects, the electronic susceptibility at frequency  $\omega$  is given by

$$4\pi\chi_e = F_s \frac{\omega_p^2}{(\omega_g^2 - \omega^2)}, \quad (3.22)$$

where  $\omega_p$ ,  $\omega_g$  and  $F_s$  are the plasma frequency, frequency of the optical band gap and oscillator strength, respectively. Here, I assume that all electronic oscillators are lumped into one effective electronic oscillator having energy gap,  $E_g$ . The oscillator strength is invariant with temperature and the square of the plasma frequency is inversely proportional to the volume of the material. It is a fact that the shift of the lattice absorption frequency is negligibly small compared with the change of operating temperature for most of the optical glasses [23] and nonlinear crystals [24]. This means that the temperature variation of  $\chi_l$  is almost zero. Differentiating Eq. (3.21) with respect to temperature,  $T$ , and by use of Eq. (3.22), we have

$$2n \frac{dn}{dT} = F_s \left[ \left( \frac{1}{\omega_g^2 - \omega^2} \right) \frac{d}{dT} (\omega_p^2) + \omega_p^2 \frac{d}{dT} \left( \frac{1}{\omega_g^2 - \omega^2} \right) \right] \quad (3.23)$$

or,

$$2n \frac{dn}{dT} = F_s \left[ \left( -3\alpha \frac{\omega_p^2}{\omega_g^2 - \omega^2} \right) - \frac{\omega_p^2}{(\omega_g^2 - \omega^2)^2} \frac{d}{dT} (\omega_g^2) \right], \quad (3.24)$$

where  $\alpha$  is the thermal expansion coefficient, and  $n$  and  $dn/dT$  are the room temperature refractive index and its variation with temperature,  $T$ , respectively.

Recently, we observed that the temperature coefficient of the peak energy in reflectivity, sometimes called the peak energy due to an excitonic transition,  $E_{eg}$ , yields the dominant contribution to  $dn/dT$  through the second term in Eq. [3.24] for optical fiber glasses [25] and some optical glasses [26]. Further, we observed in analyzing thermo-optic coefficients of  $\text{LiNbO}_3$  and  $\text{LiTaO}_3$  crystals [27] from room temperature up to 500°C and for  $\text{KNbO}_3$  crystals [28] from room temperature up to 180°C, that the fitting band gap is invariant under temperature and the excitonic band gap decreases more rapidly as the temperature increases, like in other semiconductor crystals [29].

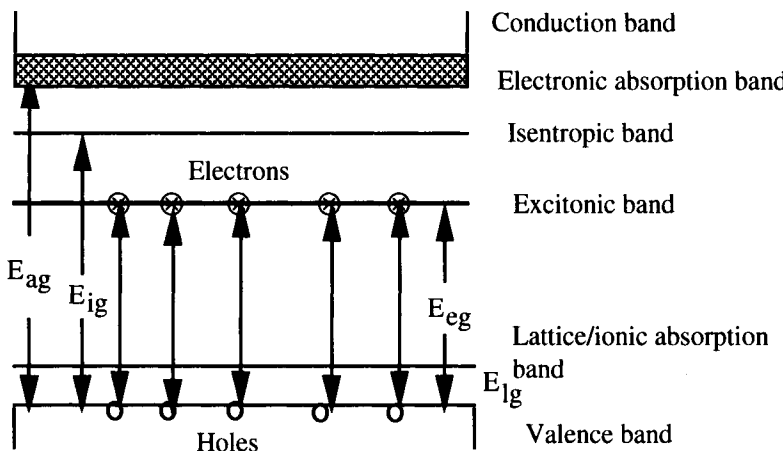


Figure 3.1: The schematic energy-level diagram for the isotropic materials; the energy levels will be shifted for an anisotropic material in an orthogonal direction (after Ref. 33).

The excitonic level lies about 1.3 eV below the conduction band as observed by Ellis *et al.* [30] and the excitonic band gap decreases with temperature, contributing to a positive thermo-optic coefficient. Matsuoka *et al.* [31] observed a temperature-insensitive peak energy corresponding to the band-to-band transition around 11.6 eV and a temperature-sensitive highest peak corresponding to the excitonic transition around 10.4 eV in  $\text{SiO}_2$  glass. As the temperature increases, the excitonic transition takes place, and the interaction between the electron and exciton dominates. This invariant energy gap with temperature has been assigned as the isentropic band gap,  $E_{ig}$ , which is similar to the isentropic thermal expansion in the temperature-entropy diagram [32]. This band gap determines the dispersion of  $2n(dn/dT)$ . In our experience, we noticed that the  $E_{ig}$  gap lies between the lowest level of the conduction band and  $E_{eg}$  for most of the optical materials. Therefore, we have assigned the energy band diagram [33] for all the optical materials as shown in Fig. 3.1.

The isentropic band,  $E_{ig}$  is lying in between the average electronic absorption band,  $E_{ag}$  and the excitonic band,  $E_{eg}$ . These bands are accounting for the thermo-optic coefficients of all optical materials. The electrons and ions are loosely bound in the ionic/ halide crystals and glasses. Therefore, an isentropic lattice/ionic band, denoted as  $E_{lg}$  is considered to account

for the thermo-optic coefficients in the long wavelength region. This energy gap is very small and is lying in the IR region. Now, by considering  $\omega_{ig}^2 = \omega_g^2 = \omega_{ag}\omega_{eg}$ , i.e., the isentropic band is the geometric mean of the electronic absorption band and the excitonic band of the materials, Eq. (3.24) transforms to

$$2n \frac{dn}{dT} = F_s \frac{\omega_p^2}{\omega_{ig}^2} \left[ -3\alpha \left( \frac{\omega_{ig}^2}{\omega_{ig}^2 - \omega^2} \right) - \left( \frac{\omega_{ig}^2}{\omega_{ig}^2 - \omega^2} \right)^2 \frac{1}{\omega_{eg}} \frac{d\omega_{eg}}{dT} \right], \quad (3.25)$$

where  $\omega_{ag}$  is the average electronic absorption band gap lying within the conduction band and has no effect on the thermo-optic coefficients, and is constant against temperature. Now, assigning  $R$ , the normalized dispersive wavelength, which is related to the wavelength  $\lambda$ , by  $R = \lambda^2/(\lambda^2 - \lambda_{ig}^2)$ , and  $F_s\omega_p^2/\omega_{ig}^2 = (n_\infty^2 - 1)$ , where  $n_\infty$  is the low-frequency refractive index in the IR region, Eq. (3.25) is written as

$$2n \frac{dn}{dT} = (n_\infty^2 - 1) \left( -3\alpha R - \frac{1}{E_{eg}} \frac{dE_{eg}}{dT} R^2 \right). \quad (3.26)$$

Eq. (3.26) is rewritten as

$$2n \frac{dn}{dT} = K^2 \left( -3\alpha R - \frac{1}{E_{eg}} \frac{dE_{eg}}{dT} R^2 \right), \quad (3.27)$$

where the constant,  $K$ , is related to  $n_\infty$  by  $K^2 = n_\infty^2 - 1$ .

This model resembles the Prod'homme model [15] which can be rearranged and written as

$$2n \frac{dn}{dT} = (n^2 - 1) \left[ -3\alpha \left( \frac{n^2 + 2}{3} \right) + \frac{1}{P} \frac{dP}{dT} \left( \frac{n^2 + 2}{3} \right) \right], \quad (3.28)$$

where  $P$  is the electronic polarizability and  $(I/P)(dP/dT)$  is its temperature coefficient. All other terms remain the same as in Eq. (3.27). In the present model, the temperature coefficient of the excitonic band gap is used instead of the temperature coefficient of the calculated electronic polarizability. The constant,  $K$ , is similar, but we have instead used the low frequency refractive index,  $n_\infty$ . In the Prod'homme model, there is no explicit consideration of dispersion, i.e., the wavelength dependence, but only a constant  $(n^2 + 2)/3$  is multiplied by both factors of Eq. (3.28). There is no

direct experimental evidence showing the measurement of the temperature coefficient of the electronic polarizability. By contrast, the present model is physically meaningful because it takes into account both the physical parameters  $\alpha$  and  $dE_{eg}/dT$ , which are both measured with greater accuracy, instead of considering the calculated  $dP/dT$  values. In addition, a basic understanding of the model is easy to grasp. As the temperature increases, usually the optical materials, such as glass, crystals, and semiconductors expand and more electrons are excited to the excitonic band from the valence band, and excitonic transition takes place.

When a constant  $dn/dT$  is assumed for a small temperature interval, Eq. (3.27) is transformed to

$$2n \frac{dn}{dT} = GR + HR^2. \quad (3.29)$$

Eq. (3.29) is a form of Sellmeier relation that represents the product of the refractive index and the thermo-optic coefficient. The constants  $G$  and  $H$  are related to the thermal expansion coefficient,  $\alpha$ , and the temperature coefficient of the excitonic band gap  $E_{eg}$ , respectively, by the relations  $G = -3\alpha K^2$ ,  $H = (-1/E_{eg})(dE_{eg}/dT)K^2$ . It is clear from Eq. (3.29) that the product is controlled by two factors which normally compete with one another to give positive or negative values of  $dn/dT$ . The first factor, the contribution from the thermal expansion coefficient  $\alpha$ , is negative because  $\alpha$  is normally positive for optical glasses, fiber glasses, nonlinear crystals, and semiconductors. Its contribution is also small because  $\alpha$  is of the order of  $10^{-6}/^\circ\text{C}$ . On the other hand, in the second factor, the temperature variation of the excitonic band gap is of the order of  $10^{-4} \text{ eV}/^\circ\text{C}$  and is normally negative for the glasses [31], nonlinear crystals [29], and semiconductors [34]. Since the first factor is also negative ( $-1/E_{eg}$ ), contribution of  $H$  is positive and larger than the first one to yield positive values of  $dn/dT$ . The value of  $R$  is greater than 1 in the UV region and almost has unity in the IR region.

For analyzing thermo-optic coefficients of ionic/halide crystals, an additional term is to be added in equation (3.29). This term is due to the variation of the lattice/ionic absorption frequency with temperature. Therefore, the Sellmeier equation for ionic/halide crystals takes the form

$$2n \frac{dn}{dT} = GR + HR^2 + LR_{ip}^2, \quad (3.30)$$

where  $L$ , the optical constant, is related to the lattice absorption band gap  $E_{lg}$ , as  $L = (-1/E_{lg})(dE_{lg}/dT)K^2$ . The normalized isentropic phonon/lattice wavelength,  $R_{ip}$  is related to the wavelength  $\lambda$ , by  $R_{ip} = \lambda^2/(\lambda^2 - \lambda_{ip}^2)$ . It is to be noted that this contribution is small.

The above two Sellmeier Eqs. (3.29 and 3.30) are used to satisfactorily characterize the thermo-optic coefficients of the presently available optical materials. The optical constants  $G$ ,  $H$ ,  $L$ ,  $\lambda_{ig}$ , and  $\lambda_{ip}$  are called Sellmeier coefficients for the thermo-optic coefficients.

### 3.4 Derivation of Sellmeier Coefficients

From a set of measured ( $n$ ,  $dn/dT$ , and  $\lambda$ ) data, optical constants  $G$  and  $H$  are evaluated by scanning the band gap ( $\lambda_{ig}$ ) values from the lowest to the highest one. The constants  $G$  and  $H$  are chosen in a manner such that the deviation between the experiment and computation is minimum, i.e., by adopting least squares procedure and one of the optical constants, say  $G$ , is nearly equal to the experimental value which is predetermined by knowing the thermal expansion coefficient  $\alpha$  and the value of nondispersive refractive index  $n_\infty$ .

As the thermo-optic coefficient is not constant, i.e., nonlinear over a wide range of temperature, we have fitted ( $2n$ ,  $dn/dT$ ,  $\lambda$ ) data at some suitable temperature increments/decrements (intervals) for some optical materials in the same form as in Eq. (3.29) by keeping  $G$  as a constant, since the thermal expansion coefficient is approximately constant from room temperature to the measured temperature. The optical constant  $H$  and the fitting gap  $E_{ig}$  are computed at the said temperature intervals. The constants are then plotted against temperature and interestingly, the variation of  $H$  is observed to be a quadratic function of temperature. However, the variation of fitting gap  $E_{ig}$  is negligibly small (0.01 nm/ $^\circ$ C). On the other hand,  $H$  is strongly dependent on temperature. The quadratic equation for  $H$  indicates that the variation of excitonic band gap with temperature is not linear in the measured temperature region. The temperature variations of excitonic band gap ( $dE_{eg}/dT$ ) are calculated at different temperatures and are plotted to show the almost linear dependency. The excitonic band gaps ( $E_{eg}$ ) at different temperatures are also shown for some optical materials. The band gap decreases asymptotically with temperature. This type of characteristic curve has been experimentally observed in many nonlinear crystals [29]. In

the following paragraphs, the thermo-optic coefficients of different groups of optical materials are analyzed. The Sellmeier coefficients are shown in Tables 3.1 for the crystals, and Table 3.2 for optical glasses.

**Table 3.1: Sellmeier Coefficients for Some Crystals and Semiconductors,  $[2n(dn/dT) = GR + HR^2 + LR_{ip}^2]$ ; Thermal Expansion Coefficient, Isentropic and Excitonic Band Gaps, and Variation of Excitonic Band Gap with Temperature**

Materials	Polarization	$n_\infty$	$G$ $L (X 10^{-3})$ <----[ 10 <sup>-6</sup> / °C ] ----->	Band gaps $E_{ig}$ , $E_{ip}$ , $E_{eg}$			Expansion Coeff. $\alpha [ 10^{-6}/ ^\circ C ]$	Expt. [Ref.]	Fit	$dE_{eg}/dT$ [10 <sup>-4</sup> eV/ °C]	Fit	Refs. for $n$ , $dn/dT$ , and Eqn.
				Isentropic	lattice	Excitonic						
ADA	o	1.530	-114.4750	-15.4885	0.165	7.50	7.00	29.00 [42]	28.50	--	0.80	[40, 8]
	e	1.500	-2.9697	33.6589	0.180	6.90	6.50	1.00	0.80	--	-1.75	
AD*A	o	1.530	-114.4750	-15.4885	0.165	7.50	7.00	--	20.00	--	0.80	[40, 8]
	e	1.500	-12.1100	31.6589	0.180	6.90	6.50	--	12.00	--	-1.65	
ADP	o	1.516	-150.6780	8.0121	0.150	8.27	8.00 [37]	38.00 [39]	38.40	--	-0.50	[40, 41, 5]
	e	1.470	-33.5894	28.9714	0.140	8.90	8.50	27.20	27.30	--	-2.10	[35, 8, 37]
AD*P	o	1.530	-150.6780	8.0121	0.150	8.27	8.00	--	38.00	--	-0.50	[40, 8]
	e	1.470	-33.5894	26.9714	0.140	8.90	8.50	--	27.30	--	-2.00	
AgCl		2.002	-292.3780	63.0232	0.230	5.50	5.00	32.40	32.40	--	-1.10	[129]
AgGaS <sub>2</sub>	o	2.400	-398.8000	1122.0000	0.260	4.77	2.70 [84]	14.40 [82]	2.80	-4.85 [83]	-6.40	[79, 81]
	e	2.300	255.0000	457.2000	0.328	3.78	2.70	-5.66	-2.00	--	-2.90	
ALON		1.770	-365.2930	373.9230	0.195	6.36	3.00	56.60	57.00	--	-5.30	[114]
Al <sub>2</sub> O <sub>3</sub>	o	1.755	-45.2665	83.5457	0.150	8.27	5.85	7.15	7.21	--	-2.40	[7, 115,
	e	1.748	-39.8961	81.9579	0.155	8.00	5.42	6.65	6.47	--	-2.20	116]
BaF <sub>2</sub>		1.400	-83.4102	39.0353	0.110	11.30	6.00	18.40 [7]	14.50	--	-2.40	[130]
			-31902.0000	60.000								
BaF <sub>2</sub>		1.400	-96.0080	48.9224	0.140	8.90	6.00	18.40	16.50	--	-3.10	[7]
				6.4628	60.000							

**Table 3.1: (Continued)**

Materials	Polarization	$n_\infty$	<i>G</i>	<i>H</i>	Band gaps $E_{ig}$ , $E_{ip}$ , $E_{eg}$			Expansion Coeff.		$dE_{eg}/dT$	Refs. for $n$ , $dn/dT$ , and Eqn.			
			$L (X 10^{-3})$	Isentropic/lattice Excitonic	$\mu\text{m}$	[eV]	[eV]	[Ref.]	$\alpha [10^{-6}/^\circ\text{C}]$	[ $10^{-4}$ eV/ $^\circ\text{C}$ ]	Expt. [Ref.]	Fit	Expt. [Ref.]	Fit
			<----[ $10^{-6}/^\circ\text{C}$ ] ----->											
BaF <sub>2</sub>		1.400	-115.9840	65.4513	0.160	7.80	6.00		18.40	20.10	--	-4.10	[10]	
				142.1930	60.000									
BBO	<i>o</i>	1.610	-19.3007	-34.9683	0.0652	19.00	6.43	[69]	4.00	[75]	4.00	--	+1.40	[66, 73–75]
	<i>e</i>	1.520	-141.4210	110.8630	0.073	17.00	6.43		36.00		36.00	--	-5.40	
BeO	<i>o</i>	1.520	-32.9658	60.9064	0.03	41.0	4.00		7.47		8.38	--	-1.90	[117]
	<i>e</i>	1.53	-24.6110	70.9506	0.034	36.5	4.70		5.64		6.12	--	-2.50	
BGO		2.300	-219.6180	57.9295	0.180	6.90	4.50		16.80		17.10	--	-0.61	[118]
BNN	<i>x</i>	2.250	-182.5760	73.1998	0.350	3.54	2.50		10.40	[111]	15.00	--	-0.45	[111]
	<i>y=z</i>	2.160	-124.7710	428.4920	0.248	5.00	3.00		11.40		11.30	--	-3.50	
C(diamond)		2.380	-18.7033	65.1738	0.085	14.60	12.00		1.25		1.26	--	-1.70	[133, 134]
CaCO <sub>3</sub>	<i>o</i>	1.613	-121.6890	122.4940	0.115	10.80	10.00		25.10		25.00	--	-7.60	[113]
	<i>e</i>	1.472	+12.7011	20.4803	0.137	9.05	6.83		-3.70		-3.70	--	-1.20	
CaF <sub>2</sub>		1.300	-74.3524	47.9117	0.080	15.50	8.00		18.70	[7]	18.10	--	-5.55	[3]
				11.5103	50.000									
CaF <sub>2</sub>		1.300	-77.7534	44.7453	0.130	9.50	8.00		18.70	[7]	18.80	--	-5.19	[7]
				60.7785	50.000									
CaF <sub>2</sub>		1.300	-79.0806	44.6212	0.140	8.90	8.00		18.70	[7]	19.10	--	-5.17	[10]
				89.0224	50.000									
CaMoO <sub>4</sub>	<i>o</i>	1.910	-93.7427	47.7368	0.310	4.00	3.00		11.80		11.80	--	-0.50	[119]

**Table 3.1: (Continued)**

Materials	Polarization	$n_\infty$	G	H	Band gaps $E_{ig}$ , $E_{ip}$ , $E_{eg}$			Expansion Coeff.	$dE_{eg}/dT$		Refs. for $n$ , $dn/dT$ , and Eqn.	
			$L (X 10^{-3})$	$<----[ 10^{-6}/^{\circ}\text{C} ] ----->$	μm	[eV]	[eV]	[Ref.]	Expt. [Ref.]	Fit		
CaWO <sub>4</sub>	e	1.920	-40.0200	8.03851	0.310	4.00	3.00		7.60	7.60	--	-0.10
	o	1.870	-27.1657	5.12541	0.310	4.00	3.00		12.38	3.60	--	-0.10
	e	1.870	-40.1307	8.96004	0.310	4.00	3.00		6.35	5.40	--	-0.10
CDA	o	1.540	-29.0445	-46.2754	0.161	6.90	6.00		7.00 [42]	12.00	--	+2.00
	e	1.530	-205.0850	124.8060	0.187	6.20	5.00		51.00	45.00	--	-4.60
	o	1.540	-204.4210	127.1350	0.120	10.30	9.50		51.00 [42]	49.70	--	-8.80
CdGeP <sub>2</sub>	e	1.530	-40.4922	-10.2249	0.080	15.50	10.00		8.70	10.09	--	+0.70
	o	3.121	-8.1660	1049.1200	0.4988	2.49	1.99 [85]		0.04 [86]	0.03	-2.3 [85]	-2.40
	e	3.140	-235.0070	1321.7100	0.539	2.30	1.72		0.89	0.89	-2.5	-2.60
CdF <sub>2</sub>		1.500	-125.2880		88.5095	0.150	8.27	5.00	21.80 [7]	21.70	--	-3.70
					0.0280	50.000						[7]
CdS	o	1.710	-17.8000	348.0000	0.360	3.44	3.00		2.50 [135]	3.10	-5.0 [130]	-2.10
	e	1.720	-20.6000	379.2000	0.360	3.44	3.00		4.60	3.50	--	-2.20
CdSe	o	2.450	-23.9000	323.0000	0.450	2.76	2.40		2.90 [135]	1.60	-4.6 [130]	-1.55
	e	2.470	-23.6000	343.8000	0.450	2.76	2.40		4.90	1.50	--	-1.62
CdSiP <sub>2</sub>	o	3.180	-261.1100	1604.9000	0.353	3.51	2.10 [89]		11.10 [90]	12.70	-3.5 [88]	-3.70
	e	3.180	-4.1000	1315.2000	0.371	3.34	2.10	0.00	0.02	-3.5	--	-3.10
CdTe		2.665	-91.7544	604.3350	0.5146	2.41	1.47 [141]	5.00	5.00	-2.9 [141]	-1.50	[11, 140]
CdTe		2.683	-90.1873	639.8820	0.481	2.58	2.14 [141]	5.00	4.90	-2.9 [141]	-2.20	[11, 136]
CsBr		1.430	-297.2830		60.5160	0.360	3.44	3.00	47.00	47.40	--	-1.74
					50.6273	200.000						[131]

**Table 3.1: (Continued)**

Materials	Polarization	$n_\infty$	$G$	$H$	Band gaps $E_{ig}$ , $E_{ip}$ , $E_{eg}$			Expansion Coeff.		$dE_{eg}/dT$	Refs. for $n$ , $dn/dT$ , and Eqn.	
			$L (X 10^{-3})$ <----[ $10^{-6}/^\circ\text{C}$ ] ----->	$\mu\text{m}$	[eV]	[eV]	[Ref.]	$\alpha [10^{-6}/^\circ\text{C}]$ Expt. [Ref.]	Fit	Expt. [Ref.]	Fit	
CsI		1.520	-377.3430	102.4440 37.0207	0.198 200.000	6.26	5.00	48.60	48.00	—	-3.91	[131]
CuGaS <sub>2</sub>	o	2.290	-122.8220	357.7850	0.313	3.96	2.50 [91]	0.77 [92]	0.77	-2.2 [92]	-1.72	[79]
	e	2.470	-117.8550	368.6930	0.338	3.67	2.43	0.77	0.77	-1.5 [93]	-1.76	
DLAP	x	1.480	-206.2320	81.8664	0.160	7.75	5.83	—	57.70	—	-4.01	[76]
	y	1.540	-111.1290	39.4953	0.160	7.75	7.07	—	27.00	—	-2.01	
	z	1.550	-307.5360	89.6214	0.160	7.75	7.32	—	73.10	—	-4.68	
GaAs		3.320	-150.0250	1452.1500	0.411	3.02	2.17 [141]	5.00	5.00	-4.2 [141]	-3.10	[99, 140]
GaP		3.015	-129.1680	690.8060	0.3174	3.91	3.03 [141]	5.30	5.30	-3.7 [141]	-2.60	[99, 140]
GaN		2.350	-75.9980	322.9200	0.280	4.43	4.00	5.59	5.60	—	-2.86	[99]
GaSe	o	2.632	-119.1000	615.6000	0.342	3.63	3.00	11.50 [108]	6.70	-4.8 [107]	-3.10	[105-107]
	e	2.355	-144.1000	1314.3000	0.370	3.35	3.00	9.67	10.60	—	-8.70	[99]
Ge		4.001	-257.6750	3475.3000	0.6563	1.89	1.36 [141]	5.7	5.70	-3.7 [141]	-3.20	[144, 140]
HfO <sub>2</sub> :Y <sub>2</sub> O <sub>3</sub>		1.980	-67.1742	89.3484	0.173	7.17	5.90	—	7.70	—	-1.80	[122]
HgS	o	1.250	-433.1000	459.1000	0.385	3.22	2.80	—	25.30	-2.5 [104]	-2.30	[102-104]
	e	1.310	-338.7000	578.8000	0.395	3.14	2.80	—	15.98	—	-2.30	
InAs		3.500	-149.3520	2179.3700	1.9515	0.60	4.43 [141]	4.40	4.40	-3.5 [141]	-2.80	[99, 140]
InP		3.100	-116.1420	592.3540	0.9140	1.36	2.20 [141]	4.50	4.50	-2.9 [141]	-1.50	[99, 140]
KBr		1.500	-301.4510	171.5900 23.1720	0.135 160.000	9.10	6.60	38.70 [7]	40.20	—	-9.10	[7]
KBr		1.500	-324.8960	203.3960	0.140	8.86	6.60	38.70 [7]	43.30	—	-10.70	[128]
				331372 X 10	160.000							

**Table 3.1: (Continued)**

Materials	Polarization	$n_{\infty}$	$G$	$H$	Band gaps $E_{ig}$ , $E_{ip}$ , $E_{eg}$			Expansion Coeff.		$dE_{eg}/dT$	Refs. for $n$ , $dn/dT$ , and Eqn.	
			$L (X 10^{-3})$	Isentropic/lattice	Excitonic	$\alpha [10^{-6}/^{\circ}\text{C}]$	Expt. [Ref.]	Fit	$[10^{-4} \text{ eV}/^{\circ}\text{C}]$	Expt. [Ref.]	Fit	
			<----[ $10^{-6}/^{\circ}\text{C}$ ] ----->		$\mu\text{m}$	[eV]	[eV]	[Ref.]				
KCl		1.430	-224.1240	117.1120 299.2220	0.135 160.000	9.19 6.00	37.10	[7]	35.70	--	-6.70	[7]
KCl		1.430	-231.2620	135.5470 508.7530	0.135 160.000	9.19 6.00	37.10		37.00	--	-7.80	[128]
KDA	o	1.530	-303.7200	170.2220	0.190	6.90 5.00	47.00	[42]	65.00	--	-6.30	[40, 8]
	e	1.500	-86.9424	21.0408	0.210	5.90 5.00	24.00		23.20	--	-0.80	
KDP	o	1.470	-157.8360	32.6350	0.110	11.30 10.00	44.00	[39]	45.30	--	-2.80	[40, 41, 58]
	e	1.460	-86.2661	12.3940	0.140	8.90 8.00	22.00		25.40	--	-0.90	[35, 36]
KD*P	o	1.470	-99.6083	21.1153	0.170	7.29 5.30	24.90	[44]	28.60	--	-1.00	[5, 40,
	e	1.450	-138.3930	65.6926	0.170	7.29 5.30	44.00		41.80	--	-3.00	8, 35]
KI		1.530	-337.5380	183.7250	0.189	6.56 5.00	40.30		42.00	--	-6.90	[128]
				107131X10 <sup>2</sup>	200.000							
KNO	x	2.120	-52.9953	156.0920	0.282	4.40 4.10 [60]	5.00 [59]		5.10	--	-1.80	[58]
	y	2.150	-152.4170	27.9796	0.362	3.40 3.10	14.00		14.00	--	-0.20	
	z	2.040	-5.12731	267.2700	0.2526	4.90 4.10	0.50		0.54	--	-3.50	
KTP	x	1.670	-52.4727	70.6357	0.210	5.90 4.10 [60]	6.8-11 [63]	9.80	--	-1.62	[61, 62, 64]	
	y	1.700	-51.6979	75.8637	0.227	5.50 4.10	9.0-9.8		9.10	--	-1.65	
	z	1.800	-3.03864	47.9739	0.290	4.30 4.10	-1.3-0.6		0.60	--	-0.88	
KTP	x	1.670	-51.7317	106.8120	0.200	6.20 4.10 [60]	6.8-11 [63]	9.60	--	-2.45	[50, 61, 62]	
	y	1.700	-52.8840	126.4280	0.215	5.80 4.10	9.0-9.8		9.30	--	-2.74	
	z	1.800	5.50571	111.8990	0.214	5.80 4.10	-1.3-0.6	-0.80	--	-2.05		

Table 3.1: (Continued)

Materials	Polarization	$n_\infty$	$G$ $L (X 10^{-3})$ $<----[ 10^{-6}/^{\circ}\text{C} ] ----->$	$H$ $\mu\text{m}$	Band gaps $E_{\text{ig}}$ , $E_{\text{ip}}$ , $E_{\text{eg}}$			Expansion Coeff.		$dE_{\text{eg}}/dT$		Refs. for $n$ , $dn/dT$ , and Eqn.
					Isentropic/lattice	Excitonic	$\alpha [ 10^{-6}/^{\circ}\text{C}]$	Expt. [Ref.]	Fit	Expt. [Ref.]	Fit	
LBO	<i>x</i>	1.530	-127.7020	122.1340	0.053	23.40	7.80 [69]	32.40 [68]	32.90	--	-7.10	[65 - 67]
	<i>y</i>	1.530	373.3387	-415.1040	0.0327	37.90	7.80	-92.40	-91.80	---	+24.10	
	<i>z</i>	1.550	-446.9500	419.3340	0.0435	28.50	7.80	106.40	106.20	---	-23.30	
LiF		1.340	-158.3480	110.8230	0.090	13.80	8.00	33.20 [7]	33.20	---	-11.10	[7]
				153.4570	40.000							
LiF		1.340	-176.8010	125.2570	0.090	13.80	8.00	33.20 [7]	37.00	---	-12.60	[128]
				121.0350	40.000							
LIO	<i>o</i>	1.809	-203.8850	-131.8000	0.130	9.54	6.00	31.20 [54]	29.90	---	3.47	[50, 55, 27]
	<i>e</i>	1.700	-323.4600	53.5749	0.190	6.53	6.00	58.00	57.10	---	-1.70	
LNO	<i>o</i>	2.113	-173.5490	163.0330	0.280	4.43	3.90 [56]	16.70 [53]	16.70	-2.0 [56]	-2.12	[4, 48, 27]
	<i>e</i>	2.098	-21.4246	174.5430	0.282	4.41	3.90	2.00	2.10	-2.0	-2.51	[49, 52]
LTO	<i>o</i>	2.029	-196.4220	200.1090	0.185	6.70	4.50 [56]	21.00 [57]	21.00	-2.0	-2.88	[51, 27]
	<i>e</i>	2.032	-53.5020	145.8320	0.267	4.64	4.20	5.70	5.70	---	-2.10	
LiYF <sub>4</sub>	<i>o</i>	1.447	-26.7781	23.4390	0.120	10.30	8.20	8.30	8.20	---	-1.80	[132]
	<i>e</i>	1.469	-34.4546	26.0227	0.110	11.30	9.80	13.30	9.90	---	-2.20	
MgAl <sub>2</sub> O <sub>4</sub>		1.560	-69.2415	71.0157	0.290	4.28	3.50	6.97	16.10	---	-1.97	[115]
MgF <sub>2</sub>	<i>o</i>	1.290	-37.2043	39.3186	0.095	13.10	8.00	9.40 [7]	9.30	---	-4.70	[7]
				15.9824	40.000							
	<i>e</i>	1.290	-56.7859	57.3986	0.080	15.50	8.00	13.70 [7]	14.20	---	-6.90	
MgO		1.720	-62.4416	107.0410	0.132	9.39	8.81	10.60	10.60	---	-4.80	[123, 124]
				104.1330	0.138	9.00	8.07	10.60	10.41	---	-4.30	

**Table 3.1: (Continued)**

Materials	Polarization	$n_\infty$	$G$	$H$	Band gaps $E_{ig}$ , $E_{ip}$ , $E_{eg}$			Expansion Coeff.		$dE_{eg}/dT$	Refs. for $n$ , $dn/dT$ , and Eqn.		
			$L (X 10^{-3})$	$\text{Isentropic/lattice}$	Excitonic	$\mu\text{m}$	[eV]	[eV]	[Ref.]	$\alpha [10^{-6}/^\circ\text{C}]$	Expt. [Ref.]	Fit	
NaCl		1.400	-224.7430 <----[ 10 <sup>-6</sup> /°C ] ---->	122.0700 46.1208	0.150 80.000	8.30	7.00		41.10	39.00	---	-8.90	[130]
NaCl		1.400	-232.5270	131.6540 46.5769	0.150 80.000	8.30	7.00		41.10	40.40	---	-9.60	[128]
NaCl		1.400	-250.9910	139.2630 317.5410	0.150 80.000	8.30	7.00		39.60 [7]	43.60	---	-10.10	[7]
NaF		1.250	-106.1070	61.7984 107.2360	0.120 80.000	10.30	8.00		33.50	31.40	---	-8.80	[128]
NaF		1.250	-108.1170	72.6030 822.2110	0.130 80.000	9.50	8.00		32.20 [7]	32.00	---	-10.30	[7]
PbMoO <sub>4</sub>	o	2.132	-215.9160	-11.2558	0.350	3.50	3.00		20.30	20.30	---	+0.10	[119]
	e	2.127	-91.9798	-18.4567	0.350	3.50	3.00		8.70	8.70	---	+0.16	
PbS		4.099	-9137.5400	-4411.2300	1.430	0.87	1.13 [141]	19.00	190.00	+5.2 [141]	+3.20	[143, 140]	
PbSe		4.785	-1275.2300	-7095.1900	2.2133	0.56	0.95 [141]	19.40	19.40	+4.0 [141]	+3.10	[143, 140]	
PbTe		5.745	-1899.3500	-11010.2000	1.9073	0.65	0.77 [141]	19.80	19.80	+4.5 [141]	+2.70	[143, 140]	
RDA	o	1.530	-263.4890	150.5630	0.180	6.90	5.10	49.00 [42]	65.50	---	-5.70	[40, 8]	
	e	1.500	-142.2770	71.5459	0.190	6.50	5.10	17.00	37.00	---	-3.10		
RD*A	o	1.530	-202.4150	102.2690	0.190	6.50	5.10	---	65.50	---	-3.90		
	e	1.500	-142.2770	88.5459	0.190	6.50	5.10	---	53.70	---	-3.80		
RDP	o	1.480	-166.6340	56.1215	0.110	11.30	7.90	45.80 [42]	46.70	---	-3.70	[40, 8]	
	e	1.460	-171.4140	86.2442	0.200	6.20	5.50	39.20	51.30	---	-4.20		

**Table 3.1: (Continued)**

Materials	Polarization	$n_\infty$	$G$	$H$	Band gaps $E_{ig}$ , $E_{ip}$ , $E_{eg}$			Expansion Coeff.		$dE_{eg}/dT$	Refs. for $n$ , $dn/dT$ , and Eqn.	
			$L \times 10^{-3}$	$\text{Isentropic/lattice }$	$\mu\text{m}$	[eV]	[eV]	[Ref.]	$\alpha [10^{-6}/^\circ\text{C}]$	Expt. [Ref.]	Fit	
Si		3.450	-86.1087	1159.2000	0.4196	2.96	2.26 [141]	2.62	2.62	-2.8 [141]	-2.40	[144, 140]
a-Si		3.400	-43.8250	829.6600	0.6170	2.00	2.60 [146]	1.30 [146]	1.38	-5.6 [146]	-2.20	[145-147]
c-Si		3.421	-78.7560	1904.2000	0.3148	3.94	3.38 [34]	2.50	2.49	-5.37 [34]	-6.10	[146-149]
c-Si		3.421	-92.5980	1625.7500	0.3333	3.72	3.38 [34]	2.50	2.90	-5.37 [34]	-5.20	[144, 146-149]
c-Si		3.421	-89.8691	1364.6500	0.3346	3.71	3.40 [150]	2.50	2.80	-4.6 [150]	-4.30	[150]
$\alpha\text{-SiO}_2$	o	1.515	-61.1840	43.9990	0.120	10.30	8.90	6.88	15.70	--	-3.02	[1]
	e	1.520	-70.1182	49.2875	0.120	10.30	8.90	12.38	17.80	--	-3.32	
SrF <sub>2</sub>		1.330	-85.7210	49.8663	0.110	11.30	7.90	17.90 [7]	17.50	--	-5.10	[7]
SrF <sub>2</sub>				1681.6800	40.000							
SrF <sub>2</sub>		1.330	-156.8210	119.6520	0.110	11.30	7.90	17.90	35.00	--	-12.30	[10]
TeO <sub>2</sub>	o	2.180	-58.7374	77.4969	0.270	4.60	4.20	4.90	5.20	--	-0.90	[125]
	e	2.320	-192.3890	199.1830	0.220	5.60	5.00	15.00	14.60	--	-3.20	
TiO <sub>2</sub>	o	2.432	-132.2530	64.5269	0.300	4.10	3.50	8.97	8.98	--	-0.46	[126]
	e	2.683	-127.5650	45.2141	0.300	4.10	3.50	6.86	6.87	--	-0.26	
Tl <sub>3</sub> AsSe <sub>3</sub>	o	3.300	-477.9090	130.8100	1.350	0.92	0.60	18.00	16.10	--	-0.08	[109, 110]
	e	3.100	-908.1540	1089.2400	0.505	2.46	2.00	28.00	35.20	--	-2.50	

**Table 3.1: (Continued)**

Materials	Polarization	$n_\infty$	$G$	$H$	Band gaps $E_{ig}$ , $E_{ip}$ , $E_{eg}$			Expansion Coeff.	$dE_{eg}/dT$ [ $10^{-4}$ eV/ $^{\circ}$ C]	Refs. for $n$ , $dn/dT$ , and Eqn.		
			$L$ ( $\times 10^{-3}$ ) <----[ $10^{-6}/^{\circ}$ C ] ----->	$\mu\text{m}$	[eV]	[eV]	[Ref.]					
Tl [Br:I] (KRS-5)		2.200	-1315.6700	231.6840 113.1610	0.290 160.000	4.30 8.38	3.50 7.50	58.00 7.70	57.50 7.80	-- --	-2.11 -2.84	[2]
YAG		1.750	-48.2648	78.0333	0.148	8.38	7.50	7.70	7.80	--	-2.84	[121]
$\text{Y}_2\text{O}_3$		1.890	-51.0773	77.2278	0.150	8.27	7.50	6.56	6.60	--	-2.24	[114]
$\beta$ -ZnS		2.150	-74.1348	256.9390	0.275	4.51	3.77	6.80 [7]	6.82	---	-2.67	[7]
ZnSe		2.350	-98.9475	392.1820	0.310	4.00	3.48	7.30	7.29	-4.8 [141]	-3.02	[11]
ZnSe		2.570	-113.1560	363.7430	0.3057	4.06	3.73 [141]	7.00 [7]	7.10	-4.8 [141]	-2.60	[7]
ZnSiAs <sub>2</sub>	o	3.171	-190.2000	1644.6000	0.390	3.18	2.90 [94]	7.20 [95]	7.00	-3.5 [88]	-2.80	[78, 88]
	e	3.206	-89.1000	1616.2000	0.404	3.07	2.90	2.80	3.20	---	-2.70	
ZnSiP <sub>2</sub>	o	2.900	-164.5000	1859.3000	0.331	3.75	3.10 [96]	7.90 [86]	7.40	-2.8 [97]	-3.10	[87, 88]
	e	2.890	-86.2000	1813.0000	0.336	3.69	3.00	3.20	3.90	-3.0	-3.00	
ZnGeP <sub>2</sub>	o	3.121	-132.4160	1042.4600	0.3898	3.18	2.63 [97]	5.00	5.00	-2.5 [88]	-3.13	[77]
	e	3.158	-210.8390	1217.7700	0.3889	3.19	2.31	7.80	7.80	---	-3.14	
ZrO <sub>2</sub> : 12%Y <sub>2</sub> O <sub>3</sub>		2.000	-91.2056	115.4850	0.167	7.43	7.23	10.20	10.10	--	-2.78	[127]

**Table 3.2: Sellmeier Coefficients for Various Optical Glasses at 20°C, [2n(dn/dT) = GR + HR<sup>2</sup>]; Thermal Expansion Coefficient, Isentropic and Excitonic Band Gaps, and Variation of Excitonic Band Gap with Temperature**

Glasses	$n_{\infty}$	$G$	$H$	Band gaps			Expansion Expt.[Ref.]	Coeff Fit	$dE_{eg}/dT$ [10 <sup>-4</sup> eV/°C]	Refs. for $n, dn/dT$ and Eq.	
				Isentropic μm	$E_{ig}$ [eV]	$E_{eg}$ [eV]					
<----[10 <sup>-6</sup> / °C] ---->											
<b>Ohara</b>	<b>Schott</b>										
BAL4	BaLF4	1.549	-33.1615	38.4818	0.1512	8.20	7.39	7.9 [18]	7.9	-2.0	[18, 156]
BAL11	BaK1	1.544	-29.8957	36.3157	0.1446	8.58	7.36	7.2 [18]	7.2	-1.9	[18, 156]
BAL23	PSK3	1.522	-24.0703	32.3867	0.1286	9.64	8.60	6.1 [18]	6.1	-2.1	[18, 156]
BSM4	SK4	1.581	-29.6823	35.7490	0.1335	9.29	8.72	6.6 [18]	6.6	-2.1	[18, 156]
BSM24	SSK4A	1.587	-29.6234	39.4928	0.1465	8.46	7.46	6.5 [18]	6.5	-1.9	[18, 156]
NSL5	SK5	1.481	-29.3886	31.5514	0.1432	8.66	7.50	8.2 [18]	8.2	-2.0	[18, 156]
S-LAM2	LaF2	1.705	-42.3372	46.8995	0.1703	7.28	6.54	7.4 [18]	7.4	-1.6	[18, 156]
S-BSL7	BK7	1.488	-26.2676	32.3516	0.1304	9.51	8.30	7.2 [18]	7.2	-2.2	[18, 156]
S-FSL5	FK5	1.460	-30.5877	27.0300	0.1358	9.13	7.06	9.0 [18]	9.0	-1.7	[18, 156]
SLAL10	LaK10	1.665	-36.1597	42.5887	0.1528	8.12	7.29	6.8 [18]	6.8	-1.8	[18, 156]
SSL6	—	1.470	-18.1234	30.8473	0.1467	8.45	8.21	5.2 [18]	5.2	-2.2	[18, 156]
ZSL1	ZK1	1.505	-28.4466	36.6849	0.1439	8.62	7.58	7.5 [18]	7.5	-2.2	[18, 156]
—	KzFS6	1.540	-20.9066	29.8877	0.1550	8.00	7.52	5.1 [18]	5.1	-1.6	[19, 156]
PBH6	SF6	1.751	-50.2619	70.4245	0.2241	5.53	5.10	8.1 [18]	8.1	-1.7	[18, 156]
<b>Others</b>											
as1723 (at 28 °C)		1.513	-34.0879	57.9421	0.119	10.4	6.0	9.0 [17]	8.8	-2.7	[6, 25]
fs7940 (at 26 °C)		1.43	-1.26595	33.7930	0.117	10.6	10.2	0.16~0.6	0.6	-3.3	[6, 25]
vc7913 (at 28 °C)		1.43	-1.23171	32.2137	0.118	10.5	10.2	“ [151]	0.4	-3.1	[6, 25]
fs7940 + silica [152]											
+ SiO <sub>2</sub> [35]		1.43	-2.38947	32.6348	0.108	11.5	10.2	0.16~0.6	0.76	-3.2	[6, 25]

**Table 3.2: (Continued)**

Glasses	$n_\infty$	$G$	$H$	Band gaps			Expansion Expt.[Ref.]	Coeff Fit	$dE_{eg}/dT$ [10 <sup>-4</sup> eV/ °C]	Refs. for $n, dv/dT$ and Eq. [153]
				Isentropic μm	$E_{ig}$ [eV]	$E_{eg}$ [eV]				
Borosilicate-717	1.46	-17.6270	26.5232	0.106	11.6	10.4	5.1 [16]	5.1	-2.4	[16, 26]
Silica-739	1.44	-1.9969	25.5833	0.106	11.6	10.4	0.62 [16]	0.6	-2.5	[16, 26]
Soda lime-710	1.60	-36.1213	41.1111	0.105	11.4	9.6	7.75 [16]	7.8	-2.5	[16, 26]
Lead silicate	1.50	-30.0274	40.9336	0.103	14.0	5.5	7.95 [16]	8.0	-1.8	[16, 26]
Vitreous silica	1.435	-1.9436	27.2883	0.106	11.6	10.4	0.61 [12]	0.6	-2.7	[12, 25]
<b>Soda-Lime-Silica</b>										
$25\text{Na}_2\text{O}.\text{pCaO}.(75 - \text{p})\text{SiO}_2$										
$\text{p} = 0$	1.47	-50.3250	37.6279	0.104	11.4	9.3	14.45 [153]	14.45	-3.01	[154]
$= 5$	1.49	-53.7544	39.8834	0.104	11.4	9.3	14.65 ["]	14.65	-3.03	[154]
$= 10$	1.505	-57.6322	40.5481	0.104	11.4	9.3	15.15 ["]	15.15	-2.97	[154]
$= 15$	1.52	-60.5962	45.4648	0.104	11.4	9.3	15.45 ["]	15.45	-3.23	[154]
$= 20$	1.535	-64.4885	48.7405	0.104	11.4	9.3	15.85 ["]	15.85	-3.34	[154]
$(25 - \text{p})\text{Na}_2\text{O}.\text{pCaO}.75\text{SiO}_2$										
$\text{p} = 0$	1.47	-50.3250	37.6279	0.104	11.4	9.3	14.45 ["]	14.45	-3.01	[154]
$= 2.5$	1.48	-43.7855	38.8743	0.104	11.4	9.6	12.20 ["]	12.20	-3.12	[154]
$= 5$	1.487	-39.7869	38.2908	0.104	11.4	9.6	10.95 ["]	10.95	-3.03	[154]
$= 7.5$	1.491	-34.8578	40.6628	0.104	11.4	9.6	9.50 ["]	9.50	-3.19	[154]
$= 10$	1.497	-32.3908	39.4112	0.104	11.4	9.6	8.70 ["]	8.70	-3.05	[154]
<b>Fluoride BGZA (4)</b>										
	1.45	-53.5987	15.3175	0.270	4.6	4.3	16.9 [155]	16.8	-0.6	[155]
$L = 15914.2 \lambda_{ip} = 24$										

The experimental value of  $dE_{eg}/dT$  for  $\text{SiO}_2$  glass is  $-2.3 \pm 0.5$  ( $10^{-4}\text{eV/ }^\circ\text{C}$ ) [31]; therefore the fit values of  $dE_{eg}/dT$  for other glasses (except fluoride) are within the experimental accuracy.

### 3.4.1 Nonlinear Crystals

The nonlinear crystals, such as ammonium dihydrogen phosphate, (ADP), potassium dihydrogen phosphate, (KDP), and their isomorphs have been used as the primary group of workhorse crystals in nonlinear optics and electro-optical devices since the mid-1960s. The temperature dependence of the refractive indices of ADP and KDP crystals along with deuterated potassium dihydrogen phosphate, KD\*P were measured by Phillips [5] in 1966. Data were taken between 150 and 298 K from  $0.365 \mu\text{m}$  to  $0.691 \mu\text{m}$  and were fitted to the following form

$$n(T) - n(298) = cf(n).(298 - T), \quad (3.31)$$

where  $f = n^2 + a \cdot n + b$ , and  $T$  is the absolute temperature. In the same time, Yamazaki and Ogawa [35] reported their measurements between 100 and 300 K for KDP, and 150 and 300 K for ADP and KD\*P only at three, and two wavelengths in the visible region, respectively. They used a fit of the form

$$(n - n_{300}) = a + bT + cT^2, \quad (3.32)$$

where  $a$ ,  $b$ , and  $c$  are some constants.

In 1981, Onaka and Kawamura [36] measured the temperature variation of the refractive indices of KDP at eight wavelengths from  $0.405 \mu\text{m}$  to  $0.546 \mu\text{m}$ . In 1982, Onaka and Takeda [37] reported the temperature dependence of the refractive indices for ADP at four wavelengths from  $0.365 \mu\text{m}$  to  $0.546 \mu\text{m}$ . The temperature dependence was fitted to the following formula

$$\Delta n_{o,e} = n_{o,e}(T) - n_{o,e}(298) = a_{o,e}(298 - T)^2 + b_{o,e}(298 - T), \quad (3.33)$$

where the constants  $a_{o,e}$  and  $b_{o,e}$  were determined from the experimental data using the least-square method. They reported some numerical values of thermo-optic coefficients for KDP and ADP crystals.

In 1982, Ghosh and Bhar [38] reported double-pole Sellmeier fits to the indices of KDP, ADP, and KD\*P and represented each of the four Sellmeier parameters as varying linearly with temperature. Simultaneously, data on thermo-optic coefficients for nine of the isomorphs of KDP were reported

by Barnes *et al.* [8] at five wavelengths in the visible region from 0.405  $\mu\text{m}$  to 0.633  $\mu\text{m}$ . There is a review paper entitled *Electro-optic, Linear, and Nonlinear Optical Properties of KDP and Its Isomorphs* by Eimerl [43] on nonlinear optical properties and room temperature Sellmeier coefficients.

However, there is no physical explanation or a suitable model to account for the thermo-optic coefficients and their dispersions for these important nonlinear optical materials. So, we have used all the above experimental data and also some estimated values within the measured values allowable to analyze Eq. (3.29) above. The computed optical constants are shown in Table 3.1. The calculated values and the experimental data are cited in Table 3.3. Thus, the Sellmeier coefficients cited in Tables 2.1 and 3.1 can be used to calculate refractive indices for any wavelength within the transmission region at any operating temperature. It is worthwhile to see the characteristic behavior of dispersion of  $dn/dT$ , i.e., to estimate the  $dn/dT$  values beyond the measured wavelength region both in the UV and in the IR region. Hence, experimental data are plotted in Figs. 3.2 to 3.6 for ADA, CDA, CD\*A, KDA, and RDA and in Figs. 3.7 to 3.10 for ADP, KDP, KD\*P, and RDP crystals, respectively. Thermo-optic coefficients are negative for all these KDP isomorphs crystals, except for ADA extraordinary polarization. Thermal expansion coefficients are dominant to contribute negative  $dn/dT$  to these crystals. Since the thermal expansion coefficient is lowest and minimum for ADA extraordinary polarization, the  $dn/dT$  values are positive. Similarly, it is the case for extraordinary polarization in ADP crystal, in which the  $dn/dT$  values are negative but the absolute value is very small. The  $dn/dT$  values asymptotically decrease from high negative to less negative values in the UV to near-IR region for most of the crystals. However, in some cases the opposite behavior is also observed. But, the thermo-optic coefficients are decreasing asymptotically from high positive values to less positive values for ADA (e) crystal; and from positive to negative values (the absolute value is within 1.5 ppm) in ADP (e) crystal. Since the  $dn/dT$  values are different in orthogonal polarizations in ADA and ADP crystal, it is possible to use these crystals efficiently in temperature-tuned optical devices.

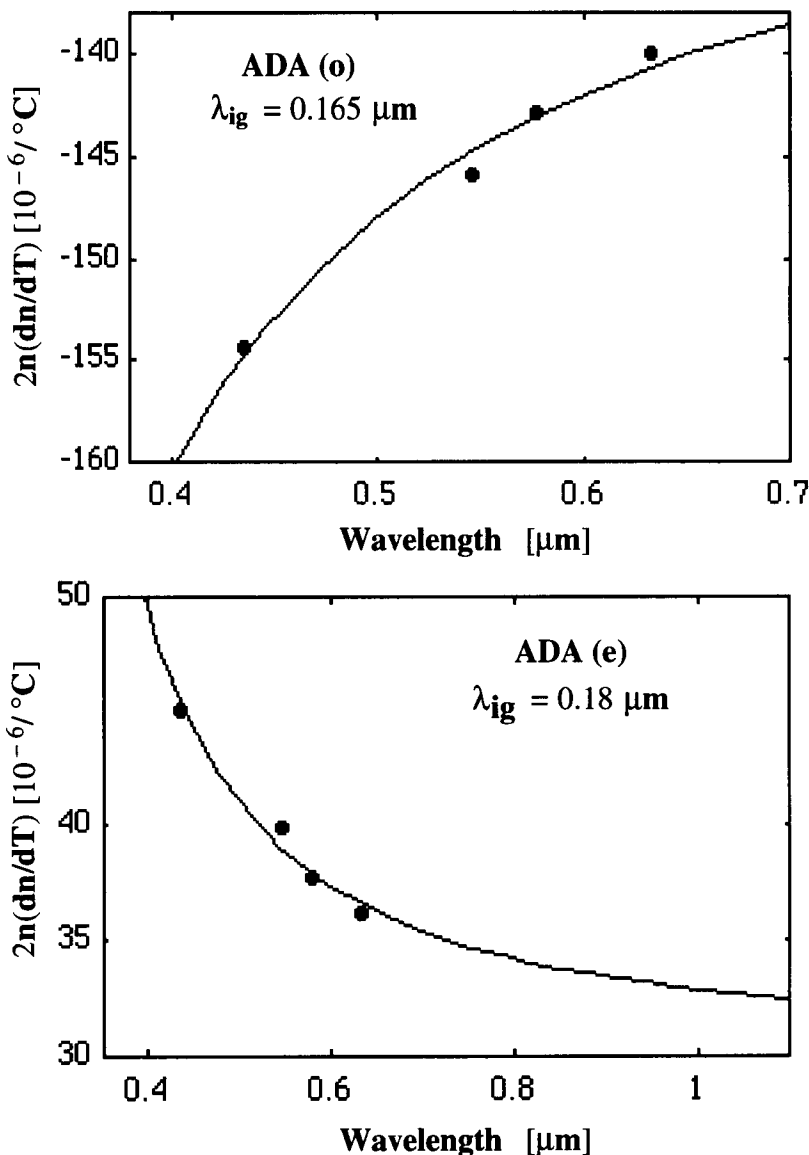


Figure 3.2:  $2n(dn/dT)$  versus wavelength for the ADA crystal: Curves are computed values from the optical constants  $G$ ,  $H$ , and  $E_{ig}$  from Table 3.1; solid circles are the experimental data [40, 8] at  $33^{\circ}\text{C}$ .

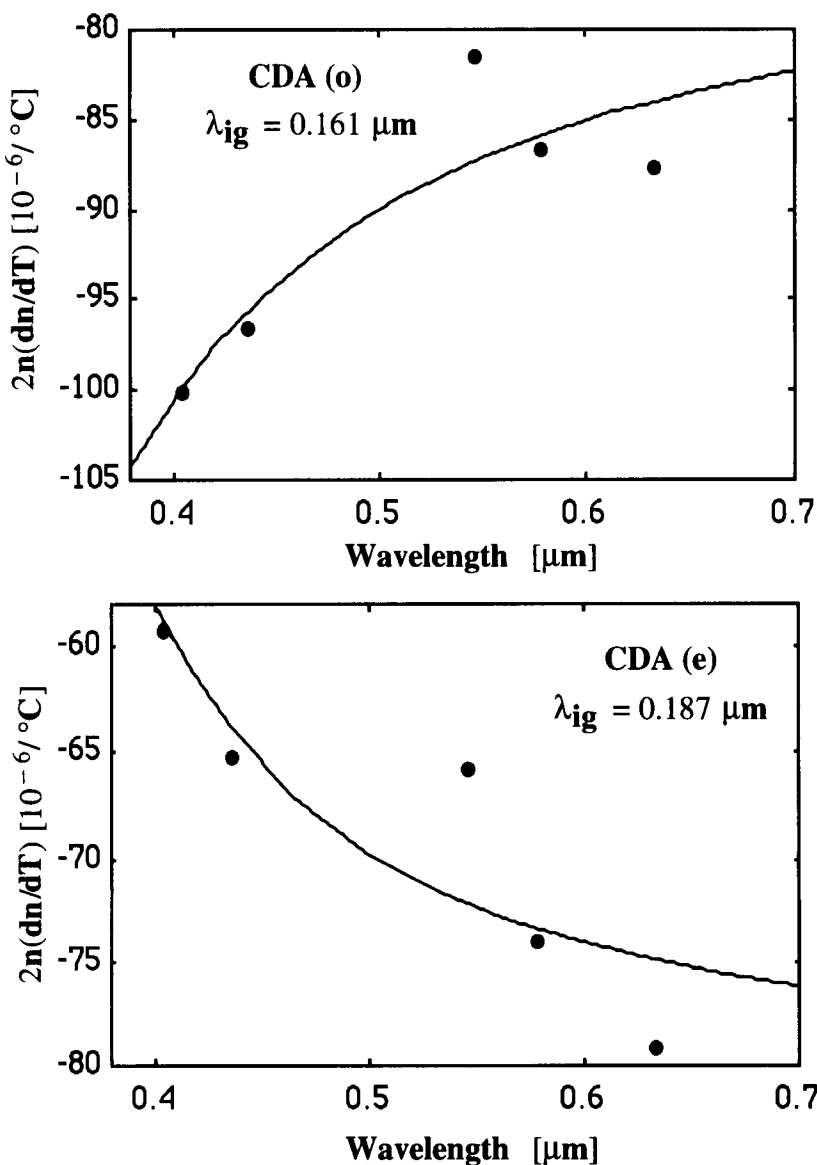


Figure 3.3:  $2n(dn/dT)$  versus wavelength at  $33^\circ\text{C}$  for the CDA crystal: Curves are the computed values from the optical constants  $G$ ,  $H$ , and  $E_{ig}$  from Table 3.1; the experimental points [40, 8] are shown as solid circles.

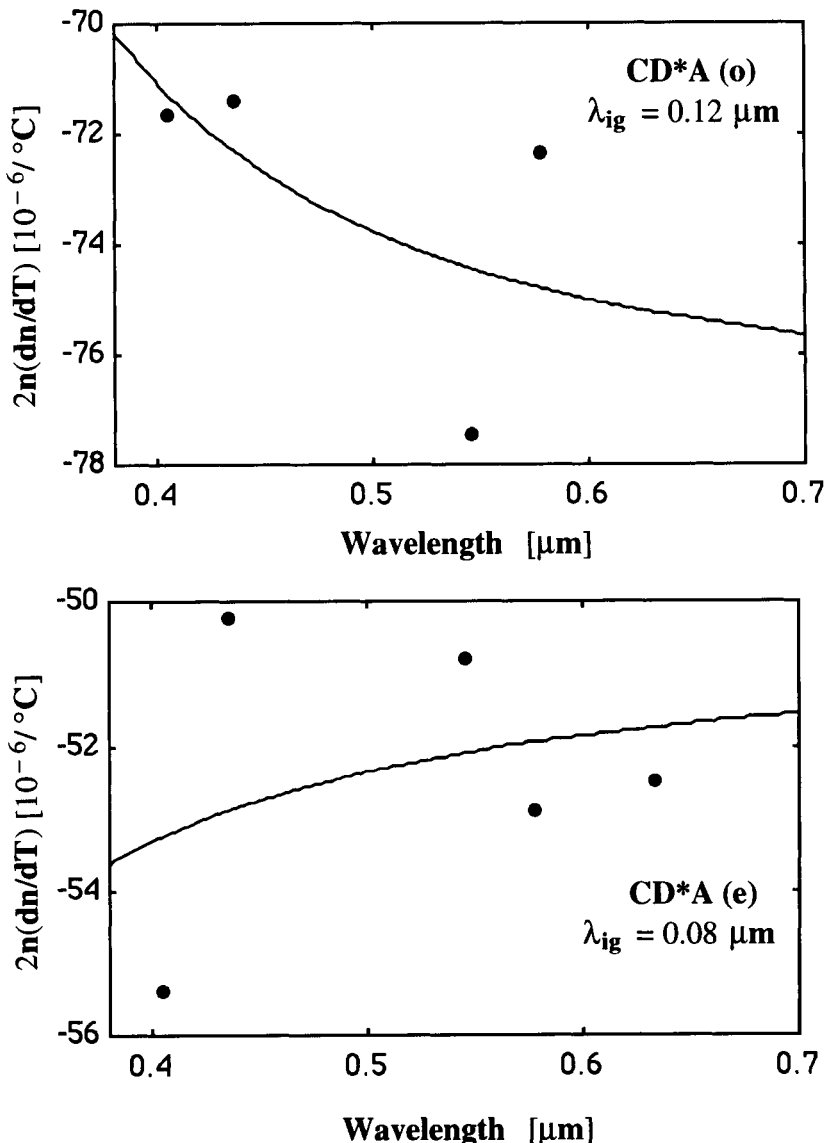


Figure 3.4:  $2n(dn/dT)$  versus wavelength at  $33^\circ\text{C}$  for the CD\*A crystal: Solid curves are the computed values from the optical constants  $G$ ,  $H$ , and  $E_{ig}$  from Table 3.1; the experimental points [40, 8] are shown as solid circles.

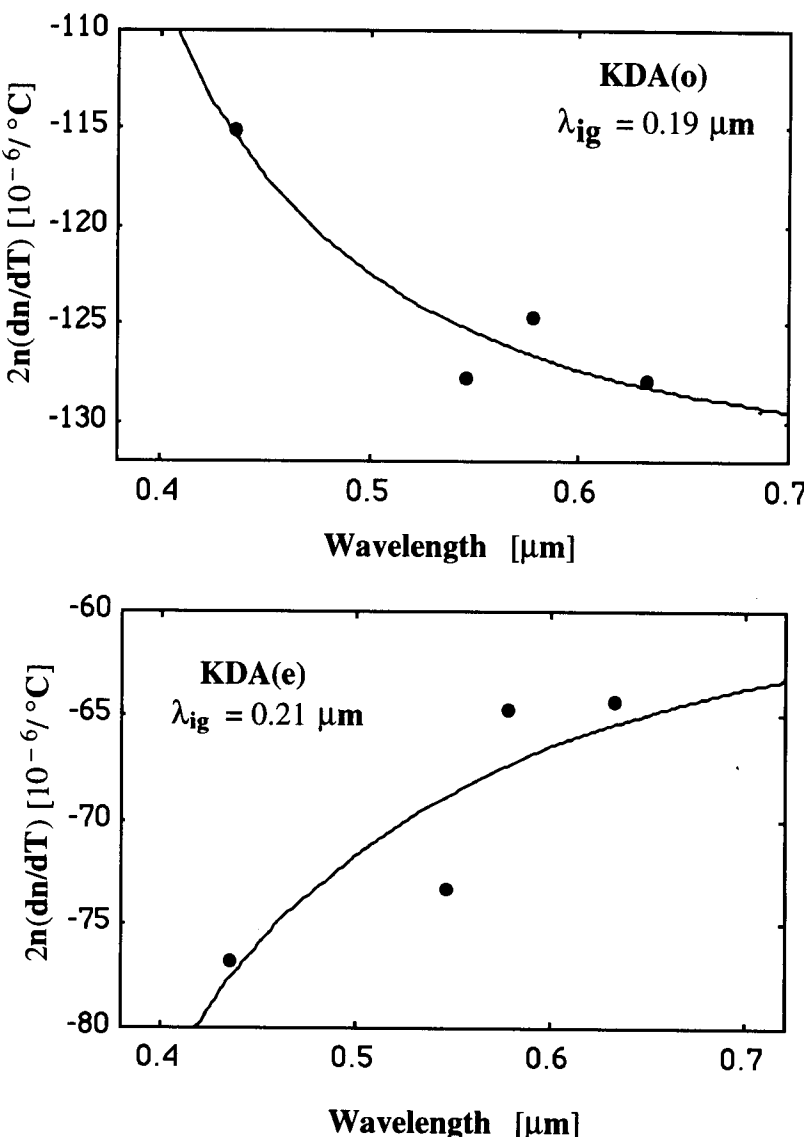


Figure 3.5:  $2n(dn/dT)$  versus wavelength at  $33^\circ\text{C}$  for the KDA crystal: Solid curves are the computed values from the optical constants  $G$ ,  $H$ , and  $E_{ig}$  from Table 3.1; the experimental points [40, 8] are shown as solid circles.

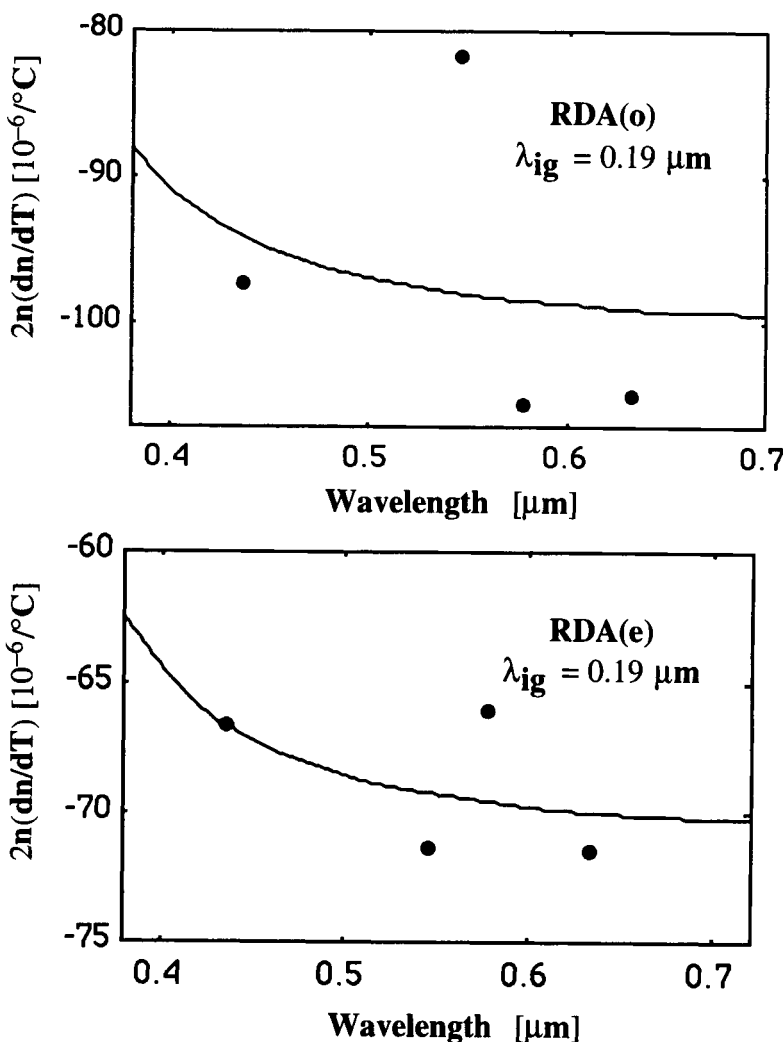


Figure 3.6:  $2n(dn/dT)$  versus wavelength at  $33^\circ\text{C}$  for the RDA crystal: Solid curves are the computed values from the optical constants  $G$ ,  $H$ , and  $E_{\text{ig}}$  from Table 3.1; the experimental points [40, 8] are shown as solid circles.

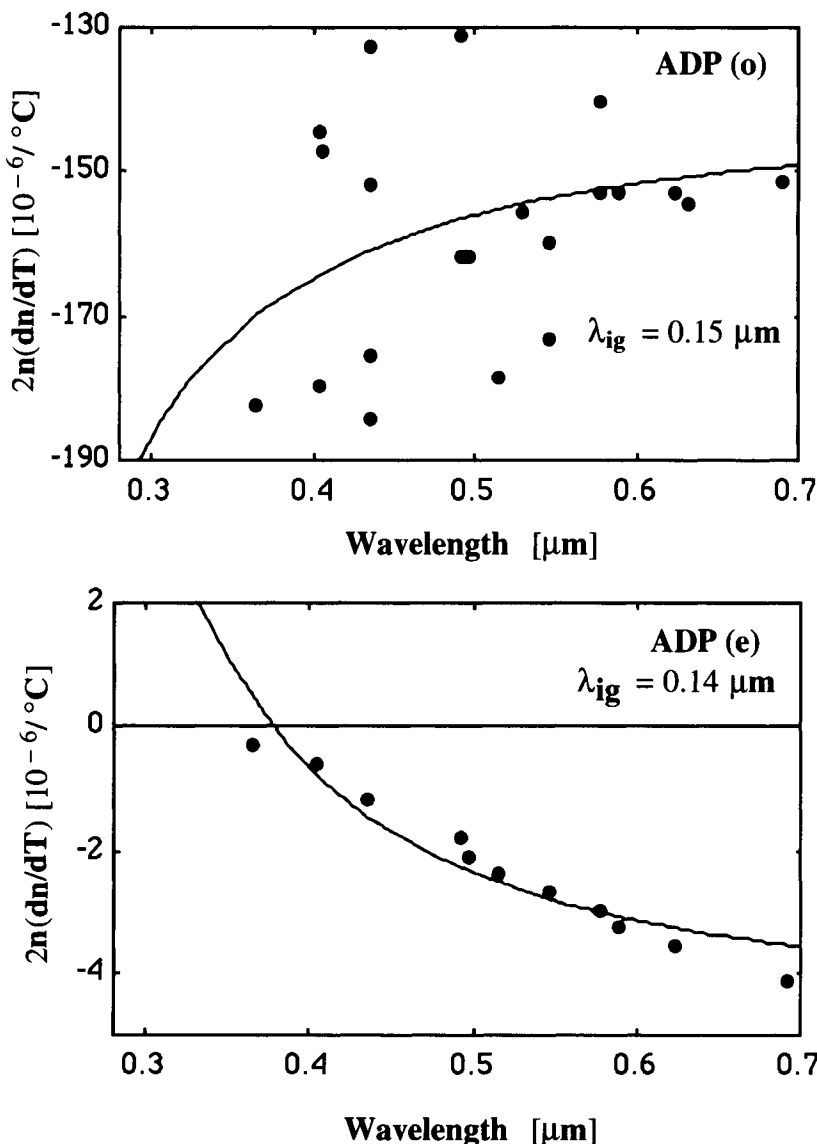


Figure 3.7:  $2n(dn/dT)$  versus wavelength at  $33^\circ\text{C}$  for the ADP crystal: Solid curves are the computed values from the optical constants  $G$ ,  $H$ , and  $E_{ig}$  from Table 3.1; the experimental points [40, 41, 5, 35, 37, 8] are shown as solid circles.

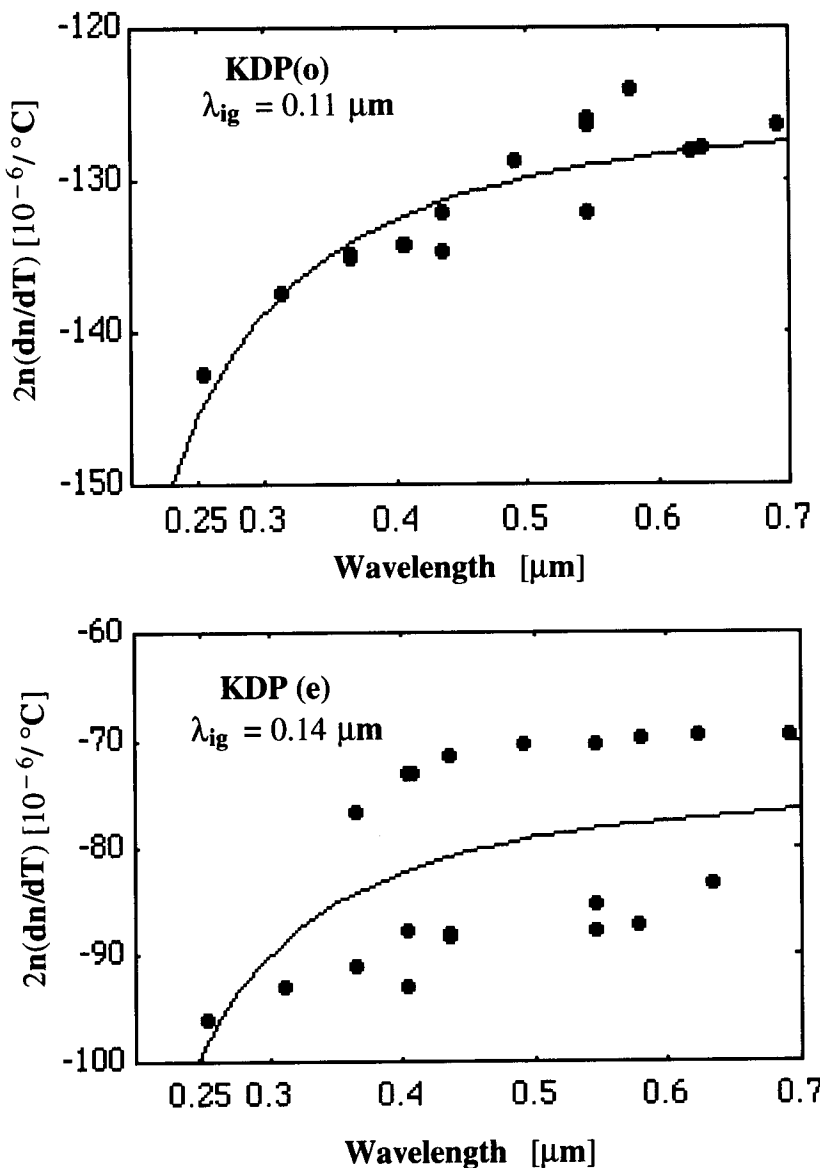


Figure 3.8:  $2n(dn/dT)$  versus wavelength at  $33^\circ\text{C}$  for the KDP crystal: Solid curves are the computed values from the optical constants  $G$ ,  $H$ , and  $E_{ig}$  from Table 3.1; the experimental points [40, 41, 5, 35, 36, 8] are shown as solid circles.

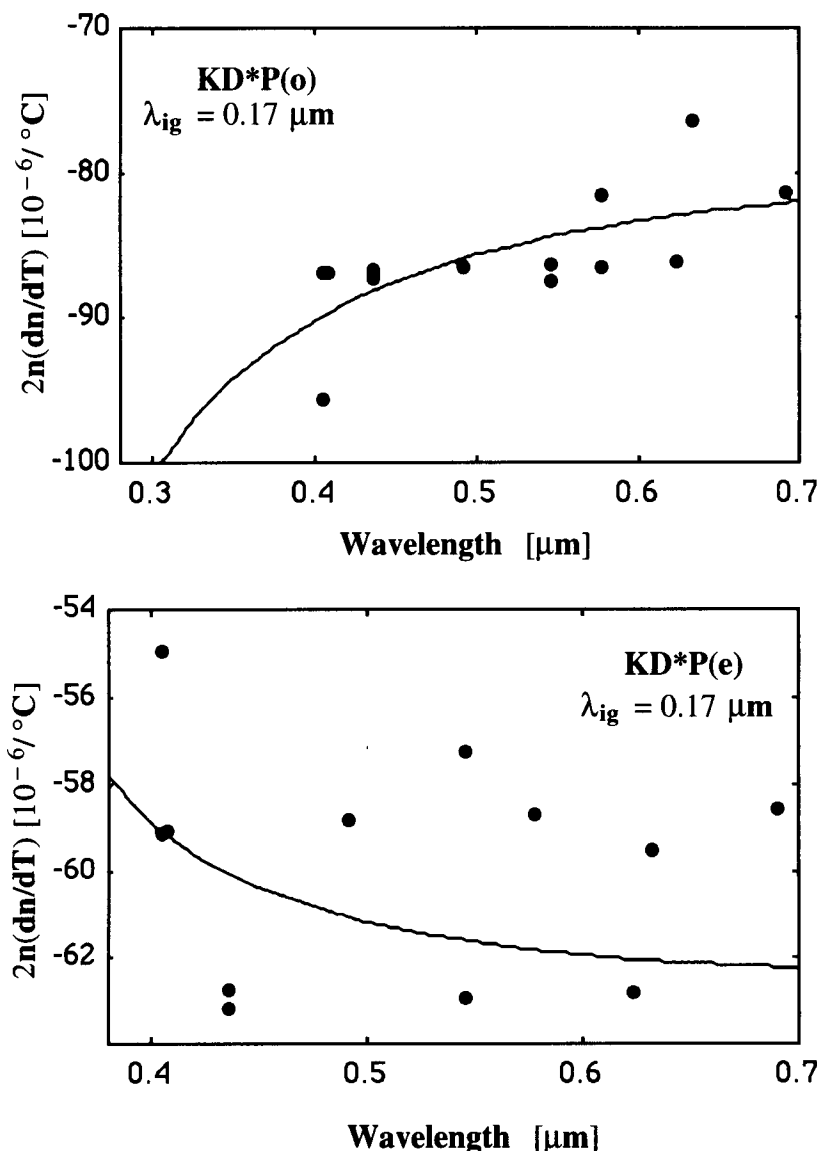


Figure 3.9:  $2n(dn/dT)$  versus wavelength at  $33^{\circ}\text{C}$  for the KD\*P crystal: Solid curves are the computed values from the optical constants  $G$ ,  $H$ , and  $E_{ig}$  from Table 3.1; the experimental points [40, 5, 35, 8] are shown as solid circles.

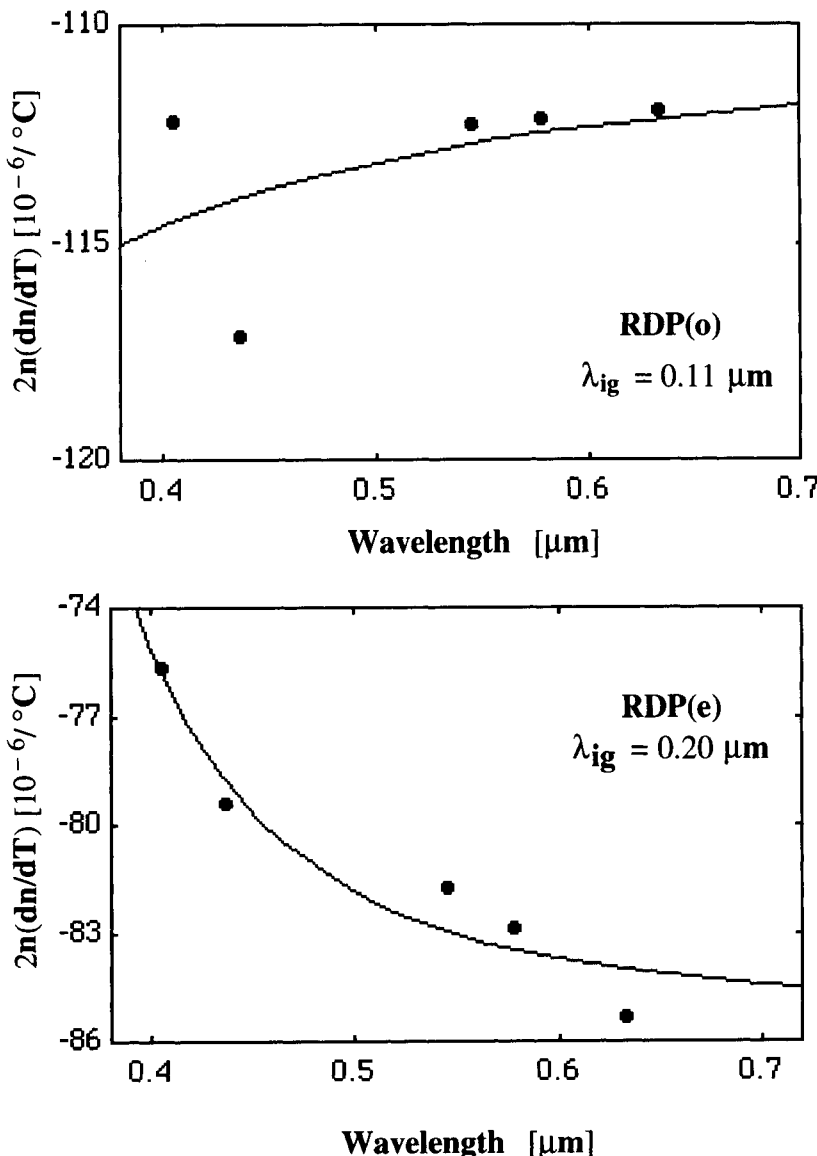


Figure 3.10:  $2n(dn/dT)$  versus wavelength at  $33^{\circ}\text{C}$  for the RDP crystal: Solid curves are the computed values from the optical constants  $G$ ,  $H$ , and  $E_{ig}$  from Table 3.1; the experimental points [40, 8] are shown as solid circles.

**Table 3.3: Refractive Index and Thermo-Optic Coefficients of KDP Isomorphs at 33°C**

Crystal [Ref.]	Wavelength [ μm]	Refractive index	<i>dn/dT</i> [(10 <sup>-6</sup> )/K]		Differ- ence	Av. Dev.	RMS <-[10 <sup>-6</sup> ]>
			Expt. values	Computed (This work)			
ADA(o) [40] [8]	0.436	1.59196	-48.5	-48.59	0.091	0.57	0.97
	0.546	1.57888	-43.9	-45.84	1.936		
	0.578	1.57632	-45.3	-45.36	0.056		
	0.633	1.57263	-44.5	-44.72	0.218		
ADA(e) [40] [8]	0.436	1.53491	12.7	14.77	-2.067	0.65	1.05
	0.546	1.52413	13.1	12.81	0.294		
	0.578	1.52209	12.4	12.48	-0.079		
	0.633	1.51924	11.9	12.05	-0.149		
ADP(o) [40] [41] [5] [35] [8] [37]	0.365	1.54613	-59.0	-54.88	-4.112	3.1	3.8
	0.405	1.53961	-47.8	-53.22	5.418		
	0.4047	1.53965	-47.0	-53.23	6.259		
	0.4360	1.53578	-49.4	-52.29	2.886		
	0.4916	1.53010	-52.9	-51.11	-1.771		
	0.5145	1.52875	-58.3	-50.73	-7.611		
	0.5460	1.52664	-52.3	-50.31	-1.992		
	0.5780	1.52477	-46.0	-49.96	3.958		
	0.5893	1.52416	-50.2	-49.85	-0.361		
	0.6234	1.52245	-50.2	-49.56	-0.628		
	0.6330	1.52201	-50.8	-49.49	-1.310		
	0.6907	1.51951	-49.9	-49.13	-0.729		
ADP (e) [40] [41] [5] [35] [8] [37]	0.3650	1.49717	-0.10	0.149	-0.249	0.098	0.12
	0.4047	1.49159	-0.20	-0.259	0.059		
	0.4358	1.48830	-0.40	-0.481	0.081		
	0.4916	1.48391	-0.60	-0.756	0.156		
	0.4965	1.48359	-0.70	-0.775	0.075		
	0.5145	1.48249	-0.80	-0.838	0.038		
	0.5461	1.48081	-0.90	-0.932	0.032		
	0.5779	1.47937	-1.00	-1.010	0.010		
	0.5893	1.47890	-1.10	-1.034	-0.066		
	0.6234	1.47763	-1.20	-1.097	-0.103		
	0.6907	1.47553	-1.40	-1.193	-0.207		
CDA(o) [40] [8]	0.405	1.58992	-31.5	-31.38	-0.123	0.75	1.01
	0.436	1.58441	-30.5	-30.19	-0.308		
	0.546	1.57202	-25.9	-27.77	1.873		
	0.578	1.56963	-27.6	-27.36	-0.245		
	0.633	1.56625	-28.0	-26.80	-1.200		

**Table 3.3: (Continued)**

Crystal [Ref.]	Wavelength [ μm]	Refractive index	$\frac{dn}{dT}$ [( $10^{-6}$ )/K]		Differ- ence	Av. Dev.	RMS $<-[10^{-6}]>$
			Expt. values	Computed (This work)			
CDA(e) [40] [8]	0.405	1.56660	-18.9	-18.85	-0.053	0.83	1.13
	0.436	1.56157	-20.9	-20.46	-0.440		
	0.546	1.55044	-21.2	-23.27	2.070		
	0.578	1.54837	-23.9	-23.69	-0.208		
	0.633	1.54552	-25.6	-24.23	-1.375		
CD*A(o) [40] [8]	0.405	1.58522	-22.6	-22.49	-0.108	0.54	0.64
	0.436	1.57990	-22.6	-22.90	0.296		
	0.546	1.56808	-24.7	-23.73	-0.968		
	0.578	1.56584	-23.1	-23.88	0.779		
CD*A(e) [40] [8]	0.405	1.56456	-17.7	-17.00	-0.696	0.70	0.92
	0.436	1.55956	-15.1	-16.94	1.845		
	0.546	1.54858	-16.4	-16.81	0.409		
	0.578	1.54655	-17.1	-16.78	-0.317		
	0.633	1.54376	-17.0	-16.75	-0.252		
KDA(o) [40] [8]	0.436	1.58159	-36.4	-36.53	0.125	0.40	0.50
	0.546	1.56924	-40.7	-39.89	-0.806		
	0.578	1.56684	-39.8	-40.38	0.584		
	0.633	1.56341	-40.9	-41.00	0.098		
KDA(e) [40] [8]	0.436	1.52932	-23.1	-25.35	2.249	2.1	2.2
	0.546	1.51938	-21.3	-24.04	2.741		
	0.578	1.51753	-25.1	-23.80	-1.299		
	0.633	1.51498	-21.2	-23.47	2.275		
KDP(o) [40] [41] [8] [5] [35] [36]	0.2537	1.56636	-45.4	-46.25	0.848	1.7	2.9
	0.3126	1.54112	-43.0	-44.65	1.653		
	0.3650	1.52028	-43.6	-44.11	0.511		
	0.4047	1.52337	-44.1	-43.45	-0.651		
	0.4358	1.51984	-42.3	-43.21	0.911		
	0.5461	1.51155	-41.7	-42.69	0.990		
	0.3653	1.52923	-40.1	-43.85	3.748		
	0.4047	1.52337	-40.1	-43.45	3.349		
	0.4078	1.52298	-43.1	-43.42	0.323		
	0.4358	1.51984	-43.5	-43.21	-0.289		
	0.4916	1.51504	-42.5	-42.90	0.400		
	0.5461	1.51155	-41.7	-42.69	0.990		
	0.5791	1.50981	-41.1	-42.59	1.495		
	0.6234	1.50777	-42.5	-42.49	-0.006		
	0.6907	1.50514	-42.0	-42.38	0.384		

**Table 3.3: (Continued)**

Crystal [Ref.]	Wavelength [ μm]	Refractive index	$dn/dT$ Expt. values [ $(10^{-6})/\text{K}$ ] (This work)	Computed	Differ- ence	Av. Dev.	RMS $<-[10^{-6}]>$
	0.5460	1.51155	-32.8	-42.69	9.891		
	0.6330	1.50737	-39.4	-42.48	3.075		
KDP(e) [40, 41]	0.2537	1.51593	-30.7	-32.46	1.760	2.4	2.5
[8, 5]	0.3126	1.49432	-31.1	-29.62	-1.482		
[35, 36]	0.3650	1.48425	-30.7	-28.33	-2.366		
	0.4047	1.47930	-29.7	-27.72	-1.984		
	0.4358	1.47638	-29.4	-27.36	-2.042		
	0.5461	1.46984	-29.9	-26.58	-3.320		
	0.3653	1.48420	-25.8	-28.33	2.528		
	0.4047	1.47930	-24.7	-27.72	3.016		
	0.4078	1.47897	-24.7	-27.68	2.976		
	0.4358	1.47638	-24.2	-27.36	3.158		
	0.4916	1.47252	-23.9	-26.89	2.993		
	0.5461	1.46984	-23.9	-26.58	2.680		
	0.5791	1.46856	-23.7	-26.43	2.734		
	0.6234	1.46712	-23.7	-26.28	2.577		
	0.6907	1.46540	-23.7	-26.10	2.396		
	0.4050	1.47927	-31.5	-27.71	-3.788		
	0.4360	1.47637	-28.8	-27.36	-1.444		
	0.5460	1.46984	-29.0	-26.58	-2.420		
	0.5780	1.46860	-28.7	-26.44	-2.261		
	0.6330	1.46685	-25.4	-26.25	0.847		
KD*P(o) [5]	0.4047	1.51890	-28.6	-29.57	0.967	1.4	2.0
[40]	0.4078	1.51850	-28.6	-29.51	0.912		
[8]	0.4358	1.51550	-28.6	-29.07	0.470		
[35]	0.4916	1.51110	-28.6	-28.42	-0.178		
	0.5461	1.50790	-28.6	-27.99	-0.612		
	0.5779	1.50630	-27.1	-27.80	0.696		
	0.6234	1.50440	-28.6	-27.57	-1.025		
	0.6907	1.50220	-27.1	-27.33	0.228		
	0.405	1.51883	-30.0	-29.56	-0.438		
	0.436	1.51554	-33.7	-29.07	-4.634		
	0.546	1.50785	-29.9	-27.99	-1.910		
	0.578	1.50632	-30.0	-27.80	-2.205		
	0.633	1.50410	-31.6	-27.53	-4.067		
KD*P(e) [40, 8]	0.405	1.47754	-18.6	-24.09	5.492	3.5	3.8
	0.436	1.47368	-21.3	-24.38	3.076		

**Table 3.3: (Continued)**

Crystal [Ref.]	Wavelength [ μm]	Refractive index	$dn/dT$ [( $10^{-6}$ )/K]		Differ- ence	Av. Dev.	RMS $<-[10^{-6}]>$
			Expt. values	Computed (This work)			
RDA(o)	0.546	1.46830	-19.5	-24.76	5.255		
	0.578	1.46707	-25.2	-24.80	-0.397		
	0.633	1.46534	-20.3	-24.86	4.557		
	0.436	1.57341	-30.9	-31.41	0.509	1.1	1.3
	[40]	0.546	1.56136	-36.2	-33.98	-2.224	
	[8]	0.578	1.55902	-33.8	-34.36	0.564	
RDA(e)	0.633	1.55568	-33.7	-34.86	1.156		
	0.436	1.53421	-19.7	-21.71	2.008	1.08	1.23
	[40]	0.546	1.52409	-23.4	-22.72	-0.678	
	[8]	0.578	1.52222	-21.7	-22.86	1.156	
RDP(o)	0.633	1.51964	-23.5	-23.02	-0.485		
	0.405	1.52075	-36.9	-37.64	0.742	0.4	0.6
	[40]	0.436	1.51733	-38.6	-37.55	-1.050	
	[8]	0.546	1.50917	-37.2	-37.34	0.143	
	0.578	1.50749	-37.2	-37.31	0.106		
RDP(e)	0.633	1.50502	-37.2	-37.26	0.059		
	0.405	1.48989	-26.7	-25.46	-1.244	1.1	1.4
	[40]	0.436	1.48689	-27.6	-26.48	-1.116	
	[8]	0.546	1.48002	-25.4	-28.02	2.617	
	0.578	1.47889	-28.0	-28.21	-0.206		
	0.633	1.47684	-28.9	-28.44	-0.464		

The nonlinear crystals, such as lithium niobate,  $\text{LiNbO}_3$  (LNO), lithium iodate,  $\text{LiIO}_3$  (LIO), and lithium tantalate,  $\text{LiTaO}_3$  (LTO) have been used as the second group of workhorse crystals in nonlinear optics [45] since the mid-1960s. So far there has been no satisfactory formulation of the dispersion of thermo-optic coefficients for these crystals except for LNO. However, the temperature dispersion equation [4] of LNO cannot be interpreted in a physically meaningful model and cannot be used to assess many high-power nonlinear-optical devices (NLOD's). Temperature stability and tunability [46, 47] calculated from the different measured thermo-optic coefficients [48-52] of these crystals by different workers often widely differ from those of the experiments. The thermo-optic coefficients have been analyzed recently [27] and are shown in Table 3.1. The experimental values and the computed curves are shown in Figs. 3.11 and 3.12 for LNO and LIO, respectively. Some experimental data and computed values are shown in Table 3.4. Although there are only four data points for LIO crystal, the fit was excellent. The error bars for the LIO crystal are calculated by the accuracy of the  $dn/dT$  measurement, which is  $\pm 1.0 \times 10^{-6}/^\circ\text{C}$ . It is interesting to note that the fitted gap  $E_{\text{ig}}$  is close to the reflectivity peak in the electronic absorption spectra. From the fitted constants  $G$  and  $H$ , the thermal expansion coefficient  $\alpha$  and the temperature coefficient of the band gap are computed and are also shown in Table 3.1. These values are compared with the experimental values and agree reasonably well within the experimental accuracy. The  $dn/dT$  values are negative in LIO crystal. The first factor, i.e., the contribution from the thermal expansion coefficient, is dominant in this crystal. We have used 6 eV as the value for the excitonic band gap of LIO crystal, to calculate  $dE_{\text{eg}}/dT$  from the evaluated constants, since there is no reported value of it at this moment.

Because the thermo-optic coefficient is not constant up to  $500^\circ\text{C}$ , we have fitted  $(2n, dn/dT, \lambda)$  data at  $50^\circ\text{C}$  increments from 25 to  $500^\circ\text{C}$  for LNO [4, 49, 52] and LTO crystals [51] in the same form as in Eq. (3.29) by keeping  $G$  as a constant, since the thermal expansion coefficient is approximately constant [53] from room temperature to  $500^\circ\text{C}$ . The optical constant  $H$  and the fitting gap  $E_{\text{ig}}$  are computed at the above temperature interval for these two crystals. The constants are then plotted against temperature and, interestingly, the variation is a quadratic function of temperature. However, the variation of fitting gap  $E_{\text{ig}}$  is negligibly small. On the other hand,  $H$  is

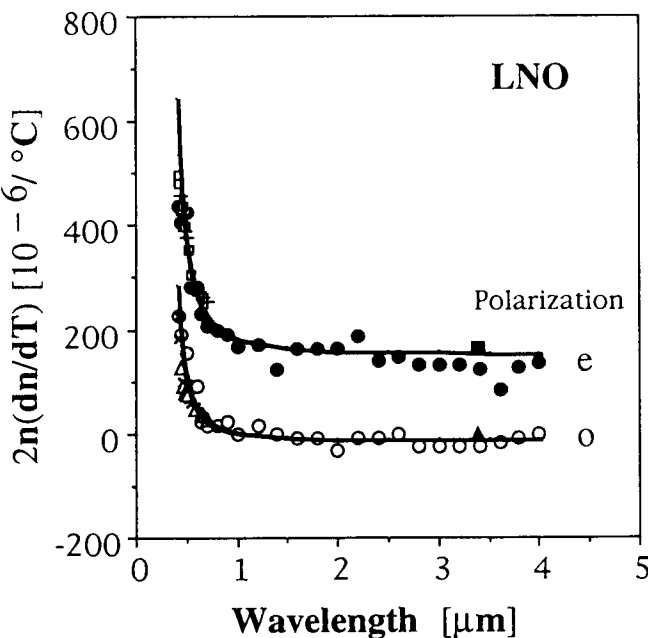


Figure 3.11:  $2n(dn/dT)$  versus wavelength for LNO crystal at room temperature: The solid curves are the computed values and the points are the experimental values; open circles [48], open triangles [4], crosses [49], filled triangle [52], filled circles [48], pluses [4], open squares [49], and filled square [52] (after Ref. 27 with permission from OSA).

strongly dependent on temperature. The optimum fitted equations for LNO and LTO crystals are

For LNO:

$$H_o(T) = 159.75384 + 0.093435T - 0.000047759T^2, \quad (3.34)$$

$$H_e(T) = 179.66405 + 0.383470T + 0.000042605T^2. \quad (3.35)$$

For LTO:

$$H_o(T) = 199.11300 + 0.033678T + 0.00024602T^2, \quad (3.36)$$

$$H_e(T) = 130.17849 + 0.574140T + 0.00082996T^2. \quad (3.37)$$

These equations indicate that the variations of excitonic band gap with temperature are not linear in the stated temperature region. The temperature

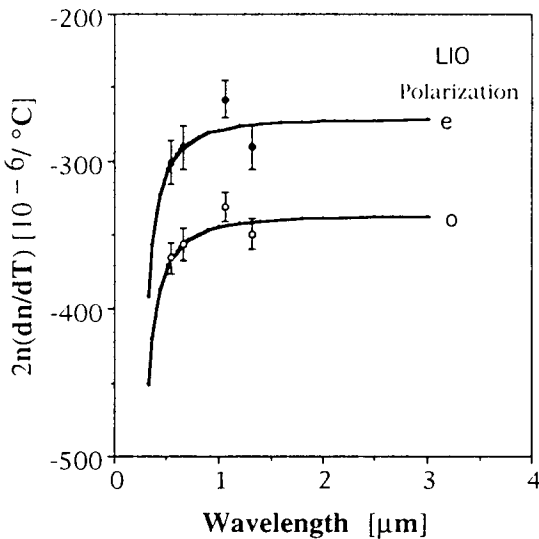


Figure 3.12:  $2n(dn/dT)$  versus wavelength for LIO crystal at room temperature: The solid curves are the computed values and the points are the experimental values; filled and open circles [50] (after Ref. 27 with permission from OSA).

variations of excitonic band gap ( $dE_{eg}/dT$ ) are calculated at different temperatures and are plotted in Fig. 3.13. The behavior is almost linear for both polarizations. The excitonic band gaps ( $E_{eg}$ ) at different temperatures are also shown in the same figure. The band gap decreases asymptotically with temperature. The optical constants cited in Table 3.1 along with Eqs. (3.34) to (3.37) can be used to calculate thermo-optic coefficients at any temperature and wavelength. These thermo-optic coefficients along with the room temperature refractive indices calculated from the room temperature Sellmeier coefficients in Table 2.1 can be used either to formulate the temperature-dependent Sellmeier equations or to assess the currently available NLOD's more accurately, which are described in the next chapter.

Refractive indices of KNO were measured by Zysset *et al.* [58] in the orthorhombic phase at six different temperatures between 22 and 180°C in the wavelength range from 0.4 to 3.4  $\mu\text{m}$  with the maximum experimental error  $\pm 2.5 \times 10^{-4}$ . They formulated 18 sets of Sellmeier coefficients by using a two-term oscillator model with an IR correction term for six tem-

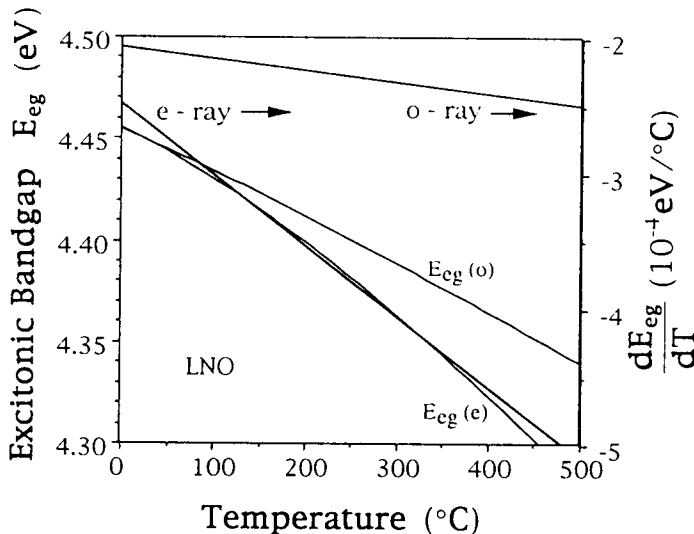


Figure 3.13: A schematic plot of the variations of the excitonic band gap with temperature ( $dE_{eg}/dT$ ) and the band gap ( $E_{eg}$ ) versus temperature for LNO crystal (after Ref. 27 with permission from OSA).

peratures along  $x$ ,  $y$ , and  $z$  axes, respectively. For unified notations,  $x$ ,  $y$ , and  $z$  axes have been used instead of  $a$ ,  $b$ , and  $c$  axes. These Sellmeier coefficients are not able to analyze the formation of three temperature dependent Sellmeier coefficients along the three optic axes. Zysett *et al.* [58] tried to analyze the thermo-optic coefficients in terms of the quadratic polarization optical effect induced by the spontaneous polarization of the orthorhombic phase. However, it was noticed that the basic assumption of the temperature-independent quadratic polarization optic coefficients is not fulfilled. Also, the comparison between the quadratic polarization optic coefficients of KNO crystal from optical, electro-optical, and from the indirect calculation of the temperature dependence of the refractive indices is not explained quantitatively and even qualitatively.

We have used their experimental [58] and calculated values of refractive indices for 22 different wavelengths between 0.4 and  $3.4 \mu\text{m}$  to compute thermo-optic coefficients at five temperatures. The optimum fitted constants  $G$  and  $H$  are shown in Table 3.1 along with the other parameters at  $22^\circ\text{C}$ . The other physical parameters are compared with the experimental values and agree reasonably well within the experimental accuracy. The

experimental values and the computed curves are shown in Fig. 3.14 along two optic axes  $x$  and  $z$ , respectively. Thermo-optic coefficients along the  $y$  axis are negative and in this case the contribution from the thermal expansion coefficient is dominant. It is interesting to note that the fit gap  $E_{ig}$  is slightly above the reflectivity peak [60] of this crystal. The comparison between the experimental data and the calculated values of thermo-optic coefficients are shown in Table 3.4. Since the thermo-optic coefficient is not constant up to 180°C, we have fitted [2n( $dn/dT$ ),  $\lambda$ ] data at four other measured temperatures, i.e., at 50, 75, 100, and 140°C by considering separate constant  $dn/dT$  at the stated temperature interval. In the fitting analyses, the same form of Eq. (3.29) was used by keeping  $G$  as a constant, since the thermal expansion coefficient is approximately constant [59] from room temperature up to 180°C. As we have noticed, the fitting isentropic band gap is invariant under temperature like previous LNO, LTO, etc. crystals. The fitting and experimental points at 140°C are also shown in Fig. 3.14 along the  $x$  and  $z$  axes, respectively. Henceforth, the optical constants  $H$ , computed at the above mentioned five temperatures, are expressed as a quadratic functions of temperature as shown below.

$$H_x(T) = 143.04726 + 0.38005T + 0.0014781T^2, \quad (3.38)$$

$$H_y(T) = 11.92604 + 0.76106T - 0.00412735T^2, \quad (3.39)$$

and

$$H_z(T) = 241.79441 + 0.96897T + 0.0035473T^2, \quad (3.40)$$

where  $T$  is the temperature in degree centigrade. The analyses indicate that the variation of excitonic band gap with temperature is not linear within the stated temperature region. Therefore, the value of  $E_{eg}$  and  $dE_{eg}/dT$  are calculated and shown in Fig. 3.15. The variation of  $dE_{eg}/dT$  is almost linear and  $E_{eg}$  is decreasing asymptotically against temperature. The above optical constants are used to calculate refractive indices at any operating temperature and henceforth to assess the currently available nonlinear optical devices precisely. These are described in the next chapter.

Gettemy *et al.* [50] reported the variation of refractive indices of KTP crystal to determine the average power limit of nonlinear interaction at four wavelengths from 0.532 to 1.32  $\mu\text{m}$  from  $-160$  to  $35^\circ\text{C}$ . They quoted the least squares fit of  $dn/dT$  values at  $35^\circ\text{C}$  with the experimental accuracy of  $\pm 5.5 \times 10^{-6}/^\circ\text{C}$ . Kato [61] analyzed the above experimental values to

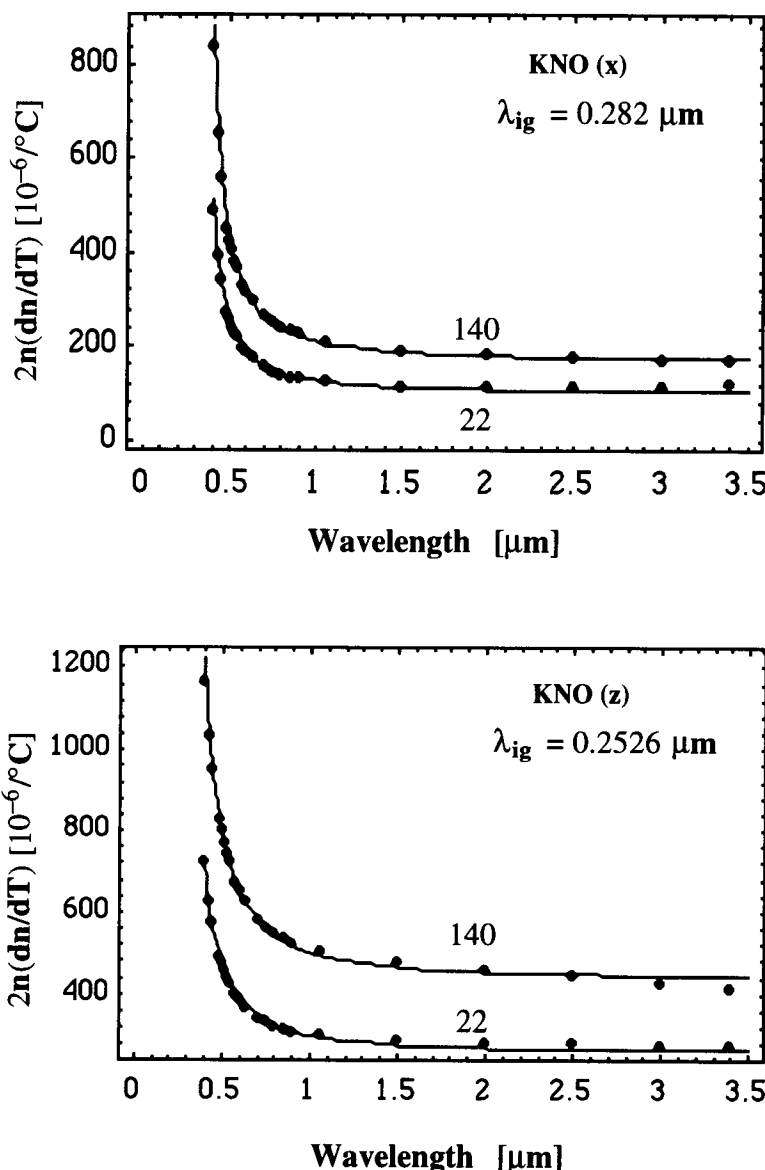


Figure 3.14:  $2n(dn/dT)$  versus wavelength for KNO crystal: Solid curves are the computed values; points are the experimental values [58] for  $x$  and  $z$  axes; temperatures are indicated along the curves as 22°C and (2) 140°C, respectively (after Ref. 28 with permission from AIP).

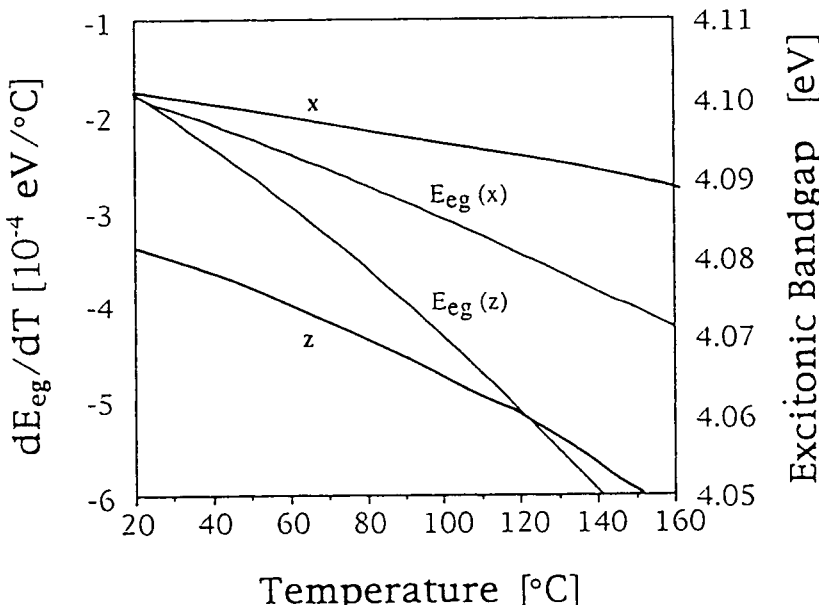


Figure 3.15: The schematic plot of the variations of the excitonic band gap with temperature ( $dE_{eg}/dT$ ) as marked (x) and (z) for the respective axis and the excitonic band gap ( $E_{eg}$ ) versus temperature for KNO crystal (after Ref. 28 with permission from AIP).

characterize the phase-matching bandwidths of several nonlinear interactions. Then he predicted the following empirical formula for thermo-optic coefficients along the three optic axes:

$$\frac{dn_x}{dT} = (1.323\lambda^{-3} - 4.385\lambda^{-2} + 12.307\lambda^{-1} + 7.709) \quad (10^{-6}/^{\circ}\text{C}), \quad (3.41)$$

$$\frac{dn_y}{dT} = (5.014\lambda^{-3} - 20.030\lambda^{-2} + 33.016\lambda^{-1} + 7.498) \quad (10^{-6}/^{\circ}\text{C}), \quad (3.42)$$

and

$$\frac{dn_z}{dT} = (3.896\lambda^{-3} - 13.332\lambda^{-2} + 22.762\lambda^{-1} + 21.151) \quad (10^{-6}/^{\circ}\text{C}). \quad (3.43)$$

Wiechmann *et al.* [64] measured the refractive indices of flux-grown KTP crystal using the minimum deviation method at nine wavelengths from 0.502 to 1.13  $\mu\text{m}$  at different temperatures from 15 to 40°C. Using the data points and employing a polynomial fit, they derived the following three equations to describe the wavelength dependence of the thermo-optic coefficients:

$$\frac{dn_x}{dT} = (0.1427\lambda^{-3} - 0.4735\lambda^{-2} + 0.8711\lambda^{-1} + 0.0952) \quad (10^{-5}/^\circ\text{C}), \quad (3.44)$$

$$\frac{dn_y}{dT} = (0.4269\lambda^{-3} - 1.4761\lambda^{-2} + 2.1232\lambda^{-1} - 0.2113) \quad (10^{-5}/^\circ\text{C}), \quad (3.45)$$

and

$$\frac{dn_z}{dT} = (1.2415\lambda^{-3} - 4.4414\lambda^{-2} + 5.9129\lambda^{-1} - 1.2101) \quad (10^{-5}/^\circ\text{C}). \quad (3.46)$$

Since these empirical formulae have no physical significance, we have fitted the above experimental values in my model by using Eq. (3.29). The optimum fitted constants are shown in Table 3.1 along with the other physical parameters. The experimental points and the fitted curves are shown in Fig. 3.16 to Fig. 3.18 for the thermo-optic coefficients along  $x$ ,  $y$ , and  $z$  axes, respectively, at room temperature. The error bars are also indicated by considering the accuracy of the thermo-optic coefficients measurement. Since there is no peak energy in reflectivity data for KTP crystal, we have used the energy gap 4.1 eV as  $E_{\text{eg}}$  for calculating  $dE_{\text{eg}}/dT$ . These values are compared with the experimental values of other crystals [29] and agree reasonably well within the experimental accuracy. The experimental and calculated values of thermo-optic coefficients at the measured wavelengths are shown in Table 3.4.

Recently, lithium triborate,  $\text{LiB}_3\text{O}_5$  (LBO), and barium beta-borate,  $\beta\text{-BaB}_3\text{O}_5$  (BBO) are important nonlinear crystals. In particular, LBO and KNO are important to make temperature-tuned nonlinear optical devices. The thermo-optic coefficients of LBO crystal were measured by Velsko *et al.* [67] at five wavelengths from 0.365 to 1.064  $\mu\text{m}$ . According to

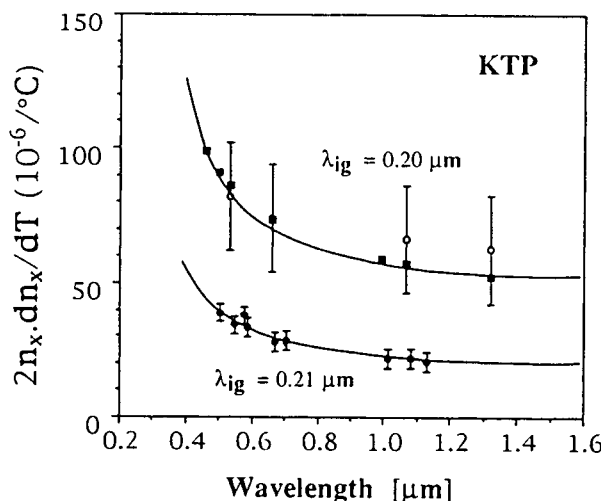


Figure 3.16:  $2n_x(dn_x/dT)$  versus wavelength for the KTP crystal: Solid curves are the computed values; points are the experimental data; solid circle [64], open circle [50], and solid square [61] at  $25^\circ\text{C}$  (after Ref. 62 with permission from IEEE).

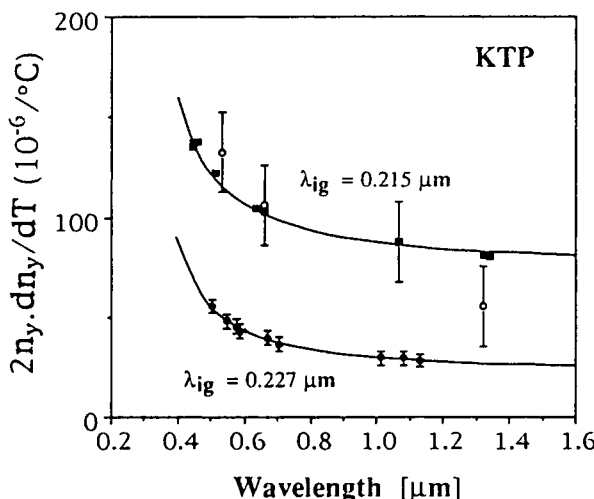


Figure 3.17:  $2n_y(dn_y/dT)$  versus wavelength for KTP crystal: Solid curves are the computed values; points are the experimental values; solid circle [64], open circle [50], and solid square [61] at  $25^\circ\text{C}$  (after Ref. 62 with permission from IEEE).

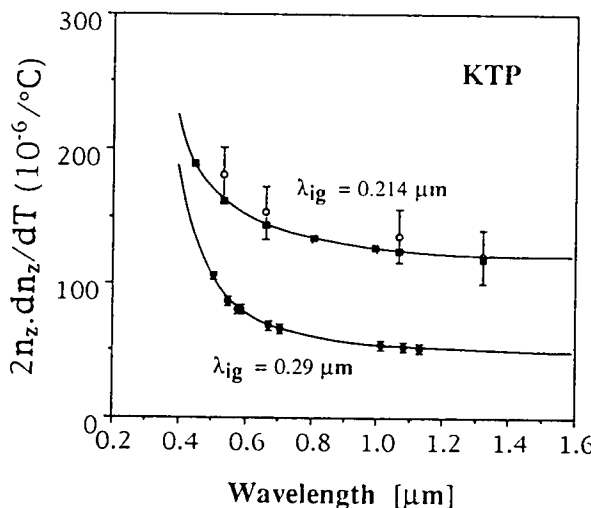


Figure 3.18:  $2n_z(dn_z/dT)$  versus wavelength for KTP crystal: Solid curves are the computed values; points are the experimental values; solid circle [64], open circle [50], and solid square [61] at  $25^\circ\text{C}$  (after Ref. 62 with permission from IEEE).

their observation, the change in refractive index with temperature was to be linear over the range  $20 - 65^\circ\text{C}$ . The thermal dependence of the refractive indices were linear least squares fits to the following weighted mean values near room temperature

$$\frac{dn_x}{dT} = -1.8 \pm 0.2 \quad (10^{-6}/^\circ\text{C}) \text{ [wavelength independent]}, \quad (3.47)$$

$$\frac{dn_y}{dT} = -13.6 \pm 0.1 \quad (10^{-6}/^\circ\text{C}) \text{ [wavelength independent]}, \quad (3.48)$$

and

$$\frac{dn_z}{dT} = -6.3 \pm 0.6 + (2.1 \pm 0.8)\lambda \quad (10^{-6}/^\circ\text{C}) \quad (\lambda \text{ in } \mu\text{m}). \quad (3.49)$$

Kato [70] has examined the above  $dn/dT$  values to characterize the temperature phase-matching bandwidths. Then he has expressed the following wavelength dependent  $dn/dT$  values along three axes of LBO crystal.

$$\frac{dn_x}{dT} = (-3.76\lambda + 2.30) \quad (10^{-6}/^\circ\text{C}), \quad (3.50)$$

$$\frac{dn_y}{dT} = (6.01\lambda - 19.40) \times 10^{-6}/^\circ\text{C}, \quad (3.51)$$

and

$$\frac{dn_z}{dT} = (1.50\lambda - 9.70) \times 10^{-6}/^\circ\text{C}. \quad (3.52)$$

These equations are unable to explain the temperature-dependent Type-II phase-matched nonlinear optical devices. Also, there is no physical significance of these empirical formulae.

Therefore, we have used all the quoted experimental values including the precision of Velsko *et al.* [67] for computation by using Eq. (3.29). The optimum fitted constants  $G$  and  $H$  are shown in Table 3.1 along with the other physical parameters at 20°C. Since there are no experimental values of the excitonic band gaps at present, we have used the absorption gap of 7.78 eV to calculate the variation of band gap with temperature. The average  $dE_{eg}/dT$  values agrees reasonably well with the experimental values of  $-2.3 \pm 0.5 \times 10^{-5}$  eV/°C for optical glasses. The experimental points and the fitted curves are shown in Fig. 3.19. Also, the experimental and computed values are shown in Table 3.4. It is quite clear that the band edge data are more temperature sensitive and dispersive. Since the thermal expansion coefficient is not constant along the  $y$  axis for LBO, the experimentally measured noncritically phase-matched (NCPM) second harmonic generated (SHG) temperatures [70 - 72] for the fundamental wavelength from 0.95 to 1.31 μm, the room temperature Sellmeier coefficients, and the computed optical constants  $G$  and  $H$  at 20°C are used to calculate the  $G$ 's at these NCPM temperatures. The optical constants  $G$ 's are now expressed as a function of temperature  $T$  and are shown below along the  $y$  axis

$$G_y(T) = 372.170 - 2.199 \times 10^{-1}T + 1.1748 \times 10^{-3}T^2 - 2.05077 \times 10^{-6}T^3, \quad (3.53)$$

where  $T$  is the temperature in degrees centigrade.

It is worthwhile to examine Eq. [3.53] at higher temperatures. As the temperature increases, the value of  $G$  decreases and it corresponds to the shift of the thermal expansion coefficient from more negative to the less negative values. This behavior was observed experimentally [68] in measuring thermal expansion coefficients along the  $y$  axis of LBO. Again, the NCPM temperatures [70-72] in the fundamental wavelength region of 1.40

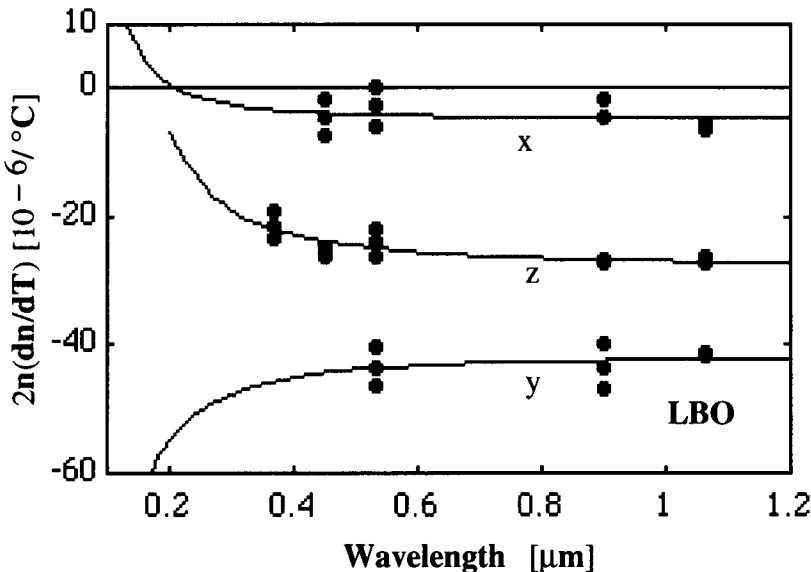


Figure 3.19:  $2n(dn/dT)$  versus wavelength for the LBO crystal: Curves are the computed values; solid circles are the experimental data of Velsko *et al.* [67] at 20°C (after Ref. 66 with permission from AIP).

-  $1.75 \mu\text{m}$ , the room temperature Sellmeier coefficients, and the optical constants  $G$  and  $H$  are used to calculate different values of  $H$  along the  $z$  axis. These values are then expressed as a nonlinear function of temperature  $T$  by

$$\begin{aligned} H_z(T) = & 410.66123 + 1.667 \times 10^{-1} T - 5.1887 \times 10^{-4} T^2 \\ & + 5.56251 \times 10^{-7} T^3. \end{aligned} \quad (3.54)$$

As the temperature rises, the value of  $H_z$  increases for LBO, similar to the characteristics of the LNO crystal. The experimental and computed values of thermo-optic coefficients at the measured wavelengths are compared in Table 3.4.

Eimerl *et al.* [75] have reported the negative values of  $dn/dT$  for BBO crystal at three wavelengths from  $0.405 \mu\text{m}$  to  $1.014 \mu\text{m}$  by measuring the refractive indices at several temperatures between 20 and 80°C. The temperature dependence was found to be linear, and a linear least squares fit was made to the data at each of three wavelengths. The dispersion of the thermo-optic coefficients is comparable to the experimental accuracy.

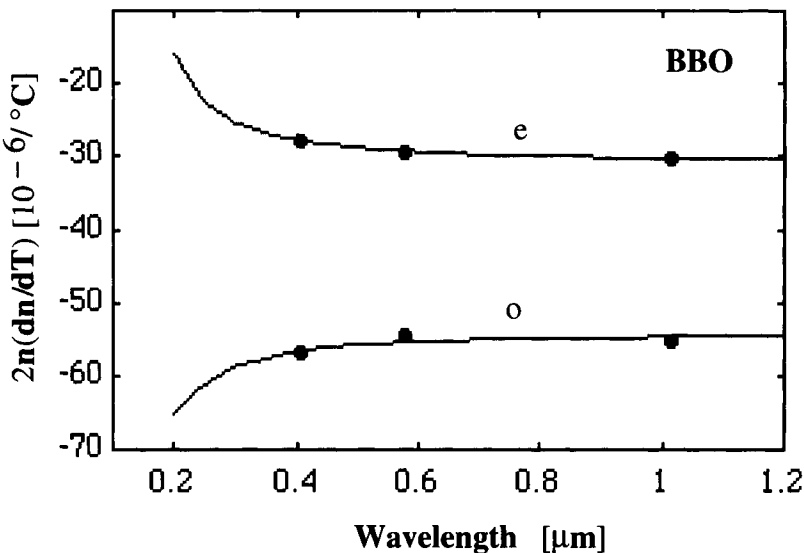


Figure 3.20:  $2n(dn/dT)$  versus wavelength for the BBO crystal: Curves are the computed values; solid circles are the experimental data of Eimerl *et al.* [75] at  $20^{\circ}\text{C}$  (after Ref. 66 with permission from AIP).

Therefore, they have used the following averaged values

$$\frac{dn_o}{dT} = -16.6 \left(10^{-6}/^{\circ}\text{C}\right), \quad (3.55)$$

and

$$\frac{dn_e}{dT} = -9.3 \left(10^{-6}/^{\circ}\text{C}\right). \quad (3.56)$$

The experimental values are used to fit in the above Eq. (3.29). The optimum fitted constants  $G$  and  $H$  are shown in Table 3.1 along with the other physical parameters at  $20^{\circ}\text{C}$ . The comparison between the experimental and computed values of the thermo-optic coefficients is also shown in Table 3.4. We have used the absorption gap of 6.43 eV to calculate the variation of band gap with temperature. It is interesting to note that the fit gap  $E_{ig}$  is close to the peak position ‘D’ of the x-ray photoemission spectra’s (XPS) valence band, as denoted by French *et al.* [69] for LBO and BBO crystals. The experimental values and the computed curves are shown in Fig. 3.20.

Eimerl *et al.* [76] measured the thermo-optic coefficients of deuterated L-arginine phosphate, DLAP, at several wavelengths from 0.405 to 1.014

$\mu\text{m}$  over the temperature interval 20 to 60°C. The three indices of refraction are unequally affected by temperature with  $n_y$  being least temperature sensitive and  $n_z$  the most. Furthermore, for  $n_x$  and  $n_y$ , the dispersion of  $dn/dT$  is comparable to the precision with which  $dn/dT$  is determined. However, the measured dispersion in the thermo-optic coefficient  $dn_z/dT$  is statistically significant. There is no analysis for this important optical phenomena. Here, these values are analyzed in Eq. (3.29) satisfactorily. The optical constants  $G$ ,  $H$ , and the isentropic band gaps are shown in Table 3.1. The experimental values and the calculated curves are shown in Fig. 3.21 for the thermo-optic coefficients along  $x$ ,  $y$ , and  $z$  axes, respectively. It can be seen that the  $dn/dT$  values are negative along three axes of DLAP crystal throughout the transmission region; and the values are decreasing from high negative to less negative values. The calculated and experimental values of thermo-optic coefficients at the measured wavelengths are compared in Table 3.4. The optical constants cited in Tables 2.1 and 3.1 can be used to explain the temperature-dependent nonlinear optical behavior of this crystal.

The thermo-optic coefficients of other important infrared nonlinear crystals such as GaSe along with HgS and  $\text{Tl}_3\text{AsSe}_3$  have been analyzed [101]. The optical constants are shown in Table 3.1. The experimental points and the calculated curves are shown in Fig. 3.22 for  $\text{Tl}_3\text{AsSe}_3$  crystal. The fit is excellent. The thermo-optic coefficients are negative for ordinary polarization, while its values are positive for extraordinary polarization. This characteristic is similar to that of ADA crystal. The experimental and calculated values at the measured wavelengths are compared in Table 3.4.

There is another important nonlinear crystal, barium sodium niobate, banana,  $\text{Ba}_2\text{NaNb}_5\text{O}_{15}$  (BNN), which was investigated by Singh *et al.* [111]. This crystal is suitable to make SHG of 1.064  $\mu\text{m}$  laser. The thermo-optic coefficients at room temperature have been analyzed and the optical constants are shown in Table 3.1. Some experimental and calculated values at some wavelengths are compared in Table 3.4.

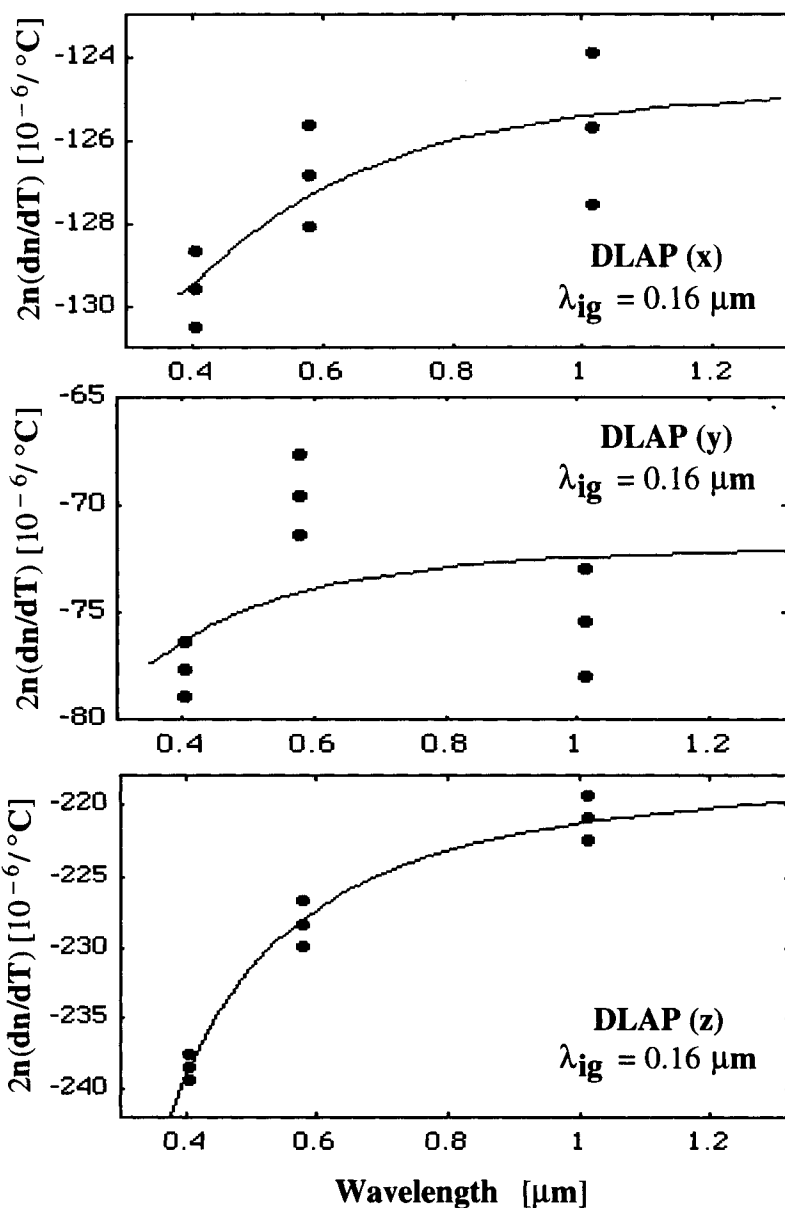


Figure 3.21:  $2n(dn/dT)$  versus wavelength for the DLAP crystal: Curves are the computed values; solid circles are the experimental data of Eimerl *et al.* [76] at  $25^\circ\text{C}$ .

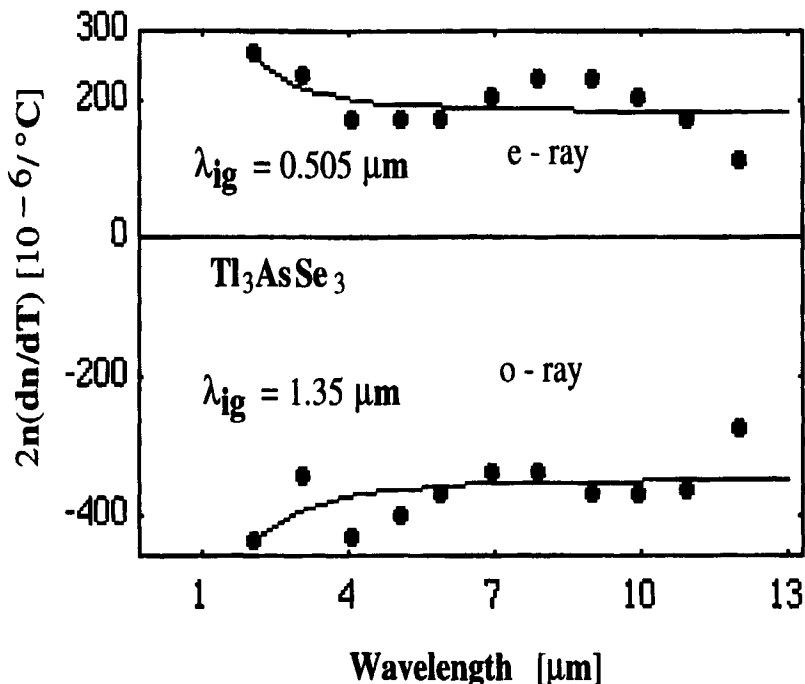


Figure 3.22:  $2n(dn/dT)$  versus wavelength for the  $\text{Tl}_3\text{AsSe}_3$  crystal: Curves are the computed values; solid circles are the experimental data of Ewbank *et al.* [110].

**Table 3.4: Refractive Index and Thermo-Optic Coefficients of Some Important Nonlinear Crystals**

Crystal [Ref.]	Wavelength [ μm]	Refractive index	$dn/dT$ [(10 <sup>-6</sup> )/K]		Differ- ence	Av. RMS Dev. Dev. [10 <sup>-6</sup> ]
			Expt. values	Computed (This work)		
BBO (o) [75, 66]	0.4047 0.5790	1.69212 1.67086	-16.8 -16.4	-16.75 -16.58	-0.084 0.235	0.15 0.17
at 25°C	1.0140	1.65584	-16.6	-16.50	0.141	
BBO (e) [75, 66]	0.4047 0.5790	1.56756 1.55241	-8.8 -9.4	-8.85 -9.42	0.006 -0.005	0.008 0.009
at 25°C	1.0140	1.54160	-9.8	-9.77	0.014	
BNN (x)	1.064 1.33	2.25801 2.24329	-25.0 ---	-24.95 -24.88	-0.05	
[111]	2.36	2.20471	---	-24.98		
(y)	1.064 1.33 2.36	2.25671 2.24245 2.20702	80.0 ---	76.90 73.70 70.67	-3.1	
D-LAP (x) [76]	0.40466 0.57907	1.52092 1.50655	-42.6 ± 0.3 -42.1 ± 0.4	-42.55 -42.26	-0.350 0.155	0.32 0.38
at 25°C	1.01400	1.49660	-42.0 ± 0.6	-41.89	-0.106	
D-LAP (y) [76]	0.40466 0.57907	1.59218 1.57309	-24.4 ± 0.4 -22.1 ± 0.6	-23.94 -23.53	-0.460 1.427	0.95 1.15
at 25°C	1.01400	1.55936	-24.2 ± 0.8	-23.22	-0.976	
D-LAP (z) [76]	0.40466 0.57907	1.60270 1.58101	-74.4 ± 0.3 -72.2 ± 0.5	-74.44 -72.08	0.040 -0.124	0.32 0.37
at 25°C	1.014	1.56642	-70.5 ± 0.5	-70.59	0.085	0.25 0.40
GaSe (o)	0.98 1.064	2.80891 2.79592	118.10 112.50	117.94 113.16	-0.16 0.66	
[105 – 107]	5.3 10.6 (e) 1.064	2.72357 2.69725 2.40785 2.40713	91.90 92.1 337.50 319.50	92.00 92.25 336.30 319.20	-0.10 0.15 -1.20 -0.30	
	5.3 10.6	2.39690 2.37485	246.21 247.11	246.65 247.01	0.44 0.10	
HgS (o) [102 – 104]	0.98 5.3 10.6 (e) 1.064	2.71777 2.62797 2.59380 3.00941 2.88774	24.00 5.36 5.23 70.00 42.45	23.90 5.44 5.13 69.90 42.37	-0.10 0.08 -0.10 -0.10 -0.08	0.10 0.08 0.20 0.35
	5.3 10.6	2.84480	42.00	42.40	0.40	
KNO (x) [58]	0.405 0.43	2.45528 2.41479	98.93 81.07	98.821 80.255	0.109 0.815	0.75 0.96

**Table 3.4: (Continued)**

Crystal [Ref.]	Wavelength [ $\mu\text{m}$ ]	Refractive index	$dn/dT$ [ $(10^{-6})/\text{K}$ ]		Differ- ence	Av. RMS Dev. Dev. [ $10^{-6}$ ]
			Expt. values	Computed (This work)		
at 22°C [28]	0.45	2.38949	71.07	70.303	0.767	
	0.488	2.35294	57.86	57.858	-0.001	
	0.50	2.34369	55.00	55.035	-0.035	
	0.5145	2.33363	51.79	52.104	-0.318	
	0.53	2.32403	48.93	49.439	-0.509	
	0.54	2.31839	47.50	47.929	-0.429	
	0.58	2.29930	42.50	43.121	-0.621	
	0.60	2.29143	40.36	41.270	-0.910	
	0.633	2.28030	37.86	38.777	-0.917	
	0.70	2.26291	34.29	35.169	-0.884	
	0.75	2.25310	32.50	33.289	-0.789	
	0.80	2.24516	31.07	31.850	-0.778	
	0.86	2.23742	29.64	30.524	-0.881	
	0.90	2.23307	29.29	29.816	-0.531	
	1.064	2.21971	27.50	27.835	-0.335	
	1.50	2.19942	25.71	25.644	0.071	
	2.0	2.18335	25.71	24.828	0.886	
	2.5	2.16757	26.07	24.558	1.513	
	3.0	2.15004	26.43	24.516	1.913	
	3.4	2.13424	27.14	24.575	2.568	
KNO (y) [58]	0.405	2.55081	-20.00	-12.932	-7.068	5.5
	0.43	2.49772	-27.86	-38.732	10.872	6.4
at 22°C [28]	0.45	2.46519	-32.14	-42.031	9.891	
	0.488	2.41901	-37.50	-41.457	3.957	
	0.50	2.40746	-38.21	-40.861	2.651	
	0.5145	2.39497	-39.29	-40.107	0.817	
	0.53	2.38311	-40.00	-39.316	-0.684	
	0.54	2.37617	-40.35	-38.828	-1.522	
	0.58	2.35282	-41.07	-37.104	-3.966	
	0.60	2.34326	-41.43	-36.377	-5.053	
	0.633	2.32980	-41.43	-35.348	-6.082	
	0.70	2.30891	-40.71	-33.765	-6.945	
	0.75	2.29720	-39.64	-32.899	-6.741	
	0.80	2.28776	-39.93	-32.219	-7.711	
	0.86	2.27860	-38.21	-31.579	-6.631	
	0.90	2.27347	-37.50	-31.232	-6.268	
	1.064	2.25780	-35.71	-30.247	-5.463	
	1.50	2.23433	-31.43	-29.158	-2.272	
	2.0	2.21609	-27.86	-28.806	0.946	

Table 3.4: (Continued)

Crystal [Ref.]	Wavelength [ $\mu\text{m}$ ]	Refractive index	$dn/dT [ (10^{-6})/\text{K}]$		Differ- ence	Av. RMS Dev. Dev. [ $10^{-6}$ ]
			Expt. values	Computed (This work)		
KNO (z) [58] at 22°C [28]	2.5	2.19835	-24.29	-28.769	4.479	
	3.0	2.17872	-20.00	-28.883	8.883	
	3.4	2.16105	-16.43	-29.046	12.616	
	0.405	2.30978	156.43	153.164	3.266	1.44
	0.43	2.27737	137.86	135.092	2.768	
	0.45	2.25706	126.43	124.558	1.872	
	0.488	2.22764	110.36	110.365	-0.005	
	0.50	2.22017	106.79	106.964	-0.174	
	0.5145	2.21205	102.86	103.353	-0.493	
	0.53	2.20429	99.29	99.994	-0.704	
	0.54	2.19973	97.14	98.059	-0.919	
	0.58	2.18427	90.71	91.726	-1.016	
	0.60	2.17789	87.86	89.213	-1.353	
	0.633	2.16886	84.64	85.760	-1.120	
	0.70	2.15474	79.64	80.611	-0.971	
	0.75	2.14677	77.14	77.851	-0.711	
	0.80	2.14030	75.36	75.701	-0.341	
KTP (x) [64, 62]	0.86	2.13400	73.93	73.691	0.239	
	0.90	2.13046	72.86	72.606	0.254	
	1.064	2.11957	71.07	69.523	1.547	
	1.5	2.10307	68.57	66.052	2.518	
	2.0	2.09005	67.86	64.782	3.078	
	2.5	2.07730	67.50	64.418	3.082	
	3.0	2.06317	67.14	64.449	2.691	
	3.4	2.05046	67.14	64.641	2.499	
	0.50157	1.78599	10.85	11.262	-0.412	0.38
	0.54607	1.77626	9.56	10.050	-0.490	0.50
	0.57897	1.77069	10.64	9.385	1.255	
	0.58756	1.76940	9.33	9.235	0.095	
	0.66781	1.75991	7.86	8.170	-0.310	
	0.70652	1.75650	8.06	7.809	0.251	
	1.01398	1.74139	6.15	6.398	-0.248	
	1.08303	1.73938	6.36	6.249	0.111	
	1.1287	1.73818	5.91	6.167	-0.257	
KTP(y) [64, 62]	0.50157	1.79758	15.40	15.289	0.111	0.16
	0.54607	1.78703	13.41	13.535	-0.125	0.18
	0.57897	1.78100	12.71	12.588	0.122	
	0.58756	1.77961	12.06	12.377	-0.317	
	0.66781	1.76939	11.20	10.887	0.313	

**Table 3.4: (Continued)**

Crystal [Ref.]	Wavelength [ $\mu\text{m}$ ]	Refractive index	$d\nu/dT$ [ $(10^{-6})/\text{K}$ ]		Differ- ence	Av. RMS Dev. Dev. [ $10^{-6}$ ]
			Expt. values	Computed (This work)		
	0.70652	1.76574	10.30	10.388	-0.088	
	1.01398	1.74960	8.45	8.475	-0.025	
	1.08303	1.74746	8.43	8.276	0.154	
	1.1287	1.74619	8.02	8.166	-0.146	
KTP (z)	0.50157	1.89768	27.79	27.320	0.470	0.21 0.28
	0.54607	1.88257	23.00	23.594	-0.594	
[64, 62]	0.57897	1.87407	21.48	21.726	-0.246	
	0.58756	1.87213	21.43	21.322	0.108	
	0.66781	1.85799	18.51	18.600	-0.090	
	0.70652	1.85301	17.90	17.736	0.164	
	1.01398	1.83159	14.74	14.630	0.110	
	1.08303	1.82885	14.36	14.325	0.035	
	1.1287	1.82722	14.22	14.159	0.061	
KTP (x)	0.459	1.79898	27.40	27.484	-0.084	0.85 1.07
[50]	0.497	1.78726	25.50	25.276	0.224	
[61, 62]	0.532	1.77902	24.14	23.783	0.357	
	0.532	1.77902	23.00	23.783	-0.783	
	0.66	1.76039	20.89	20.604	0.286	
	0.66	1.76039	21.00	20.604	0.396	
	0.994	1.74152	17.00	17.830	-0.830	
	1.064	1.73941	16.50	17.579	-1.079	
	1.32	1.73347	15.09	17.001	-1.911	
	1.064	1.73941	19.00	17.579	1.421	
	1.32	1.73347	19.00	17.001	1.999	
KTP (y)	0.459	1.81175	38.15	38.565	-0.415	1.82 2.58
	0.446	1.81714	37.34	40.082	-2.742	
[50]	0.532	1.79000	32.09	32.793	-0.703	
[61, 62]	0.532	1.79000	37.00	32.793	4.207	
	0.636	1.77267	29.39	28.615	0.775	
	0.660	1.76990	28.98	27.986	0.994	
	0.660	1.76990	30.00	27.986	2.014	
	0.994	1.74974	24.97	23.907	1.063	
	1.064	1.74749	23.11	23.544	-0.434	
	1.320	1.74120	23.07	22.711	0.359	
	1.064	1.74749	25.00	23.544	1.456	
	1.320	1.74120	16.00	22.711	-6.711	
KTP(z)	0.446	1.92638	49.07	50.872	-1.802	1.46 1.76
[50]	0.532	1.88673	42.71	43.949	-1.239	
[61, 62]	0.532	1.88673	48.00	43.949	4.051	

**Table 3.4: (Continued)**

Crystal [Ref.]	Wavelength [ $\mu\text{m}$ ]	Refractive index	$dn/dT$ [ $(10^{-6})/\text{K}$ ]		Differ- ence	Av. RMS Dev. Dev. [ $10^{-6}$ ]
			Expt. values	Computed (This work)		
	0.807	1.84284	36.30	36.734	-0.434	
	0.660	1.85870	38.58	39.245	-0.665	
	0.660	1.85870	41.00	39.245	1.755	
	0.994	1.83184	34.49	35.160	-0.670	
	1.064	1.82895	34.00	34.793	-0.793	
	1.32	1.82103	32.44	33.958	-1.518	
	1.064	1.82895	37.00	34.793	2.207	
	1.320	1.82103	33.00	33.958	-0.958	
LBO (x) [65–67]	0.450	1.58433	$-1.5 \pm 0.9$	-1.23	-0.268	0.28 0.31
	0.532	1.57844	$-0.9 \pm 1.0$	-1.39	0.490	
	0.900	1.56739	$-1.5 \pm 1.0$	-1.65	0.146	
	1.064	1.56466	$-1.9 \pm 0.2$	-1.69	-0.214	
LBO (y) [65–67]	0.532	1.60666	$-13.5 \pm 1.0$	-13.54	0.039	0.20 0.24
	0.900	1.59382	$-13.6 \pm 1.1$	-13.29	-0.308	
	1.064	1.59040	$-13.0 \pm 0.1$	-13.27	0.266	
LBO (z) [65–67]	0.365	1.64083	$-6.5 \pm 0.6$	-6.67	0.169	0.23 0.27
	0.450	1.62833	$-7.8 \pm 0.2$	-7.33	-0.466	
	0.532	1.62155	$-7.4 \pm 0.6$	-7.70	0.296	
	0.900	1.60868	$-8.4 \pm 0.1$	-8.30	-0.102	
	1.064	1.60541	$-8.3 \pm 0.2$	-8.40	0.096	
LIO (o) [50, 55]	0.532	1.89817	-96.4	-96.38	-0.017	1.50 1.97
	0.660	1.87862	-94.9	-94.42	-0.477	
at 25°C	1.064	1.85702	-89.3	-92.30	2.998	
[27]	1.320	1.85148	-94.4	-91.89	-2.507	
LIO (e) [50, 55]	0.532	1.74802	-86.1	-85.92	-0.184	2.7 3.6
	0.660	1.73301	-83.9	-83.38	-0.521	
at 25°C	1.064	1.71650	-75.2	-80.67	5.473	
[27]	1.320	1.71256	-84.9	-80.12	-4.775	
LNO (o) [4, 48]	0.42	2.41081	47.27	44.765	2.505	2.9 4.1
	0.45	2.37955	40.00	31.708	8.292	
[49, 52]	0.50	2.34222	32.73	19.895	12.835	
at 25°C	0.55	2.31637	20.00	13.555	6.445	
	0.60	2.29758	20.00	9.702	10.298	
[27]	0.65	2.28320	5.45	7.160	-1.710	
	0.70	2.27236	3.64	5.380	-1.740	
	0.80	2.25637	3.64	3.092	0.548	
	0.90	2.24533	5.45	1.715	3.735	
	1.0	2.23720	0.00	0.813	-0.813	
	1.2	2.22568	3.64	-0.268	3.908	

**Table 3.4: (Continued)**

Crystal [Ref.]	Wavelength [ μm]	Refractive index	$d\nu/dT$ [ $10^{-6}$ /K]		Differ- ence	Av. RMS Dev. Dev. [ $10^{-6}$ ]
			Expt. values	Computed (This work)		
[48]	1.4	2.21735	0.00	-0.874	0.874	
	1.6	2.21040	-1.82	-1.252	-0.568	
	1.8	2.20411	-1.82	-1.505	-0.315	
	2.0	2.19794	-7.27	-1.684	-5.586	
	2.2	2.19168	-1.82	-1.816	-0.004	
	2.4	2.18516	-1.82	-1.918	0.098	
	2.6	2.17828	0.00	-1.998	1.998	
	2.8	2.17097	-5.45	-2.063	-3.387	
	3.0	2.16315	-5.45	-2.118	-3.332	
	3.2	2.15480	-5.45	-2.165	-3.285	
	3.4	2.14580	-5.45	-2.206	-3.244	
	3.6	2.13620	-3.64	-2.243	-1.397	
	3.8	2.12580	-1.82	-2.276	0.456	
	4.0	2.11470	0.00	-2.308	2.308	
	0.42	2.41081	47.30	44.765	2.535	
	0.43	2.39942	38.00	39.616	-1.616	
	0.4471	2.38222	26.36	32.697	-6.337	
	0.46	2.37084	21.00	28.626	-7.626	
[27]	0.4713	2.36182	19.50	25.657	-6.157	
	0.49	2.34857	17.50	21.664	-4.164	
	0.4922	2.34713	17.20	21.255	-4.055	
	0.5016	2.34124	16.21	19.632	-3.422	
	0.52	2.33081	14.00	16.935	-2.935	
	0.55	2.31637	13.00	13.555	-0.555	
	0.58	2.30444	11.00	11.041	-0.041	
	0.5876	2.30174	10.30	10.505	-0.205	
	0.61	2.29443	9.00	9.112	-0.112	
	0.64	2.28595	7.50	7.595	-0.095	
	0.6678	2.27917	7.35	6.457	0.893	
	0.67	2.27867	7.15	6.376	0.774	
	0.7076	2.27090	6.35	5.156	1.194	
	3.39	2.14626	0.13	-2.204	2.334	
LNO (e)	0.42	2.30330	94.55	117.159	-22.609	5.7 7.3
[4, 48]	0.45	2.27726	89.09	96.167	-7.077	
[49, 52]	0.50	2.24600	94.55	76.569	17.981	
at 25°C	0.55	2.22430	63.64	65.679	-2.039	
	0.60	2.20849	63.64	58.876	4.764	
[27]	0.65	2.19620	52.73	54.293	-1.563	
	0.70	2.18722	47.27	51.012	-3.742	

**Table 3.4: (Continued)**

Crystal [Ref.]	Wavelength [ $\mu\text{m}$ ]	Refractive index	$dn/dT \text{ [ } (10^{-6})/\text{K} \text{ ] }$		Differ- ence	Av. RMS Dev. Dev. [ $10^{-6}$ ]
			Expt. values	Computed (This work)		
[48]	0.80	2.17370	45.45	46.723	-1.273	
	0.90	2.16439	43.64	44.091	-0.451	
	1.0	2.15751	38.18	42.347	-4.167	
	1.2	2.14776	40.00	40.244	-0.244	
	1.4	2.14071	29.10	39.073	-9.973	
	1.6	2.13486	38.18	38.364	-0.184	
	1.8	2.12952	38.18	37.913	0.267	
	2.0	2.12430	38.18	37.621	0.559	
	2.2	2.11900	43.64	37.433	6.207	
	2.4	2.11353	32.73	37.317	-4.587	
	2.6	2.10774	34.55	37.254	-2.704	
	2.8	2.10158	30.91	37.233	-6.323	
	3.0	2.09500	30.91	37.244	-6.334	
	3.2	2.08795	30.91	37.284	-6.374	
	3.4	2.08040	29.09	37.348	-8.258	
	3.6	2.07230	20.00	37.434	-17.434	
	3.8	2.06362	30.91	37.540	-6.630	
	4.0	2.05431	32.73	37.667	-4.937	
LTO (o) [51]	0.42	2.30334	108.00	117.158	-9.158	
	0.43	2.29385	105.00	108.944	-3.944	
	0.4471	2.27949	100.20	97.777	2.423	
	0.46	2.26997	96.20	91.121	5.079	
	0.4713	2.26243	92.80	86.219	6.581	
	0.49	2.25133	88.00	79.553	8.447	
	0.4922	2.25012	87.00	78.866	8.134	
	0.5016	2.24519	83.80	76.123	7.677	
	0.5145	2.23893	81.26	72.805	8.455	
	0.52	2.23643	79.00	71.526	7.474	
	0.55	2.22430	68.50	65.679	2.821	
	0.58	2.21426	63.60	61.258	2.342	
	0.5876	2.21199	62.90	60.307	2.593	
	0.61	2.20584	61.90	57.818	4.082	
	0.64	2.19863	60.80	55.078	5.722	
	0.6678	2.19297	60.20	52.999	7.201	
	0.67	2.19255	60.00	52.850	7.150	
	0.7076	2.18599	55.00	50.597	4.403	
	3.39	2.08079	35.70	37.344	-1.644	
LTO (o)	0.468	2.23142	11.0	10.82	0.199	0.17
[51]	0.480	2.22519	10.3	10.19	0.084	0.18

**Table 3.4: (Continued)**

Crystal [Ref.]	Wavelength [μm]	Refractive index	$dn/dT \text{ [ } (10^{-6})/\text{K} \text{ ] }$		Differ- ence	Av. RMS Dev. Dev. [10 <sup>-6</sup> ]
			Expt. values	Computed (This work)		
at 25°C [27]	0.509	2.21216	8.6	8.89	-0.270	
	0.644	2.17474	5.6	5.43	0.126	
LTO (e) [51]	0.468	2.23670	57.6	53.92	3.679	2.7
	0.480	2.23000	48.4	51.19	-2.791	2.8
at 25°C [27]	0.509	2.21670	43.2	45.96	-2.759	
	0.644	2.17920	35.5	33.97	1.532	
Tl <sub>3</sub> AsSe <sub>3</sub> (Ord.)	2.056	3.419	-64.220	-63.745	-0.4754	4.3
	3.059	3.380	-50.460	-57.953	7.4928	
at 25°C [109]	4.060	3.364	-64.220	-55.286	-8.9340	
	5.035	3.357	-59.630	-54.076	-5.5538	
[110]	5.856	3.354	-55.050	-53.492	-1.5576	
	6.945	3.349	-50.460	-53.059	2.5992	
	7.854	3.345	-50.460	-52.849	2.3894	
	9.016	3.340	-55.050	-52.693	-2.3568	
	9.917	3.336	-55.050	-52.628	-2.4217	
	10.961	3.331	-55.050	-52.597	-2.4533	
	12.028	3.327	-41.280	-52.575	11.2955	
Tl <sub>3</sub> AsSe <sub>3</sub> (e)	2.056	3.227	41.280	41.391	-0.1107	4.1
	3.059	3.199	36.700	34.000	2.7000	
at 25°C [109]	4.060	3.177	27.520	31.684	-4.1636	
	5.035	3.171	27.520	30.607	-3.0867	
[110]	5.856	3.168	27.520	30.092	-2.5723	
	6.945	3.164	32.110	29.689	2.4215	
	7.854	3.162	36.700	29.472	7.2284	
	9.016	3.158	36.700	29.306	7.3943	
	9.917	3.155	32.110	29.223	2.8872	
	10.961	3.152	27.520	29.155	-1.6350	
	12.028	3.147	18.350	29.128	-10.7780	

Ternary chalcopyrite semiconductor crystals are important for second harmonic generation of the CO<sub>2</sub> laser. Thermo-optic coefficients of zinc germanium phosphide, ZnGeP<sub>2</sub>, cadmium germanium phosphide, CdGeP<sub>2</sub>, and copper gallium sulphide, CuGaS<sub>2</sub> were measured by Boyd *et al.* [77-79]. We analyzed those values in the begining of 1980's [80]. We have reanalyzed these values and the optical constants  $G$ ,  $H$ , and  $E_{ig}$  are shown in Table 3.1. The experimental data and the computed curves are shown in Figs. 3.23, 3.24 for CdGeP<sub>2</sub>; and ZnGeP<sub>2</sub> and CuGaS<sub>2</sub>, respectively. The thermo-optic coefficients are one-order magnitude greater than that of the previous other nonlinear crystals. The larger positive values at the band-edge region are decreasing asymptotically in the near IR and IR region for these crystals. The variation of band gap with temperature is dominated in these crystals to account for the large positive values of  $dn/dT$ . The experimental data are compared with the calculated values as shown in Table 3.5. The fit is excellent. The thermo-optic coefficients of some other ternary semiconductor crystals, such as ZnSiAs<sub>2</sub>, CdSiP<sub>2</sub>, ZnSiP<sub>2</sub>, and AgGaS<sub>2</sub> have also been analyzed in this model. The optical constants are shown in Table 3.1 with other different optical and physical parameters. Some of these optical constants were evaluated [100] from the values of  $dB/dT$ , the change of birefringence with temperature. A typical plot of the change of birefringence with temperature versus wavelength is shown in Fig. 3.25. for ZnSiAs<sub>2</sub>, CdSiP<sub>2</sub>, and ZnSiP<sub>2</sub> crystals.

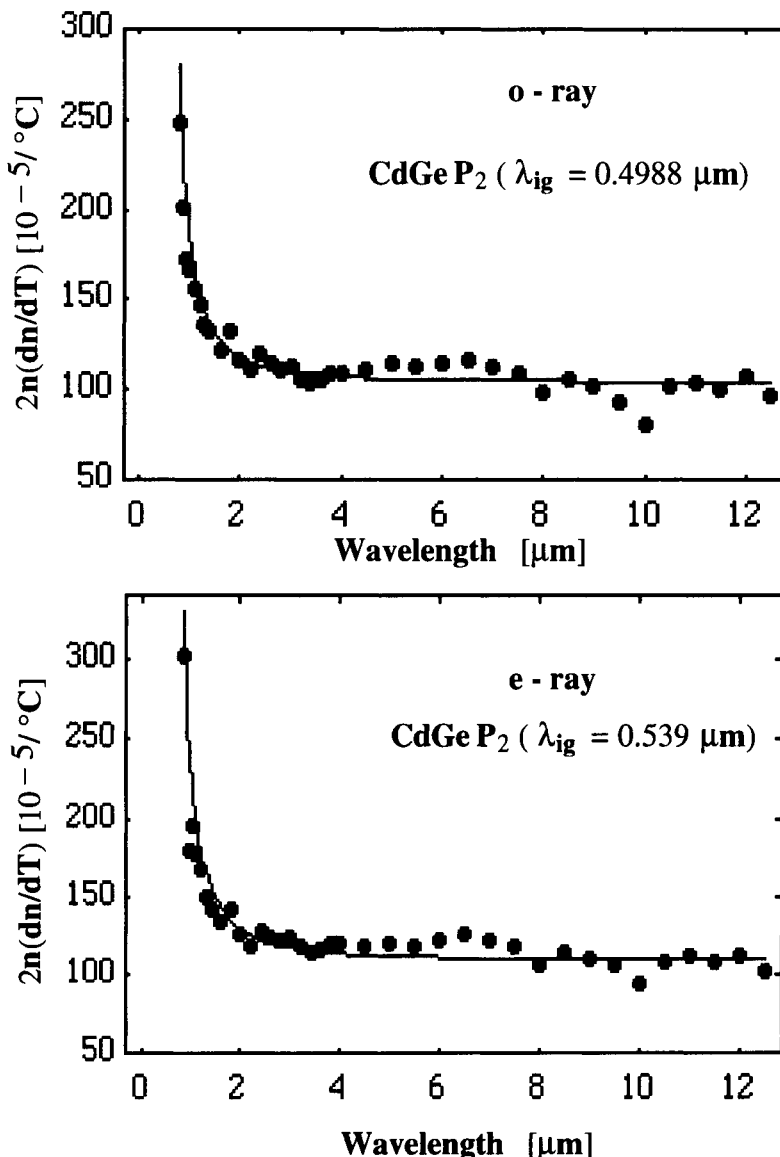


Figure 3.23:  $2n(dn/dT)$  versus wavelength for the CdGeP<sub>2</sub> crystal: Curves are the computed values; solid circles are the experimental data of Boyd *et al.* [78] at 25°C.

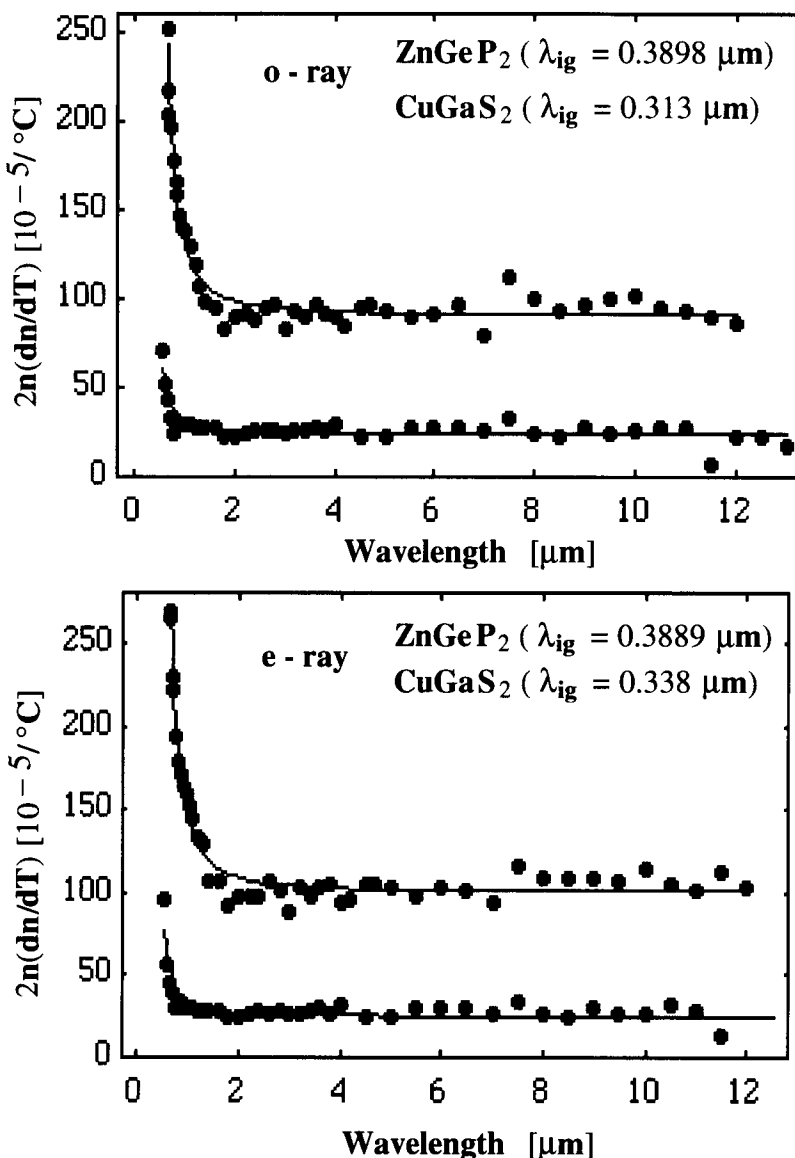


Figure 3.24:  $2n(dn/dT)$  versus wavelength for the  $\text{CuGaS}_2$  and  $\text{ZnGeP}_2$  crystal: Curves are the computed values; solid circles are the experimental data of Boyd *et al.* [79, 77] at  $25^{\circ}\text{C}$ .

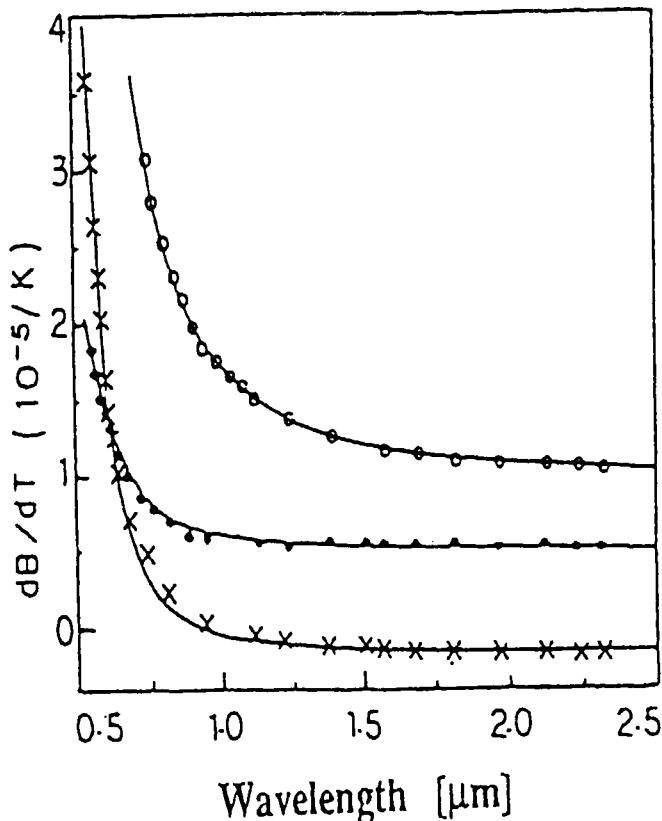


Figure 3.25: Change of birefringence with temperature versus wavelength: solid curves are the computed values; points are the experimental values [88];  $\odot$ , ZnSiAs<sub>2</sub>;  $\bullet$ , ZnSiP<sub>2</sub>; and  $\times$ , CdSiP<sub>2</sub> (after Ref. 100 with permission from OSA).

**Table 3.5: Refractive Index and Thermo-Optic Coefficients of Some Chalcopyrite Crystals**

Crystal [Ref.]	Wavelength [ μm]	Refractive index	<i>dn/dT</i> [(10 <sup>-5</sup> )/K]		Differ- ence	Av. Dev. [10 <sup>-5</sup> ]	RMS Dev.
			Expt. values	Computed (This work)			
AgGaS <sub>2</sub> (o) [79, 81]	0.633	2.55339	22.500	22.400	-0.100	0.25	0.30
	1.06	2.45083	17.500	17.260	-0.240		
	10.6	2.34665	15.020	15.430	0.410		
	(e) 0.633	2.50711	24.000	23.990	-0.010	0.25	0.30
	1.06	2.39658	17.520	17.560	0.040		
	10.6	2.29245	15.660	15.560	-0.100		
CdGeP <sub>2</sub> (Ord.) at 20°C [78]	0.800	3.48330	35.560	40.114	-4.5542	1.8	3.9
	0.850	3.44030	29.110	35.290	-6.1797		
	0.900	3.40590	53.720	31.912	21.8082		
	0.950	3.37890	25.550	29.424	-3.8741		
	1.000	3.35600	24.800	27.537	-2.7370		
	1.100	3.32320	23.600	24.859	-1.2593		
	1.200	3.29900	22.250	23.087	-0.8368		
	1.300	3.28110	20.710	21.838	-1.1278		
	1.400	3.26690	20.200	20.922	-0.7223		
	1.600	3.24700	18.680	19.681	-1.0014		
	1.800	3.23420	20.560	18.893	1.6672		
	2.000	3.22550	18.110	18.357	-0.2468		
	2.200	3.22020	17.120	17.969	-0.8493		
	2.400	3.21590	18.700	17.685	1.0152		
	2.600	3.21280	17.770	17.467	0.3031		
	2.800	3.20960	17.300	17.301	-0.0010		
	3.000	3.20650	17.690	17.172	0.5183		
	3.200	3.20490	16.610	17.062	-0.4522		
	3.400	3.20260	16.100	16.977	-0.8774		
	3.600	3.20030	16.390	16.909	-0.5188		
	3.800	3.19810	17.190	16.853	0.3375		
	4.000	3.19630	17.040	16.804	0.2357		
	4.500	3.19240	17.440	16.713	0.7266		
	5.000	3.18870	17.860	16.654	1.2064		
	5.500	3.18300	17.710	16.625	1.0848		
	6.000	3.18000	18.080	16.597	1.4833		
	6.500	3.17680	18.380	16.579	1.8009		
	7.000	3.17350	17.690	16.569	1.1208		
	7.500	3.17030	17.120	16.564	0.5559		
	8.000	3.16690	15.510	16.564	-1.0539		
	8.50	3.16240	16.580	16.573	0.0073		

**Table 3.5: (Continued)**

Crystal [Ref.]	Wavelength [ μm]	Refractive index	<i>dn/dT</i> [ (10 <sup>-5</sup> )K ]		Differ- ence	Av. Dev.	RMS Dev. [10 <sup>-5</sup> ]
			Expt. values	Computed (This work)			
CdGeP <sub>2</sub> (Extra. ord.)	9.00	3.15850	16.200	16.581	-0.3807		
	9.50	3.15470	14.750	16.590	-1.8402		
	10.00	3.15080	12.880	16.602	-3.7217		
	10.50	3.14350	16.140	16.633	-0.4925		
	11.00	3.13720	16.590	16.659	-0.0692		
	11.50	3.13210	15.930	16.680	-0.7505		
	12.00	3.12410	17.140	16.718	0.4220		
	12.50	3.11650	15.480	16.754	-1.2742		
	0.85	3.49420	43.350	47.282	-3.9320	2.0	4.0
	0.90	3.45050	61.380	41.255	20.1250		
	0.95	3.41670	26.160	36.993	-10.833		
	1.00	3.39020	28.750	33.841	-5.0907		
	1.10	3.35050	26.370	29.542	-3.1722		
	1.20	3.32220	25.080	26.787	-1.7070		
	1.30	3.30250	22.520	24.885	-2.3646		
	1.40	3.28670	21.420	23.517	-2.0966		
	1.60	3.26430	20.570	21.699	-1.1294		
	1.80	3.25020	21.750	20.564	1.1858		
	2.00	3.24060	19.310	19.802	-0.4924		
	2.20	3.23400	18.250	19.262	-1.0124		
	2.40	3.22870	19.610	18.868	0.7424		
	2.60	3.22430	19.310	18.570	0.7397		
	2.80	3.22060	18.960	18.340	0.6196		
	3.00	3.21750	19.220	18.159	1.0613		
	3.20	3.21560	18.240	18.008	0.2316		
	3.40	3.21320	17.650	17.890	-0.2398		
	3.60	3.21080	17.940	17.793	0.1465		
	3.80	3.20830	18.720	17.715	1.0048		
	4.00	3.20630	18.610	17.648	0.9620		
	4.50	3.20260	18.490	17.518	0.9724		
	5.00	3.19910	18.750	17.430	1.3201		
	5.50	3.19340	18.510	17.382	1.1276		
	6.00	3.19060	19.030	17.338	1.6918		
	6.50	3.18760	19.560	17.308	2.2517		
	7.00	3.18460	19.020	17.288	1.7319		
	7.50	3.18160	18.520	17.275	1.2450		
	8.00	3.17850	16.730	17.268	-0.5378		
	8.50	3.17430	17.920	17.271	0.6493		

**Table 3.5: (Continued)**

Crystal [Ref.]	Wavelength [ μm]	Refractive index	<i>dn/dT</i> [(10 <sup>-5</sup> )/K]		Differ- ence	Av. Dev.	RMS Dev. [10 <sup>-5</sup> ]
			Expt. values	Computed (This work)			
	9.00	3.17070	17.280	17.274	0.0064		
	9.50	3.16720	16.690	17.279	-0.5886		
	10.00	3.16360	14.720	17.286	-2.5662		
	10.50	3.15740	16.980	17.310	-0.3297		
	11.00	3.15170	17.620	17.332	0.2880		
	11.50	3.14700	17.020	17.350	-0.3300		
	12.00	3.14020	17.850	17.381	0.4693		
	12.50	3.13320	16.110	17.413	-1.3034		
CuGaS <sub>2</sub> (Ord.)	0.55	2.76300	12.950	10.875	2.0746	0.6	0.9
at 20°C	0.60	2.69830	9.720	9.387	0.3327		
[79]	0.65	2.65770	8.080	8.400	-0.3202		
	0.70	2.62930	6.370	7.710	-1.3399		
	0.75	2.61000	4.640	7.201	-2.5609		
	0.80	2.59250	5.260	6.823	-1.5633		
	0.85	2.57860	6.060	6.530	-0.4697		
	0.90	2.56810	5.640	6.294	-0.6544		
	0.95	2.55910	5.870	6.105	-0.2347		
	1.00	2.55170	5.860	5.948	-0.0882		
	1.10	2.54060	5.750	5.707	0.0435		
	1.20	2.53220	5.440	5.532	-0.0916		
	1.30	2.52590	5.480	5.400	0.0801		
	1.40	2.52090	5.440	5.299	0.1415		
	1.60	2.51350	5.320	5.154	0.1655		
	1.80	2.50920	4.490	5.057	-0.5672		
	2.00	2.50510	4.520	4.991	-0.4712		
	2.20	2.50190	4.950	4.943	0.0065		
	2.40	2.49930	5.290	4.908	0.3821		
	2.60	2.49750	5.080	4.880	0.2000		
	2.80	2.49590	5.150	4.858	0.2916		
	3.00	2.49450	4.990	4.841	0.1488		
	3.20	2.49320	5.160	4.828	0.3324		
	3.40	2.49220	5.090	4.816	0.2739		
	3.60	2.49100	5.630	4.807	0.8227		
	3.80	2.48970	5.330	4.800	0.5296		
	4.00	2.48840	5.760	4.795	0.9652		
	4.50	2.48690	4.530	4.782	-0.2521		
	5.00	2.48430	4.390	4.776	-0.3860		
	5.50	2.48030	5.680	4.775	0.9045		

**Table 3.5: (Continued)**

Crystal [Ref.]	Wavelength [ μm]	Refractive index	<i>dn/dT</i> [(10 <sup>-5</sup> )/K]		Differ- ence	Av. Dev.	RMS Dev. [10 <sup>-5</sup> ]
			Expt. values	Computed (This work)			
	6.00	2.47740	5.620	4.775	0.8452		
	6.50	2.47440	5.440	4.776	0.6642		
	7.00	2.47140	5.110	4.778	0.3323		
	7.50	2.46740	6.670	4.782	1.8877		
	8.00	2.46390	4.910	4.787	0.1234		
	8.50	2.45890	4.700	4.794	-0.0942		
	9.00	2.45390	5.680	4.802	0.8778		
	9.50	2.44910	4.930	4.810	0.1199		
	10.00	2.44290	5.190	4.821	0.3690		
	10.50	2.43720	5.660	4.831	0.8288		
	11.00	2.43110	5.610	4.842	0.7677		
	11.50	2.42750	1.260	4.849	-3.5887		
	12.00	2.41710	4.810	4.869	-0.0588		
	12.50	2.40940	4.800	4.884	-0.0837		
	13.00	2.39990	3.490	4.902	-1.4124		
CuGaS <sub>2</sub> (Extra. ord.)	0.55	2.78130	17.320	13.709	3.6109	0.8	1.1
	0.60	2.70190	10.570	11.446	-0.8759		
	0.65	2.65700	8.610	9.994	-1.3841		
	0.70	2.62660	7.640	9.009	-1.3694		
[79]	0.75	2.60560	5.890	8.303	-2.4129		
	0.80	2.58860	6.220	7.782	-1.5616		
	0.85	2.57370	6.510	7.386	-0.8764		
	0.90	2.56300	5.940	7.072	-1.1319		
	0.95	2.55380	6.080	6.821	-0.7407		
	1.00	2.54640	5.980	6.615	-0.6348		
	1.10	2.53490	6.030	6.301	-0.2708		
	1.20	2.52650	5.570	6.075	-0.5049		
	1.30	2.51990	5.740	5.907	-0.1668		
	1.40	2.51480	5.750	5.778	-0.0277		
	1.60	2.50730	5.620	5.595	0.0247		
	1.80	2.50280	4.820	5.473	-0.6533		
	2.00	2.49910	4.730	5.389	-0.6594		
	2.20	2.49560	5.200	5.330	-0.1300		
	2.40	2.49310	5.640	5.285	0.3549		
	2.60	2.49130	5.410	5.250	0.1598		
	2.80	2.48940	5.730	5.224	0.5063		
	3.00	2.48800	5.440	5.202	0.2377		
	3.20	2.48710	5.350	5.184	0.1658		

**Table 3.5: (Continued)**

Crystal [Ref.]	Wavelength [ μm]	Refractive index	$dn/dT$ [ $(10^{-5})/\text{K}$ ]		Differ- ence	Av. Dev.	RMS Dev. [ $10^{-5}$ ]
			Expt. values	Computed (This work)			
ZnGeP <sub>2</sub> (Ord.) at 20°C [77]	3.40	2.48530	5.660	5.172	0.4884		
	3.60	2.48410	6.000	5.160	0.8396		
	3.80	2.48310	5.360	5.151	0.2091		
	4.00	2.48160	6.290	5.144	1.1459		
	4.50	2.48010	4.990	5.128	-0.1381		
	5.00	2.47720	5.120	5.120	-0.0005		
	5.50	2.47280	6.120	5.120	1.0005		
	6.00	2.46940	6.080	5.119	0.9611		
	6.50	2.46570	6.240	5.121	1.1193		
	7.00	2.46210	5.520	5.123	0.3966		
	7.50	2.45820	6.950	5.128	1.8223		
	8.00	2.45390	5.520	5.134	0.3864		
	8.50	2.44900	4.940	5.141	-0.2013		
	9.00	2.44350	6.210	5.151	1.0593		
	9.50	2.43760	5.440	5.161	0.2787		
	10.00	2.43110	5.500	5.174	0.3265		
	10.50	2.42340	6.730	5.189	1.5414		
	11.00	2.41790	5.720	5.199	0.5208		
	11.50	2.41210	2.580	5.211	-2.6307		
	0.64	3.50520	35.940	34.577	1.3628	0.9	1.2
	0.66	3.47560	31.230	32.441	-1.2111		
	0.68	3.44770	29.520	30.678	-1.1577		
	0.70	3.42330	28.630	29.186	-0.5556		
	0.75	3.37300	26.220	26.318	-0.0984		
	0.80	3.33570	24.690	24.267	0.4230		
	0.85	3.30630	24.120	22.744	1.3764		
	0.90	3.28300	22.340	21.573	0.7675		
	0.95	3.26380	21.320	20.651	0.6687		
	1.00	3.24780	21.180	19.911	1.2691		
	1.10	3.22320	20.110	18.800	1.3098		
	1.20	3.20540	18.630	18.015	0.6155		
	1.30	3.19240	16.840	17.434	-0.5937		
	1.40	3.18200	15.340	16.994	-1.6539		
	1.60	3.16660	15.100	16.380	-1.2802		
	1.80	3.15620	13.200	15.979	-2.7787		
	2.00	3.14900	14.190	15.700	-1.5097		
	2.20	3.14330	14.600	15.500	-0.9000		
	2.40	3.13880	14.140	15.352	-1.2116		

**Table 3.5: (Continued)**

Crystal [Ref.]	Wavelength [ μm]	Refractive index	$dn/dT$ [ $10^{-5}$ /K]		Differ- ence	Av. Dev.	RMS Dev. [ $10^{-5}$ ]
			Expt. values	Computed (This work)			
	2.60	3.13570	15.130	15.236	-0.1057		
	2.80	3.13270	15.480	15.147	0.3327		
	3.00	3.13040	13.260	15.076	-1.8160		
	3.20	3.12840	14.940	15.019	-0.0787		
	3.40	3.12630	14.400	14.974	-0.5735		
	3.60	3.12570	15.580	14.930	0.6497		
	3.80	3.12370	14.580	14.901	-0.3210		
	4.00	3.12230	14.260	14.875	-0.6146		
	4.20	3.12090	13.570	14.853	-1.2829		
	4.50	3.11860	15.310	14.828	0.4818		
	4.70	3.11740	15.510	14.814	0.6961		
	5.00	3.11490	15.050	14.800	0.2498		
	5.50	3.11310	14.490	14.775	-0.2851		
	6.00	3.11010	14.580	14.764	-0.1838		
	6.50	3.10570	15.600	14.765	0.8351		
	7.00	3.10400	12.850	14.757	-1.9072		
	7.50	3.09940	18.150	14.766	3.3836		
	8.00	3.09610	16.100	14.772	1.3282		
	8.50	3.09190	15.160	14.783	0.3768		
	9.00	3.08800	15.560	14.795	0.7654		
	9.50	3.08360	16.270	14.810	1.4604		
	10.00	3.07880	16.530	14.827	1.7025		
	10.50	3.07380	15.400	14.847	0.5529		
	11.00	3.06890	15.250	14.867	0.3831		
	11.50	3.06230	14.740	14.896	-0.1555		
	12.00	3.05520	14.240	14.927	-0.6871		
ZnGeP <sub>2</sub> (Extra. ord.)	0.64	3.58020	37.580	38.079	-0.4990	1.0	1.3
	0.66	3.54670	37.340	35.733	1.6068		
	0.68	3.51600	32.530	33.788	-1.2584		
	0.70	3.48850	31.820	32.147	-0.3274		
[77]	0.75	3.43240	28.260	28.985	-0.7253		
	0.80	3.39150	26.430	26.713	-0.2833		
	0.85	3.35930	25.390	25.024	0.3656		
	0.90	3.33360	24.610	23.726	0.8836		
	0.95	3.31240	24.260	22.705	1.5549		
	1.00	3.29540	23.010	21.879	1.1306		
	1.10	3.26880	22.080	20.643	1.4367		
	1.20	3.24930	20.510	19.770	0.7398		

**Table 3.5: (Continued)**

Crystal [Ref.]	Wavelength [ μm]	Refractive index	<u><math>dn/dT</math> [(10<sup>-5</sup>)/K]</u>		Differ- ence	Av. Dev.	RMS Dev. [10 <sup>-5</sup> ]
			Expt. values	Computed (This work)			
	1.30	3.23460	20.120	19.127	0.9931		
	1.40	3.22440	16.550	18.631	-2.0809		
	1.60	3.20770	16.750	17.948	-1.1977		
	1.80	3.19650	14.400	17.500	-3.1002		
	2.00	3.18890	15.290	17.188	-1.8983		
	2.20	3.18290	15.280	16.965	-1.6850		
	2.40	3.17800	15.490	16.800	-1.3100		
	2.60	3.17450	16.800	16.672	0.1284		
	2.80	3.17170	16.050	16.571	-0.5210		
	3.00	3.16930	13.960	16.491	-2.5312		
	3.20	3.16710	16.280	16.428	-0.1476		
	3.40	3.16470	15.460	16.378	-0.9181		
	3.60	3.16320	16.290	16.334	-0.0442		
	3.80	3.16160	16.530	16.299	0.2310		
	4.00	3.16080	15.020	16.266	-1.2460		
	4.20	3.15950	15.140	16.241	-1.1009		
	4.50	3.15610	16.600	16.218	0.3816		
	4.70	3.15490	16.710	16.202	0.5078		
	5.00	3.15330	16.430	16.182	0.2483		
	5.50	3.15180	15.420	16.152	-0.7317		
	6.00	3.14800	16.300	16.143	0.1574		
	6.50	3.14450	16.130	16.138	-0.0083		
	7.00	3.14200	15.010	16.134	-1.1235		
	7.50	3.13780	18.590	16.141	2.4491		
	8.00	3.13500	17.430	16.144	1.2863		
	8.50	3.13110	17.370	16.154	1.2159		
	9.00	3.12720	17.500	16.166	1.3338		
	9.50	3.12310	17.110	16.181	0.9295		
	10.00	3.11830	18.410	16.200	2.2104		
	10.50	3.11370	16.840	16.218	0.6215		
	11.00	3.10870	16.340	16.240	0.0998		
	11.50	3.10080	18.320	16.278	2.0423		
	12.00	3.09490	16.590	16.305	0.2846		
ZnSiAs <sub>2</sub>	1.064	3.33518	29.520	29.609	0.089	0.065	0.070
(o)	5.3	3.20621	23.010	22.945	0.065		
[78, 88]	10.6	3.17627	23.000	22.961	0.039		
(e)	1.064	3.37101	31.150	31.185	-0.035	0.02	0.03
	5.3	3.23262	23.910	23.905	0.005		
	10.6	3.20275	23.890	23.912	0.022		

### 3.4.2 Other Oxide and Laser Crystals

Quartz ( $\text{SiO}_2$ ) is an important crystal which was used by Franken *et al.* [112] for SHG of ruby laser. Surprisingly, there is no analysis of the thermo-optic coefficients for both ordinary and extraordinary polarizations. There is a systematic data reported by Micheli [1] from 0.202 to 0.643  $\mu\text{m}$ . Similarly, Micheli [113] reported the values of thermo-optic coefficients for calcite crystal ( $\text{CaCO}_3$ ) from 0.211 to 0.643  $\mu\text{m}$ . We have analyzed these historical data in the present model satisfactorily. The optical constants  $G$ ,  $H$ , and  $E_{ig}$  are shown in Table 3.1. The calculated and experimental values are shown in Table 3.6. To show the characteristic behavior of dispersion of thermo-optic coefficients, the  $2n(dn/dT)$  values are plotted in Fig. 3.26 for calcite, and quartz crystals, the upper and lower figures, respectively. Thermo-optic coefficients are decreasing asymptotically from a small positive value to a small negative value from UV to near-IR in the transmission region for both polarizations in the quartz crystal. Both the thermal expansion coefficient and the variation of band gap with temperature are contributing equally to the thermo-optic coefficients in this crystal. On the other hand, the thermo-optic coefficients are decreasing from a large positive value to a small positive value from the UV to the near-IR in calcite crystal. Since the thermal expansion coefficient is negative for extraordinary polarization in calcite crystal, the thermo-optic coefficients are positive and less dispersive compared to the ordinary polarization.

The thermo-optic coefficients of some other oxide crystals, such as ALON [114],  $\text{Al}_2\text{O}_3$  [115, 116], BeO [117], BGO [118]; laser crystals  $\text{CaMO}_4$  [119],  $\text{CaWO}_4$  [120], YAG [121];  $\text{HfO}_2:\text{Y}_2\text{O}_3$ , [122];  $\text{MgAl}_2\text{O}_4$  [115],  $\text{MgO}$  [123, 124],  $\text{PbMoO}_4$  [119],  $\text{TeO}_2$  [125],  $\text{TiO}_2$  [99, 126],  $\text{Y}_2\text{O}_3$  [114], and  $\text{ZrO}_2:\text{Y}_2\text{O}_3$  [127] have been analyzed here by using Eq. (3.29), satisfactorily. The optical constants  $G$ ,  $H$ , and  $E_{ig}$  are shown in Table 3.1. The experimental values are compared with the calculated values which are shown in Table 3.6. The characteristic behavior of dispersions are shown in Figs. 3.27-3.32 for  $\text{Al}_2\text{O}_3$  and ALON, BeO,  $\text{CaWO}_4$ ,  $\text{TeO}_2$ , YAG and  $\text{HfO}_2:\text{Y}_2\text{O}_3$ , and,  $\text{MgO}$  and  $\text{ZrO}_2:\text{Y}_2\text{O}_3$  crystals, respectively. It is quite interesting to note that the thermo-optic coefficients are positive for most of the oxide crystals, except  $\text{CaMO}_4$  [119],  $\text{CaWO}_4$  and  $\text{PbMoO}_4$ . Also, the dispersion is significant in most crystals.

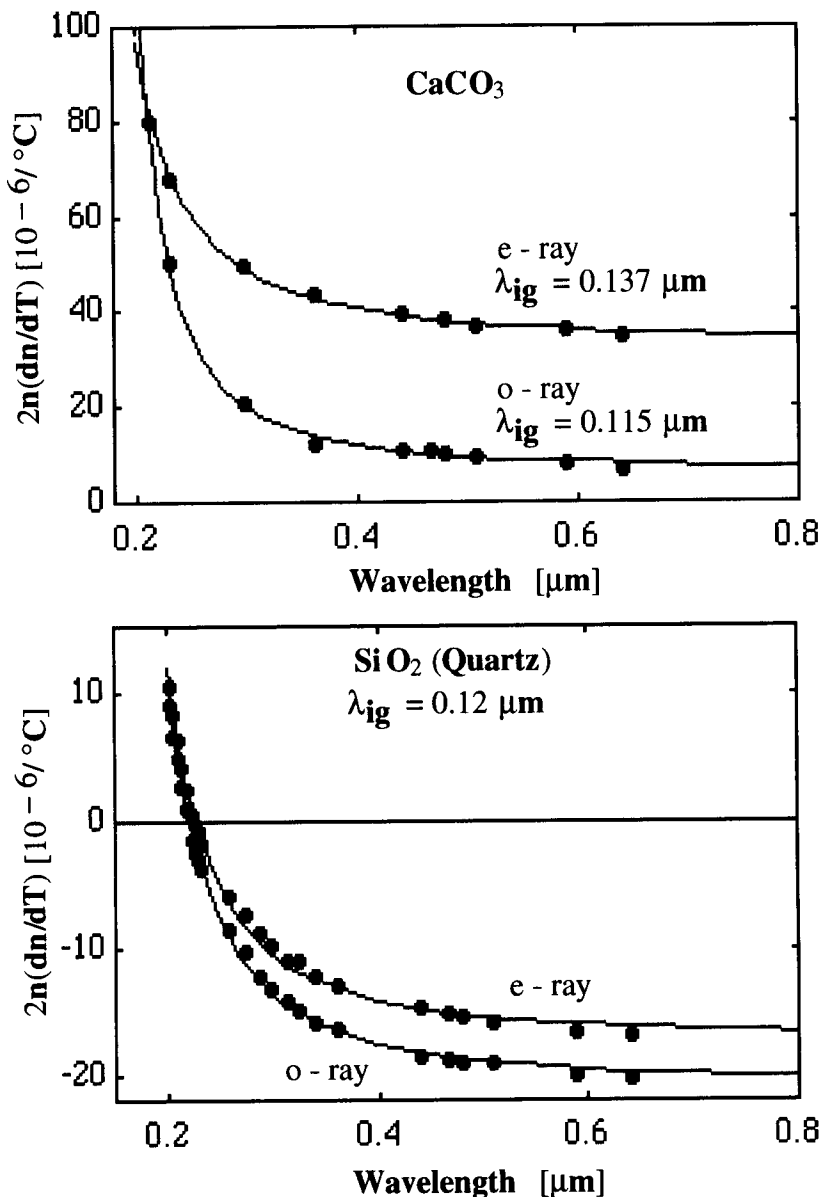


Figure 3.26:  $2n(dn/dT)$  versus wavelength for CaCO<sub>3</sub> and SiO<sub>2</sub> crystals: Curves are the computed values; solid circles are the experimental data of Micheli [4], and [113], respectively, at 25°C.

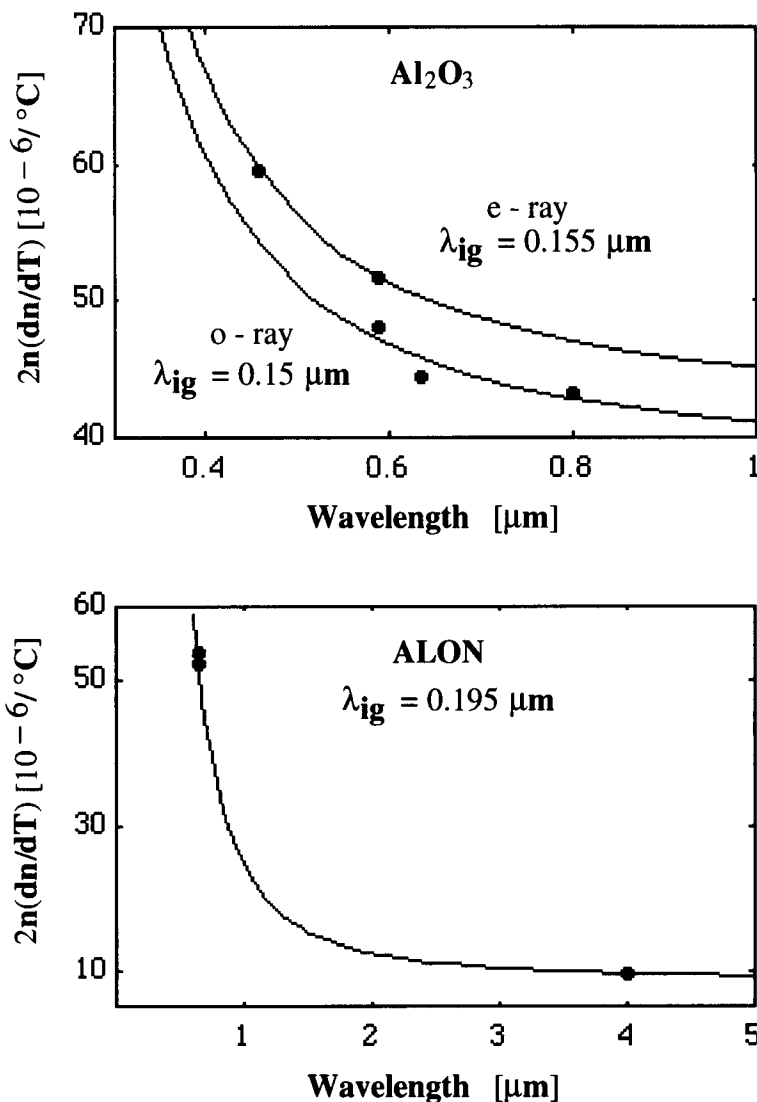


Figure 3.27:  $2n(dn/dT)$  versus wavelength for  $\text{Al}_2\text{O}_3$  and ALON crystals: Curves are the computed values; solid circles are the experimental data [115, 116] for  $\text{Al}_2\text{O}_3$  at  $20^\circ\text{C}.$ , and [114] at  $25^\circ\text{C}$  for ALON, respectively.

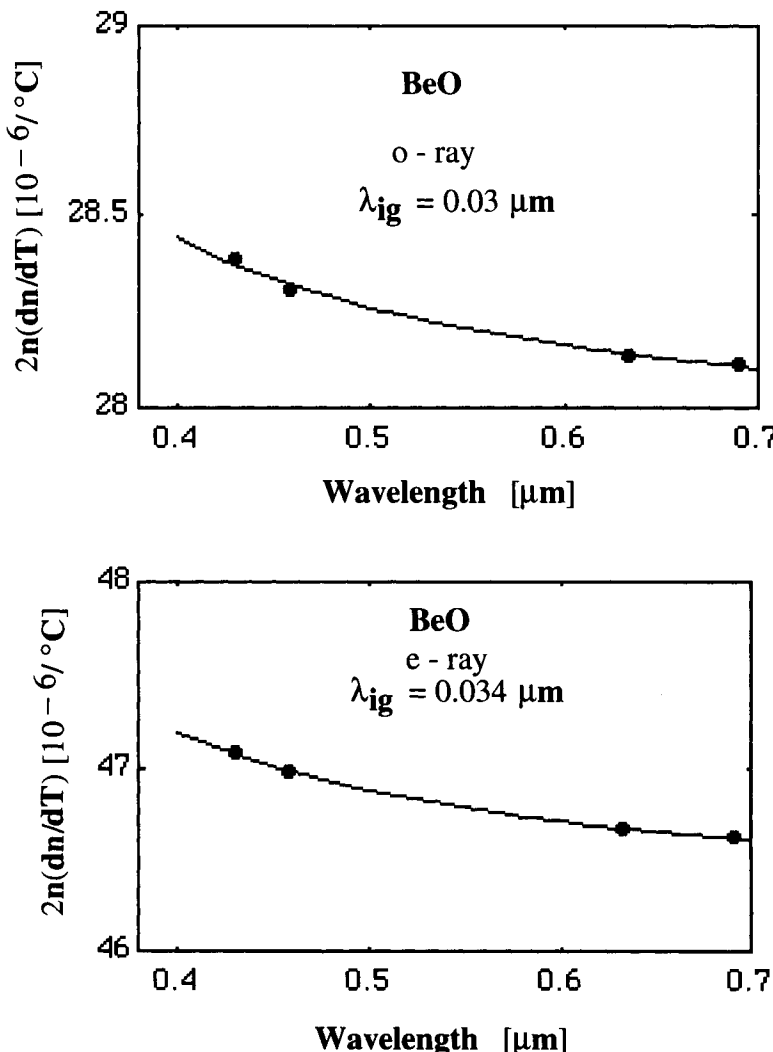


Figure 3.28:  $2n(dn/dT)$  versus wavelength for BeO crystal: Curves are the computed values; solid circles are the experimental data [117] at  $25^\circ C$ .

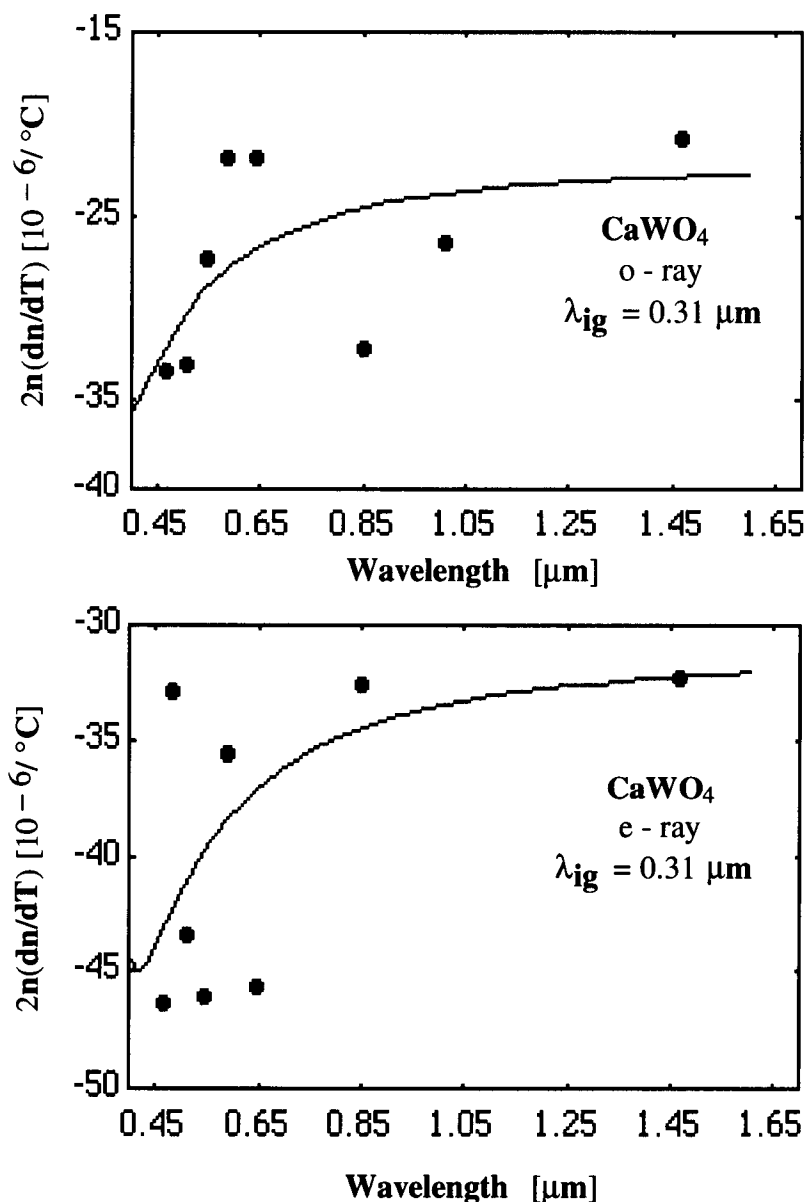


Figure 3.29:  $2n(dn/dT)$  versus wavelength for  $\text{CaWO}_4$  crystal: Curves are the computed values; solid circles are the experimental data [120] at  $25^{\circ}\text{C}$ .

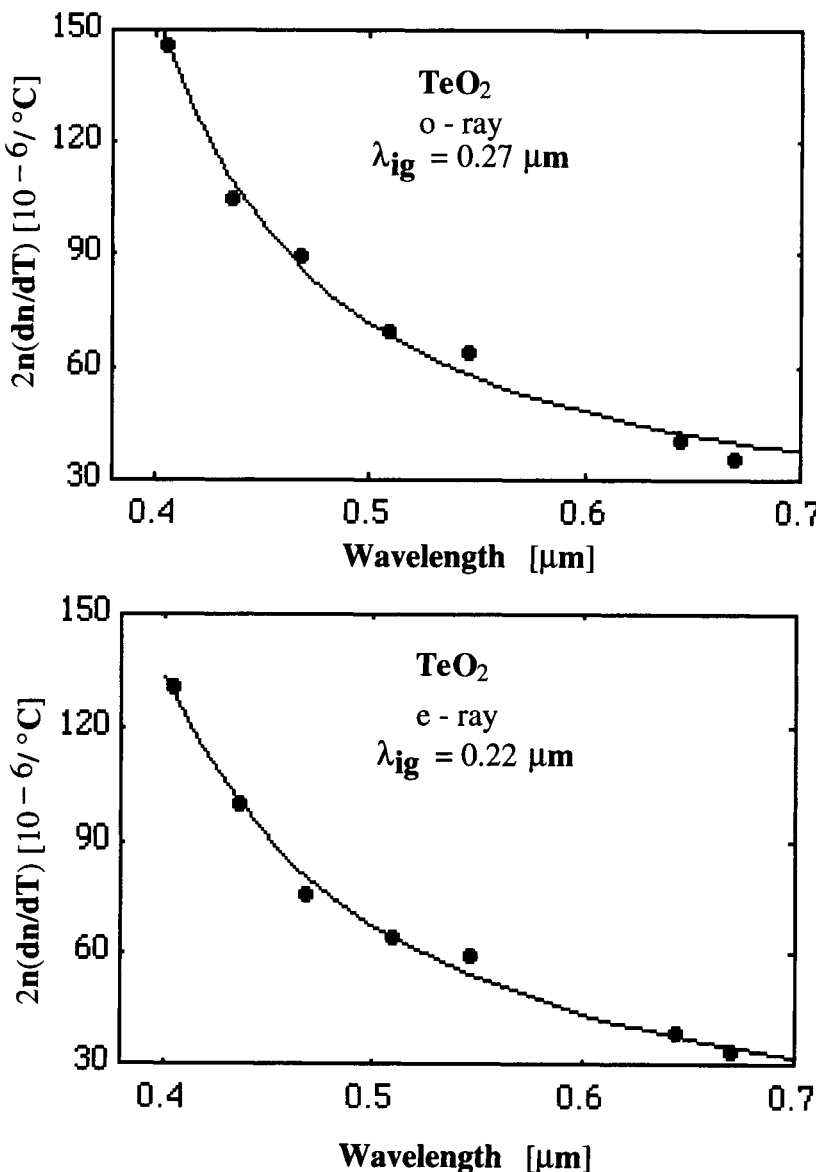


Figure 3.30:  $2n(dn/dT)$  versus wavelength for  $\text{TeO}_2$  crystal: Curves are the computed values; solid circles are the experimental data [125] at  $20^\circ\text{C}$ .

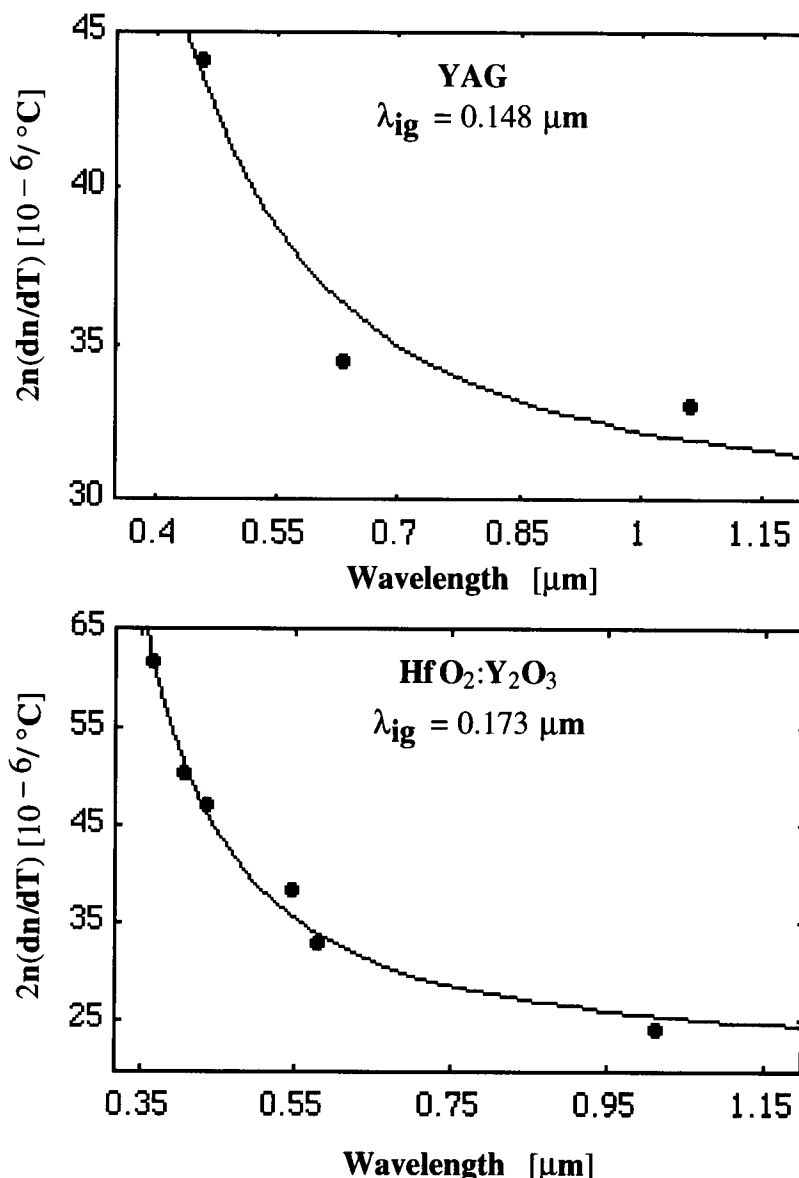


Figure 3.31:  $2n(dn/dT)$  versus wavelength for YAG and  $\text{HfO}_2:\text{Y}_2\text{O}_3$  crystals: Curves are the computed values; solid circles are the experimental data [121] for YAG, and [122] for  $\text{HfO}_2:\text{Y}_2\text{O}_3$ , respectively at  $25^{\circ}\text{C}$ .

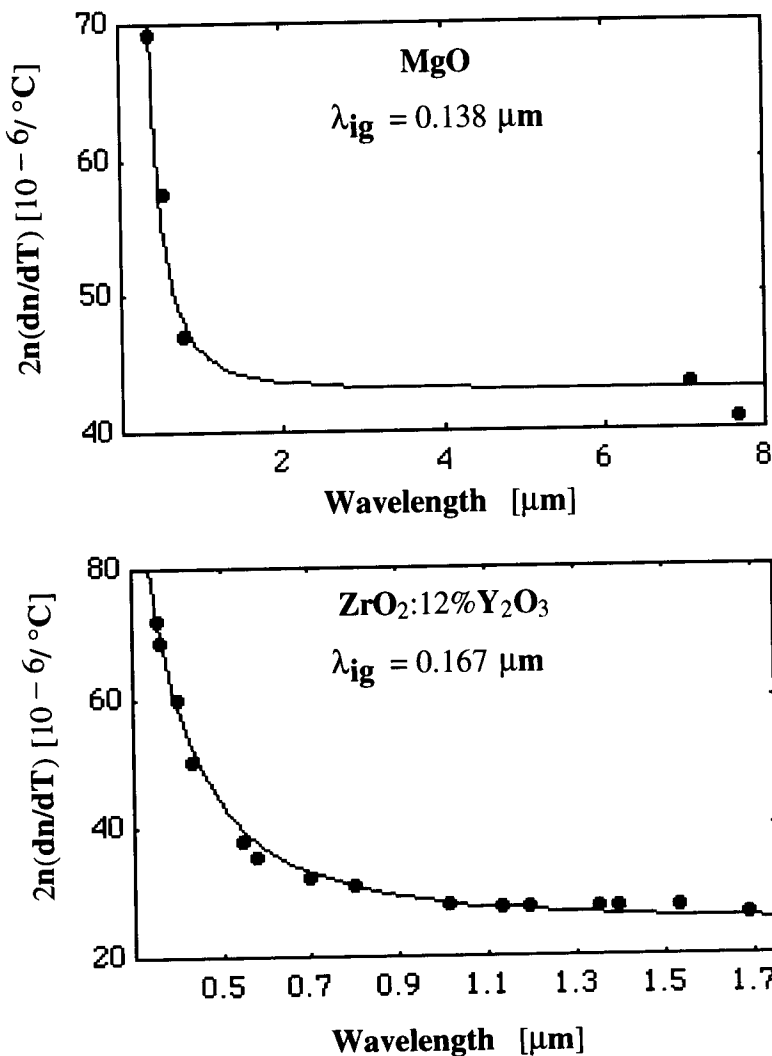


Figure 3.32:  $2n(\text{dn}/dT)$  versus wavelength for MgO and ZrO<sub>2</sub>:Y<sub>2</sub>O<sub>3</sub> crystals: Curves are the computed values; solid circles are the experimental data [123, 124] for MgO at 20°C, and [127] for ZrO<sub>2</sub>:Y<sub>2</sub>O<sub>3</sub> at 25°C, respectively.

**Table 3.6: Refractive Index and Thermo-Optic Coefficients of Some Oxide Crystals**

Crystal [Ref.]	Wavelength [ μm]	Refractive index	$dn/dT$ [( $10^{-6}$ )/K] Expt. Computed values (This work)	Differ- ence	Av. Dev.	RMS Dev. [ $10^{-6}$ ]
ALON [114]	0.63	1.7861	15.00	14.807	0.193	0.13 0.16
	0.63	1.7860	14.60	14.793	-0.193	
	4.00	1.7042	2.80	2.800	0.000	
Al <sub>2</sub> O <sub>3</sub> (o) [115, 116]	0.589	1.76816	13.60	13.327	0.273	0.26 0.29
	0.633	1.76599	12.58	12.974	-0.394	
at 20 °C	0.799	1.76030	12.29	12.169	0.121	
Al <sub>2</sub> O <sub>3</sub> (e)	0.458	1.77008	16.80	16.800	0.000	0.0 0.0
	0.589	1.75997	14.70	14.700	0.000	
BeO(o) [117]	0.430	1.73091	8.20	8.200	0.003	0.002 0.002
	0.458	1.72635	8.20	8.200	-0.004	
at 25°C	0.633	1.71573	8.20	8.200	-0.001	
	0.690	1.71427	8.20	8.200	0.001	
BeO(e) [117]	0.430	1.75705	13.40	13.400	0.002	0.002 0.002
	0.458	1.75304	13.40	13.400	-0.003	
at 25°C	0.633	1.74169	13.40	13.400	-0.001	
	0.690	1.73991	13.40	13.400	0.001	
BGO [118]	0.51	2.63327	-32.39	-33.340	-0.900	
	0.5893	2.55690	-32.93	-33.420	-0.500	
	0.6438	2.52430	-32.95	-33.650	-0.700	
	1.06	2.43266	---	-33.860		
	1.55	2.40535	---	-33.900		
CaCO <sub>3</sub> (o) at 25°C [113]	0.211	1.85692	21.50	20.136	1.364	0.8 0.9
	0.231	1.80233	13.97	15.184	-1.214	
	0.298	1.72771	6.04	7.562	-1.522	
	0.361	1.69316	3.60	4.811	-1.211	
	0.441	1.67423	3.25	3.122	0.128	
	0.467	1.67051	3.19	2.776	0.414	
	0.480	1.66877	3.05	2.627	0.423	
	0.508	1.66549	2.87	2.348	0.522	
	0.589	1.65835	2.40	1.774	0.626	
	0.643	1.65504	2.08	1.514	0.566	
CaCO <sub>3</sub> (e) at 25°C [113]	0.231	1.54541	21.98	22.106	-0.126	0.16 0.18
	0.298	1.51508	16.41	16.182	0.228	
	0.361	1.50224	14.49	14.242	0.248	
	0.441	1.49373	13.18	13.104	0.076	
	0.480	1.49108	12.87	12.777	0.094	
	0.508	1.48956	12.34	12.593	-0.253	
	0.589	1.48640	12.13	12.217	-0.087	

**Table 3.6:** (*Continued*)

Crystal [Ref.]	Wavelength [ μm]	Refractive index	<u><math>dn/dT</math></u> [( $10^{-6}$ )/K] Expt. Computed values (This work)	Differ- ence	Av. Dev.	RMS Dev. [ $10^{-6}$ ]
CaMoO <sub>4</sub> [119] (o) [119] (e)	0.643	1.48490	11.85	12.048	-0.198	
	0.588	1.99147	-9.60	-9.610	-0.010	
	0.633	1.98445	---	-10.260		
	1.064	1.95672	---	-11.610		
	0.588	2.00095	-10.00	-10.000	0.000	
	0.633	1.99328	---	-9.720		
	1.064	1.96332	---	-8.690		
	0.6438	1.91220	-5.70	-6.980	1.276	0.96
	0.5896	1.91840	-5.70	-7.230	1.534	1.11
	0.5461	1.92490	-7.10	-7.510	0.413	
CaWO <sub>4</sub> (o) at 25°C [120]	0.5086	1.93150	-8.60	-7.830	-0.770	
	0.4678	1.94210	-8.60	-8.280	-0.325	
	0.8521	1.89860	-8.50	-6.450	-2.048	
	1.0140	1.89370	-7.00	-6.270	-0.735	
	1.4695	1.88500	-5.50	-6.050	0.552	
	0.6438	1.91220	-11.90	-9.690	-2.250	1.19
	0.5896	1.93470	-9.20	-9.910	0.731	1.44
	0.5461	1.94170	-11.90	-10.220	-1.636	
	0.5086	1.94900	-11.10	-10.560	-0.558	
	0.4678	1.96020	-11.80	-10.990	-0.844	
CaWO <sub>4</sub> (e) at 25°C [120]	0.4800	1.95640	-8.40	-10.860	2.486	
	0.8521	1.91320	-8.50	-8.980	0.477	
	1.0140	1.90820	-7.00	-8.740	1.743	
	1.4695	1.89860	-8.50	-8.480	-0.024	
	0.3650	2.18411	14.10	14.190	-0.091	0.31
	Y <sub>2</sub> O <sub>3</sub> at 25°C [122]	0.4046	2.16082	11.70	11.940	-0.239
	0.4358	2.14735	11.00	10.750	0.251	
	0.5460	2.11822	9.10	8.430	0.665	
	0.5780	2.11289	7.80	8.050	-0.249	
	1.01398	2.08269	5.80	6.150	-0.345	
MgAl <sub>2</sub> O <sub>4</sub> [115]	0.589	1.71583	9.00	9.420	-0.420	
	1.064	1.70191	---	2.370		
	0.365	1.77188	19.50	19.708	-0.208	0.58
	0.546	1.74082	16.50	15.632	0.868	0.64
	0.768	1.72867	13.60	14.264	-0.664	
PbMoO <sub>4</sub> (o) (e)	0.589	2.40869	-75.00	-74.870	0.130	
	1.064	2.30258	---	-55.650		
	0.589	2.27669	-41.00	-40.910	0.090	
	1.064	2.20373	---	-28.670		
$\alpha$ -SiO <sub>2</sub> (o) at 25°C [1]	0.202	1.63810	3.21	3.213	-0.003	0.11
	0.206	1.63333	2.53	2.509	0.021	0.14
	0.210	1.62892	1.93	1.890	0.040	
	0.214	1.62483	1.24	1.345	-0.105	

**Table 3.6: (Continued)**

Crystal [Ref.]	Wavelength [ μm]	Refractive index	$dn/dT$ [(10 <sup>-6</sup> )/K] Expt. Computed values (This work)	Differ- ence	Av. Dev.	RMS [ 10 <sup>-6</sup> ]
$\alpha\text{-SiO}_2$ (e) at 25°C [1]	0.219	1.62013	0.75	0.747	0.003	
	0.224	1.61583	0.17	0.228	-0.058	
	0.226	1.61421	-0.08	0.039	-0.119	
	0.228	1.61265	-0.27	-0.140	-0.130	
	0.231	1.61040	-0.52	-0.392	-0.128	
	0.257	1.59474	-1.86	-1.972	0.112	
	0.274	1.58720	-2.35	-2.628	0.278	
	0.288	1.58217	-2.79	-3.037	0.247	
	0.298	1.57905	-3.11	-3.276	0.166	
	0.313	1.57497	-3.48	-3.574	0.094	
	0.325	1.57216	-3.52	-3.771	0.251	
	0.340	1.56909	-3.93	-3.976	0.046	
	0.361	1.56546	-4.18	-4.208	0.028	
	0.441	1.55624	-4.75	-4.742	-0.008	
	0.467	1.55422	-4.85	-4.848	-0.002	
	0.480	1.55333	-4.99	-4.893	-0.097	
	0.508	1.55163	-5.14	-4.978	-0.162	
	0.589	1.54790	-5.39	-5.149	-0.241	
	0.643	1.54606	-5.49	-5.226	-0.264	
	0.202	1.65841	2.67	2.818	-0.149	0.10
	0.206	1.65265	1.98	2.054	-0.074	0.12
	0.210	1.64735	1.43	1.382	0.048	
	0.214	1.64246	0.83	0.788	0.042	
	0.219	1.63684	0.27	0.138	0.132	
	0.224	1.63172	-0.48	-0.426	-0.054	
	0.226	1.62980	-0.75	-0.632	-0.118	
	0.228	1.62794	-0.93	-0.827	-0.103	
	0.231	1.62528	-1.12	-1.101	-0.019	
	0.257	1.60686	-2.65	-2.821	0.171	
	0.274	1.59811	-3.23	-3.536	0.306	
	0.288	1.59225	-3.85	-3.981	0.131	
	0.298	1.58864	-4.15	-4.242	0.092	
	0.313	1.58395	-4.50	-4.566	0.066	
	0.325	1.58071	-4.69	-4.780	0.090	
	0.340	1.57720	-5.01	-5.004	-0.006	
	0.361	1.57306	-5.21	-5.256	0.046	
	0.441	1.56262	-5.93	-5.836	-0.094	
	0.467	1.56036	-6.01	-5.951	-0.059	
	0.480	1.55937	-6.10	-6.001	-0.099	
	0.508	1.55748	-6.16	-6.092	-0.068	
	0.589	1.55338	-6.42	-6.279	-0.141	
	0.643	1.55139	-6.53	-6.362	-0.168	

**Table 3.6: (Continued)**

Crystal [Ref.]	Wavelength [ μm]	Refractive index	$dn/dT$ [(10 <sup>-6</sup> )/K] Expt. Computed values (This work)	Differ- ence	Avg. Dev.	RMS Dev. [ 10 <sup>-6</sup> ]
TeO <sub>2</sub> (o) at 20°C [125]	0.4047	2.43150	30.00	29.990	0.012	0.64
	0.4358	2.38340	22.00	22.820	-0.824	0.77
	0.4678	2.34780	19.00	18.350	0.647	
	0.5086	2.31500	15.00	14.790	0.213	
	0.5461	2.29310	14.00	12.650	1.350	
	0.6440	2.25620	9.00	9.490	-0.488	
	0.6700	2.25000	8.00	8.960	-0.963	
TeO <sub>2</sub> (e) at 20°C [125]	0.4047	2.61570	25.00	24.510	0.486	0.47
	0.4358	2.55830	19.50	19.650	-0.149	0.61
	0.4678	2.51640	15.00	16.160	-1.164	
	0.5086	2.47790	13.00	13.070	-0.067	
	0.5461	2.45200	12.00	11.050	0.953	
	0.6440	2.40860	8.00	7.780	0.219	
	0.6700	2.38000	7.00	7.270	-0.268	
TiO <sub>2</sub> (o) [126]	0.405	2.96880	4.00	4.000	0.000	
	0.589	2.61137	---	-11.700		
	1.064	2.47795	---	-13.600		
	(e)	0.405	3.37038	-9.00	-9.000	0.000
	0.589	2.90881	---	-15.400		
	1.064	2.74047	---	-15.500		
YAG at 25°C [121]	0.4580	1.85177	11.90	11.720	0.182	0.33
	0.6330	1.83253	9.40	9.890	-0.494	0.35
	1.0600	1.81783	9.10	8.790	0.314	
Y <sub>2</sub> O <sub>3</sub> [114]	0.663	1.92163	8.30	8.310	0.010	
	1.064	1.90106	---	7.440		
	10.6	1.58072	---	8.280		
Zr:Y <sub>2</sub> O <sub>3</sub> at 25°C [127]	0.361	2.25362	16.00	15.729	0.271	0.24
	0.365	2.24989	15.30	15.418	-0.118	0.29
	0.405	2.21990	13.50	13.020	0.481	
	0.436	2.20303	11.40	11.747	-0.347	
	0.546	2.16698	8.75	9.214	-0.464	
	0.580	2.16012	8.25	8.763	-0.513	
	0.700	2.14366	7.50	7.729	-0.229	
	0.800	2.13521	7.20	7.233	-0.033	
	1.010	2.12442	6.55	6.660	-0.110	
	1.130	2.12033	6.50	6.475	0.025	
	1.190	2.11859	6.50	6.404	0.096	
	1.350	2.11457	6.50	6.261	0.239	
	1.390	2.11367	6.50	6.234	0.266	
	1.530	2.11070	6.50	6.155	0.345	
	1.690	2.10753	6.20	6.090	0.110	

### 3.4.3 Halide Crystals/Glasses

The halide crystals such as AgCl, BaF<sub>2</sub>, CaF<sub>2</sub>, CdF<sub>2</sub>, CsBr, CsI, KBr, KCl, KI, LiF, LiYF<sub>4</sub>, MgF<sub>2</sub>, NaCl, NaF, SrF<sub>2</sub>, and KRS-5 are useful in many optical and opto-electronic applications. The thermo-optic coefficients of these crystals were measured in different laboratories and some of those values were analyzed by Li [128] in his review paper. He used the following equation for analyzing  $dn/dT$

$$2n \frac{dn}{dT} = a(n^2 - 1) + b + \frac{c\lambda^4}{(\lambda^2 - d)^2} + \frac{e\lambda^4}{(\lambda^2 - f)^2}, \quad (3.57)$$

where,  $a$ ,  $b$ ,  $c$ ,  $d$ ,  $e$  and  $f$  are optical constants computed from the thermo-optic and refractive index values. This equation does not bear physical significance.

We have used the experimental values of thermo-optic coefficients from different sources for computation in the model of Eq [3.29]. The optical constant  $G$  is now chosen in such a way that there should be twice the calculated values (both electrons and optical phonons are contributing to  $dn/dT$ ). The electrons and ions are loosely bound in the halide/ ionic crystals. As a consequence, there is a variation of IR-absorption band with temperature. The fitted optical constants  $G$ ,  $H$ ,  $L$ ,  $E_{ig}$ , and  $E_{ip}$  are shown in Table 3.1. It is meaningless to predict the thermo-optic coefficients of these halide crystals for the whole transmission range without having a datum. Evidently, the ionic contribution is mainly affected in the near IR or IR region. For halide crystals, the values of thermo-optic coefficients are negative. This is due to the dominant contribution from the thermal expansion coefficient. The experimental values are compared as shown in Table 3.7. The refractive indices of BGZA(4) [4-mol % AlF<sub>3</sub> doped 31.68BaF<sub>2</sub>-3.84GdF<sub>3</sub>-60.48ZrF<sub>4</sub> mol %] glass were measured at 25, 50, 100, 150, 200, and 250°C from 0.40 to 5.5 μm by Mitachi and Miyashita [155]. They used the Pro'dhomme's model to explain the temperature dependence of the refractive-index dispersion. However, the explanation is not so appealing compared to the present one. There is no experimental confirmation of the calculated polarizability coefficient which they had calculated. Thermo-optic coefficients at 25°C are fitted in this model and

the optical constants are shown in Table 3.2. The calculated and the experimental values of thermo-optic coefficients are cited in Table 3.7.

The dispersion behaviors of  $2n(dn/dT)$  are shown in Figs. 3.33 to 3.44 for BaF<sub>2</sub>, CaF<sub>2</sub>, BGZA(4) and CdF<sub>2</sub>, CsBr and CsI, KBr, KCl, KI and LiYF<sub>4</sub>, LiF, NaCl, NaF, SrF<sub>2</sub>, and MgF<sub>2</sub> and KRS-5, crystals, respectively. The thermo-optic coefficients are mostly negative throughout the transmission region for these crystals. But there is a strong dispersion of  $dn/dT$  near the UV and the visible region of the spectrum for these halide crystals. As we have analyzed the LiYF<sub>4</sub> crystal, there is no significant contribution from the lattice/ionic part. This may be due to the strong yttrium-fluoride bonding. In the case of MgF<sub>2</sub>, the thermo-optic coefficients are positive for both ordinary and extraordinary polarizations. This is due to the smaller thermal expansion coefficient in this crystal. On the other hand, there are large negative values of  $dn/dT$  in CsBr, CsI and KRS5 crystals, due to the larger values of the thermal expansion coefficients. The dispersion characteristics are analyzed in this model satisfactorily. Table 3.7 and the figures speak for themselves to the validity of this sound physical model.

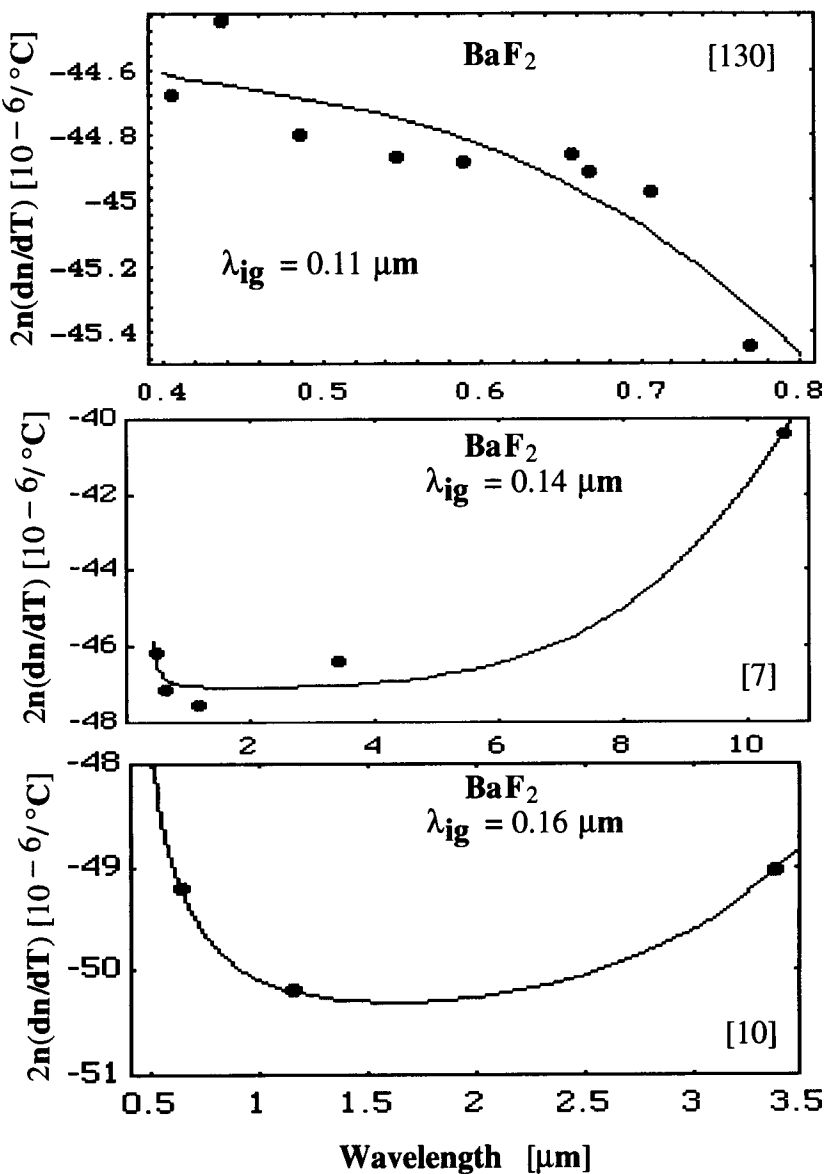


Figure 3.33:  $2n(dn/dT)$  versus wavelength for  $\text{BaF}_2$  crystal: Curves are the computed values; solid circles are the experimental data [130], Feldman *et al.* [7] and Lipson *et al.* [10].

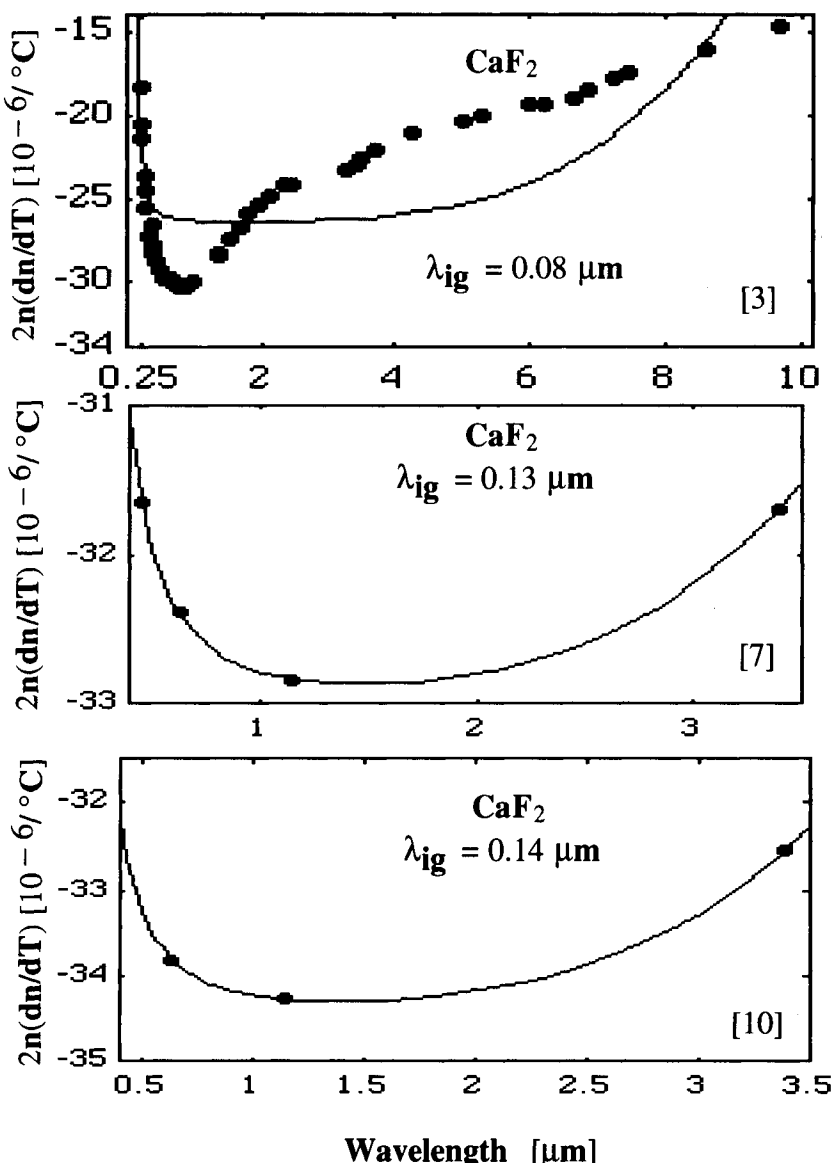


Figure 3.34:  $2n(dn/dT)$  versus wavelength for  $\text{CaF}_2$  crystal: Curves are the computed values; solid circles are the experimental data Malitson [3], the top figure; Feldman *et al.* [7], the middle figure; and Lipson *et al.* [10], the bottom figure.

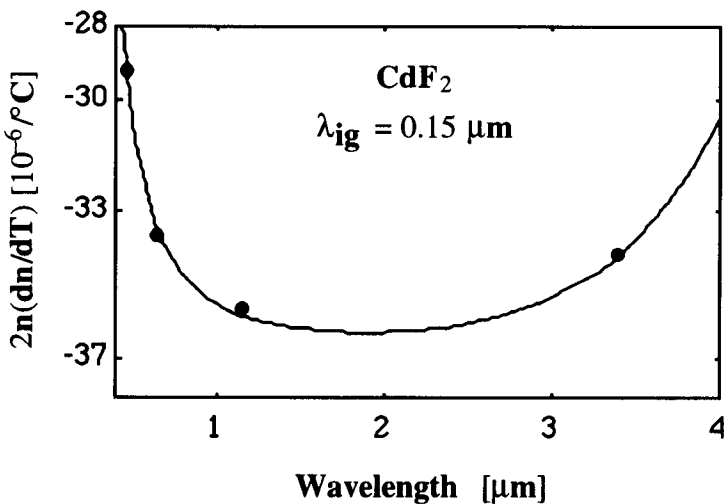
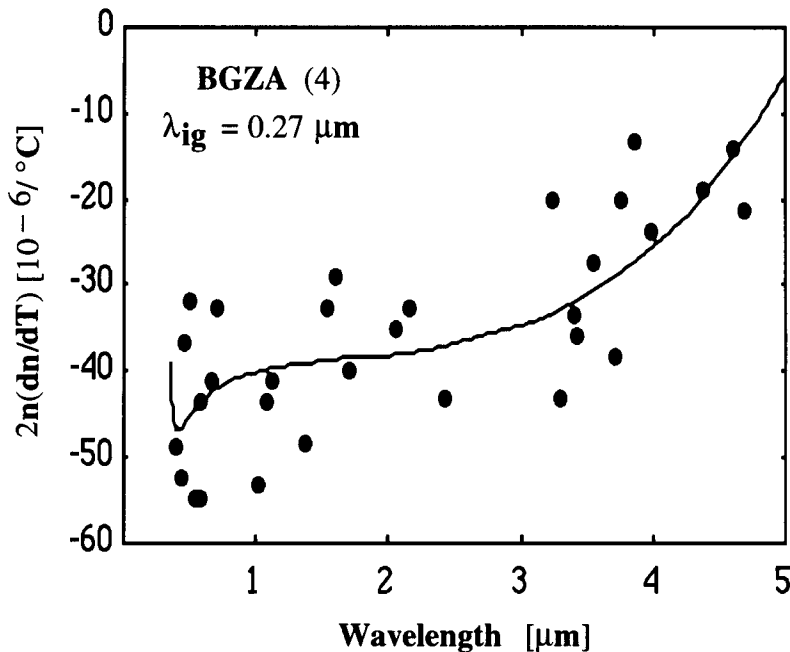


Figure 3.35:  $2n(dn/dT)$  versus wavelength for BGZA(4) fluoride glass and CdF<sub>2</sub> crystal: Curves are the computed values; solid circles are the experimental data [155] for BGZA(4), and [7] for CdF<sub>2</sub> crystal.

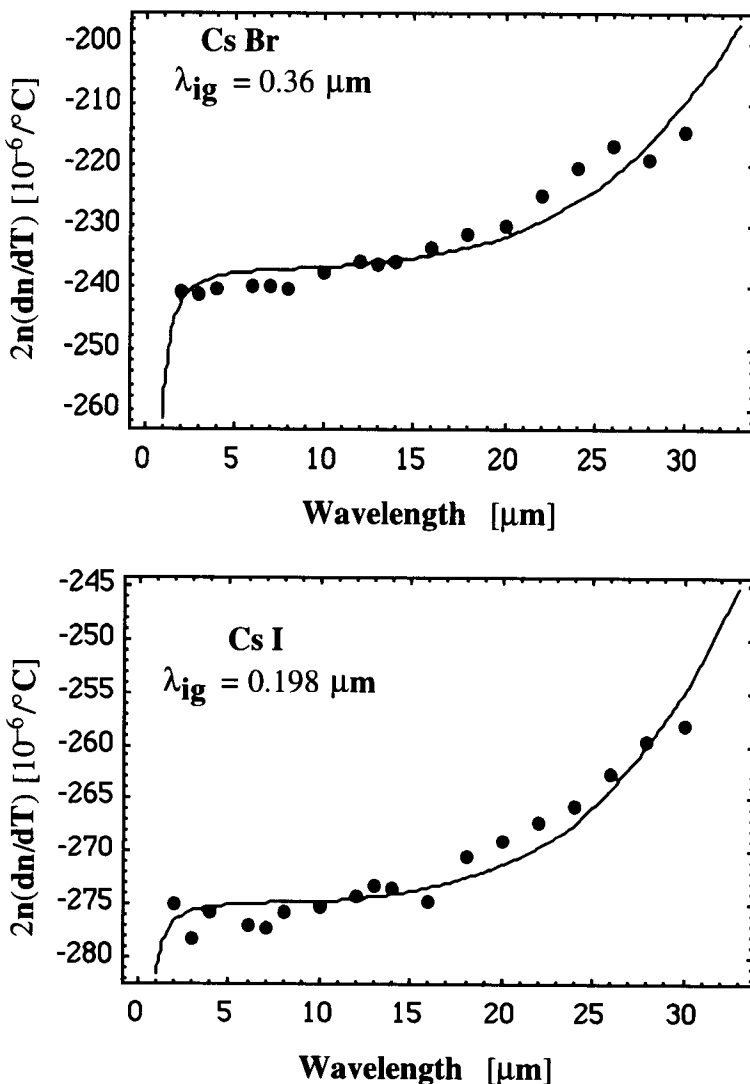


Figure 3.36:  $2n(dn/dT)$  versus wavelength for  $\text{CsBr}$  and  $\text{CsI}$  crystals: Curves are the computed values; solid circles are the experimental data [131].

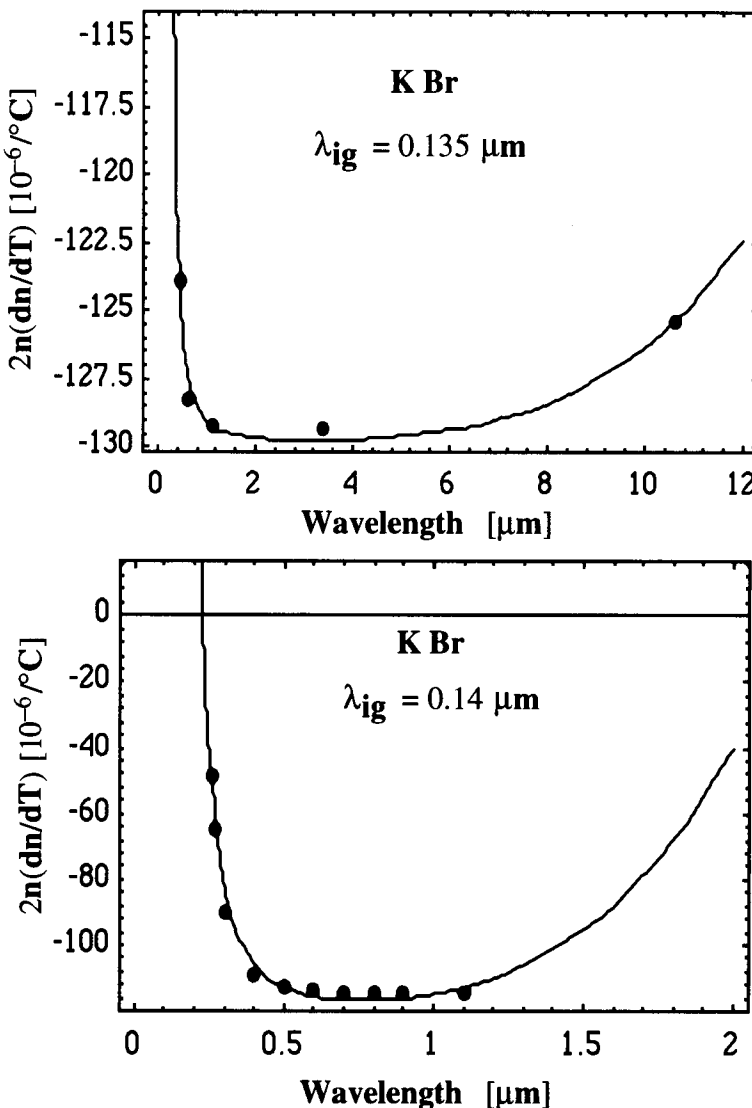


Figure 3.37:  $2n(dn/dT)$  versus wavelength for KBr crystal: Curves are the computed values; solid circles are the experimental data [7], the top figure; [128], the bottom figure.

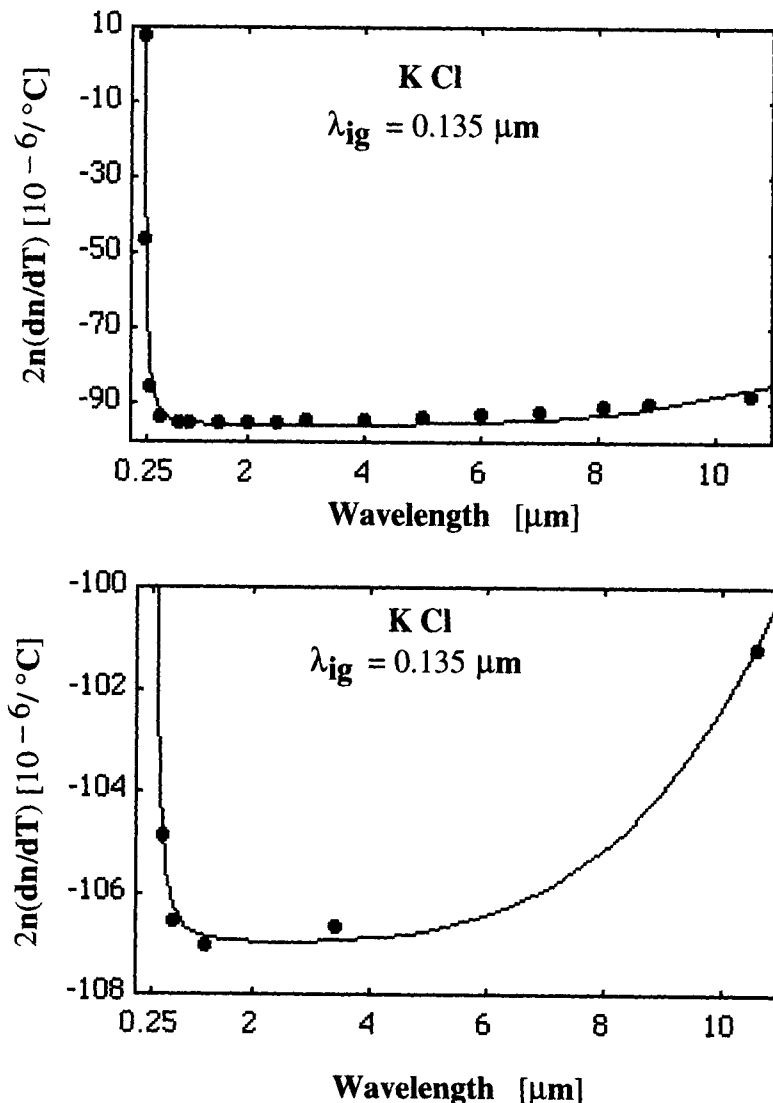


Figure 3.38:  $2n(dn/dT)$  versus wavelength for KCl crystal: Curves are the computed values; solid circles are the experimental data [128], the top figure; [7], the bottom figure.

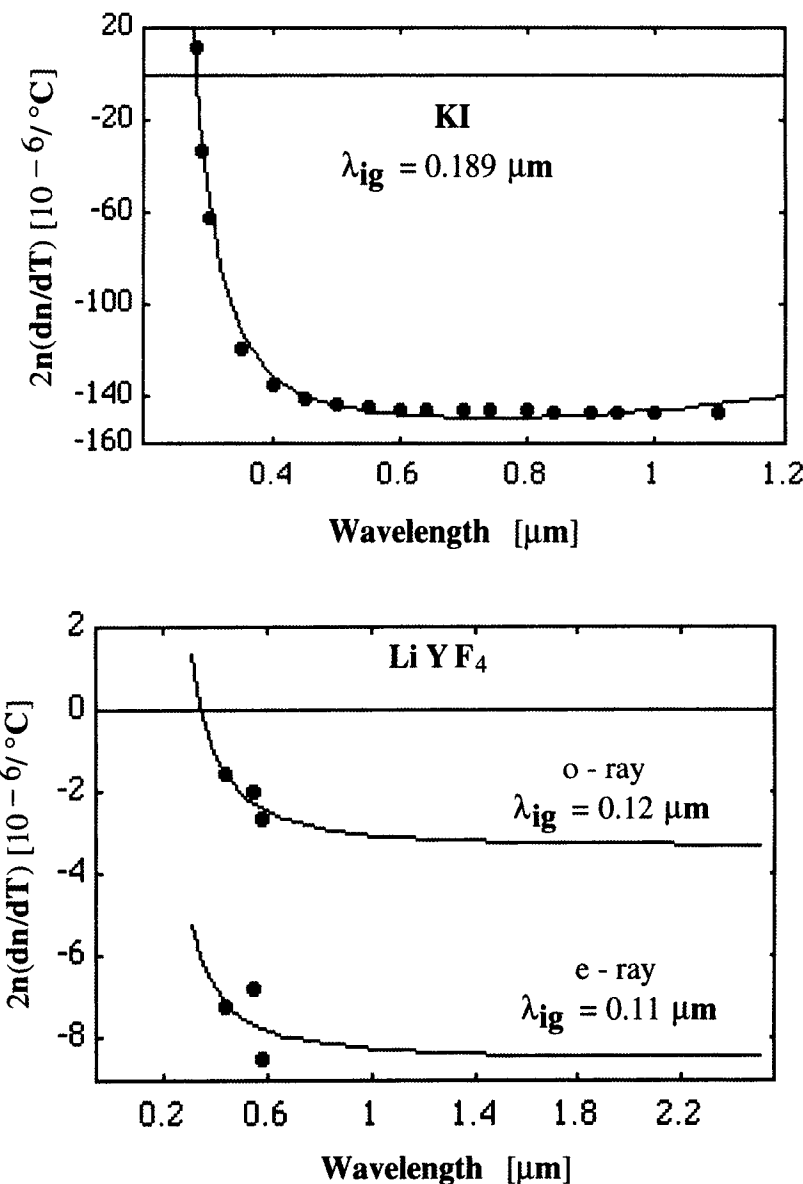


Figure 3.39:  $2n(dn/dT)$  versus wavelength for KI and LiYF<sub>4</sub> crystals: Curves are the computed values; solid circles are the experimental data [128], the top figure; [132], the bottom figure.

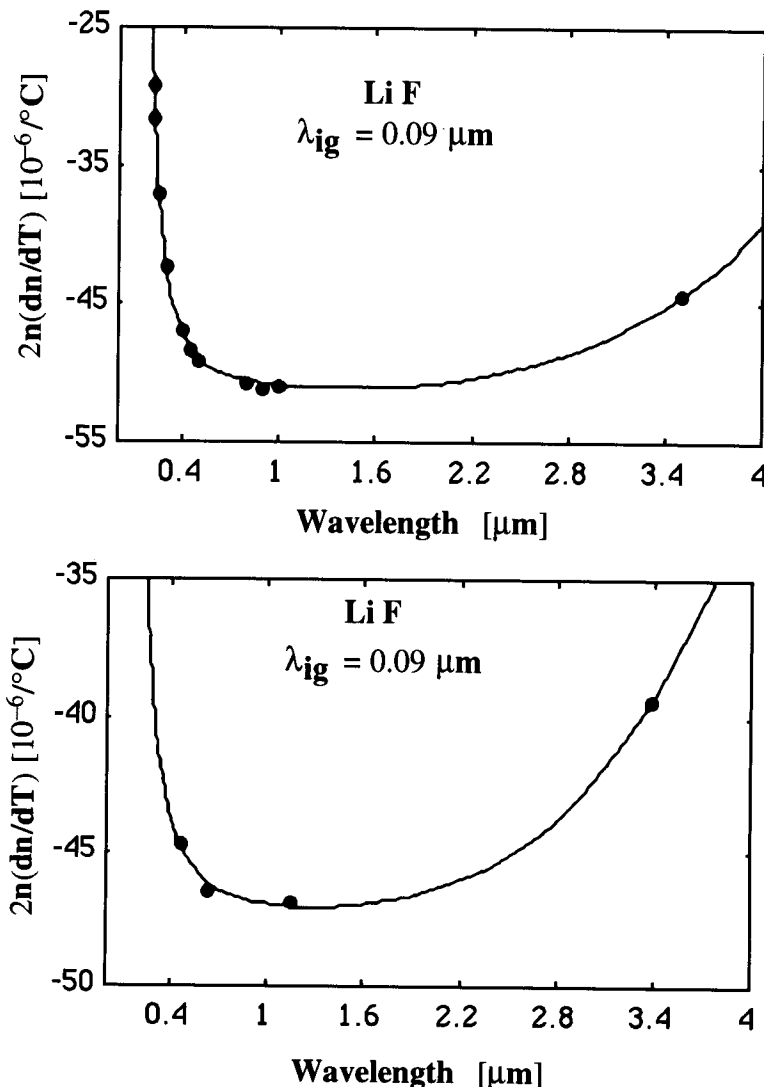


Figure 3.40:  $2n(dn/dT)$  versus wavelength for LiF crystal: Curves are the computed values; solid circles are the experimental data [128], the top figure; [7], the bottom figure.

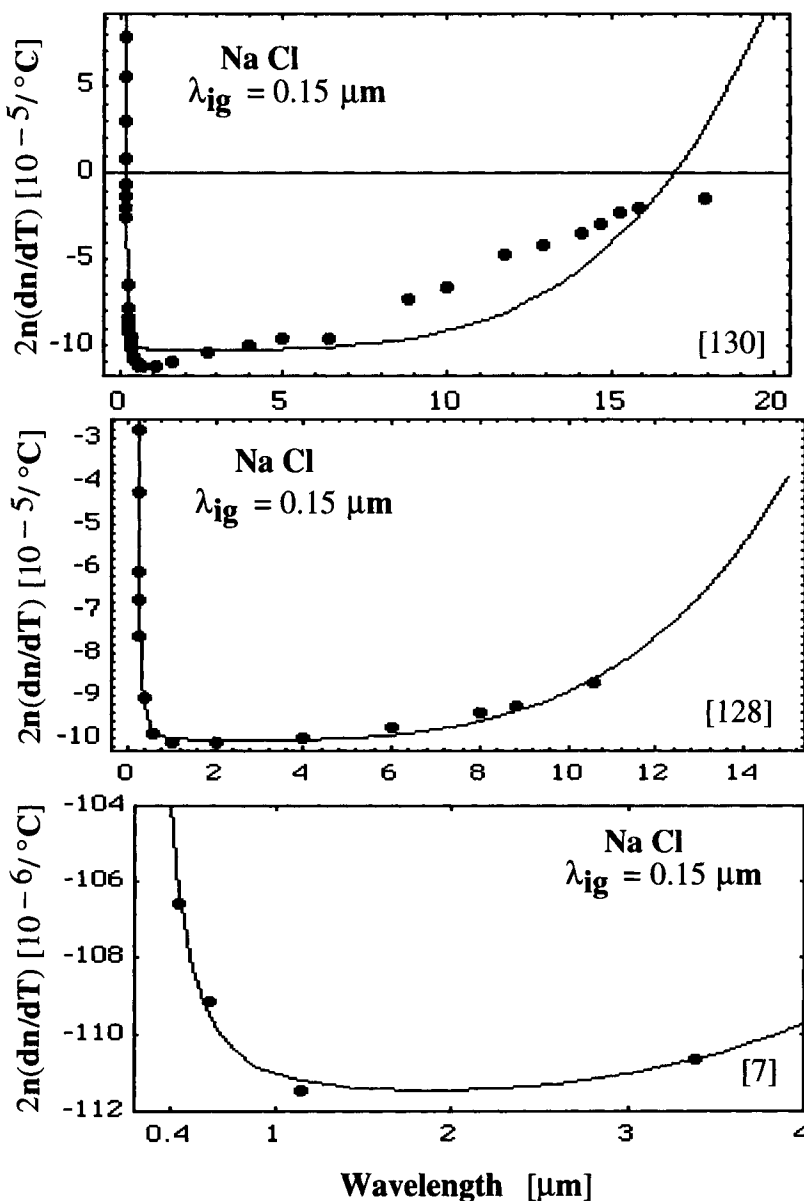


Figure 3.41:  $2n(dn/dT)$  versus wavelength for NaCl crystal: Curves are the computed values; solid circles are the experimental data [130], the top figure; [128], the middle figure; and [7], the bottom figure.

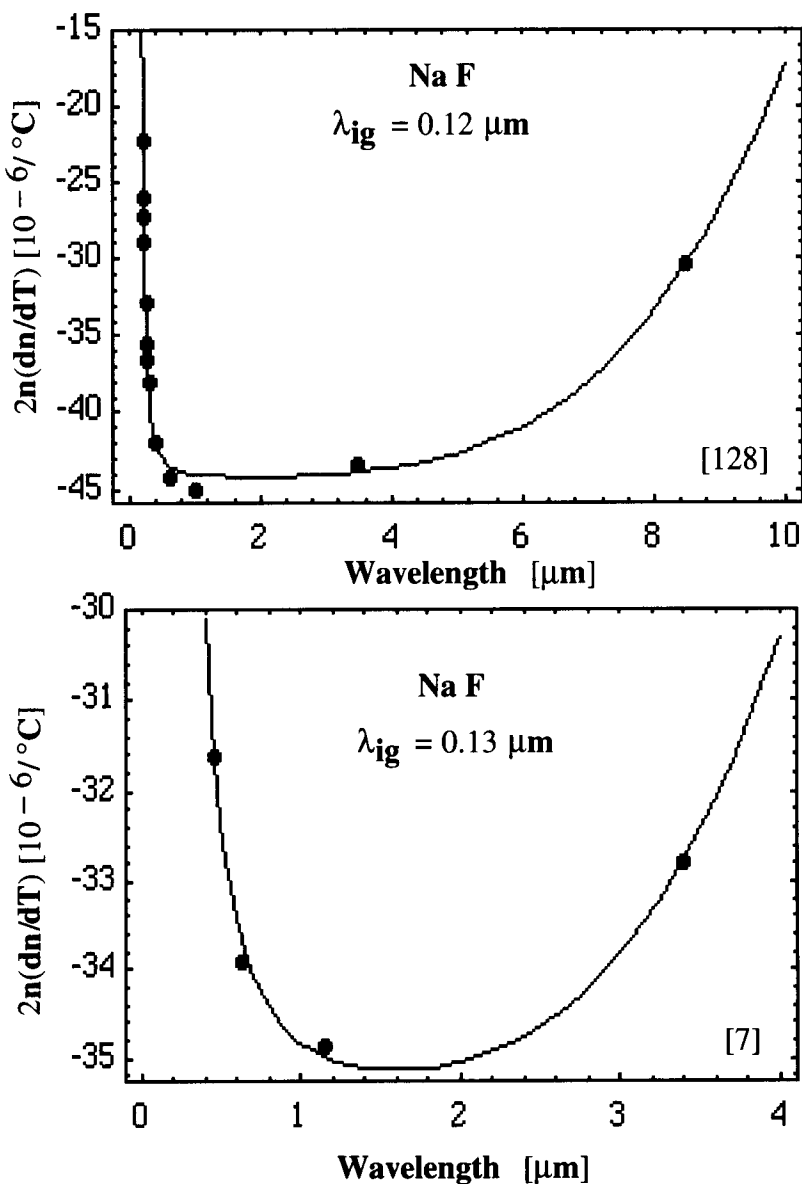


Figure 3.42:  $2n(dn/dT)$  versus wavelength for NaF crystal: Curves are the computed values; solid circles are the experimental data [128], the top figure; and [7], the bottom figure.

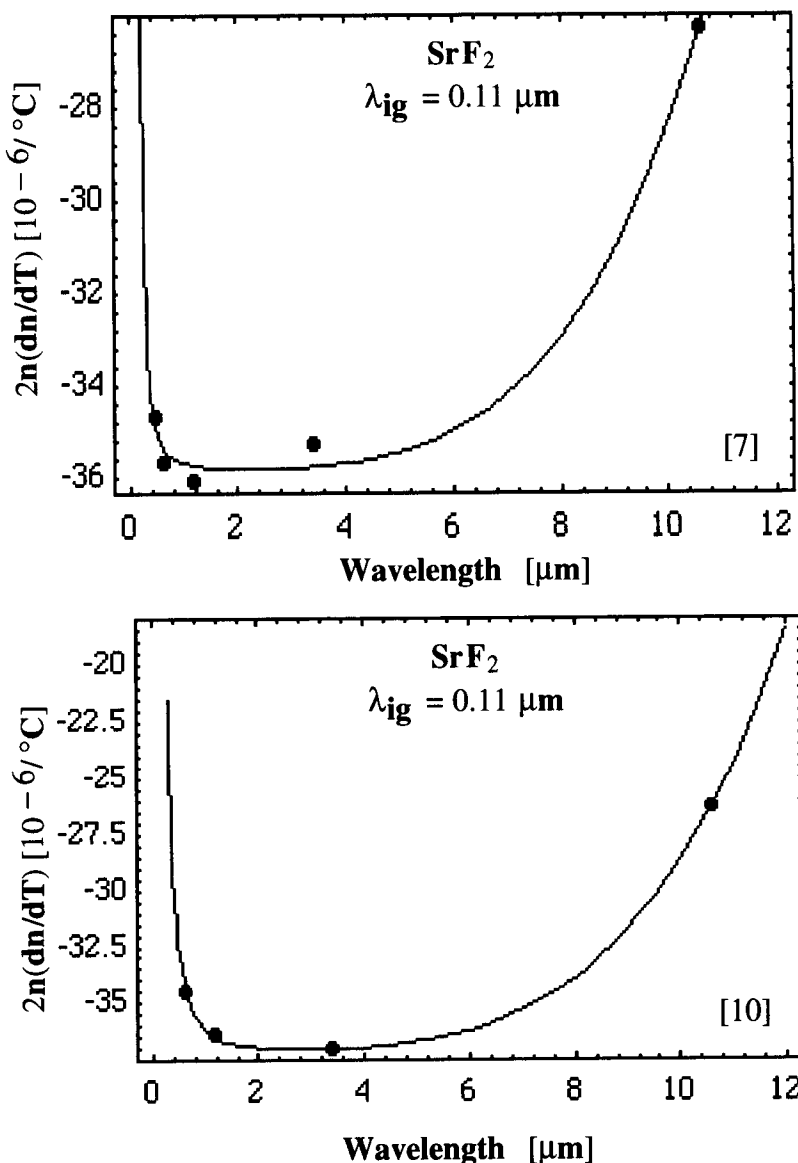


Figure 3.43:  $2n(dn/dT)$  versus wavelength for  $\text{SrF}_2$  crystal: Curves are the computed values; solid circles are the experimental data [7], the top figure; and [10], the bottom figure.

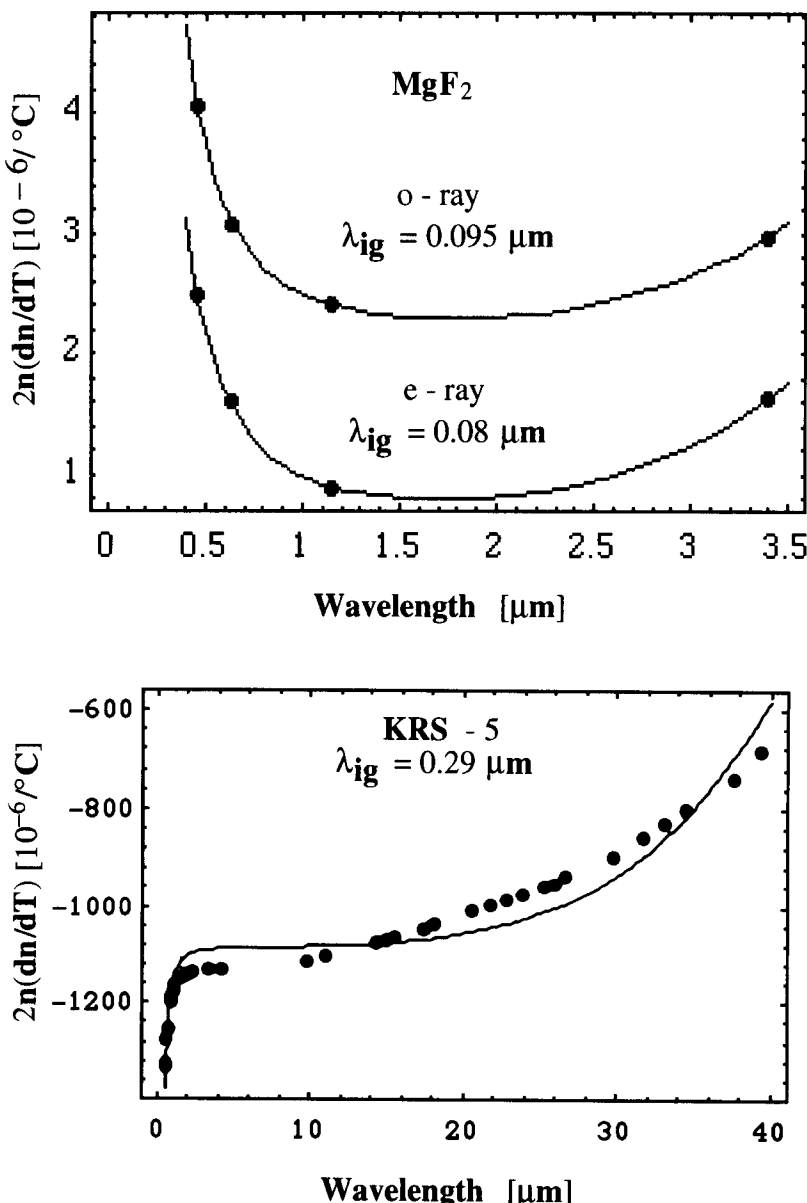


Figure 3.44:  $2n(dn/dT)$  versus wavelength for MgF<sub>2</sub> and KRS-5 crystals: Curves are the computed values; solid circles are the experimental data [7], the top figure; and [2], the bottom figure.

**Table 3.7: Refractive Index and Thermo-Optic Coefficients of Halide Crystals and Glasses**

Crystal [Ref.]	Wavelength [μm]	Refractive index	$\frac{dn}{dT} \text{ [ } (10^{-6})/\text{K}]$	Differ- ence	Av. Dev.	RMS [10 <sup>-6</sup> ]
Temp.			Expt values (This work)	Computed		
AgCl	0.633	2.05682	-61.00	-61.550	0.550	
	1.064	2.01987	---	-58.760		
	1.55	2.00988	---	-57.980		
BaF <sub>2</sub> [130]	0.4046563	1.48440	-15.10	-15.030	-0.021	0.036
at 25°C	0.4358342	1.48175	-15.00	-15.070	0.065	
(dn/dT)	0.4861327	1.47855	-15.20	-15.110	-0.038	
	0.5460740	1.47586	-15.20	-15.160	-0.039	
	0.5892620	1.47442	-15.20	-15.200	-0.023	
	0.6562793	1.47273	-15.20	-15.260	0.032	
	0.6678149	1.47248	-15.20	-15.270	0.025	
	0.7065188	1.47175	-15.30	-15.320	0.041	
	0.7678580	1.47080	-15.40	-15.410	-0.041	
BaF <sub>2</sub> [10]	0.6328	1.47326	-16.70	-16.700	0.000	0.000
	1.15	1.46765	-17.10	-17.100	0.000	
	3.39	1.45955	-16.80	-16.800	0.000	
BaF <sub>2</sub> [7]	0.4579	1.48021	-15.60	-15.670	0.065	0.108
at 20°C	0.6328	1.47326	-16.00	-15.900	-0.096	
	1.15	1.46765	-16.20	-16.030	-0.172	
	3.39	1.45955	-15.90	-16.110	0.206	
	10.6	1.39253	-14.50	-14.500	-0.002	
BGZA4 [155]	0.404656	1.52756	-16.00	-15.332	-0.667	2.12
	0.435835	1.52459	-17.20	-15.296	-1.904	2.56
	0.447100	1.52357	-12.00	-15.232	3.232	
at 25°C	0.501500	1.51994	-10.40	-14.836	4.436	
	0.546074	1.51787	-18.00	-14.528	-3.472	
	0.576959	1.51663	-18.00	-14.345	-3.655	
	0.587561	1.51622	-14.40	-14.287	-0.113	
	0.667815	1.51391	-13.60	-13.929	0.329	
	0.706519	1.51308	-10.80	-13.796	2.996	
	1.01398	1.50904	-17.60	-13.218	-4.382	
	1.08297	1.50844	-14.40	-13.149	-1.251	
	1.12866	1.50809	-13.60	-13.109	-0.491	
	1.36220	1.50651	-16.00	-12.953	-3.047	
	1.52952	1.50555	-10.80	-12.865	2.065	
	1.60660	1.50486	-9.60	-12.830	3.230	
	1.6932	1.50456	-13.20	-12.785	-0.415	

**Table 3.7: (Continued)**

Crystal [Ref.]	Wavelength [μm]	Refractive index	$dn/dT$ [ $(10^{-6})/\text{K}$ ]		Differ- ence	Av. Dev.	RMS Dev. [ $10^{-6}$ ]
			Expt values	Computed (This work)			
CaF <sub>2</sub> [3] at 19°C	2.0581	1.50247	-11.60	-12.581	0.981		
	2.1526	1.50187	-10.80	-12.517	1.717		
	2.4374	1.50022	-14.40	-12.277	-2.123		
	3.2389	1.49384	-6.80	-11.034	4.234		
	3.3036	1.49347	-14.40	-10.880	-3.520		
	3.4115	1.49240	-11.20	-10.606	-0.594		
	3.4199	1.49211	-12.00	-10.585	-1.415		
	3.5524	1.49081	-9.20	-10.206	1.006		
	3.7077	1.48927	-12.80	-9.699	-3.101		
	3.7601	1.48883	-6.80	-9.512	2.712		
	3.8480	1.48813	-4.40	-9.178	4.778		
	3.9788	1.48632	-8.00	-8.638	0.638		
	4.3769	1.48174	-6.40	-6.591	0.191		
	4.5960	1.47902	-4.80	-5.172	0.372		
	4.6885	1.47783	-7.20	-4.501	-2.699		
	0.228803	1.47635	-6.20	-7.630	1.427	1.038	1.158
	0.24827	1.46793	-7.00	-7.940	0.940		
	0.2537	1.42798	-7.50	-8.220	0.723		
	0.2652	1.46233	-8.10	-8.140	0.042		
	0.28035	1.45828	-8.40	-8.280	-0.116		
	0.296728	1.45467	-8.80	-8.410	-0.391		
	0.394148	1.44852	-9.20	-8.780	-0.422		
	0.34662	1.44694	-9.40	-8.670	-0.733		
	0.365015	1.44490	-9.60	-8.730	-0.867		
	0.4046563	1.44151	-9.80	-8.840	-0.959		
	0.4358342	1.43949	-10.00	-8.900	-1.096		
	0.4861327	1.43703	-10.20	-8.980	-1.221		
	0.546074	1.43494	-10.40	-9.040	-1.359		
	0.589262	1.43381	-10.40	-9.070	-1.326		
	0.643847	1.43268	-10.40	-9.110	-1.294		
	0.6562793	1.43246	-10.40	-9.110	-1.288		
	0.6678149	1.43226	-10.50	-9.120	-1.382		
	0.7065188	1.43167	-10.50	-9.130	-1.366		
	0.767858	1.43088	-10.60	-9.150	-1.445		
	0.85212	1.43002	-10.60	-9.180	-1.424		
	0.8944	1.42966	-10.60	-9.190	-1.415		
	1.01398	1.42879	-10.50	-9.200	-1.296		
	1.3622	1.42691	-10.00	-9.240	-0.763		

**Table 3.7: (Continued)**

Crystal [Ref.]	Wavelength [ $\mu\text{m}$ ]	Refractive index	$dn/dT$ [ $(10^{-6})/\text{K}$ ] Expt Computed values (This work)	Differ- ence	Av. Dev.	RMS Dev. [ $10^{-6}$ ]
	1.39506	1.42675	-9.90 -9.240	-0.661		
	1.52952	1.42612	-9.60 -9.250	-0.354		
	1.7012	1.42531	-9.40 -9.250	-0.147		
	1.81307	1.42478	-9.10 -9.260	0.157		
	1.97009	1.42401	-8.90 -9.260	0.362		
	2.1526	1.42306	-8.70 -9.270	0.566		
	2.32542	1.42212	-8.50 -9.270	0.768		
	2.4374	1.42147	-8.50 -9.270	0.769		
	3.3026	1.41561	-8.20 -9.260	1.056		
	3.3036	1.49347	-14.40 -10.880	-3.520		
	3.422	1.41467	-8.10 -9.250	1.151		
	3.507	1.41398	-8.00 -9.250	1.246		
	3.7067	1.41229	-7.80 -9.230	1.433		
	4.258 0	1.40713	-7.50 -9.170	1.674		
	5.01882	1.39873	-7.30 -9.020	1.723		
	5.3034	1.39520	-7.20 -8.940	1.740		
	6.014	1.38539	-7.00 -8.650	1.646		
	6.238	1.38200	-7.00 -8.520	1.524		
	6.63306	1.37565	-6.90 -8.270	1.367		
	6.8559	1.37186	-6.70 -8.100	1.395		
	7.268	1.36443	-6.50 -7.720	1.223		
	7.4644	1.36070	-6.40 -7.520	1.117		
	8.602	1.33500	-6.00 -5.890	-0.108		
	9.724	1.30756	-5.60 -3.310	-2.291		
CaF <sub>2</sub> [10]	0.6328	1.43288	-11.80 -11.800	0.000	0.00	0.00
	1.15	1.42798	-12.00 -12.000	0.000		
	3.39	1.41493	-11.50 -11.500	0.000		
CaF <sub>2</sub> [7]	0.4579	1.43830	-11.00 -11.000	-0.003	0.003	0.004
	0.6328	1.43288	-11.30 -11.310	0.007		
at 20°C	1.15	1.42798	-11.50 -11.500	-0.004		
	3.39	1.41493	-11.20 -11.200	0.000		
CdF <sub>2</sub> [7]	0.4579	1.58500	-9.20 -9.240	0.037	0.25	0.41
	0.6328	1.57400	-10.70 -10.610	-0.095		
at 20°C	1.15	1.55000	-11.50 -11.570	0.067		
	3.39	1.54000	-11.10 -11.910	0.808		
CsBr [131]	2.0	1.67041	-72.04 -72.617	0.577	0.68	0.81
	3.0	1.66891	-72.27 -71.701	-0.569		
	4.0	1.66806	-72.05 -71.399	-0.646		

**Table 3.7: (Continued)**

Crystal [Ref.]	Wavelength [μm]	Refractive index	<i>dn/dT</i> [(10 <sup>-6</sup> )/K] Expt values (This work)	Computed	Differ- ence	Av. Dev.	RMS Dev. [10 <sup>-6</sup> ]
at 27°C	6.0	1.66669	-71.95	-71.208	-0.742		
	7.0	1.66575	-72.04	-71.186	-0.854		
	8.0	1.66479	-72.23	-71.178	-1.052		
	10.0	1.66253	-71.50	-71.180	-0.320		
	12.0	1.65977	-71.05	-71.173	0.128		
	13.0	1.65822	-71.23	-71.157	-0.073		
	14.0	1.65652	-71.18	-71.128	-0.052		
	16.0	1.65276	-70.59	-71.017	0.427		
	18.0	1.64844	-70.22	-70.809	0.589		
	20.0	1.64357	-70.00	-70.468	0.468		
	22.0	1.63812	-68.68	-69.955	1.275		
	26.0	1.62538	-66.68	-68.224	1.544		
	28.0	1.61768	-67.77	-66.911	-0.859		
	30.0	1.60965	-66.63	-65.189	-1.441		
CsI [131]	2.0	1.74585	-78.73	-79.215	0.485	0.42	0.49
	3.0	1.74385	-79.82	-79.035	-0.785		
	4.0	1.74297	-79.09	-78.979	-0.111		
	at 27°C	6.0	1.74174	-79.55	-78.960	-0.590	
	7.0	1.74116	-79.63	-78.965	-0.665		
	8.0	1.74068	-79.23	-78.966	-0.264		
	10.0	1.73920	-79.14	-78.983	-0.157		
KBr [128]	12.0	1.73746	-78.95	-78.984	0.034		
	13.0	1.73659	-78.64	-78.969	0.329		
	14.0	1.73552	-78.77	-78.949	0.179		
	16.0	1.73324	-79.27	-78.867	-0.403		
	18.0	1.73059	-78.13	-78.716	0.586		
	20.0	1.72764	-77.82	-78.471	0.651		
	22.0	1.72440	-77.45	-78.102	0.652		
	24.0	1.72079	-77.18	-77.583	0.403		
	26.0	1.71668	-76.50	-76.884	0.384		
	28.0	1.71247	-75.82	-75.946	0.126		
	30.0	1.70775	-75.59	-74.745	-0.845		
	0.26	1.70575	-14.20	-15.860	1.665	0.83	1.03
	0.27	1.68725	-19.20	-18.920	-0.278		
	0.30	1.64825	-27.30	-25.150	-2.154		
	0.40	1.59117	-34.40	-33.300	-1.099		
	0.50	1.56964	-35.90	-35.910	0.014		
	0.60	1.55894	-36.50	-37.030	0.530		

**Table 3.7: (Continued)**

Crystal [Ref.]	Wavelength [ $\mu\text{m}$ ]	Refractive index	$\frac{dn}{dT} [ (10^{-6})/\text{K}]$	Differ- ence	Avg. Dev.	RMS Dev. [ $10^{-6}$ ]
			Expt values (This work)	Computed		
	0.70	1.55278	-36.80	-37.520	0.720	
	0.80	1.54888	-36.90	-37.650	0.753	
	0.90	1.54626	-37.00	-37.520	0.518	
	1.1	1.54303	-37.10	-36.520	-0.583	
KBr	0.4579	1.57700	-39.30	-39.420	0.121	0.105
[7]	0.6328	1.55700	-41.20	-40.940	-0.262	
at 20°C	1.15	1.54200	-41.90	-41.910	0.008	
	3.39	1.53600	-42.10	-42.240	0.136	
	10.6	1.52500	-41.10	-41.100	-0.001	
KCl	0.21	1.67539	2.30	-0.120	2.423	0.81
[128]	0.23	1.62226	-14.20	-11.510	-2.693	
at 20°C	0.30	1.54558	-27.50	-24.860	-2.635	
	0.50	1.49679	-31.30	-30.650	-0.653	
	0.80	1.48291	-31.90	-31.840	-0.060	
	1.0	1.47983	-32.00	-32.070	0.074	
	1.5	1.47668	-32.10	-32.290	0.194	
	2.0	1.47536	-32.10	-32.370	0.271	
	2.5	1.47449	-32.10	-32.410	0.307	
	3.0	1.47374	-32.00	-32.420	0.425	
	4.0	1.47223	-31.90	-32.420	0.524	
	5.0	1.47048	-31.80	-32.370	0.570	
	6.0	1.46842	-31.50	-32.240	0.741	
	7.0	1.46600	-31.30	-32.000	0.702	
	8.1	1.46290	-31.00	-31.560	0.562	
	8.9	1.46036	-30.80	-31.090	0.290	
	10.6	1.45409	-30.10	-29.510	-0.590	
KCl	0.4579	1.50200	-34.90	-34.950	0.050	0.06
[7]	0.6328	1.48800	-35.80	-35.710	-0.093	
at 20°C	1.15	1.47800	-36.20	-36.150	-0.054	
	3.39	1.47300	-36.20	-36.300	0.098	
	10.6	1.45400	-34.80	-34.800	-0.001	
KI	0.28	1.88949	2.90	-0.009	2.909	0.95
[128]	0.29	1.85931	-9.00	-8.476	-0.524	
	0.30	1.83484	-17.00	-14.852	-2.148	
at	0.35	1.75948	-33.90	-31.336	-2.564	
20°C	0.40	1.72093	-39.10	-37.731	-1.369	
	0.45	1.69789	-41.30	-40.846	-0.454	
	0.50	1.68280	-42.50	-42.579	0.079	

Table 3.7: (Continued)

Crystal [Ref.]	Wavelength [ μm]	Refractive index	<i>dn/dT</i> [(10 <sup>-6</sup> )/K] Expt Computed values (This work)	Differ- ence	Av. Dev.	RMS Dev. [10 <sup>-6</sup> ]
LiF [128] at 20°C	0.55	1.67229	-43.10 -43.623	0.523		
	0.60	1.66464	-43.60 -44.280	0.680		
	0.64	1.65991	-43.80 -44.627	0.827		
	0.70	1.65442	-44.10 -44.945	0.845		
	0.74	1.65154	-44.20 -45.056	0.856		
	0.80	1.64805	-44.30 -45.102	0.802		
	0.84	1.64615	-44.40 -45.063	0.663		
	0.90	1.64379	-44.50 -44.911	0.411		
	0.94	1.64248	-44.50 -44.749	0.249		
	1.00	1.64080	-44.60 -44.416	-0.184		
	1.10	1.63861	-44.70 -43.613	-1.087		
	0.21	1.43368	-10.20 -9.980	-0.220	0.11	0.14
	0.22	1.42912	-11.10 -11.080	-0.020		
	0.25	1.41892	-13.10 -13.320	0.217		
LiF [7] at 20°C	0.30	1.40871	-15.00 -15.270	0.272		
	0.40	1.39894	-16.80 -16.890	0.090		
	0.45	1.39633	-17.30 -17.280	-0.021		
	0.50	1.39444	-17.60 -17.550	-0.054		
	0.80	1.38898	-18.30 -18.200	-0.100		
	0.90	1.38798	-18.40 -18.280	-0.116		
	1.0	1.38711	-18.40 -18.340	-0.057		
	3.5	1.35853	-16.30 -16.300	0.001		
	0.4579	1.39600	-16.00 -16.050	0.046	0.056	0.07
	0.6328	1.39130	-16.70 -16.590	-0.111		
LiYF <sub>4</sub> (o) [132] at 20°C	1.15	1.38593	-16.90 -16.970	0.065		
	3.39	1.36038	-14.50 -14.500	-0.001		
	0.4358	1.46136	-0.54 -0.524	-0.016	0.07	0.08
LiYF <sub>4</sub> (e) [7] at 20°C	0.5461	1.45599	-0.67 -0.776	0.106		
	0.5780	1.45499	-0.91 -0.820	-0.090		
	0.4358	1.48389	-2.44 -2.397	-0.043	0.2	0.2
MgF <sub>2</sub> (o) [7] at 20°C	0.5461	1.47826	-2.30 -2.585	0.285		
	0.5780	1.47705	-2.86 -2.618	-0.242		
	0.4579	1.38117	1.47 1.470	0.001	0.001	0.002
MgF <sub>2</sub> {e} [7]	0.6328	1.37697	1.12 1.120	-0.003		
	1.15	1.37269	0.88 0.880	0.002		
	3.39	1.35604	1.10 1.100	0.000		
MgF <sub>2</sub> {e}	0.4579	1.39313	0.89 0.820	0.068	0.07	0.07
	0.6328	1.38875	0.58 0.490	0.087		

**Table 3.7: (Continued)**

Crystal [Ref.]	Wavelength [ $\mu\text{m}$ ]	Refractive index	$dn/dT [ (10^{-6})/\text{K}]$		Differ- ence	Av. Dev.	RMS Dev. [ $10^{-6}$ ]
			Expt values	Computed (This work)			
at 20°C	1.15	1.38425	0.32	0.260	0.064		
	3.39	1.36645	0.60	0.530	0.073		
NaCl	0.202	1.78271	31.34	29.624	1.716	3.20	4.5
[130]	0.206	1.76509	22.90	21.162	1.738		
	0.210	1.74948	15.70	14.286	1.414		
at 60°C	0.214	1.73554	8.61	8.623	-0.013		
	0.219	1.72010	2.35	2.848	-0.498		
	0.224	1.70651	-1.87	-1.823	-0.047		
	0.226	1.70152	-3.82	-3.445	-0.375		
	0.229	1.69446	-5.98	-5.654	-0.326		
	0.231	1.69001	-7.57	-6.995	-0.575		
	0.257	1.64632	-19.79	-18.243	-1.547		
	0.274	1.62720	-23.96	-22.129	-1.831		
	0.288	1.61491	-26.02	-24.316	-1.704		
	0.298	1.60754	-27.27	-25.515	-1.755		
	0.313	1.59821	-28.62	-26.918	-1.702		
	0.325	1.59191	-29.87	-27.790	-2.080		
	0.340	1.58620	-30.68	-28.639	-2.041		
	0.361	1.57748	-31.94	-29.575	-2.365		
	0.441	1.55892	-34.25	-31.447	-2.803		
	0.467	1.55509	-34.54	-31.775	-2.765		
	0.480	1.55343	-34.68	-31.911	-2.769		
	0.508	1.55032	-35.17	-32.157	-3.013		
	0.589	1.54387	-36.22	-32.626	-3.594		
	0.643	1.54093	-36.36	-32.822	-3.538		
	0.656	1.54034	-36.52	-32.860	-3.660		
	1.10	1.53106	-36.42	-33.395	-3.025		
	1.60	1.52810	-35.57	-33.533	-2.037		
	2.70	1.52518	-34.27	-33.620	-0.650		
	3.96	1.52215	-32.86	-33.626	0.766		
	4.96	1.51923	-31.72	-33.559	1.839		
	6.40	1.51398	-31.49	-33.273	1.783		
	8.85	1.50194	-24.05	-31.821	7.771		
	10.02	1.49472	-22.00	-30.425	8.425		
	11.79	1.48186	-16.00	-26.972	10.972		
	12.97	1.47192	-14.00	-23.460	9.460		
	14.14	1.46092	-12.00	-18.724	6.724		
	14.73	1.45491	-10.00	-15.766	5.766		

**Table 3.7: (Continued)**

Crystal [Ref.]	Wavelength [ $\mu\text{m}$ ]	Refractive index	$\frac{dn}{dT} [10^{-6}/\text{K}]$	Differ- ence	Av. Dev.	RMS Dev. [ $10^{-6}$ ]
			Expt values (This work)	Computed		
NaCl [7] at 20°C	15.32	1.44859	-8.00	-12.368	4.368	
	15.91	1.44194	-7.00	-8.482	1.482	
	17.90	1.41654	-5.00	9.297	-14.297	
	0.4579	1.55800	-34.20	-34.15	-0.052	0.07
	0.6328	1.54200	-35.40	-35.54	0.136	0.08
	1.15	1.53100	-36.40	-36.31	-0.085	
	3.39	1.52400	-36.30	-36.30	0.001	
	0.21	1.74676	21.60	21.19	0.405	0.29
	0.22	1.71499	7.20	7.35	-0.154	
	0.24	1.67116	-8.40	-8.09	-0.309	
NaCl [128] at 20°C	0.25	1.65537	-12.90	-12.66	-0.243	
	0.27	1.63124	-18.80	-18.66	-0.135	
	0.28	1.62184	-20.80	-20.70	-0.097	
	0.30	1.60665	-23.70	-23.65	-0.053	
	0.40	1.56746	-29.00	-29.45	0.446	
	0.60	1.54343	-32.10	-31.82	-0.276	
	1.0	1.53200	-33.00	-32.67	-0.332	
	2.0	1.52654	-33.20	-32.98	-0.225	
	4.0	1.52174	-33.00	-33.03	0.034	
	6.0	1.51534	-32.30	-32.79	0.486	
	8.0	1.50643	-31.30	-31.90	0.600	
	8.8	1.50210	-30.80	-31.25	0.448	
	10.6	1.49065	-29.30	-28.84	-0.456	
NaF [128] at 20°C	0.210	1.37516	-8.10	-7.745	-0.355	0.19
	0.220	1.36849	-9.50	-9.432	-0.068	
	0.224	1.36619	-10.00	-9.976	-0.024	
	0.230	1.36306	-10.60	-10.682	0.082	
	0.250	1.35477	-12.10	-12.376	0.276	
	0.270	1.34879	-13.20	-13.441	0.241	
	0.280	1.34639	-13.60	-13.831	0.231	
	0.300	1.34246	-14.20	-14.427	0.227	
	0.400	1.33189	-15.80	-15.757	-0.043	
	0.600	1.32500	-16.70	-16.405	-0.295	
	1.0	1.32143	-17.10	-16.663	-0.437	
	3.5	1.31152	-16.60	-16.734	0.134	
	8.5	1.26393	-12.00	-11.996	-0.004	
NaF [7]	0.4579	1.32900	-11.90	-11.93	0.028	0.035
	0.6328	1.32500	-12.80	-12.73	-0.070	0.04

**Table 3.7: (Continued)**

Crystal [Ref.]	Wavelength [ $\mu\text{m}$ ]	Refractive index	$\frac{dn}{dT} [ (10^{-6})/\text{K}]$		Differ- ence	Av. Dev.	RMS Dev. [ $10^{-6}$ ]
			Expt values	Computed (This work)			
at 20°C	1.15	1.32100	-13.20	-13.24	0.042		
	3.39	1.31200	-12.50	-12.50	-0.001		
SrF <sub>2</sub> [7]	0.4579	1.44300	-12.00	-12.06	0.062	0.089	0.11
	0.6328	1.43700	-12.40	-12.31	-0.093		
at 20°C	1.15	1.43200	-12.60	-12.47	-0.128		
	3.39	1.42300	-12.40	-12.56	0.162		
TlBr (45.7%)	10.6	1.34000	-9.80	-9.80	-0.002		
	0.576960	2.62911	-254.0	-255.909	1.909	6.37	7.36
ThI (54.3%)	0.579016	2.62659	-253.0	-255.731	2.731		
	0.643857	2.56604	-249.0	-250.559	1.559		
[2]	0.69075	2.53619	-247.0	-247.566	0.566		
	0.85212	2.47608	-242.0	-240.634	-1.366		
(KRS5)	0.89440	2.46636	-241.0	-239.405	-1.595		
	1.01398	2.44566	-240.0	-236.761	-3.239		
at 19°C	1.12866	2.43236	-240.0	-234.972	-5.028		
	1.3673	2.41528	-238.0	-232.606	-5.394		
	1.3950	2.41393	-238.0	-232.403	-5.597		
	1.52952	2.40808	-238.0	-231.605	-6.395		
	1.6921	2.40287	-238.0	-230.883	-7.117		
	1.7092	2.40245	-238.0	-230.815	-7.185		
	1.8333	2.39999	-238.0	-230.356	-7.644		
	1.9701	2.39698	-238.0	-230.028	-7.972		
	2.3253	2.39220	-238.0	-229.368	-8.632		
	3.4188	2.38528	-237.0	-228.511	-8.489		
	4.258	2.38287	-237.0	-228.274	-8.726		
	9.724	2.37269	-235.0	-228.262	-6.738		
	11.035	2.36995	-233.0	-228.273	-4.727		
	14.29	2.36149	-228.0	-228.038	0.038		
	14.98	2.35958	-227.0	-227.891	0.891		
	15.48	2.35810	-226.0	-227.764	1.764		
	17.40	2.35159	-223.0	-227.083	4.083		
	18.16	2.34885	-220.0	-226.692	6.692		
	20.57	2.33942	-216.0	-224.883	8.883		
	21.79	2.33414	-214.0	-223.578	9.578		
	22.76	2.32970	-212.0	-222.315	10.315		
	23.82	2.32476	-210.0	-220.663	10.663		
	25.16	2.31808	-207.0	-218.145	11.145		
	25.97	2.31357	-206.0	-216.385	10.385		

**Table 3.7: (Continued)**

Crystal [Ref.]	Wavelength [ $\mu\text{m}$ ]	Refractive index	$\frac{dn}{dT} [(10^{-6})/\text{K}]$	Differ- ence	Av. Dev.	RMS Dev. [ $10^{-6}$ ]
			Expt values (This work)	Computed		
	26.63	2.31018	-202.0	-214.752	12.752	
	29.81	2.29099	-195.0	-204.656	9.656	
	31.70	2.27840	-188.0	-196.444	8.444	
	33.00	2.26927	-183.0	-189.638	6.638	
	34.48	2.25838	-177.0	-180.581	3.581	
	37.56	2.23343	-165.0	-156.515	-8.485	
	39.38	2.21708	-154.0	-138.356	-15.644	

The thermo-optic coefficients of NaCl crystal which are cited in [130] are the collected data from different sources [ From F. J. Micheli, Ann. Physik **4**, 7 (1902) from 0.202 to 0.643  $\mu\text{m}$ ; from E. Liebreich, Verhandl. Deut. Physik. Ges. **13**, 709, (1911) from 0.656 to 15.91  $\mu\text{m}$ , and from H. Rubens and E. F. Nichols, Weid. Ann. **60**, 454 (1897) from 17.93 to 22.3  $\mu\text{m}$ ]. Considering the crystal quality and measurement accuracy, the present fit is sufficient to explain these historical data.

Similarly, the thermo-optic coefficients of KRS5 crystal were measured by Rodney and Malitson [2]. The quoted average residual is  $\pm 7 \times 10^{-5}$  at room temperature. Therefore the present fit is within the experimental accuracy.

We have used only the experimental data of other halide crystals [128] and the fit is self explanatory.

### 3.4.4 Semiconductors

There are many semiconductors from diamond (C) to zinc selenide, ZnSe. The thermo-optic coefficients have been measured for some of the important semiconductors. We have analyzed these measured data in the previous model satisfactorily. In particular, the important semiconductors such as germanium, Ge, and silicon, Si, are of great importance in opto-electronic and optical studies. The refractive indices and thermo-optic coefficients were recommended by Li [144] from 1.9 to 18.0  $\mu\text{m}$  for Ge, and from 1.2 to 14  $\mu\text{m}$  for Si at 10 and 14 different temperatures from 100 to 550 K, and 100 to 750 K, respectively. Remarkably, there is no analysis of these data. The room temperature thermo-optic coefficients have been analyzed [140] and the optical constants  $G$ ,  $H$ , and  $E_{\text{ig}}$  are shown in Table 3.1. The experimental values are compared with the calculated values which are shown in Table 3.8. The dispersion curves of  $2n(dn/dT)$  at room temperature are shown in Fig. 3.45. The thermo-optic coefficients of Ge at different temperatures are also analyzed by varying  $G$  at per with the variation of the thermal expansion coefficient at the different measured temperature and by keeping the same form of Eq. (3.29). The fit is excellent. The optical constants  $G$ ,  $H$ , and the fitting isentropic bandgaps  $E_{\text{ig}}$  are shown in Table 3.9. The average value of the fitting gaps is considered to be the isentropic band gap, which is 0.6639  $\mu\text{m}$ . The calculated temperature variation of the excitonic band gap agrees well with the experimental values as cited in Table 3.1. The constants  $G$  and  $H$  are expressed as a quadratic function of temperature  $T$  and are given by

$$\begin{aligned} G(T) = & 0.324038 - 2.09205 \times 10^{-2} T + 5.03979 \times 10^{-5} T^2 \\ & - 4.14345 \times 10^{-8} T^3, \end{aligned} \quad (3.58)$$

and

$$\begin{aligned} H(T) = & 14.3362 + 9.12441 \times 10^{-2} T - 8.63548 \times 10^{-5} T^2 \\ & + 4.13818 \times 10^{-8} T^3. \end{aligned} \quad (3.59)$$

The recommended and computed values of  $2n(dn/dT)$  are shown in Fig. 3.46 at these temperatures for Ge crystal. Similarly, the experimental and

computed values of thermo-optic coefficients for Si at room temperature are shown in Table 3.8 and in Fig. 3.45. The optical constants  $G$ ,  $H$ , and  $E_{ig}$  are shown in Table 3.1.

Recently, Jellison and Modine [150] have measured the refractive indices of Si for four selected wavelengths from 0.4 to 0.78  $\mu\text{m}$  at ten different temperatures from 25 to 490°C. They tried to explain the change of the refractive index of Si as a function of temperature with the density change due to thermal expansion and the temperature-dependent polarizability. The explanation for thermo-optic coefficients is not at all satisfactory compared to the present one. The room temperature values of thermo-optic coefficients of Si were analyzed and reported [140] satisfactorily. The recent values of the thermo-optic coefficients [150] of Si are analyzed in this model. The optical constants  $G$ ,  $H$ , and the fitting isentropic bandgaps  $E_{ig}$  are also shown in Table 3.1. This gap is very near the temperature insensitive band gap [34]. The calculated temperature variation of the excitonic band gap agrees well with the experimental values as cited in Table 3.1. The experimental values of  $dn/dTs$  for Si [150] at the different measured temperature intervals are fitted in this model, Eq. (3.29) by keeping  $G$  as a constant, since  $\alpha$  is approximately a constant. The evaluated optical constants  $G$ ,  $H$ , and the fitting isentropic bandgaps  $E_{ig}$  are also shown in Table 3.10. The average value of  $G$  is  $-8.94733$  and the isentropic band gap is  $0.3187 \mu\text{m}$  (3.89 eV), which is exactly the same as the experimental value. The optical constant  $H$  is expressed as a quadratic function of temperature,  $T$ , which is shown below

$$\begin{aligned} H(T) = & 129.12 + 1.28516 \times 10^{-1} T + 8.5665 \times 10^{-4} T^2 \\ & - 1.81241 \times 10^{-6} T^3. \end{aligned} \quad (3.60)$$

The experimental and computed thermo-optic coefficients are shown in Table 3.11 at 25 and 285°C. The characteristic behavior of dispersion is shown in Fig. 3.47 at 25 and 450°C, respectively. The fit is satisfactory and therefore the present model is sufficient to explain the nonlinear behavior of thermo-optic coefficients. The existing models were unable to characterize the same behavior.

The thermo-optic coefficients of other semiconductor materials such as diamond, CdTe, CdS, GaAs, GaP, InAs, InP, PbS, PbSe, PbTe, ZnS, and ZnSe have been analyzed satisfactorily in this model. Some experimental values are compared with the calculated ones as cited in Table 3.11. The

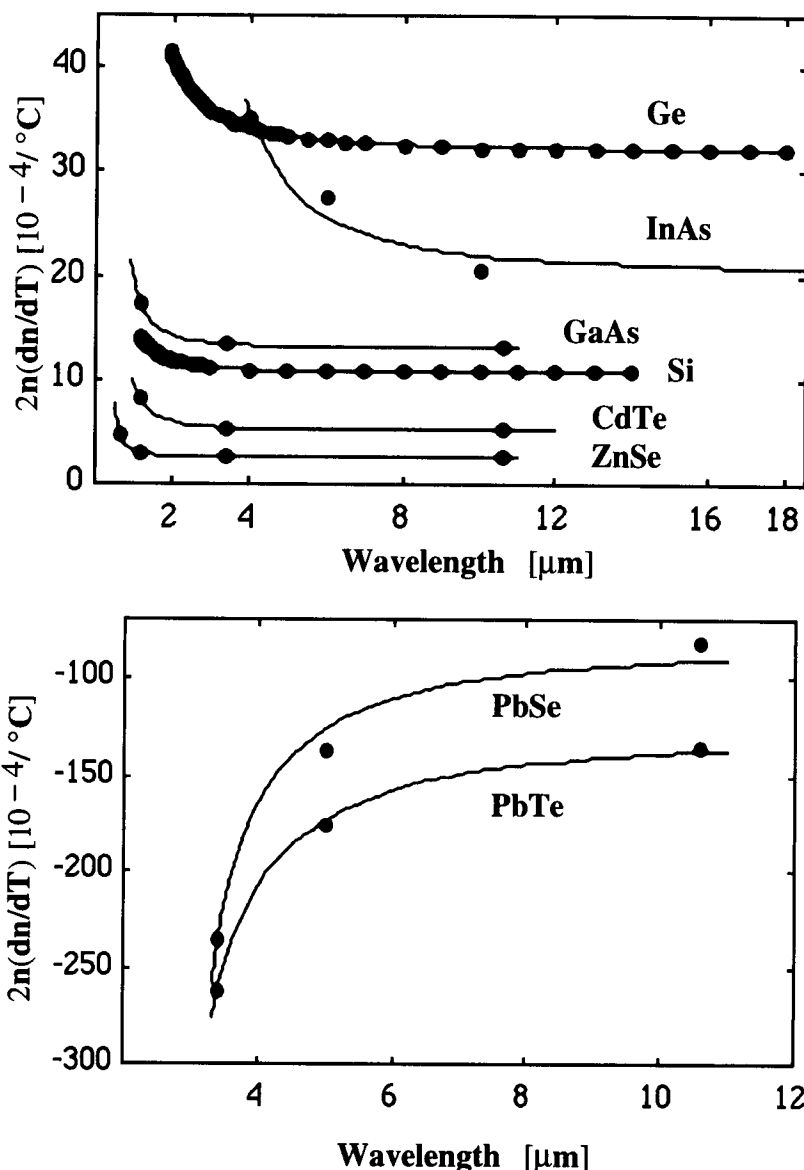


Figure 3.45:  $2n(dn/dT)$  versus wavelength for some important semiconductors at  $20^{\circ}\text{C}$ : Solid curves are the computed values; solid circles are the experimental data.

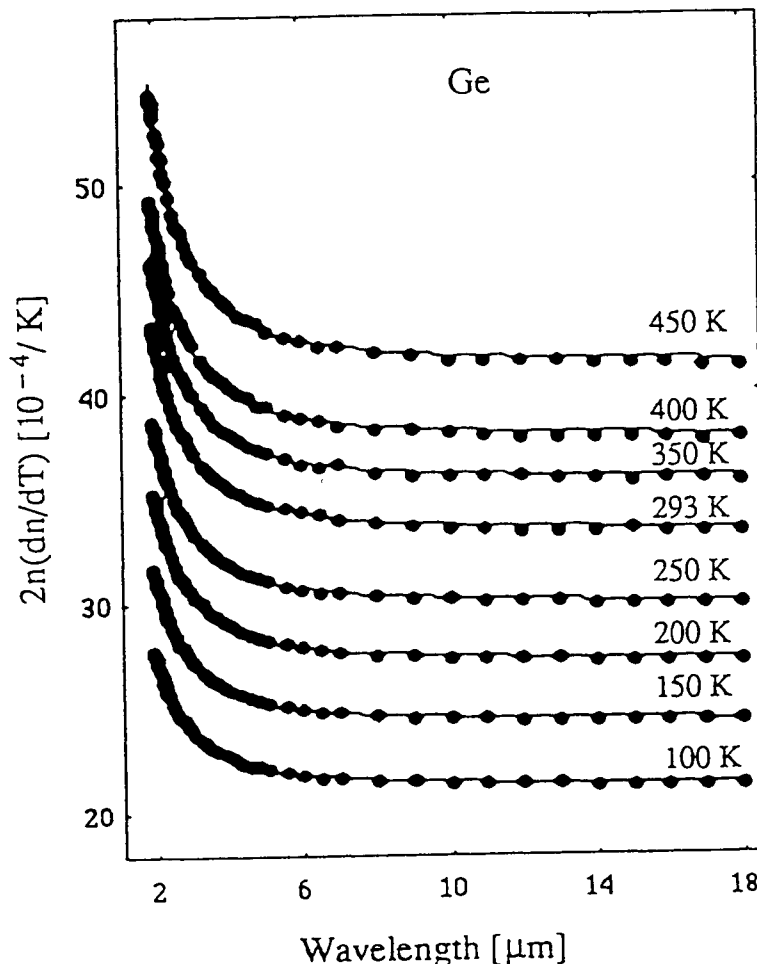


Figure 3.46:  $2n(dn/dT)$  versus wavelength for Ge semiconductor at different temperatures: Solid curves are the computed values; solid circles are the recommended values [144].

**Table 3.8: Refractive Index and Thermo-Optic Coefficients of Ge and Si Semiconductors**

Material [Ref.]	Wavelength [ μm]	Refractive index	$\frac{dn}{dT} [(10^{-4})/K]$		Differ- ence	Av. Dev.	RMS $<-[10^{-6}]>$
			Recom. values	Computed (This work)			
Ge at 20°C [144]	1.90	4.1117	5.057	5.093	-0.0360	1.69	1.89
	1.92	4.1094	5.036	5.066	-0.0304		
	1.94	4.1072	5.015	5.041	-0.0257		
	1.96	4.1050	4.995	5.016	-0.0211	Note:	
	1.98	4.1029	4.975	4.992	-0.0174	The comput-	
	2.00	4.1008	4.956	4.970	-0.0137	ed values are	
	2.05	4.0959	4.911	4.916	-0.0052	superior to	
	2.10	4.0914	4.869	4.867	0.0017	the estimated	
	2.15	4.0872	4.830	4.822	0.0076	uncertainty	
	2.20	4.0832	4.794	4.781	0.0127	in the	
	2.25	4.0795	4.760	4.743	0.0167	recommended	
	2.30	4.0761	4.728	4.708	0.0198	values of	
	2.40	4.0698	4.669	4.646	0.0235	$50 \times 10^{-6}$ .	
	2.50	4.0642	4.618	4.544	0.0279		
	2.60	4.0593	4.572	4.544	0.0279		
	2.70	4.0549	4.531	4.503	0.0283		
	2.80	4.0509	4.494	4.466	0.0278		
	2.90	4.0474	4.461	4.434	0.0272		
	3.00	4.0442	4.431	4.405	0.0261		
	3.20	4.0387	4.380	4.356	0.0244		
	3.40	4.0341	4.337	4.316	0.0215		
	3.60	4.0302	4.301	4.282	0.0186		
	3.80	4.0270	4.270	4.255	0.0154		
	4.00	4.0242	4.244	4.231	0.0128		
	4.25	4.0212	4.217	4.207	0.0103		
	4.50	4.0188	4.193	4.186	0.0068		
	4.75	4.0167	4.174	4.169	0.0049		
	5.00	4.0149	4.157	4.155	0.0024		
	5.50	4.0120	4.130	4.131	-0.0014		
	6.00	4.0098	4.110	4.114	-0.0039		
	6.50	4.0081	4.094	4.100	-0.0064		
	7.00	4.0068	4.081	4.090	-0.0086		
	8.00	4.0048	4.062	4.074	-0.0120		
	9.00	4.0034	4.049	4.063	-0.0144		
	10.00	4.0025	4.040	4.056	-0.0158		
	11.00	4.0017	4.033	4.050	-0.0173		
	12.00	4.0012	4.028	4.046	-0.0180		
	13.00	4.0008	4.024	4.043	-0.0186		
	14.00	4.0004	4.021	4.040	-0.0191		
	15.00	4.0001	4.019	4.038	-0.0190		

**Table 3.8: (Continued)**

Material [Ref.]	Wavelength [ μm]	Refractive index	$dn/dT$ [( $10^{-4}$ )/K] Recom. Computed values (This work)	Differ- ence	Avg. Dev.	RMS <-[ $10^{-6}$ ]->
Si at 20°C [144]	16.00	3.9999	4.016	4.036	-0.0202	
	17.00	3.9997	4.015	4.035	-0.0198	
	18.00	3.9996	4.013	4.034	-0.0206	
	1.20	3.5167	1.983	2.000	-0.0168	0.71
	1.22	3.5133	1.970	1.983	-0.0131	0.80
	1.24	3.5102	1.957	1.967	-0.0103	
	1.26	3.5072	1.945	1.953	-0.0075	
	1.30	3.5016	1.923	1.925	-0.0024	
	1.32	3.4990	1.912	1.913	-0.0009	
	1.34	3.4965	1.902	1.901	0.0009	
	1.36	3.4941	1.892	1.890	0.0020	
	1.38	3.4918	1.883	1.879	0.0036	
	1.40	3.4896	1.874	1.869	0.0046	
	1.50	3.4799	1.835	1.826	0.0089	
	1.55	3.4757	1.818	1.808	0.0099	
	1.65	3.4684	1.789	1.777	0.0116	
	1.70	3.4653	1.776	1.764	0.0117	
	1.90	3.4550	1.734	1.723	0.0110	
	2.00	3.4510	1.717	1.707	0.0098	Note:
	2.25	3.4431	1.685	1.677	0.0077	The comput-
	2.50	3.4375	1.662	1.656	0.0056	ed values are
	2.75	3.4334	1.645	1.641	0.0038	superior to
	3.00	3.4302	1.632	1.630	0.0022	the estimated
	4.00	3.4229	1.602	1.604	-0.0020	uncertainty
	5.00	3.4195	1.588	1.592	-0.0043	in the
	6.00	3.4177	1.581	1.586	-0.0050	recommended
	7.00	3.4165	1.576	1.582	-0.0063	value of
	8.00	3.4158	1.573	1.580	-0.0068	$15 \times 10^{-6}$ .
	9.00	3.4153	1.571	1.578	-0.0071	
	10.00	3.4150	1.570	1.577	-0.0069	
	11.00	3.4147	1.569	1.576	-0.0070	
	12.00	3.4145	1.568	1.575	-0.0074	
	13.00	3.4144	1.567	1.575	-0.0078	
	14.00	3.4142	1.567	1.574	-0.0075	

**Table 3.9: Optical Constants  $G$ ,  $H$ , and  $\lambda_{ig}$  for Ge at Different Temperatures [144]**

Temperature (K)	$G$ <----- $10^{-4}$ ----->	$H$	$\lambda_{ig}$ ( $\mu\text{m}$ )
100	-1.29590	22.6292	0.6700
150	-1.84989	26.2490	0.6610
200	-2.18454	29.4705	0.6569
250	-2.29773	32.2917	0.6562
293	-2.59996	34.7761	0.6562
350	-2.61396	37.4812	0.6592
400	-2.63559	39.6686	0.6628
450	-2.64179	41.6614	0.6672
500	-2.70606	43.5322	0.6720
550	-2.84064	45.2933	0.6772

**Table 3.10: Optical Constants  $G$ ,  $H$ , and  $\lambda_{ig}$  for Si at Different Temperatures [150]**

Temperature (°C)	$G$ <----- $10^{-5}$ ----->	$H$	$\lambda_{ig}$ ( $\mu\text{m}$ )
25	-8.98691	136.465	0.3346
150	-8.62008	150.092	0.3277
200	-8.42318	161.005	0.3264
245	-8.21012	218.444	0.3004
285	-8.34466	170.415	0.3267
325	-8.04132	230.392	0.2945
365	-7.96484	213.424	0.3004
410	-11.6880	137.252	0.3480
450	-10.2469	227.671	0.3100

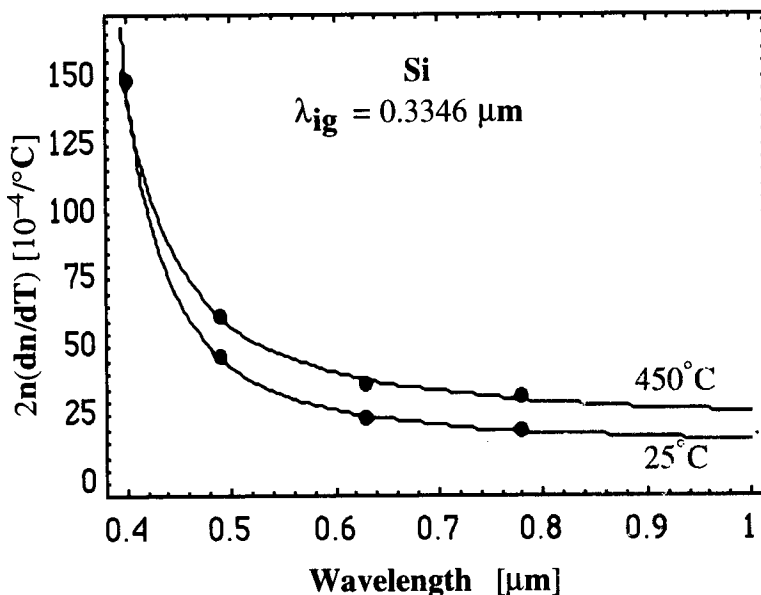


Figure 3.47:  $2n(dn/dT)$  versus wavelength for Si at 25 and  $450^{\circ}\text{C}$ : Solid curves are the computed values; solid circles are the experimental data [150].

experimental values and the computed curves are shown in Fig. 3.45 for some of these semiconductors. The characteristic behavior of dispersion of  $2n(dn/dT)$  for CdTe is shown in Fig. 3.48.

Since the thermo-optic coefficients are larger in semiconductors, thermo-optic modulators and temperature-dependent optical devices can be made efficiently by using semiconductor waveguide technology.

### 3.4.5 Optical Fiber/Optical Glasses

Wray and Neu [6] measured the thermo-optic coefficients of fused silica, Corning Code 7940, ultraviolet grade; Vycor, Corning Code 7913, optical grade and alumino silicate glass, Corning Code 1723 in the wavelength range 0.23 to  $3.4\text{ }\mu\text{m}$  and temperatures from 26 to  $826^{\circ}\text{C}$ . These experimental data are cited in most of the reference sources [130]. Only recently [25] these values have been analyzed by using this model including the updated values of thermo-optic coefficients of  $\text{SiO}_2$  glass [31]. The optical constants  $G$ ,  $H$ , and  $E_{ig}$  are shown in Table 3.2. Some experimental val-

**Table 3.11: Refractive Index and Thermo-Optic Coefficients of Some Important Semiconductors at 20°C**

Crystal [Ref.]	Wavelength [ μm]	Refractive index	$dn/dT$ [(10 <sup>-4</sup> )/K] Expt. Computed values (This work)	Differ- ence	Av. Dev.	RMS <-[10 <sup>-4</sup> ]>
a-Si	0.6328	4.18714	-1.430	-1.430	0.000	0.0 0.0
[145]	0.752	3.92542	2.710	2.710	0.000	
C	0.546	2.42339	0.101	0.102	-0.001	
(diamond)	10.60	2.34812	0.096	0.099	0.003	
CdS (o)	0.633	2.4706	1.500	1.485	0.015	0.016 0.02
[136]	1.064	2.3484	0.882	0.902	-0.020	
(e)	0.633	2.4512	1.605	1.628	-0.023	
	1.064	2.3320	0.990	0.987	0.003	
CdSe (o)	1.064	2.5367	0.891	0.887	0.004	0.02 0.03
[136]	10.60	2.4266	0.625	0.619	0.006	
(e)	1.064	2.5564	0.951	0.941	0.010	
	10.60	2.4445	0.660	0.657	0.030	
CdTe	1.15	2.8200	1.473	1.472	0.001	0.012 0.019
[140]	3.39	2.6973	0.982	1.000	-0.018	
	10.60	2.6740	0.980	0.963	0.017	
CdTe	1.15	2.8200	1.473	1.473	0.0001	0.003 0.004
[142]	6.00	2.6820	1.033	1.039	-0.0060	
	8.00	2.6773	1.032	1.035	-0.0024	
	10.00	2.6724	1.039	1.034	0.0055	
	12.00	2.6668	1.031	1.034	-0.0028	
	14.00	2.6602	1.039	1.036	0.0033	
	16.00	2.6525	1.033	1.038	-0.0055	
	18.00	2.6437	1.046	1.041	0.0046	
	20.00	2.6334	1.047	1.045	0.0023	
	22.00	2.6218	1.051	1.049	0.0011	
GaAs	1.15	3.4750	2.500	2.499	0.0013	0.01 0.01
[140]	3.39	3.3303	2.000	2.017	-0.0171	
	10.60	3.2919	2.000	1.984	0.0159	
GaN	1.15	2.3290	0.610	0.610	0.0000	
[99]	1.55	2.3169	----	0.575		
	5.30	2.2267	----	0.558		
GaP	0.546	3.4522	2.000	2.000	0.0000	0.00 0.00
[140]	0.633	3.3132	1.600	1.600	0.0000	
InAs	4.00	3.5100	5.000	5.068	-0.0678	0.19 0.21
[99, 140]	6.00	3.4400	4.000	3.719	0.2812	

**Table 3.11: (Continued)**

Crystal [Ref.]	Wavelength [ μm]	Refractive index	<u><math>dn/dT [(10^{-4})/\text{K}]</math></u>	Differ- ence	Av. Dev.	RMS Dev. $<-[10^{-4}]>$
		Expt. values	Computed (This work)			
InP	10.0	3.4200	3.000	3.217	0.2165	
[99, 140]	5.0	3.0800	0.830	0.834	-0.0042	0.017 0.02
	10.6	3.0500	0.820	0.794	0.0261	
	20.0	3.0200	0.770	0.792	0.0221	
PbS	3.39	4.1602	-21.000	-21.204	0.2043	0.44 0.47
[143,140]	5.00	4.1359	-19.000	-18.444	-0.6439	
	10.60	3.9755	-17.000	-17.500	0.4610	
PbSe	3.39	5.1204	-23.000	-23.220	0.2183	0.78 0.88
[143, 140]	5.00	4.8798	-14.000	-12.870	-1.1299	
	10.60	4.7390	-8.600	-9.590	0.9908	
PbTe	3.39	6.2576	-21.000	-21.054	0.0545	0.16 0.17
[143, 140]	5.00	5.8566	-15.00	-14.77	-0.2285	
	10.60	5.6315	-12.00	-12.18	0.1835	
Si	0.40	5.5850	13.28	13.282	-0.002	0.07 0.08
at 25°C	0.49	4.3450	5.36	5.319	0.041	
[150]	0.63	3.8770	3.12	3.253	-0.133	
	0.78	3.6950	2.72	2.624	0.096	
Si	0.40	5.9030	12.75	12.811	-0.061	0.31 0.41
at 285°C	0.49	4.4920	6.50	5.981	0.519	
[150]	0.63	3.9690	3.25	3.873	-0.623	
	0.78	3.7680	3.25	3.192	0.058	
ZnSe	0.633	2.5907	0.911	0.910	0.0014	0.005 0.006
[7]	1.15	2.4746	0.597	0.605	-0.0079	
	3.39	2.4356	0.534	0.525	0.0092	
	10.60	2.4026	0.520	0.523	-0.0025	

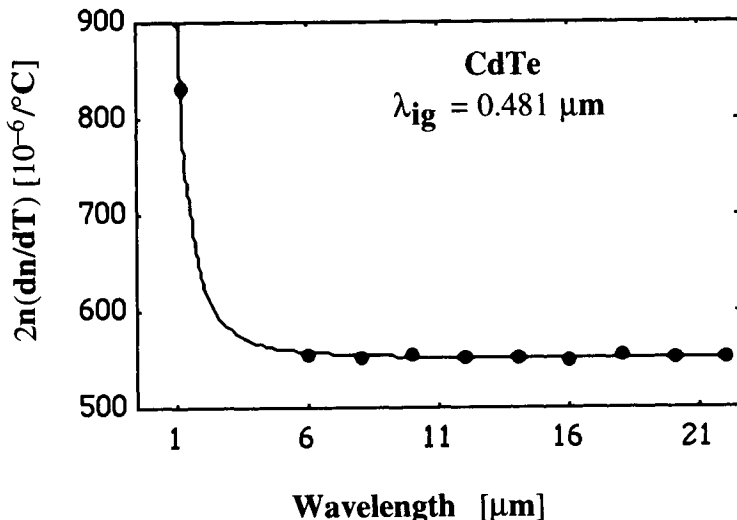


Figure 3.48:  $2n(dn/dT)$  versus wavelength for CdTe at room temperature: Solid curves are the computed values; solid circles are the experimental data [142].

ues are compared with the calculated values and are shown in Table 3.12 for fused silica, Corning Code 7940; alumino silicate, Corning Code 1723; and Vycor, Corning Code 7913. These values are also shown in Figs. 3.49 and 3.50 for these glasses to show the characteristic behavior of dispersion. It is clearly noticed that this model is also explaining the thermo-optic coefficients of the optical fiber glasses satisfactorily. Therefore, the smoothed values of thermo-optic coefficients can be used to explain the optical fiber, glass-based systems/devices.

Jewell measured the thermo-optic coefficient,  $dn/dT$ , for four National Institute of Standards and Technology (NIST) standard reference material (SRM) glasses [16] and vitreous silica [12]. He attempted to explain the behavior of the thermo-optic coefficient of these glasses by using the model suggested by Prod'homme [15]. However, he observed that for this model it is not possible to explain the linear behavior of the temperature coefficient of electronic polarizability for all glasses by correlating it to the activation energy for viscous flow, as proposed by Prod'homme. Therefore, Jewell proposed a modified model [17] by including additional factors for the various types of bridging and non-bridging oxygen ions in the glass that modify the calculation for the temperature coefficient of the electronic po-

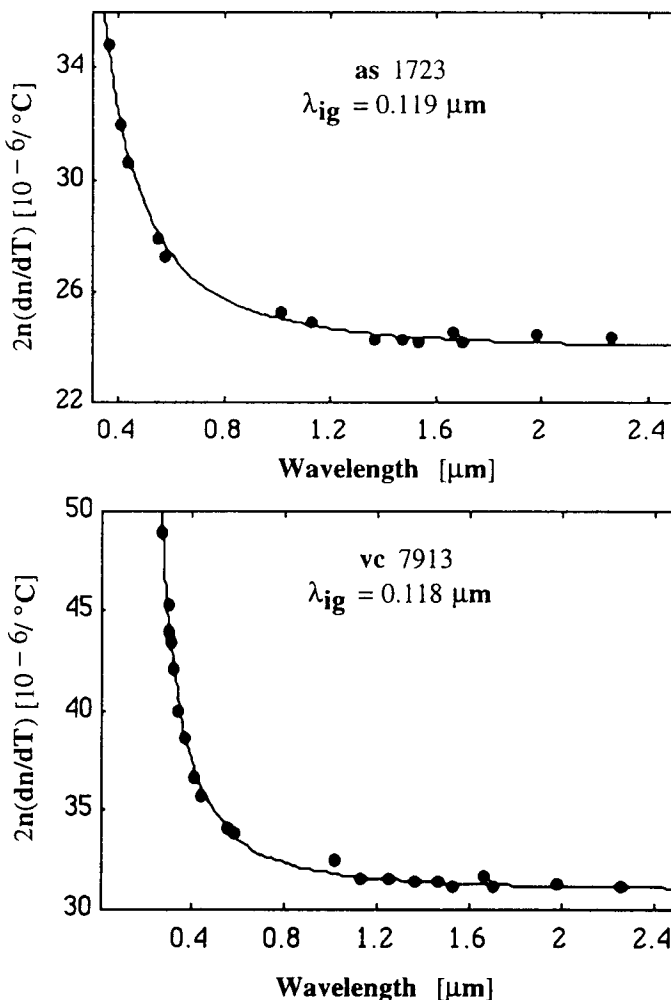


Figure 3.49:  $2n(dn/dT)$  versus wavelength for alumino-silicate 1723 and vycor 7913 Corning glasses at  $28^\circ\text{C}$ : Solid curves are the computed values; solid circles are the experimental data [6].

larizability. Nevertheless, Prod'homme's model [17] is unable to explain the thermo-optic behavior of refractive indices of different optical glasses. The thermo-optic coefficient  $dn/dT$  measured at  $0.6328 \mu\text{m}$ , is assumed to be the same at  $0.5893 \mu\text{m}$ , at which the refractive index values were measured by Jewell [16].

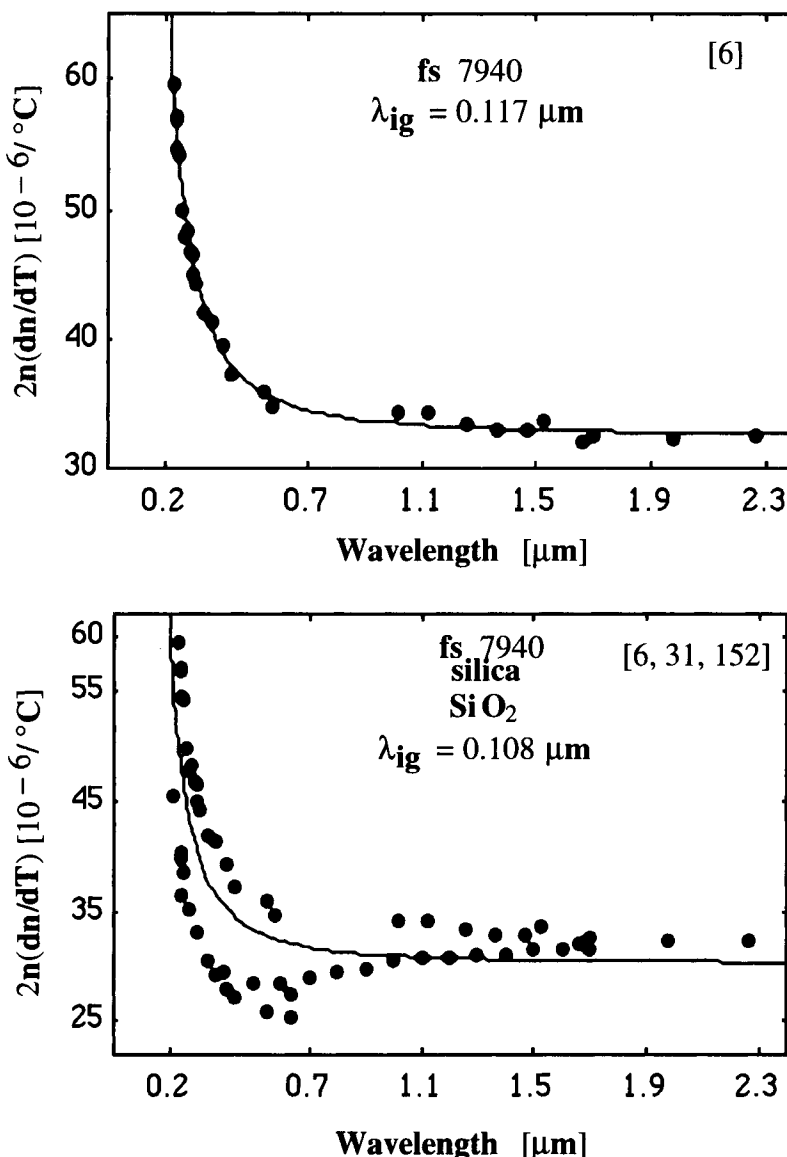


Figure 3.50:  $2n(dn/dT)$  versus wavelength for fused silica 7940; and fused silica 7940 with silica and  $\text{SiO}_2$  glass at  $26^\circ\text{C}$ : Solid curves are the computed values; solid circles are the experimental data. The references for the experimental data are shown in the figures.

**Table 3.12: Refractive Index and Thermo-Optic Coefficients of Some Optical Fiber Glasses**

Glasses [Ref.]	Wavelength [ $\mu\text{m}$ ]	Refractive index	$dn/dT$ [ $(10^{-6})/\text{K}$ ] Expt. Computed values (This work)	Differ- ence	Av. Dev.	RMS [ $10^{-6}$ ]
AS-1723 at 28°C [6]	0.36502 0.40466 0.43584 0.54607 0.57800 1.01398 1.12866 1.36728 1.47000 1.52952 1.66000 1.70100 1.98100 2.26200	1.57093 1.56405 1.56000 1.55100 1.54928 1.53854 1.53699 1.53419 1.53292 1.53224 1.53078 1.53014 1.52648 1.52245	11.1 10.2 9.8 9.0 8.8 8.2 8.1 7.9 7.9 7.9 8.0 7.9 7.9 8.0 8.0	10.95 10.27 9.88 9.05 8.90 8.13 8.06 7.98 7.96 7.95 7.93 7.93 7.91 7.91	0.151 -0.067 -0.078 -0.051 -0.104 0.073 0.038 -0.079 -0.057 -0.047 0.070 -0.027 0.089 0.091	0.07 0.08
FS-7940 at 26°C [6]	0.23021 0.23783 0.24070 0.24650 0.24827 0.26520 0.27528 0.28035 0.28936 0.29673 0.30215 0.31300 0.33415 0.36502 0.40466 0.43584 0.54607 0.57800 1.01398 1.12866 1.25400 1.36728 1.47000	1.52034 1.51496 1.51361 1.50970 1.50865 1.50023 1.49615 1.49425 1.49121 1.48892 1.48738 1.48462 1.48000 1.47469 1.46978 1.46685 1.46028 1.45899 1.45039 1.44903 1.44772 1.44635 1.44524	19.6 18.8 18.9 18.1 18.0 16.6 16.0 16.2 15.7 15.6 15.1 14.9 14.2 14.0 13.4 12.7 12.3 11.9 11.8 11.8 11.5 11.4 11.4	19.64 18.86 18.59 18.11 17.97 16.84 16.31 16.07 15.69 15.41 15.22 14.88 14.34 13.75 13.22 12.91 12.26 12.14 11.52 11.47 11.44 11.41 11.40	-0.041 -0.061 0.309 -0.007 0.032 -0.240 -0.306 0.133 0.015 0.192 -0.120 0.017 -0.142 0.247 0.181 -0.212 0.043 -0.239 0.276 0.326 0.064 -0.014 0.000	0.15 0.18

**Table 3.12: (Continued)**

Glasses [Ref.]	Wavelength [ $\mu\text{m}$ ]	Refractive index	$dn/dT$ [ $(10^{-6})/\text{K}$ ] Expt. Computed values (This work)	Differ- ence	Avg. Dev.	RMS Dev. [ $10^{-6}$ ]
	1.52952	1.44444	11.6	11.39	0.205	
	1.66000	1.44307	11.1	11.39	-0.285	
	1.70100	1.44230	11.3	11.39	-0.086	
	1.98100	1.43863	11.2	11.39	-0.186	
	2.26200	1.43430	11.3	11.40	-0.101	
FS-7940	0.23021	1.52034	19.6	16.64	2.963	1.53
+ $\text{SiO}_2$	0.23783	1.51496	18.8	16.10	2.700	1.80
[31]	0.24070	1.51361	18.9	15.91	2.988	
+ FS	0.24650	1.50970	18.1	15.57	2.526	
[152]	0.24827	1.50865	18.0	15.48	2.523	
at 26°C	0.26520	1.50023	16.6	14.68	1.923	
	0.27528	1.49615	16.0	14.29	1.708	
	0.28035	1.49425	16.2	14.12	2.081	
	0.28936	1.49121	15.7	13.84	1.860	
	0.29673	1.48892	15.6	13.64	1.963	
	0.30215	1.48738	15.1	13.50	1.601	
	0.31300	1.48462	14.9	13.25	1.651	
	0.33415	1.48000	14.2	12.85	1.354	
	0.36502	1.47469	14.0	12.40	1.598	
	0.40466	1.46978	13.4	11.99	1.405	
	0.43584	1.46685	12.7	11.76	0.941	
	0.54607	1.46028	12.3	11.25	1.049	
	0.57800	1.45899	11.9	11.16	0.741	
	1.01398	1.45039	11.8	10.68	1.123	
	1.12866	1.44903	11.8	10.64	1.162	
	1.25400	1.44772	11.5	10.61	0.891	
	1.36728	1.44635	11.4	10.59	0.807	
	1.47000	1.44524	11.4	10.58	0.818	
	1.52952	1.44444	11.6	10.58	1.021	
	1.66000	1.44307	11.1	10.57	0.528	
	1.70100	1.44230	11.3	10.57	0.726	
	1.98100	1.43863	11.2	10.58	0.623	
	2.26200	1.43430	11.3	10.59	0.706	
	0.23786	1.51519	13.3	16.10	-2.746	
	0.24472	1.51090	13.2	15.67	-2.524	
	0.24643	1.50990	12.1	15.58	-3.526	
	0.24823	1.50889	12.8	15.48	-2.677	
	0.27531	1.49635	11.8	14.29	-2.538	
	0.33419	1.48018	10.3	12.84	-2.494	
	0.36506	1.47495	9.9	12.40	-2.499	

**Table 3.12: (Continued)**

Glasses [Ref.]	Wavelength [ $\mu\text{m}$ ]	Refractive index	$dn/dT$ [ $(10^{-6})/\text{K}$ ] Expt. Computed values (This work)	Differ- ence	Av. Dev.	RMS Dev. [ $10^{-6}$ ]
	0.40470	1.47002	9.5	11.99	-2.493	
	0.43589	1.46709	9.3	11.76	-2.457	
	0.54614	1.46047	8.9	11.25	-2.349	
	0.21380	1.53433	14.8	18.12	-3.324	
	0.30000	1.48779	11.2	13.55	-2.384	
	0.40000	1.47010	10.0	12.04	-2.037	
	0.50000	1.46232	9.7	11.42	-1.680	
	0.60000	1.45804	9.7	11.11	-1.367	
	0.70000	1.45530	10.0	10.92	-0.925	
	0.80000	1.45333	10.1	10.81	-0.681	
	0.90000	1.45177	10.3	10.74	-0.476	
	1.00000	1.45044	10.5	10.68	-0.164	
	1.10000	1.44922	10.7	10.65	0.003	
	1.20000	1.44807	10.7	10.62	0.029	
	1.30000	1.44693	10.7	10.60	0.117	
	1.40000	1.44579	10.8	10.59	0.190	
	1.50000	1.44462	10.9	10.58	0.328	
	1.60000	1.44342	10.9	10.58	0.333	
	1.70000	1.44216	10.9	10.57	0.345	
Vycor 7913 at 28°C [6]	0.26520	1.49988	16.3	16.18	0.117	0.075
	0.28936	1.49074	15.2	15.05	0.151	0.10
	0.29673	1.48851	14.8	14.78	0.024	
	0.30215	1.48694	14.6	14.59	0.007	
	0.31300	1.48416	14.2	14.26	-0.063	
	0.33415	1.47949	13.5	13.73	-0.234	
	0.36502	1.47415	13.1	13.16	-0.059	
	0.40466	1.46925	12.5	12.64	-0.137	
	0.43584	1.46628	12.2	12.34	-0.138	
	0.54607	1.45960	11.7	11.70	0.000	
	0.57800	1.45831	11.6	11.59	0.014	
	1.01398	1.44968	11.2	10.99	0.213	
	1.12866	1.44831	10.9	10.94	-0.038	
	1.25400	1.44677	10.9	10.90	-0.003	
	1.36728	1.44554	10.9	10.88	0.019	
	1.47000	1.44422	10.9	10.87	0.031	
	1.52952	1.44356	10.8	10.86	-0.063	
	1.66000	1.44206	11.0	10.85	0.146	
	1.70100	1.44137	10.8	10.85	-0.054	
	1.98100	1.43750	10.9	10.85	0.045	
	2.26200	1.43298	10.9	10.87	0.029	

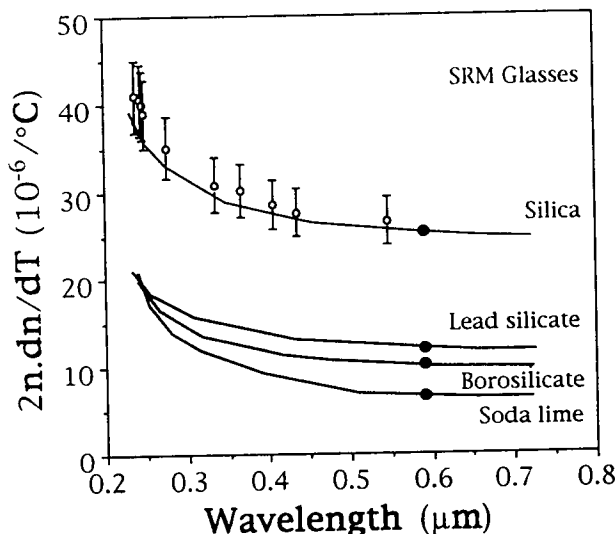


Figure 3.51:  $2n(dn/dT)$  versus wavelength at  $25^\circ\text{C}$  for SRM glasses: Solid curves are the computed values from the optical constants  $G$ ,  $H$  and  $E_{ig}$  from Table 3.2: Experimental points [31] with error bars are shown as open circles for  $\text{SiO}_2$  glass, and solid circles [16] for all glasses at  $0.5893 \mu\text{m}$  (after Ref. 26 with kind permission from Elsevier Science - NL).

By using these parameters and the thermal expansion coefficient,  $\alpha$ , the optical constants  $G$  and  $H$  were evaluated at  $25^\circ\text{C}$  and are shown in Table 3.2 along with the other optical parameters. From the evaluated constant,  $H$ , the variation of excitonic band gap with temperature was calculated by knowing the excitonic band gap at room temperature. This value is also shown in the same Table 3.2. The excitonic band gap is the average of three bands from 4.2 to 6.7 eV for lead silicate glass at room temperature which was observed by Ellis *et al.* [30]. The calculated variations of the excitonic band gaps with temperature were compared with the only available experimental value [31] and agree reasonably well, within the experimental accuracy. In this model,  $dn/dT$ s were calculated for these glasses from 0.23 to  $0.7 \mu\text{m}$  by using the evaluated constants  $G$ ,  $H$ , and the isentropic band gap  $E_{ig}$  from Table 3.2. These are shown as solid curves in Fig 3.51. The solid curve for the silicate glass is compared with the experimental val-

ues [31] of the only available  $\text{SiO}_2$  glass, which is not the same glass used by Jewell [16]. The error bar is due to the accuracy of the refractive index measurement which is  $\pm 3.0 \times 10^{-6}$ . However, the agreement is quite significant and noteworthy.

Since the thermo-optic coefficient is not constant over the stated temperature region, we have calculated the optical constants,  $H$ , with  $15^\circ\text{C}$  increments from  $25^\circ\text{C}$  up to  $115^\circ\text{C}$  for four NIST glasses by using the refractive index at  $25^\circ\text{C}$  and the linear regression equation [16] of  $dn/dT$ . In this evaluation, the band gap  $E_{\text{ig}}$ , is kept constant as discussed earlier. Again, the optical constant  $G$  is kept constant, since  $\alpha$  is almost constant from  $25^\circ\text{C}$  to  $120^\circ\text{C}$  [16] and even up to higher temperatures as observed in other nonlinear crystals and glasses. The variation of excitonic band gap with temperature,  $(dE_{\text{eg}}/dT)$ , is calculated from the optical constant  $H$  at different temperatures. These values are then plotted against temperature and fitted to straight lines for this temperature region. The schematic plot is shown in Fig. 3.52. The variation of excitonic band gap ( $E_{\text{eg}}$ ), is also plotted in the same figure for three glasses. The behavior is not linear and it will decrease more rapidly as the temperature increases, since  $dE_{\text{eg}}/dT$  is decreasing linearly against temperature. The linear relationship between  $dE_{\text{eg}}/dT$  and  $T$ , and the value of  $E_{\text{eg}}$  at room temperature was used to calculate the optical constant  $H$  at any operating temperature, and ultimately to compute the thermo-optic coefficients. The same experimental behavior is observed in other nonlinear crystals [29]. The variation of excitonic band gap ( $E_{\text{eg}}$ ), with temperature is lowest for lead silicate glass and highest for vitreous silica although the former has the lowest excitonic band gap. The explanation is very simple. There are about two electrons which have accounted for excitonic transitions ( $\text{Pb } 6s \rightarrow \text{Pb } 6p$ ) as explained by Ellis *et al.* [30] in lead silicate glass, whereas, in the same transition ( $\text{O } 2p \rightarrow \text{O } 3s$ ), the possible number of electrons involved would perhaps be 6 for silicate glasses [30]. Lead is the heaviest element and has more binding energy than the other glasses. As the temperature increases, a fewer number of electrons are excited to the higher energy band gaps compared to the loosely bound electrons in other glasses, affecting the lowest variation of band gap with temperature in lead silicate glass.

Thermo-optic coefficients,  $dn/dT$  were also analyzed in this model for two series of soda-lime-silica glasses,  $25\text{Na}_2\text{O}.\text{pCaO}.(75-\text{p})\text{SiO}_2$  and  $(25-\text{p})\text{Na}_2\text{O}.\text{CaO}.75\text{SiO}_2$ . From a set of measured ( $n$ ,  $dn/dT$ ,  $\lambda$ ) data, adopting

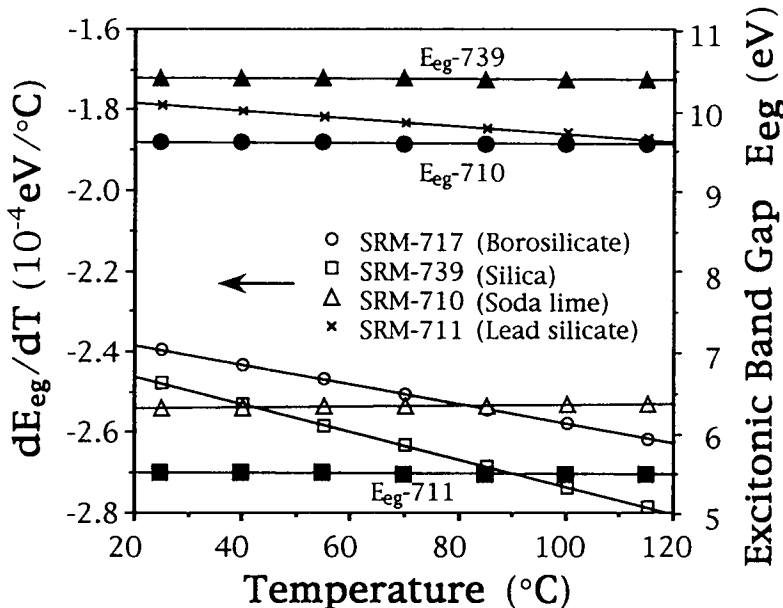


Figure 3.52: The schematic plot of the variation of the excitonic band gap with temperature,  $dE_{eg}/dT$ , versus temperature for SRM glasses. The excitonic band gap  $E_{eg}$  versus temperature is for three glasses (after Ref. 26 with kind permission from Elsevier Science - NL).

a least-squares procedure, the optical constants  $G$  and  $H$  are evaluated by an appropriate energy gap ( $E_{ig}$ ) being scanned from the lowest gap to the highest value. In this case only one datum [153] is available at  $0.5893\text{ }\mu\text{m}$  for these glasses. Therefore, it is not possible to use the fitting analyses. But a direct solution is possible to evaluate the optical constants  $G$  and  $H$  by knowing  $E_{ig}$  and  $n_\infty$ . Matsuoka *et al.* [31] observed the peak energy corresponding to the band-to-band transition around  $11.6\text{ eV}$  for  $\text{SiO}_2$  glass. Similarly, Ellis *et al.* [30] observed the  $E_{ig}$  band around  $11.4\text{ eV}$  for soda-lime glasses. Therefore,  $11.4\text{ eV}$  was used for  $E_{ig}$  band gap to calculate the normalized  $R$  for these glasses, since this value was not available in the literature for different compositions of this glass. Normally,  $E_{ig}$  is a function of composition, but its variation is rather small compared to that of the  $E_{eg}$  band gap because of the bridging oxygen ions in silicate glasses, where  $E_{eg}$  is due to the excitonic transition. The computed parameters do not vary significantly for this small variation of the  $E_{ig}$  band gap. Again,

$n_\infty$  is 0.02 less than its value at  $0.5893\text{ }\mu\text{m}$ , as is the cases for other glasses. These parameters and  $\alpha$  were used to calculate  $G$  and  $H$  at  $50^\circ\text{C}$  (Table 3.2) with the other optical parameters.  $G$  and  $H$  are plotted against composition  $p$  of CaO for two series of glasses as shown in Figs. 3.53 and 3.54, respectively. If the accuracy of  $\alpha$  and  $dn/dT$  is  $\pm 0.4 \times 10^{-6}$  and  $\pm 0.7 \times 10^{-6}$ , respectively, errors are as indicated by the bars in Fig. 3.53 for  $G$  and  $H$ , the top and bottom figure, respectively. Within the experimental accuracy,  $G$  and  $H$  vary linearly against  $p$  of CaO. The straight lines I and II represent the glasses  $25\text{Na}_2\text{O}.p\text{CaO}.(75-p)\text{SiO}_2$  and  $(25-p)\text{Na}_2\text{O}.p\text{CaO}.75\text{SiO}_2$ , respectively. Ideally, these optical constants are nonlinear against  $p$  of CaO.

Values of  $2n(dn/dT)$  have been calculated for both series of soda-lime-silica glasses. The experimental values are shown as solid circles in Fig. 3.54 for the two series of glasses.  $dn/dT$  of the  $25\text{Na}_2\text{O}.p\text{CaO}.(75-p)\text{SiO}_2$  glasses increases with increasing CaO, changing from negative to positive, while the magnitude of  $dn/dT$  for  $(25-p)\text{Na}_2\text{O}.p\text{CaO}.75\text{SiO}_2$  glasses passes through a maximum negative value.  $\alpha$  increases as CaO increases by reducing  $\text{SiO}_2$ , since CaO is more temperature sensitive than  $\text{SiO}_2$ . Also,  $n$  increases because of the replacement by the heavier calcium atom. On the other hand, when CaO substitutes for  $\text{Na}_2\text{O}$ ,  $\alpha$  decreases because a  $\text{Na}^+$  ion is replaced by the less-temperature-sensitive  $\text{Ca}^{2+}$  ion. On the short wavelength side (VUV) of the spectrum, the transparency is limited by the electronic fundamental absorption band. The fundamental edge is shifted toward the longer wavelength (VUV or UV) if the atoms forming the glasses are heavier. Therefore, the excitonic band should be shifted toward the longer wavelength side, as CaO increases in both series of glasses. Since its value is not available for different compositions at present, we took into consideration the  $E_{eg}$  band gap of 9.3 and 9.6 eV for the two series of glasses, and calculated the values of  $dE_{eg}/dT$  in Table 3.2. These values are taken from soda-lime glasses [16] which are a slightly different glass. The relative values of  $dE_{eg}/dT$  give a basic understanding on the effect of CaO for these two series of glasses. The calculated values agree quite well with the only available experimental value of pure  $\text{SiO}_2$  glass.

The temperature dependence of refractive indices of several optical glasses have been measured from  $-40$  to  $80^\circ\text{C}$  at three laser wavelengths from  $0.4358$  to  $1.06\text{ }\mu\text{m}$  for Schott glasses [19] and at seven laser wavelengths from  $0.4358$  to  $1.014\text{ }\mu\text{m}$  for Ohara glasses [18]. It was found that the refractive index is not a linear function of temperature at all wave-

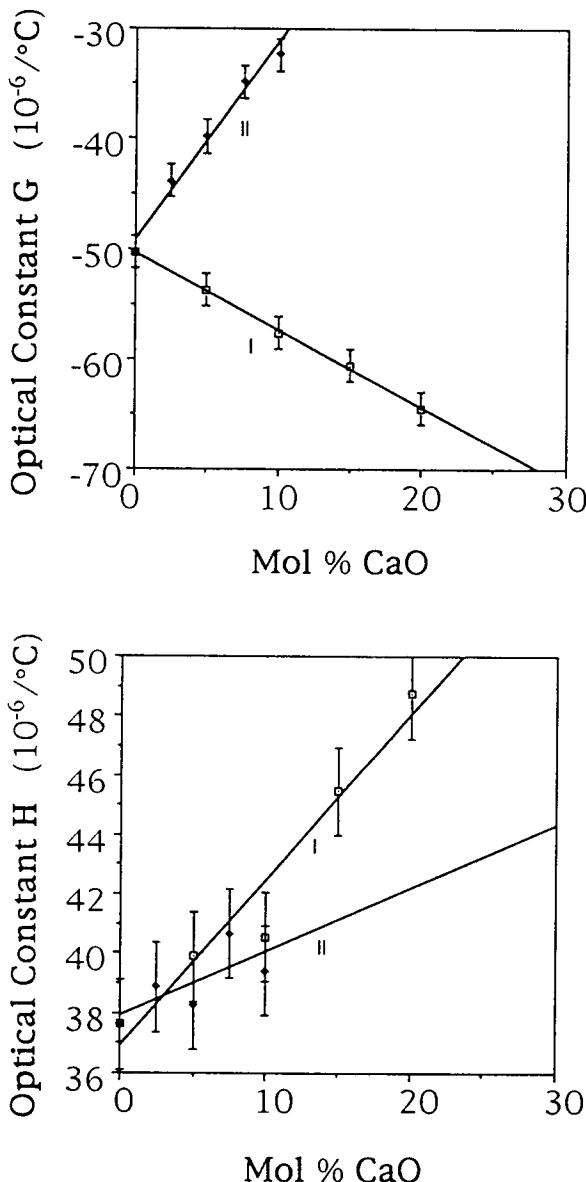


Figure 3.53: The top figure: Optical constant  $G$  versus  $p$  of  $\text{CaO}$  (mol%); I is  $25\text{Na}_2\text{O}.\text{pCaO}.(75-p)\text{SiO}_2$  glass and II is  $(25-p)\text{Na}_2\text{O}.\text{pCaO}.75\text{SiO}_2$  glass. The bottom figure: Optical constant  $H$  versus  $p$  of  $\text{CaO}$  (mol%); I is  $25\text{Na}_2\text{O}.\text{pCaO}.(75-p)\text{SiO}_2$  glass and II is  $(25-p)\text{Na}_2\text{O}.\text{pCaO}.75\text{SiO}_2$  glass (after Ref. 154 with permission from ACS).

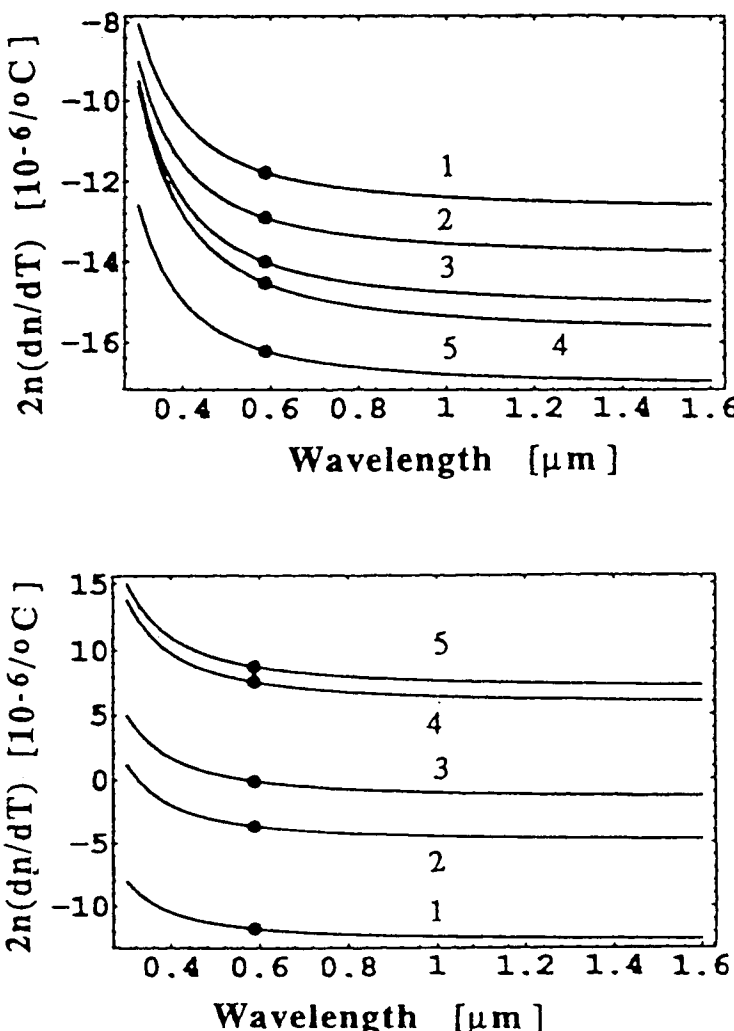


Figure 3.54: The top figure:  $2n(dn/dT)$  versus wavelength for different p of CaO (mol%) in  $25\text{Na}_2\text{O}.\text{pCaO}.(75-\text{p})\text{SiO}_2$  glass (1 is  $\text{p} = 0$ , 2 is  $\text{p} = 5$ , 3 is  $\text{p} = 10$ , 4 is  $\text{p} = 15$ , and 5 is  $\text{p} = 20$ ). The bottom figure:  $2n(dn/dT)$  versus wavelength for different p of CaO (mol%) in  $(25-\text{p})\text{Na}_2\text{O}.\text{pCaO}.75\text{SiO}_2$  glass (1 is  $\text{p} = 0$ , 2 is  $\text{p} = 2.5$ , 3 is  $\text{p} = 5$ , 4 is  $\text{p} = 7.5$ , and 5 is  $\text{p} = 10$ ); Solid circles are the experimental values (after Ref. 154 with permission from ACS).

lengths. There are no analyses or empirical equations to represent the thermo-optic coefficients for Ohara optical glasses. On the other hand, there is an empirical equation to account for the thermo-optic coefficients of Schott glasses. This equation has no physical significance. Here, we applied the present model as described earlier. From a set of measured ( $n$ ,  $dn/dT$ , and  $\lambda$ ) data, adopting least-squares procedure, the optical constants  $G$  and  $H$  are evaluated by an appropriate band gap ( $\lambda_{ig}$ ) being scanned from the lowest gap to the highest value. By following the previously described procedure, the optimum fitted constants  $G$  and  $H$  are evaluated and are shown in Table 3.2 at 20°C. Since the values of the excitonic band gaps are not available in the literature, these are calculated from the relation  $E_{ig}^2 = E_{eg} \cdot E_{ag}$ , where  $E_{ag}$  is obtained from Table 2.2. From the fitted constants  $G$  and  $H$ , the thermal expansion coefficient,  $\alpha$  and the temperature coefficient of the excitonic band gap are computed and are also shown in Table 3.2 along with the value of  $n_\infty$ . These values are compared with that of the experiment and agree reasonably well within the experimental accuracy, particularly with the only available experimental value [31] of  $dE_{eg}/dT$  for SiO<sub>2</sub> glass. The experimental and calculated values of thermo-optic coefficients are shown in Table 3.13 for various optical glasses at room temperature.

Since the thermo-optic coefficients are not the same at different temperature intervals, we have fitted [ $2n(dn/dT)$ ,  $\lambda$ ] data at five other measured temperatures, i.e., at -40, -20, 0, 40, and 60° for Ohara glasses and at two other temperatures, i.e., at -40 and 60° for Schott glasses. In the fitting analyses, the same form of Eq. (3.29) was used by keeping  $G$  as a constant, since the thermal expansion coefficient is almost constant [18, 19] from -40 to 80°. As we noticed, the fitting isentropic band gaps are consistently very close. Therefore, we calculated the average of these fitting gaps as the isentropic band gap, which is shown in Table 3.2. The experimental points and the fitting curves are shown in Figs. 3.55 to 3.58 for some selective Ohara and Schott optical glasses at -40 and 60°C, the lower and upper curves, respectively.

The agreement is satisfactory. Henceforth, the optical constant  $H$ , computed at the above mentioned temperatures, is expressed as a quadratic function of temperature,  $T$  by

$$H(T) = H_0 + H_1 T + H_2 T^2. \quad (3.61)$$

The computed optical constants are cited in Table 3.14. The analyses

**Table 3.13: Refractive Index and Thermo-Optic Coefficients of Some Ohara Optical Glasses [18] at 20°C**

Glasses (Schott)	Wavelength [ μm]	Refractive index	$dn/dT$ [(10 <sup>-6</sup> )/K] Expt. Computed values (This work)	Differ- ence	Av. RMS Dev. Dev. [10 <sup>-6</sup> ]
S-BSL7 (BK7)	0.435835	1.52621	3.30	3.334	-0.034
	0.479990	1.52236	3.10	3.072	0.028
	0.546070	1.51825	2.80	2.808	-0.008
	0.589290	1.51626	2.70	2.687	0.013
	0.632800	1.51462	2.60	2.592	0.008
	0.643850	1.51425	2.60	2.571	0.029
	1.013980	1.50686	2.20	2.236	-0.036
S-FSL5 (FK5)	0.435835	1.49596	-0.30	-0.241	-0.059
	0.479990	1.49267	-0.40	-0.439	0.039
	0.546070	1.48915	-0.60	-0.636	0.036
	0.589290	1.48743	-0.70	-0.725	0.025
	0.632800	1.48601	-0.80	-0.795	-0.005
	0.643850	1.48569	-0.80	-0.810	0.010
	1.013980	1.47915	-1.10	-1.055	-0.045
S-LAL10 (LaK10)	0.435835	1.73795	4.10	4.066	0.034
	0.479990	1.73085	3.60	3.610	-0.010
	0.546070	1.72341	3.20	3.162	0.038
	0.589290	1.71987	2.90	2.961	-0.061
	0.632800	1.71700	2.80	2.804	-0.004
	0.643850	1.71636	2.70	2.769	-0.069
	1.013980	1.70443	2.30	2.227	0.073
S-NSL5 (SK5)	0.435835	1.53332	2.20	2.186	0.014
	0.479990	1.52906	1.90	1.883	0.017
	0.546070	1.52458	1.60	1.582	0.018
	0.589290	1.52242	1.40	1.446	-0.046
	0.632800	1.52065	1.30	1.340	-0.040
	0.643850	1.52026	1.30	1.316	-0.016
	1.013980	1.51256	1.00	0.946	0.054
PBH6 (SF6)	0.435830	1.84706	16.80	16.734	0.066
	0.479990	1.82970	13.80	13.905	-0.105
	0.546070	1.81265	11.40	11.419	-0.019
	0.589290	1.80490	10.40	10.386	0.014
	0.643850	1.79750	9.50	9.454	0.046

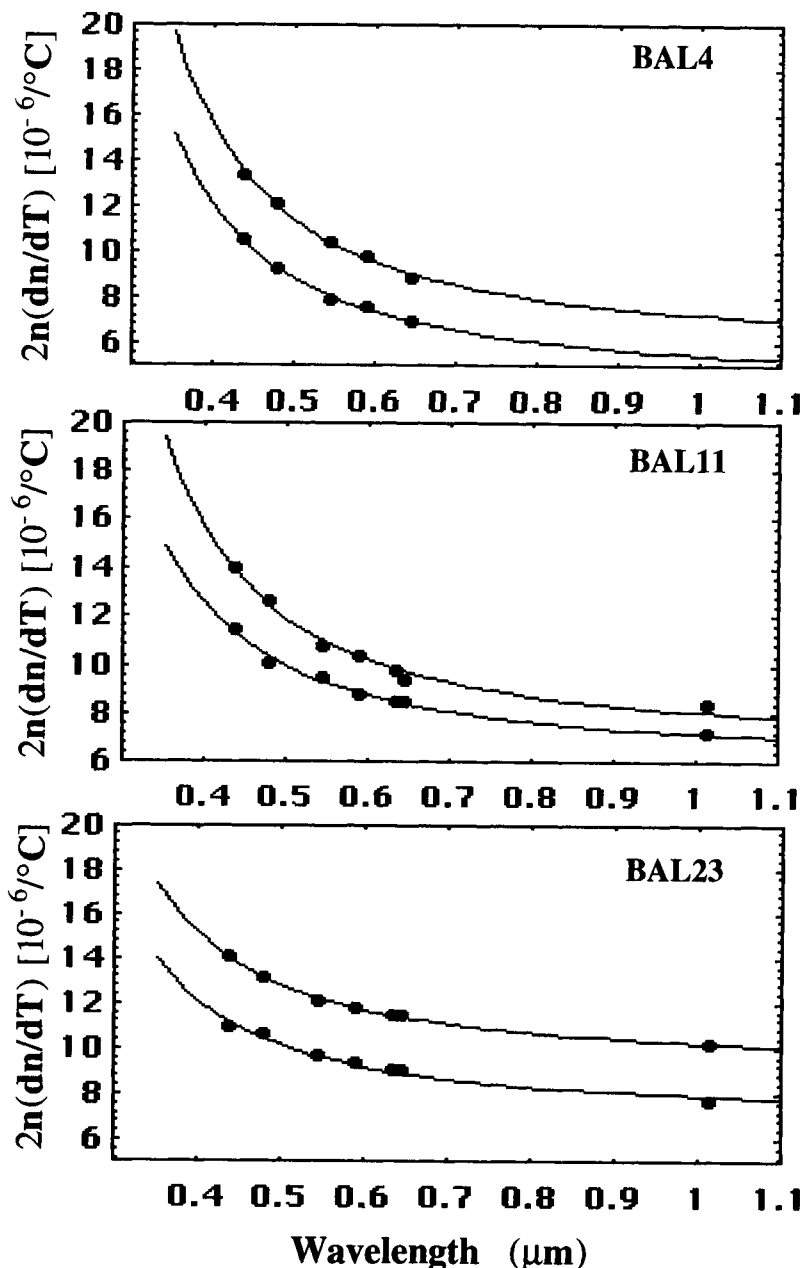


Figure 3.55:  $2n(dn/dT)$  versus wavelength for some Ohara optical glasses: Solid curves, computed values from the optical constants  $G$ ,  $H$ , and  $E_{ig}$  from Table 3.2; solid circles, experimental data; upper and lower curves,  $60$  and  $-40^{\circ}\text{C}$ , respectively, (after Ref. 156 with permission from OSA).

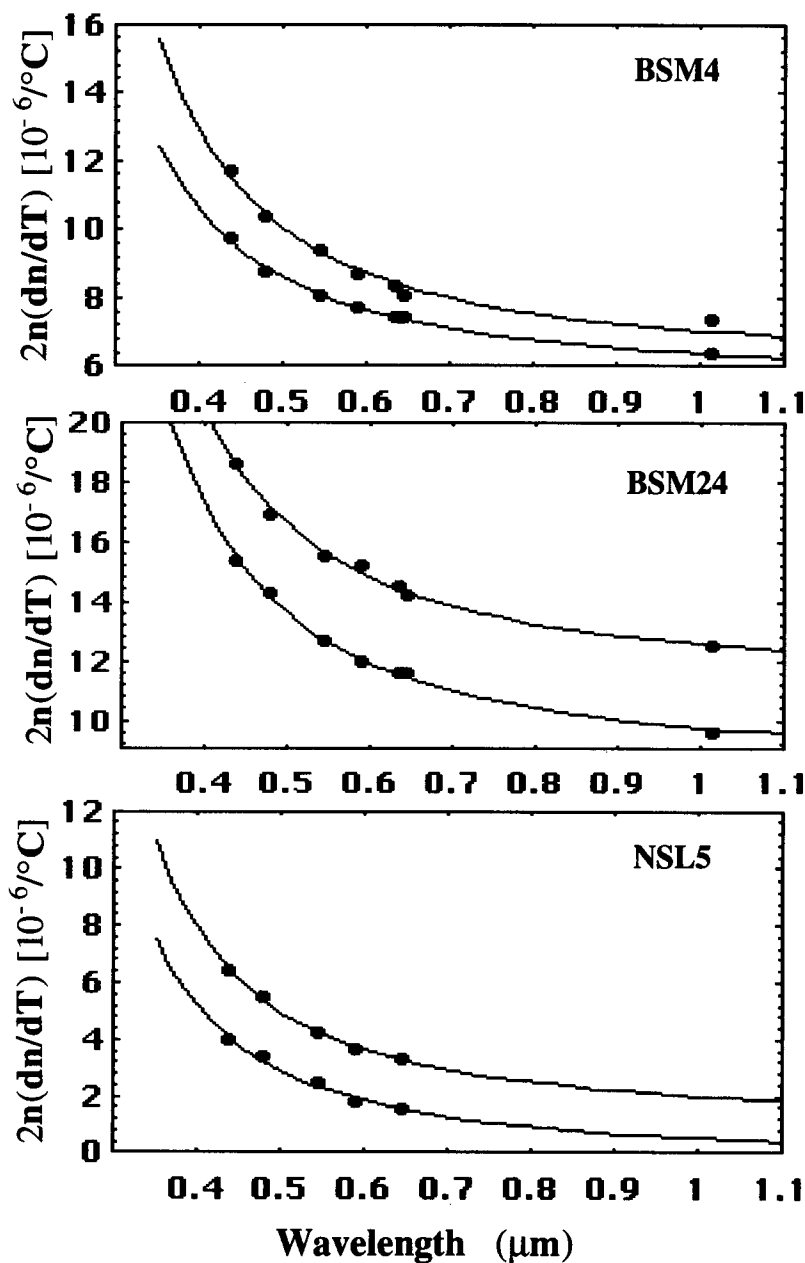


Figure 3.56:  $2n(dn/dT)$  versus wavelength for some Ohara optical glasses: Solid curves, computed values from the optical constants  $G$ ,  $H$ , and  $E_{ig}$  from Table 3.2; solid circles, experimental data; upper and lower curves, 60 and  $-40^\circ\text{C}$ , respectively, (after Ref. 156 with permission from OSA).

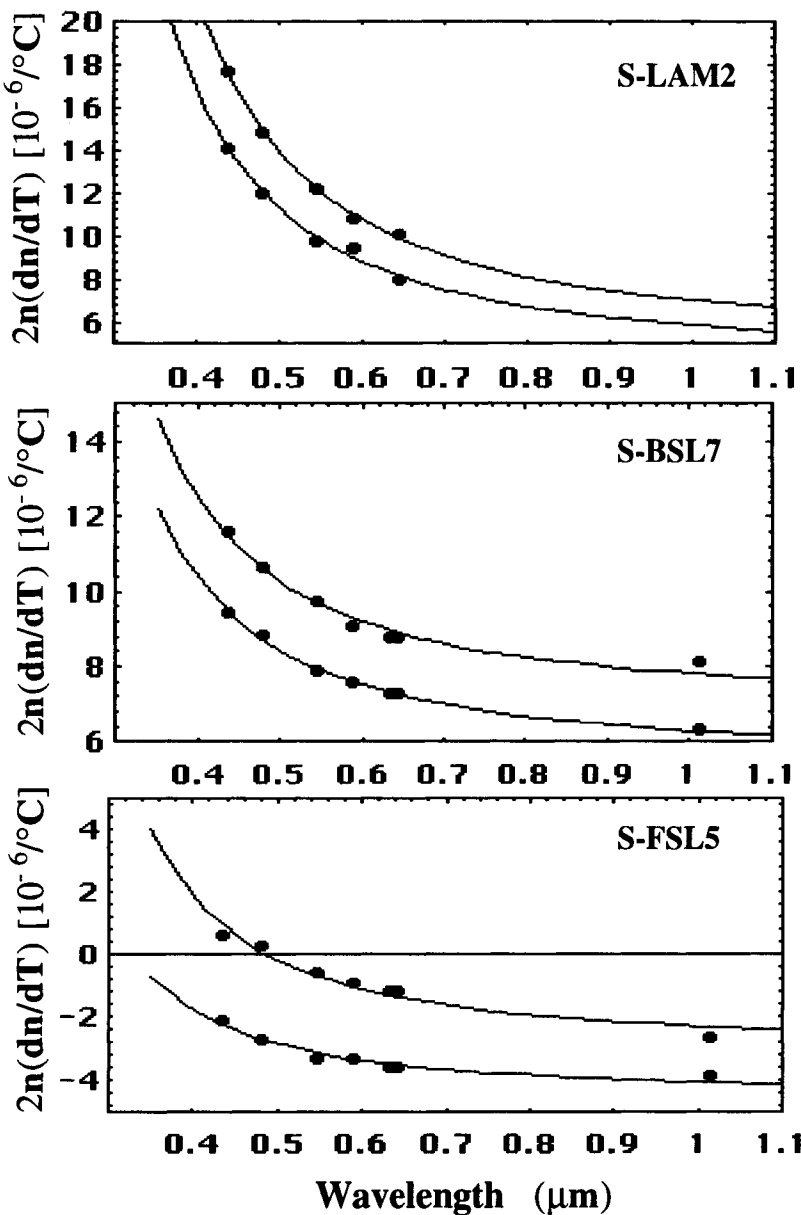


Figure 3.57:  $2n(dn/dT)$  versus wavelength for some Ohara optical glasses: Solid curves, computed values from the optical constants  $G$ ,  $H$ , and  $E_{ig}$  from Table 3.2; solid circles, experimental data; upper and lower curves, 60 and  $-40^{\circ}\text{C}$ , respectively, (after Ref. 156 with permission from OSA).

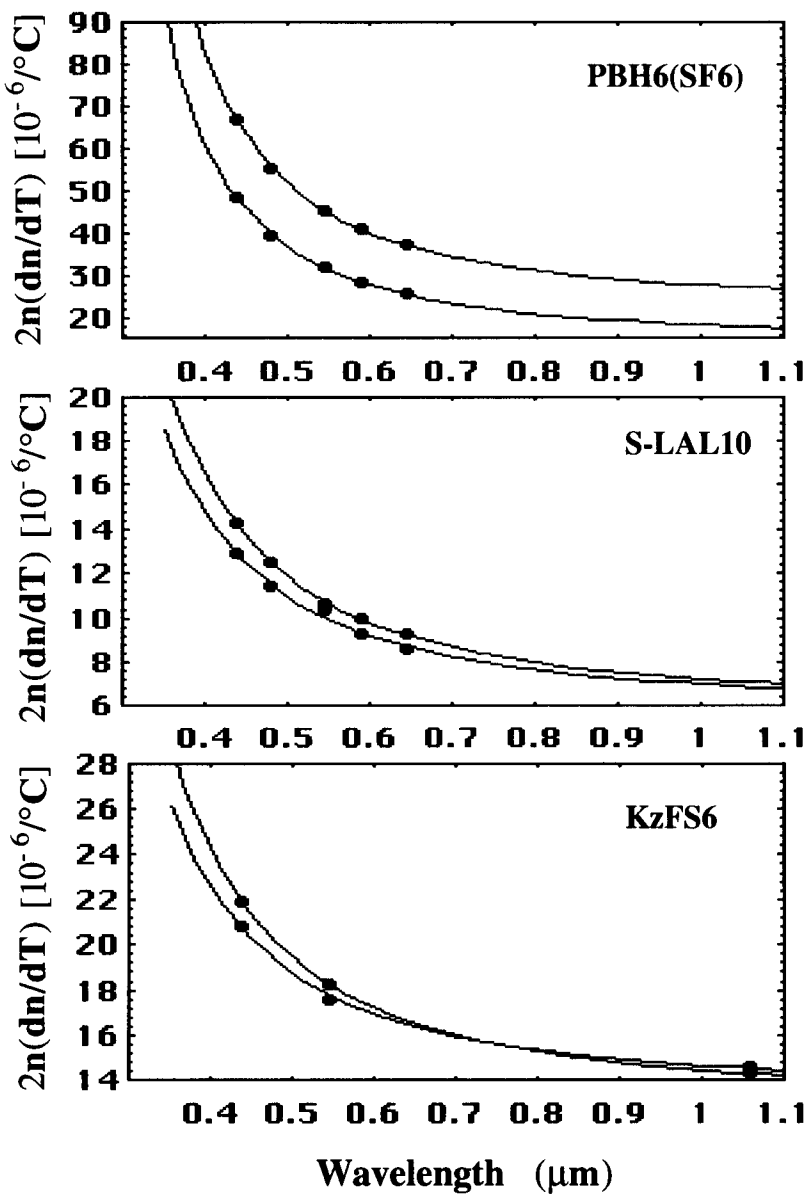


Figure 3.58:  $2n(dn/dT)$  versus wavelength for two Ohara and one Schott optical glasses: Solid curves, computed values from the optical constants,  $G$ ,  $H$ , and  $E_{ig}$  from Table 3.2; solid circles, experimental data; upper and lower curves, 60 and  $-40^{\circ}\text{C}$ , respectively, (after Ref. 156 with permission from OSA).

**Table 3.14: Temperature-Dependent Optical Constant  $H$  for Some Selected Ohara and Schott Optical Glasses**

Glasses		$H(T) = H_0 + H_1 T + H_2 T^2$ , $T$ is in °C		
Ohara	Schott	$H_0$	$H_1 [10^{-2}]$	$H_2 [10^{-4}]$
BAL4	BaLF4	37.96926	1.33955	1.26688
BAL11	BaK1	35.96333	0.55857	4.05643
BAL23	PSK3	31.92441	2.00550	1.30759
BSM4	SK4	35.61982	0.59833	-0.20871
BSM24	SSK4A	38.95158	2.35475	2.08638
NSL5	SK5	29.81815	1.26739	$3.68304 \times 10^{-2}$
S-LAM2	LaF2	46.84894	0.58643	1.25634
S-BSL7	BK7	33.30862	1.61308	-0.72125
S-FSL5	FK5	26.48068	1.37156	1.31022
SLAL10	LaK10	42.12496	$5.19464 \times 10^{-2}$	$-5.58035 \times 10^{-2}$
---	KzFS6	29.89860	-0.25575	1.00625
ZSL1	ZK1	36.19165	1.57533	1.85594
SSL6	---	30.14952	2.84301	1.61696
PBH6	SF6	69.50033	9.33476	-7.01451

indicate that the variation of excitonic band gap with temperature is not linear within the stated temperature region. The variation of  $dE_{eg}/dT$  is almost linear and  $E_{eg}$  is decreasing asymptotically against temperature. The optical constant  $G$ , the fitting gap  $\lambda_{ig}$  from Table 3.2, the room temperature Sellmeier coefficients from Table 2.2, and the constant  $H$  from Eq. (3.61) by using Table 3.14 are used to calculate refractive indices for any wavelength within the transmission region at any operating temperature more accurately. These optical constants can be used to formulate the temperature dependent Sellmeier equations to assess the temperature dependent optical characteristics of these important glasses. The author has developed software to calculate refractive index and thermo-optic coefficients for any wavelength lying within the transmission region of these optical materials.

Therefore, the present model, described in this book, is explaining the dispersion of thermo-optic coefficients of all the optical materials satisfactorily. The previous analyses are useful to characterize many optical systems/devices. The variation of some important optical parameters against temperature, such as to explain the temperature-tuned nonlinear optical devices, variations of zero-dispersion wavelength and chromatic dispersions

with temperature in the optical fiber communication systems, Abbé number, etc. are analyzed and will be discussed in the next chapter.

### 3.5 References

1. F. J. Micheli, Ann. Physik **4**, 7 (1902).
2. W. S. Rodney and I. H. Malitson, J. Opt. Soc. Am. **41**, 956 (1956).
3. I. H. Malitson, Appl. Opt. **2**, 1103 (1963).
4. M. V. Hobden and J. Warner, Phys. Lett. **22**, 243 (1966).
5. R. A. Phillips, J. Opt. Soc. Am. **56**, 629 (1966).
6. J. H. Wray and J. T. Neu, J. Opt. Soc. Am. **59**, 774 (1969).
7. A. Feldman, D. Horowitz, R. M. Waxler, and M. J. Dodge, Nat. Bur. Stand. (U.S.), Tech. Note **993**, (Feb.. 1979).
8. N. P. Barnes, D. J. Gettemy, and R. S. Adhav, J. Opt. Soc. Am. **72**, 895 (1982).
9. G. E. Jellison, Jr. and F. A. Modine, J. Appl. Phys. **76**, 3758 (1994).
10. H. H. Lipson, Y. F. Tsay, B. Bendow, and P. A. Ligor, Appl. Opt. **15**, 2352 (1976).
11. R. J. Harris, G. T. Johnston, G. A. Kepple, P. C. Krok, and H. Mukai, Appl. Opt. **16**, 436 (1977).
12. J. M. Jewell, C. Askins, and I. D. Aggarwal, Appl. Opt. **30**, 3656 (1991).
13. J. A. Stratton, *Electromagnetic Theory* (McGraw-Hill, New York, 1941); E. E. Havinga, J. Phys. Chem. Sol. **18**, 253 (1961).
14. A. J. Bosman and E. E. Havinga, Phys. Rev. **129**, 1593 (1963).
15. L. Prod'homme, Phys. Chem. Glasses **1**, 119 (1960).
16. J. M. Jewell, J. Am. Ceram. Soc. **74**, 1689 (1991).
17. J. M. Jewell, J. Non-Cryst. Solids **146**, 145 (1992).
18. *Ohara Optical Glass Catalog* (OHARA Inc., Kanagawa, 1990; 1995).
19. *Schott Optical Glass Catalog* (Schott Glass Technologies Inc., Duryea, 1992).
20. Y. Tsay, B. Bendow, and S. S. Mitra, Phys. Rev. B **8**, 2688 (1973).
21. G. N. Ramachandran, Proc. Indian Acad. Sci. Sect. A **25**, 375 (1947).
22. G. T. Johnston, Appl. Opt. **16**, 1796 (1977).
23. E. P. Markin and N. N. Sobolev, Opt. Spectrosk. **9**, 587 (1960).
24. S. V. Ivanova, V. S. Gorelik, and B. A. Strukov, Ferroelectrics **21**, 563 (1978).

25. G. Ghosh, IEEE Photon. Technol. Lett. **6**, 431 (1994).
26. G. Ghosh, J. Non-cryst. Solids **189**, 191 (1995).
27. G. Ghosh, Opt. Lett. **19**, 1391 (1994).
28. G. Ghosh, Appl. Phys. Lett. **65**, 3311 (1994).
29. M. Quintero, J. Gonzalez, and J. C. Wooley, J. Appl. Phys. **70**, 1451 (1991).
30. E. Ellis, D. W. Johnson, A. Breeze, P. M. Magee, and P. G. Perkins, Philos. Mag. B **40**, 105 (1979).
31. J. Matsuoka, N. Kitamura, S. Fujinaga, T. Kitaoka, and H. Yamashita, J. Non-Cry. Sol. **135**, 86 (1991).
32. M. W. Zemansky, *Heat and Thermodynamics* (McGraw Hill, New York, 1957), p. 210.
33. G. Ghosh, Japanese Patent 19111996 (1996).
34. G. E. Jellison, Jr. and F. A. Modine, Phys. Rev. B **27**, 7466 (1983).
35. M. Yamazaki and T. Ogawa, J. Opt. Soc. Am. **56**, 1407 (1966).
36. R. Onaka and T. Kawamura, J. Phys. Soc. Jpn. **50**, 3695 (1981).
37. R. Onaka and T. Takeda, J. Phys. Soc. Jpn. **51**, 3258 (1982).
38. G. Ghosh and G. C. Bhar, IEEE J. Quantum Electron. **QE-18**, 143 (1982).
39. W. R. Cook, J. Appl. Phys. **38**, 1637 (1967).
40. K. W. Kirby and L. G. DeShazer, J. Opt. Soc. Am. B **4**, 1072 (1987).
41. F. Zernike, J. Opt. Soc. Am. **54**, 1215 (1964);  
F. Zernike, Errata, J. Opt. Soc. Am. **55**, 210E (1965).
42. *Data Sheet* Nos. **701**, (1983); **702**, (1984); and **707**, (1991) (Quantum Technology Inc., Florida).
43. D. Eimerl, Ferroelectrics **72**, 95 (1987).
44. D. Eimerl, IEEE J. Quantum Electron. **QE-23**, 575 (1987).
45. G. D. Boyd, R. C. Miller, K. Nassau, W. L. Bond, and A. Savage, Appl. Phys. Lett. **5**, 234 (1964).
46. Y. S. Liu, Appl. Phys. Lett. **31**, 187 (1977).
47. M. S. Webb and S. P. Velsko, IEEE J. Quantum Electron. **26**, 1394 (1990).
48. G. D. Boyd, W. L. Bond, and H. L. Carter, J. Appl. Phys. **38**, 1941 (1967).
49. H. Iwasaki, H. Toyoda, and N. Niizeki, Jpn. J. Appl. Phys. **6**, 1101 (1967).
50. D. J. Gettemy, W. C. Harker, G. Lindholm, and N. P. Barnes, IEEE J. Quantum Electron. **24**, 2231 (1988).
51. H. Iwasaki, T. Yamada, N. Niizeki, and H. Toyoda, Jpn. J. Appl. Phys. **7**, 185 (1968).
52. D. S. Smith, H. D. Riccius, and R. P. Edwin, Opt. Commun. **17**, 332 (1976).
53. S. C. Abrahams, H. J. Levinstein, and J. M. Reddy, J. Phys. Chem. Solids **27**, 1019 (1966).

54. Y. V. Burak, K. Y. Borman, and I. S. Girnyk, Sov. Phys. Solid State **26**, 2223(1984).
55. K. Kato, IEEE J. Quantum Electron. **QE-21**, 119 (1985).
56. A. M. Mamedov, M. A. Osman, and L. C. Hajieva, Appl. Phys. A **34**, 189 (1984).
57. H. Iwasaki, H. Toyoda, and H. Kubota, Jpn. J. Appl. Phys. **6**, 1338 (1967).
58. B. Zysset, I. Biaggio, and P. Gunter, J. Opt. Soc. Am. B **9**, 380 (1992).
59. *Technical Catalog*, Optoelectronics Sandoz; KNbO<sub>3</sub> potassium niobate, Sandoz Ltd., CH-4002, Basel, Switzerland.
60. F. M. Michel-Calendini, H. Chermette, and J. Weber, J. Phys. C **13**, 1427 (1980).
61. K. Kato, IEEE J. Quantum Electron. **27**, 1137 (1991); IEEE J. Quantum Electron. **28**, 1974 (1992).
62. G. Ghosh, IEEE Photon. Technol. Lett. **7**, 68 (1995).
63. D. K. T. Chu, J. D. Bierlein, and R. G. Hunsperger, IEEE Trans. Ultrason. Ferroelectr. Frequency Contr. **39**, 683 (1992); *Technical Catalog*, Litton Airtron, Synoptics Group, USA.
64. W. Wiechmann, S. Kubota, T. Fukui, and H. Masuda, Opt. Lett. **18**, 1208 (1993).
65. C. Chen, Y. Wu, A. Jiang, B. Wu, G. You, R. Li; S. Lin, J. Opt. Soc. Am. B **6**, 616 (1989); and S. Lin, Z. Sun, B. Wu, and C. Chen, J. Appl. Phys. **67**, 634 (1990).
66. G. Ghosh, J. Appl. Phys. **78**, 6752 (1995).
67. S. Velsko, M. Webb, L. Davis, and C. Huang, IEEE J. Quantum Electron. **27**, 2182 (1991).
68. L. Wei, D. Guiqing, H. Qingzhen, Z. An, and L. Jingkui, J. Phys. D. Appl. Phys. B **2**, 1073 (1990).
69. R. French, J. Ling, F. Ohuchi, and C. Chen, Phys. Rev. B. **44**, 8496 (1991).
70. K. Kato, IEEE J. Quantum Electron. **30**, 2950 (1994).
71. T. Ukachi, R. Lanr, W. Bosenberg, and C. L. Tang, J. Opt. Soc. Am. B **9**, 1128 (1992).
72. S. Lin, B. Wu, F. Xie, and C. Chen, J. Appl. Phys. **73**, 1029 (1993); Appl. Phys. Lett. **59**, 1541 (1991); **60**, 2032 (1992).
73. C. Chen, B. Wu, A. Jiang, and G. You, Sci. Sinica Ser. B **28**, 235 (1985).
74. K. Kato, IEEE J. Quantum Electron. **QE-22**, 1013 (1986).
75. D. Eimerl, L. Davis, S. Velsko, E. Graham, and A. Zalkin, J. Appl. Phys. **62**, 1968 (1987).
76. D. Eimerl, S. Velsko, L. Davis, F. Wang, G. Loiacono, and G. Kennedy, IEEE J. Quanum Electron. **25**, 179 (1989).

77. G. D. Boyd, E. Buehler, and F. G. Storz, *Appl. Phys. Lett.* **18**, 307 (1971).
78. G. D. Boyd, E. Buehler, F. G. Storz, and J. H. Wernick, *IEEE J. Quantum Electron.* **QE-8**, 419 (1972).
79. G. D. Boyd, H. M. Kasper, and J. H. McFee, *IEEE J. Quantum Electron.* **QE-7**, 563 (1971).
80. G. C. Bhar and G. Ghosh, *Appl. Opt.* **19**, 1029 (1980).
81. G. C. Bhar, D. K. Ghosh, P. S. Ghosh, and D. Schmitt, *Appl. Opt.* **22**, 2492 (1983).
82. L. V. Bodnar and N. S. Orlova, *Phys. Stat. Sol. (a)* **91**, 503 (1985).
83. T. K. Gassmov and V. A. Gadzhiev, *Izv. Akad. Nauk Az. SSSR*, 108 (1976).
84. K. Sato, T. Kawakami, T. Teranishi, T. Kambara, and K. Gondaira, *J. Phys. Soc. Jpn.* **41**, 937 (1976).
85. A. S. Borshchevskii, A. A. Lebedev, I. A. Mal'tseva, K. Ovezov, V. Yu. Rud', and K. Yu. Undalov, *Fiz. Tekh. Poluprovodn.* **9**, 1949 (1975); *Sov. Phys. Semicond.* **9**, 1278 (1976).
86. A. Miller, R. G. Humphreys, and B. Chapman, *J. Phys. Paris Colloq. C3* **36**, 31 (1975).
87. G. Ambrazevicius, G. Babonas, and A. Sileika, *Phys. Stat. Sol. B* **95**, 643 (1979).
88. G. Ambrazevicius and G. Babonas, *Lit. Fiz. Sb.* **18**, 765 (1978); *Sov. Phys. Collect.* **18**, 52 (1978).
89. I. S. Gorban, Ts. A. Krys'kov, M. Tennakun, I. I. Tychina, and M. V. Chukichev, *Fiz. Tekh. Poluprovodn.* **14**, 975 (1980); *Sov. Phys. Semicond.* **14**, 577 (1980).
90. N. Itoh, T. Fujinaga, and T. Nakau, *Jpn. J. Appl. Phys.* **17**, 951 (1978).
91. N. Yamamoto, N. Tohge, and T. Miyauchi, *Jpn. J. Appl. Phys.* **14**, 192 (1975).
92. W. Horig, H. Neumann, E. Reccius, H. Weinert, G. Kuhn, and B. Schumann, *Phys. Stat. Sol. (a)* **51**, 57 (1979).
93. H. Horinaka, N. Yamamoto, and T. Miyauchi, *Jpn. J. Appl. Phys.* **17**, 521 (1978).
94. V. V. Sobolev, *Izv. Akad. Nauk SSSR, Neorg. Mater.* **9**, 1060 (1973); *Inorg. Mater. (USSR) (English Transl.)* **9**, 947 (1973).
95. M. De and S. P. Sengupta, *J. Less Common Met.* **86**, 69 (1982).
96. J. L. Shay, B. Tell, E. Buehler, and J. H. Wernick, *Phys. Rev. Lett.* **30**, 983 (1973).
97. R. G. Humphreys and B. R. Pamplin, *J. Phys. (Paris)* **36**, C3-155 (1975).
98. C. Varea de Alvarez, M. L. Cohen, S. E. Kohn, Y. Petroff, and Y. R. Shen, *Phys. Rev. B* **10**, 5175 (1974).

99. W. J. Tropf, M. E. Thomas, and T. J. Harris, in *Handbook of Optics, II Ed., Properties of Crystals and Glasses*, M. Bass, Ed. (McGraw-Hill, New York, 1995), p.33-67.
100. G. Ghosh, *Appl. Opt.* **23**, 976 (1984).
101. G. C. Bhar, G. Ghosh, and P. Ghosh, *IEEE J. Quantum Electron.* **QE-19**, 779 (1983).
102. B. Ayrault, H. Langlois, M. C. Lecocq-Mayer, and F. Lefin, *Phys. Stat. Sol. (a)* **17**, 665 (1973).
103. W. L. Bond, G. D. Boyd, and H. L. Carter, Jr. *J. Appl. Phys.* **38**, 4090 (1967).
104. G. G. Roberts and R. Zallen, *J. Phys. C* **4**, 1890 (1971).
105. G. B. Abdullaev, L. A. Kulevskii, A. M. Prokhorov, A. D. Savel'ev, E. Yu Salaev, and V. S. Smirnov, *JETP Lett.* **16**, 90 (1972).
106. M. P. Lisitsa, S. A. Boiko, and S. F. Terekhova, *Sov. Phys. Semicond.* **12**, 1249 (1978).
107. G. Antonioli, D. Bianchi, and P. Franzosi, *Appl. Opt.* **18**, 3847 (1979).
108. P. Schmid and I. P. Voitchovsky, *Phys. Stat. Sol. (b)* **65**, 249 (1974).
109. F. D. Feichtner and G. W. Roland, *Appl. Opt.* **11**, 993 (1972).
110. M. D. Ewbank, P. R. Newman, N. L. Mota, S. M. Lee, W. L. Wolfe, A. G. DeBell, and W. A. Harrison, *J. Appl. Phys.* **51**, 3848 (1980).
111. S. Singh, D. A. Draegert, and J. E. Geusic, *Phys. Rev. B* **2**, 2709 (1970).
112. P. A. Franken, A. E. Hill, C. W. Peters, and G. Weinreich, *Phys. Rev. Lett.* **7**, 118 (1961).
113. F. J. Michel, *Ann. Physik* **4**, 772 (1902).
114. C. H. Lange and D. D. Duncan, *SPIE Proc.* **1326**, 71 (1990).
115. K. Vedam, J. L. Kirk, and B. N. N. Achar, *J. Solid State Chem.* **12**, 213 (1975).
116. J. Tappin and M. L. Reily, *J. Opt. Soc. Am. A* **3**, 3610 (1986).
117. H. W. Newkirk, D. K. Smith, and J. S. Kahn, *Am. Mineralogist* **51**, 141 (1966).
118. K. Vedam and P. Hennessey, *J. Opt. Soc. Am.* **65**, 442 (1975).
119. M. J. Dodge, in *Handbook of Laser Science and Technology, Vol. IV, Optical Material; Part 2, Refractive Index*, M. J. Weber, Ed. (CRC Press, Boca Raton, 1986).
120. T. W. Houston, L. F. Johnson, P. Kisiuk, and D. J. Walsh, *J. Opt. Soc. Am.* **53**, 1286 (1963).
121. L. G. DeShazer, S. C. Rand, B. A. Wechsler, in *Handbook of Laser Science and Technology, Vol. IV, Optical Material; Part 2, Laser Crystals*, M. J. Weber, Ed. (CRC Press, Boca Raton, 1986).

122. D. L. Wood, K. Nassau, T. Y. Kometani, and D. L. Nash, *Appl. Opt.* **29**, 604 (1990).
123. R. E. Stephens and I. H. Malitson, *J. Nat. Bur. Stand.* **49**, 249 (1952).
124. T. Radhakrishnan, *Proc. Indian Acad. Sci. A* **33**, 22 (1951).
125. N. Uchida, *Phys. Rev. B* **4**, 3745 (1971).
126. J. R. DeVore, *J. Opt. Soc. Am.* **41**, 416 (1951).
127. D. L. Wood and K. Nassau, *Appl. Opt.* **21**, 2978 (1982).
128. H. H. Li, *J. Phys. Chem. Ref. Data* **5**, 329 (1976).
129. L. W. Tilton, E. K. Plyler, and R. E. Stephens, *J. Opt. Soc. Am.* **40**, 540 (1950).
130. S. S. Ballard, J. S. Browder, and J. F. Ebersole, in *American Institute of Physics Handbook, Refractive Index of Special Crystals and Certain Glasses*, D. E. Gray, Ed. (McGraw-Hill, New York, 1982) p. 6-13.
131. A. Selvarajan, J. L. Swedberg, A. G. DeBell, and W. L. Wolfe, *Appl. Opt.* **16**, 3116 (1979).
132. N. P. Barnes and D. J. Gettemy, *J. Opt. Soc. Am.* **70**, 1244 (1980).
133. G. N. Ramachandran, *Proc. Ind. Acad. Sc. A* **25**, 266 (1947).
134. J. Fontanella, R. L. Johnston, J. H. Colwell, and C. Andeen, *Appl. Opt.* **16**, 2949 (1977).
135. R. Weil and D. Neshmit, *J. Opt. Soc. Am.* **67**, 190 (1977).
136. M. P. Lisitsa, L. F. Gudymenko, V. N. Malinko, and S. F. Terekhova, *Phys. Stat. Sol.* **31**, 389 (1969).
137. N. I. Vitrikhovskii, L. F. Gudymenko, A. F. Mazinchenko, V. N. Malinko, E. V. Pidilisnyi, and S. F. Terekhova, *Ukr. Fiz. Zh.* **12**, 790 (1967).
138. G. C. Bhar, D. C. Hanna, B. Luther-Davies, and R. C. Smith, *Opt. Commun.* **6**, 323 (1972).
139. R. L. Herbst and R. L. Byer, *Appl. Phys. Lett.* **19**, 527 (1971).
140. G. Ghosh, *J. Appl. Phys.* **79**, 9388 (1996).
141. P. M. Amirtharaj and D. G. Seiler, in *Handbook of Optics, 2nd Ed., Vol. 2, Optical Properties of Semiconductors*, M. Bass, Ed. (McGraw-Hill, New York, 1995), p.36.86-36.87.
142. A. G. DeBell, E. L. Dereniak, J. Harvey, J. Nissley, J. Palmer, A. Selvarajan, and W. L. Wolfe, *Appl. Opt.* **18**, 3174 (1979).
143. J. N. Zemel, J. D. Jensen, and R. B. Schoolar, *Phys. Rev. A* **140**, 330 (1965).
144. H. H. Li, *J. Phys. Chem. Ref. Data* **9**, 561 (1980).
145. O. Yavas, N. Do, A. C. Tam, P. T. Leung, W. P. Leung, H. K. Park, C. P. Grigoropoulos, J. Boneberg, and P. Leiderer, *Opt. Lett.* **18**, 540 (1993).

146. G. D. Cody, in *Semiconductors and Semimetals, Vol. 21, Hydrogenated Amorphous Silicon, Part B, Optical Properties*, J. I. Pankove, Ed. (Academic Press, New York, 1984), p. 19-23 and 48-49.
147. G. Ghosh, *Appl. Phys. Lett.* **66**, 3570 (1995).
148. G. E. Jellison, Jr. and H. H. Burke, *J. Appl. Phys.* **60**, 841 (1986).
149. D. F. Edwards, *Handbook of Optical Constants of Solids I*, E. D. Palik, Ed. (Academic Press, New York, 1985), p. 547-569.
150. G. E. Jellison, Jr. and F. A. Modine, *J. Appl. Phys.* **76**, 3758 (1994).
151. H. Kobayashi and Y. Yamaguchi, *Jpn. J. Appl. Phys.* **29**, L2089 (1990).
152. I. H. Malitson, *J. Opt. Soc. Am.* **55**, 1205 (1965).
153. J. M. Jewell, *J. Am. Ceram. Soc.* **76**, 1855 (1993).
154. G. Ghosh, *J. Am. Ceram. Soc.* **78**, 218 (1995).
155. S. Mitachi and T. Miyashita, *Appl. Opt.* **22**, 2419 (1983).
156. G. Ghosh, *Appl. Opt.* **36**, 1540 (1997).

This page intentionally left blank

# Chapter 4

## Applications

The refractive indices of the optical materials such as crystals, semiconductors, and optical fibers have been used to make various kinds of optical systems and devices. The refractive index,  $n$ , of any optical material at any temperature,  $T$ , is related to the following equation

$$n_{o,e}(\lambda, T) = n_{o,e}(\lambda, rt) + \frac{dn_{o,e}(\lambda, T)}{dT} (T - rt), \quad (4.1)$$

where  $T$  is the temperature in degrees centigrade,  $rt$ , is the room temperature,  $n_{o,e}(\lambda, T)$  and  $n_{o,e}(\lambda, rt)$  are the refractive indices at  $T$  and room temperature, respectively, with the corresponding polarizations. Therefore, the Sellmeier coefficients, cited in Tables 2.1-2.3 for refractive indices at room temperature and the Sellmeier coefficients, cited in Tables 3.1-3.2 for thermo-optic coefficients with some special equations for some particular materials, have been used to calculate refractive indices at any operating temperature,  $T$  using Eq. (4.1). The calculated refractive indices are used to assess the presently available optical systems and devices satisfactorily, which are described in this chapter.

### 4.1 Nonlinear Optical Laser Devices

A laser is a fixed-frequency oscillator. However, a tunable or a second harmonic of the fixed-frequency laser of high power is required in several areas of research, such as spectroscopy, semiconductor analysis, photochemistry, optical communications, remote sensing, medical science, etc. Dye

lasers, versatile and efficient sources of tunable radiation for most of the visible spectrum, are available. However, solid state devices are essential to replace tunable dye lasers to avoid the handling of toxic materials and frequent changing of dyes due to their continual photodegradation. In addition, a wider tuning range, especially into the near- and far-IR, is needed. Specifically, laser-diode pumped nonlinear optical devices with some efficient nonlinear crystals will lead into the 21st century.

In 1961, Franken *et al.* [1] established the foundation of nonlinear optics by generating the second harmonic of ruby laser in a quartz crystal. In 1962, Giordmaine [2] and Maker *et al.* [3] proposed and demonstrated a new method, called *phase-matching (PM) technique* for higher conversion of *second harmonic generation (SHG)* by a judicious choice of different refractive indices in anisotropic crystals. In 1965, Giordmaine and Miller [4] built and demonstrated the first tunable *optical parametric oscillator (OPO)*. In the last three decades, the nonlinear optical parametric devices have developed significantly.

The conversion of light wave by SHG, OPO, etc. is possible by *nonlinear optical crystals* in which the refractive index  $n$  is a function of the transmitted electric field vector  $\mathbf{E}$  of the light wave, and can be expressed as

$$n(\mathbf{E}) = n_0 + n_1 \mathbf{E} + n_2 \mathbf{E}^2 + \dots, \quad (4.2)$$

where  $n_0$  is the refractive index in the absence of any electric field, and this value is used in *linear optics*. And  $n_1, n_2$ , and so on are the higher-order coefficients of  $n(\mathbf{E})$ . A dielectric polarization vector  $\mathbf{P}$ , defined as the electric dipole moment per unit volume of the substance, is related to the electric field  $\mathbf{E}$  by the following well-known equation of the medium [5, 6]

$$\mathbf{P}(\mathbf{E}) = \chi(\mathbf{E}) \cdot \mathbf{E} = \chi_0 \cdot \mathbf{E} + \chi_2 \cdot \mathbf{E}^2 + \chi_3 \cdot \mathbf{E}^3 + \dots \quad (4.3)$$

where  $\chi$  is the *dielectric susceptibility*.  $\chi_0$  is the linear susceptibility, and  $\chi_2, \chi_3$  are the *nonlinear susceptibilities* of the medium. These values are related to the linear and nonlinear refractive index as follows

$$\chi_0 \cong \frac{1}{4\pi} (n_0^2 - 1), \quad (4.4)$$

$$\chi_2 \cong \frac{1}{2\pi} n_0 n_1, \quad (4.5)$$

$$\chi_3 \cong \frac{1}{2\pi} n_0 n_2. \quad (4.6)$$

In anisotropic or biaxial crystals, the refractive index values are different along different directions of the propagating light wave inside the crystal.

We are interested in three-wave interactions in nonlinear crystals having  $\chi_2 \neq 0$ . Let two monochromatic light waves with frequencies  $\omega_1$ , and  $\omega_2$  propagate through such crystals, then two new light waves with combination frequencies will be generated. They are the sum frequency  $\omega_3$  and difference frequency  $\omega_4$ , which are simply related as

$$\omega_3 = \omega_2 + \omega_1, \quad (4.7)$$

$$\omega_4 = \omega_2 - \omega_1. \quad (4.8)$$

*Sum frequency generation* (SFG) is normally used for conversion of long-wave radiation, such as to convert CO<sub>2</sub> laser, to short-wave radition, i.e., to near-IR or visible light where efficient detectors are available. *Difference frequency generation* (DFG) is an opposite kind of interaction to convert short-wave radiation into long wave. SHG is a special kind of SFG, in which both input frequencies are the same, say  $\omega_1$ ,

$$\omega_3 = 2\omega_1. \quad (4.9)$$

A generation of higher frequencies is possible with successive SFG and/or SHG interactions. The opposite process of SFG is called OPO. In this case, an intense beam of light wave with frequency  $\omega_3$  generates two light waves with frequencies  $\omega_1$  and  $\omega_2$ .

#### 4.1.1 Noncritically Phase-Matched Second Harmonic Generations

The SHG is the most important device among other nonlinear optical devices (NLODs) in which the fundamental laser produces its harmonic, after propagating through the crystal. But the conversion efficiency depends on the PM condition, i.e., the energy and momentum must be conserved on the value of the nonlinear coefficient of the optical materials. Mathematically, the PM conditions can be written as

$$\omega_1 + \omega_1 = \omega_2, \quad (4.10)$$

$$\mathbf{K}_1 + \mathbf{K}_1 = \mathbf{K}_2, \quad (4.11)$$

where  $\omega_1$ ,  $\mathbf{K}_1$ , and  $\omega_2$ ,  $\mathbf{K}_2$  are the frequencies and propagation vectors for the fundamental and second harmonic, respectively. The Eqs. (4.10) and

(4.11) are the energy and momentum conservation equations, respectively. The momentum mismatch is obtained from Eq. (4.11) as

$$\Delta K(\theta, \lambda, T) = 2\pi \left[ \frac{n_2}{\lambda_2}(\theta, \lambda_2, T) - \frac{n_1}{\lambda_1}(\theta, \lambda_1, T) \right], \quad (4.12)$$

where  $n_1$  and  $n_2$  are the refractive indices for the fundamental and second harmonic, respectively. The propagation constant  $K$  of the electromagnetic wave is related to the refractive index  $n$  of the medium and the frequency  $\omega$  of the wave as  $K = n\omega/c = 2\pi n/\lambda$ . Each wave may be ordinary or extraordinary depending on the type of interaction. The refractive index  $n$  depends on the PM angle  $\theta$  for extraordinary rays by the equation of the index ellipsoid

$$\frac{1}{n_e^2(\theta, \lambda, T)} = \frac{\cos^2 \theta}{n_o^2(\lambda, T)} + \frac{\sin^2 \theta}{n_e^2(\lambda, T)}. \quad (4.13)$$

Therefore, the PM is possible for an angle  $\theta_m$  and temperature  $T_m$  such that  $\Delta K(\theta_m, \lambda, T_m) = 0$ . When the PM angle is  $90^\circ$ , the situation is called *noncritical phase matching* (NCPM). The temperature bandwidth,  $\Delta T$  is an important parameter for SHG. Empirical equations are given by.

$$\Delta T = \frac{2.78345\lambda_1}{2\pi L_c | dn_{1o}/dT - dn_{2e}(\theta)/dT |}, \quad (4.14)$$

for Type-I ( $o + o \Rightarrow e$ ), in a negative uniaxial crystal;

$$\Delta T = \frac{2.78345\lambda_1}{\pi L_c | dn_{1e}(\theta)/dT + dn_{1o}/dT - 2dn_{2e}(\theta)/dT |}, \quad (4.15)$$

for Type-II ( $o + e \Rightarrow e$ ), or III ( $e + o \Rightarrow e$ ), in a negative uniaxial crystal;

$$\Delta T = \frac{2.78345\lambda_1}{2\pi L_c | dn_{1e}(\theta)/dT - dn_{2o}/dT |}, \quad (4.16)$$

for Type-I ( $e + e \Rightarrow o$ ), in a positive uniaxial crystal; and

$$\Delta T = \frac{2.78345\lambda_1}{\pi L_c | dn_{1e}(\theta)/dT + dn_{1o}/dT - 2dn_{2o}/dT |}, \quad (4.17)$$

for Type-II ( $e + o \Rightarrow o$ ), or III ( $o + e \Rightarrow o$ ), in a positive uniaxial crystal, where  $\lambda_1$  is the fundamental wavelength, and  $dn_1/dT$  and  $dn_2/dT$  are the thermo-optic coefficients of the fundamental and second harmonic, respectively, with the respective polarizations as indicated by  $o$  or  $e$  for ordinary and extraordinary waves.  $L_c$  is the length of the crystal. All other symbols have their usual significance.

*Coherence length*,  $L_{coh}$  is an important parameter in NOLD. It is defined by the following equation for non-phase matchable materials

$$L_{coh} = \frac{\lambda_1}{4(n_2 - n_1)}, \quad (4.18)$$

where  $\lambda_1$  is the fundamental wavelength, and  $n_1$  and  $n_2$  represent, respectively, the refractive indices at fundamental and second harmonic wavelengths. In the case of phase matchable materials the corresponding polarizations of the fundamental and second harmonic waves should be taken into account with the PM angle. Since the refractive indices are temperature dependent,  $L_{coh}$  is also temperature dependent. The coherence length for any optical material gives a measure of dispersion. The dispersion is larger near the band edge; it falls nearly to zero near the middle of the transmission range, and it rises again near the infrared cutoff. Therefore, a peak is expected in the characteristic curve of coherence length versus transmission range. The coherence length is the traversed distance over which the desired frequency of electromagnetic wave is generated.

The *walk-off angles* are also important in NOLD. This is due to the birefringence of the anisotropic materials, the ordinary and extraordinary polarized waves, having the same frequency propagate with different velocities along the same propagation direction. Therefore, the ordinary and extraordinary waves of finite size will not overlap completely throughout the length of the nonlinear optical material. The extraordinary wave is a *walk-off* of the axis of the ordinary wave. The angle  $\rho$  is called the walk-off angle and is defined for uniaxial crystals as

$$\tan \rho = 0.5(n_e(\theta)^2)[1/n_e^2 - 1/n_o^2] \sin(2\theta) \quad (4.19)$$

for a propagation angle  $\theta$  with respect to the optic axis. In general,  $\rho$  is of the order of a few degrees for  $\theta = 45^\circ$ . But for NCPM,  $\rho$  is negligibly small. Since  $\rho$  is related to the refractive indices of both polarizations and these refractive indices are temperature-dependent, the *walk-off angle*

is also temperature-dependent. In some cases, the value is not negligibly small. The walk-off has a detrimental effect on NLOD to achieve higher conversion efficiency.

There are many books on nonlinear optics [7, 8]. However, there is no theoretical estimation of the phase-matched temperatures or explanation of temperature-tuning characteristics of various NLODs. As there are no accurate Sellmeier equations to predict the same at different temperatures, the temperature effect has been analyzed in various NLODs by using the previous analyses of refractive indices at room temperature and thermo-optic coefficients for both ordinary and extraordinary polarizations in anisotropic and biaxial crystals.

Conversion of tunable dye laser radiation of the visible spectrum to the coherent tunable UV radiation has been obtained via SHG in the nonlinear crystals ADP and KDP since the beginning of nonlinear optics. *Quantum Technology Inc.* [9], has collected data on the wavelengths that can be phase-matched with NCPM configurations in various KDP isomorphs. NCPM has the advantage of a larger angular acceptance bandwidth and a vanishing walk-off angle. Temperature tuning has an advantage over the angle tuning by phase matching. The angle tuning is very critical and thus requires every time setting of the crystal. On the other hand, only the ambient temperature of the crystal is required to vary to have a temperature-tuned NCPM. These crystals are uniaxial and negative ( $n_o > n_e$ ). Type I NCPM requires that the fundamental beam should be polarized in the XY plane, and furthermore, it should propagate in this plane at an angle of 45° to the XY axis. The generated second harmonic is then polarized along the Z axis. A crystal oven, the temperature of which was controlled by proportional temperature controller, was used to heat the crystals above ambient; a thermoelectric cooler was used down to -20°C. A special cryostat cooled by liquid nitrogen was used for much lower temperatures. A laser-pumped dye laser provided the fundamental radiation. The three dyes used were crystal violet, rhodamine 6G, and sodium fluorescein. A NCPM of the important 1.06 μm transitions to Nd:YAG and Nd:Glass is achieved in two other KDP isomorphs, CDA and CD\*A. CDA phase matches 1.064 μm at 42°C and 1.073 μm at 61°C. CD\*A (99% deuterated) phase matches 1.064 μm at about 110°C depending upon the duration level. The damage threshold of the KDP isomorphs is quite high (about 200-300 MW/cm<sup>2</sup> peak powers), with somewhat higher values for the arsenates than for the

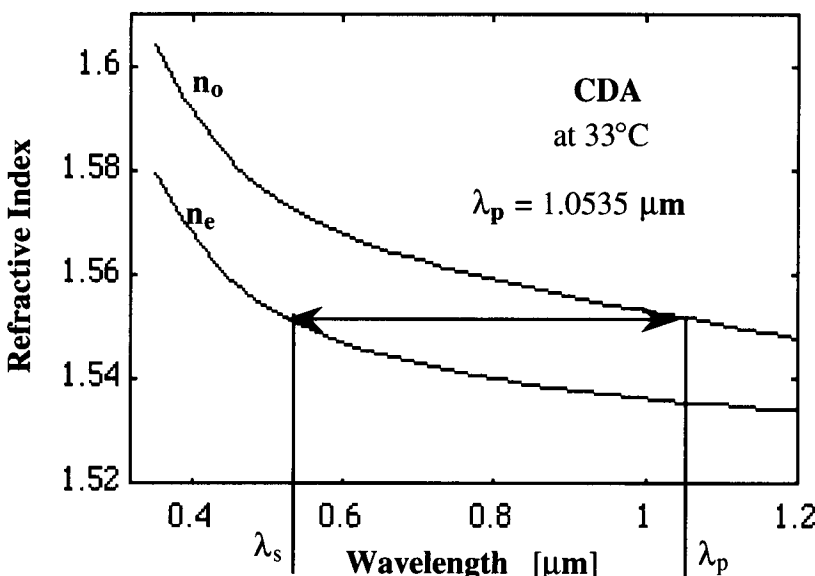


Figure 4.1: The phase matching characteristics of the fundamental and second harmonic waves in a negative uniaxial crystal, CDA at 33°C.

phosphates. Figure 4.1 shows a schematic room-temperature NCPM characteristic in a CDA crystal for SHG of  $1.0535 \mu\text{m}$  laser. At this NCPM temperature, the refractive index ( $n_o$ ) for the pump wavelength is exactly the same as the refractive index ( $n_e$ ) for the second harmonic. There is *no theoretical estimation of these NCPM temperatures*. Here, we have calculated the NCPM temperatures and the temperature bandwidths for several nonlinear interactions for these crystals by using the room temperature Sellmeier equations, Table 2.1 and thermo-optic Sellmeier coefficients, Table 3.1. The temperature bandwidths vary from less than one  $^{\circ}\text{C cm}$  to  $25^{\circ}\text{C cm}$ . The temperature bandwidth is maximum for CDA and CD\*A crystals and is minimum for ADA and ADP crystals. These are shown in Table 4.1 and the agreement is satisfactory within the experimental accuracy of the thermo-optic coefficient and the refractive index measurement.

Figure 4.2 shows the coherence length versus wavelength characteristic curve for ordinary refractive indices of ADP and KDP crystals at 33°C. It exhibits a maximum near  $1.3 \mu\text{m}$  and  $1.42 \mu\text{m}$  for KDP and ADP, respectively. The maximum coherence length in these ferroelectric crystals is of

**Table 4.1: Comparison of the NCPM Temperatures and Temperature-Bandwidths  $\Delta TL_c$  for SHG (Type I) in KDP Isomorphs Crystals**

Crystal	Fundamental Wavelength ( $\mu\text{m}$ )	<u>NCPM Temperatures</u>		<u>Temp. BW(<math>\Delta TL_c</math>)</u>		Ref. for Expt.
		Expt. (°C)	Calculated (°C)	Expt. (°C cm)	Calculated (°C cm)	
ADP	0.510	-30	-31 [Z]	-25	0.41	[9]
	0.525	30	-27 [Z]	30	0.43	[9]
	0.554	120	124 [Z]	123	0.44	[9]
AD*P	0.517	-30		-23	0.43	[9]
	0.532	30		30	0.43	[9]
	0.560	120		120	0.43	[9]
KDP	0.518	20	25 [Z]	20	2.1	[9]
	0.522	100	95 [Z]	90	2.1	[9]
KD*P	0.528	-30	0 [P]	-10	1.8	[9]
	0.531	30	40 [P]	30	1.77 [10]	[9]
	0.538	120	140 [P]	124	2.0	[9]
RDP	0.627	20		50	1.3	[9]
	0.635	80		82	1.3	[9]
ADA	0.568	-30		-25	0.3	[9]
	0.586	30		31	0.35	[9]
	0.619	120		123	0.4	[9]
AD*A	0.578	-15		-14	0.39	[9]
	0.592	30		31	0.41	[9]
	0.625	120		126	0.45	[9]
KDA	0.598	20		18	2.2	[9]
	0.603	100		98	2.2	[9]
RDA	0.679	-10		-25	2.2	[9]
	0.684	20		16	2.2	[9]
	0.695	100		100	2.3	[9]
RD*A	0.695	20		19	1.2	[9]
	0.717	100		105	1.2	[9]
CDA	1.050	20		-20	20.3	[9]
	1.064	42/48		32	21.9	[9]
	1.073	61		61	23.0	[9]
	1.078	100		100	23.7	[9]
CD*A	1.034	20		10	5.8	[9]
	1.062	100		70	6.0	[9]
	1.064	90–112		80	6.0 [11]	[9]

Z- Sellmeier from Zernike's data, P- Sellmeier from Philipps's data; Table 2.1

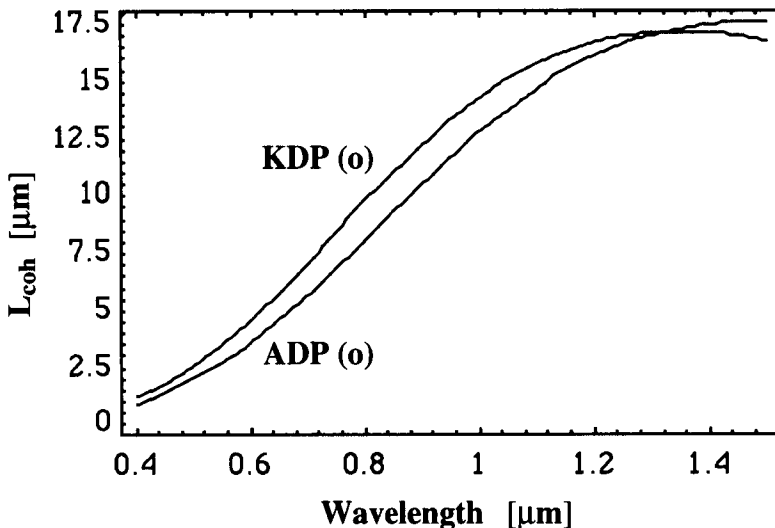


Figure 4.2: Coherence length for second harmonic generation in ADP and KDP crystals (ordinary refractive index at 33°C).

the order of 17  $\mu\text{m}$ , whereas for  $\text{ZnGeP}_2$  this value is 80  $\mu\text{m}$  [65]. This large value for  $\text{ZnGeP}_2$  is due to a wide transmission range and consequent low dispersion. This low value of coherence length in these ferroelectric crystals is due to large dispersion and the narrow transmission region. The variation of coherence length with temperature, i.e.,  $dL_{\text{coh}}/dT$ , is an important parameter. The characteristic curves are shown in Fig.4.3 for ADP and KDP crystals for ordinary refractive indices. Barnes and Piltch [64] calculated the  $dL_{\text{coh}}/dT$  values for  $\text{CdTe}$ . The variation with temperature of the coherence length is very small in ADP and KDP and is almost one fifteenth of the magnitude as that of  $\text{CdTe}$ . The variation of coherence length versus temperature is positive for these ferroelectric crystals because of negative thermo-optic coefficients.  $dL_{\text{coh}}/dT$  is determined by two factors; dispersion ( $n_2 - n_1$ ) and  $(dn_2/dT - dn_1/dT)$ . Both these factors change independently from a large to a lower value as one passes from band edge to the region of transmission cut-off. There is a similar behavior of exhibiting a maximum and a minimum in ADP and KDP to that of  $\text{CdTe}$ . This type of characteristic curve can be calculated from the Sellmeier coefficients as cited in Tables 2.1-2.3 and Tables 3.1-3.2 for any optical material.

There are three types of phase-matched interactions which can lead to a

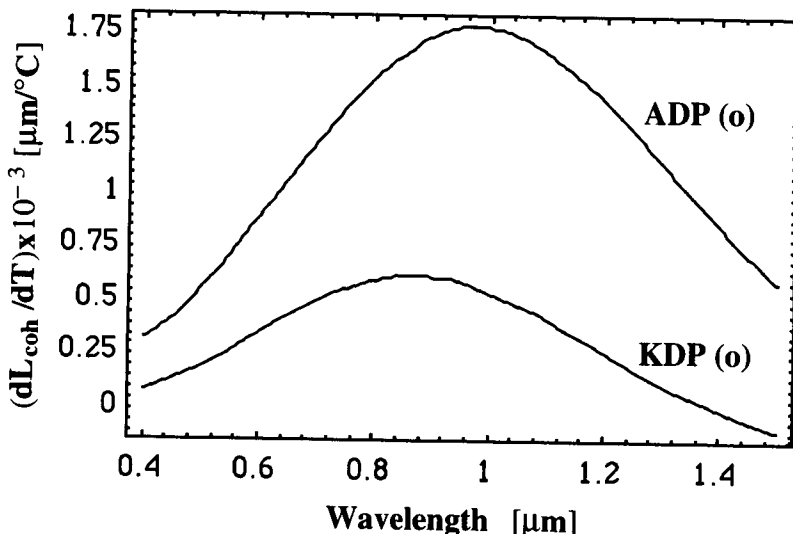


Figure 4.3: Derivative of coherence length with respect to temperature  $dL_{coh}/dT$  versus wavelength in ADP and KDP crystals (ordinary refractive index).

vanishing phase mismatch as denoted by Eimerl *et al.* [12]. Table 4.2 lists the experimental and calculated PM angles for various NLODs in BBO crystal. The calculated PM angles are compared with the other calculated and observed values of Kato [13] and Eimerl *et al.* [12] for various interactions by using 1.064  $\mu\text{m}$  laser and its harmonics. The temperature sensitivities of the PM angles are also calculated by using Sellmeier coefficients in Table 2.1 and optical constants  $G$  and  $H$  in Table 3.1, i.e., with the consideration of dispersion. Eimerl *et al.* [12] calculated the same by using an average, dispersionless values for the thermo-optic coefficients. These values are compared with the experimental data. It is shown that the present work has agreed well between the measured and the computed values for  $\theta$  and  $d\theta/dT$ . Therefore, the dispersion of thermo-optic coefficients, particularly its values at the UV edge, assesses the PM characteristics more accurately.

Recently, LBO crystal is important for various NLODs. NCPM Type-I SHG ( $\theta = 90^\circ$ ,  $\phi = 0^\circ$ ) is useful for a wide range of applications due to its higher conversion efficiency. In this configuration, the fundamental

**Table 4.2: Comparison of the Calculated and Observed PM Angles and Temperature Sensitivities of BBO for Various Parametric Three-Wave Interactions Using a 1.064- $\mu\text{m}$  Laser and its Harmonics**

Interactions	(Type)	PM angle ( $\theta$ ) in degree				$d\theta/dT$ [ $\mu\text{rad}/^\circ\text{C}$ ]		
		Expt.	Expt.	Calc.	Calc.	Calc.	Expt.	Calc.
		[13]	[12]	[12]	[24]	[12]	[12]	[24]
$1\omega + 1\omega$	(I)	22.8	22.7	22.9	22.8	14.1	$9.9 \pm 1$	12.8
	(II)	32.9	32.4	31.9	32.0	20.9	$20.9 \pm 2$	20.5
$1\omega + 2\omega$	(I)	31.3	31.1	31.1	31.2	19.2	$17.3 \pm 1$	19.6
	(II)	38.5	38.4	37.8	38.0	24.1	$26.2 \pm 2$	27.1
	(III)	59.8	58.4	58.9	58.9	50.0	$73.4 \pm 3$	64.0
$2\omega + 2\omega$	(I)	47.5	47.3	47.4	47.4	31.2	$43.7 \pm 1$	38.8
	(II)	81.0	---	82.1	81.6	191.0	---	280.0
$1\omega + 3\omega$	(I)	40.2	---	40.2	40.2	24.3	---	30.2
	(II)	46.6	---	46.1	46.2	28.8	---	39.3
$1\omega + 4\omega$	(I)	51.1	---	51.1	51.1	29.9	---	46.7
	(II)	57.2	---	56.9	56.9	35.2	---	60.0
$2\omega + 3\omega$	(I)	69.3	---	69.4	69.5	65.0	---	100.0

wave is polarized parallel to the Z-axis and is propagated in the XY-plane of the LBO crystal. The temperature-tuned NCPM phase-matched characteristics are explained thoroughly near room temperature by using the room temperature Sellmeier coefficients and the optical constants  $G$  and  $H$ , cited in Table 3.1. At the higher temperature region, however, it is not possible to explain the same. As we have analyzed, most of the semiconductors and nonlinear crystals exhibit the constancy of  $dn/dT$  throughout a small operating temperature region. Such constancies have been observed by Eimerl *et al.* [12] from 20 to 80°C in BBO and by Velsko *et al.* [14] from 16 to 35°C in a LBO crystal. However, the thermo-optic coefficients,  $dn/dT$  are not constant at the higher temperature crystals such as LNO, LTO [15], and KNO [16]. Since the thermal expansion coefficient is not constant along the Y-axis for LBO, the experimentally measured NCPM SHG temperatures, [17-19] for the fundamental wavelengths from 0.95 to 1.31  $\mu\text{m}$ , the Sellmeier coefficients, and the computed optical constants  $G$  and  $H$  at 20°C

are used to calculate the  $G$ 's at these NCPM temperatures. The optical constants  $G$ 's are now expressed as a function of temperature  $T$  and shown below along the Y-axis

$$\begin{aligned} G_y(T) = & \quad 372.170 - 2.199 \times 10^{-1} T + 1.1748 \times 10^{-3} T^2 \\ & - 2.05077 \times 10^{-6} T^3, \end{aligned} \quad (4.20)$$

where  $T$  is the temperature in degree centigrade. It is worthwhile to examine Eq. (4.20) at higher temperatures. As the temperature increases, the value of  $G$  decreases and it corresponds to the shift of the thermal expansion coefficient from more negative to the less negative values. This behavior was observed experimentally [20] in measuring thermal expansion coefficients along the Y-axis of LBO. Again, the NCPM temperatures [18, 19] in the fundamental wavelength region of 1.40 - 1.75  $\mu\text{m}$ , the room temperature Sellmeier coefficients, and the optical constants  $G$  and  $H$  are used to calculate different values of  $H$  along the Z-axis. These values are then expressed as a nonlinear function of temperature  $T$  as

$$\begin{aligned} H_z(T) = & \quad 410.66123 + 1.667 \times 10^{-1} T - 5.1887 \times 10^{-4} T^2 \\ & + 5.56251 \times 10^{-7} T^3. \end{aligned} \quad (4.21)$$

As the temperature rises, the value of  $H_z$  increases for LBO, similar to the characteristics of the LNO crystal [15].

The temperature-tuned NCPM SHG is calculated throughout the transmission region as shown in Fig. 4.4. The bold solid curve is based on this formulation by using Tables 2.1 and 3.1 and Eqs. (2.16), (3.29), (4.1), and (4.20-4.21). The tuning range is varied from 0.95 to 1.75  $\mu\text{m}$  for the fundamental wavelength by changing the temperature from  $-40$  to  $320^\circ\text{C}$ . The solid and dashed curves are made the same by using the other room temperature Sellmeier [14], [21] and the average constant thermo-optic coefficients for the X- and Y-axes, and a wavelength-dependent thermo-optic coefficient for the Z-axis of the LBO crystal as analyzed by Velsko *et al.* [14]. The calculated tuning range is 0.98-1.82  $\mu\text{m}$  for a temperature change from 0 to  $294^\circ\text{C}$ . Both curves are unable to explain the NCPM negative temperatures. We have observed NCPM Type I travelling-wave SHG by using a laser diode having a wavelength of 1.48  $\mu\text{m}$  and an output power of 100 mW in a LBO crystal at  $50^\circ\text{C}$ . Some computed and experimental NCPM temperatures are cited in Table 4.3. The experimental points

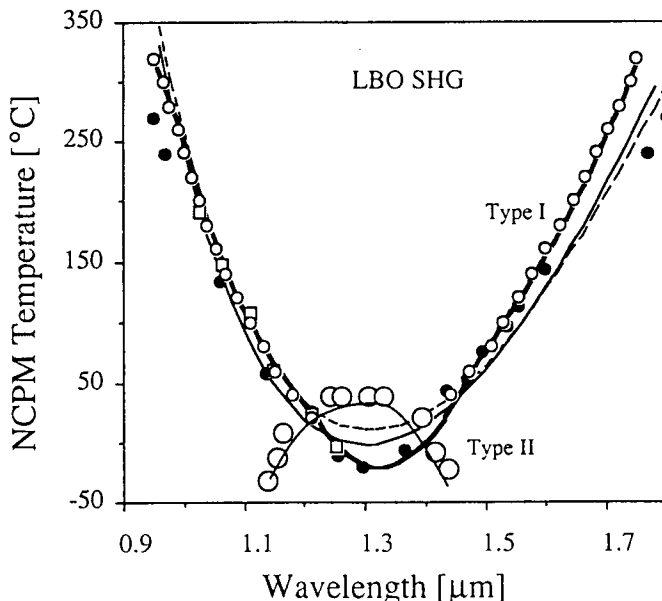


Figure 4.4: The NCPM temperatures versus fundamental wavelengths for Type I and II SHGs in LBO: The bold solid curve is calculated using optical constants in Tables 2.1 and 3.1, and Eqs. (2.16), (4.1), (4.20) and (4.21). The solid and dashed curves are also calculated using the room temperature Sellmeier coefficients of Velsko *et al.* [Ref. 14], Mao *et al.* [Ref. 21], and thermo-optic coefficients of Velsko *et al.* [Ref. 14], respectively. Experimental data are denoted as open circles [Ref. 18], squares [Ref. 17], and solid circles [Ref. 19]; and open circles [Ref. 19] for Type I and II SHGs, respectively, (after Ref. 24 with permission from AIP).

[17-19] are also shown in Fig. 4.4. The computed values based on this dispersion model interpret the experimental values to within  $\pm 4.0^\circ\text{C}$ .

Recently, Gontijo [22] measured the temperature dependence of  $\Delta n$ , i.e., the refractive index difference between the fundamental and second harmonic ( $\Delta n = n_{z,\omega} - n_{y,2\omega}$ ) in a NCPM Type-I configuration of SHG generation by using a 1.064- $\mu\text{m}$  laser. It was found that  $d(\Delta n)/dT$  is dependent on both wavelength and temperature. We have calculated the same at different temperatures and this is shown in Fig. 4.5. The nonlinear equation is written as

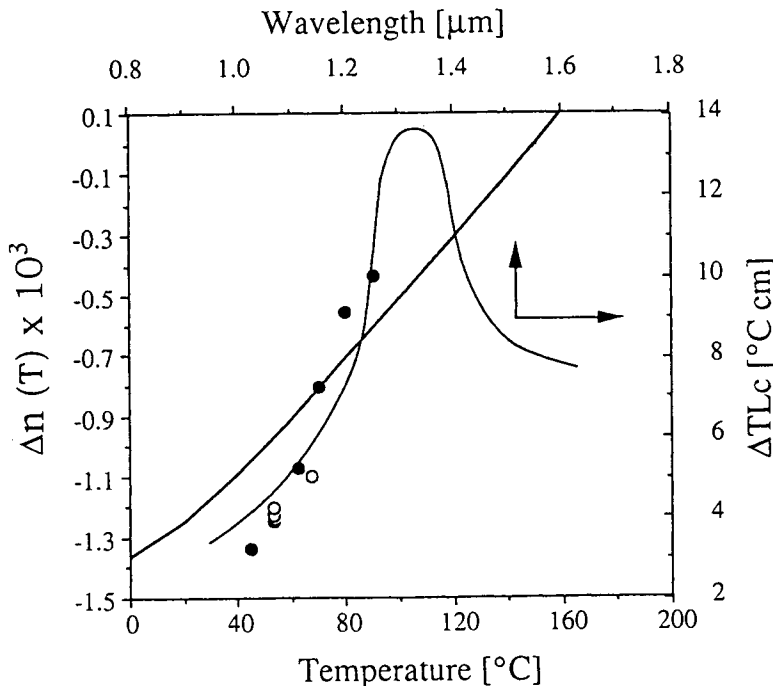


Figure 4.5: The refractive index difference  $\Delta n = n_{z,\omega} - n_{y,2\omega}$  as a function of temperature for a 1.064- $\mu\text{m}$  laser as pump; and temperature bandwidth  $\Delta TL_c$  versus pump wavelength: Experimental data points are described as solid [Ref. 17] and open circles [Ref. 23], (after Ref. 24 with permission from AIP).

$$\begin{aligned}\Delta n(T) &= -1.36245 \times 10^{-3} + 4.64015 \times 10^{-6} T + \\ &\quad 5.84559 \times 10^{-8} T^2 - 1.89162 \times 10^{-10} T^3.\end{aligned}\quad (4.22)$$

This equation is similar to the one derived from the experiment [22]. The calculated NCPM temperature is 148.7°C, whereas the experimental values are 148.5 [22], 148.1 [17], and 149.5°C [23].

In a Type-II NCPM SHG ( $\theta = 0^\circ$ ,  $\phi = 90^\circ$ ) configuration, the fundamental waves are polarized parallel to the X- and Y-axes, and are propagated in the YZ plane of the LBO crystal. The Type-II temperature-tuning curve is also shown in Fig. 4.5 with the experimental points [19] as the

open circles. The calculated retracing wavelength region is slightly narrower than that of the experiment. The calculated retracing points are at  $\lambda = 1.30 \mu\text{m}$ ,  $T = -19.6^\circ\text{C}$ , and at  $\lambda = 1.298 \mu\text{m}$ ,  $T = 32^\circ\text{C}$  for Type-I and Type-II NCPM SHG, respectively. These values are comparable to the experimental values of  $\lambda = 1.31 \mu\text{m}$ ,  $T = -20^\circ\text{C}$ , and  $\lambda = 1.30 \mu\text{m}$ , with  $T = 39^\circ\text{C}$  for the above interactions. As observed by Lin *et al.* [19] it was difficult to determine accurately the NCPM temperatures at the retracing region because of the extremely large temperature bandwidth.

The temperature bandwidths  $\Delta TL_c$  are calculated for different fundamental wavelengths and are shown in Fig. 4.5. Some values are cited in Table 4.3. The solid [17] and open circles [22, 23] are the experimental values. At the retracing region, its values are approximately three-to-four times greater than that of the low wavelength region. This was also observed by Lin *et al.* [17]. It is not possible to explain this particular behavior clearly by using other Sellmeier [19] and the dispersionless thermo-optic coefficients [14]. The experimental values are 3.9 [17], 4.2 [22], and  $4.0^\circ\text{C cm}$  [23] for Type-I NCPM SHG of a  $1.064\text{-}\mu\text{m}$  laser and are comparable to the calculated value of  $4.8^\circ\text{C cm}$ . The above stated temperature-dependent optical devices have been analyzed [24] recently for BBO and LBO crystals.

Webb and Velsko [25] have measured the temperature dependence (between  $23$  and  $65^\circ\text{C}$ ) of the PM angle  $\theta_{\text{pm}}$  for Type-I frequency doubling of a  $1.064\text{-}\mu\text{m}$  laser in LIO crystal. The measured value of  $d\theta_{\text{pm}}/dT$  is  $-14.7 \pm 1 \mu\text{rad}/^\circ\text{C}$ . We have calculated this value to be  $-13.8 \mu\text{rad}/^\circ\text{C}$  from the smoothed thermo-optic coefficients in Table 3.1 and room temperature refractive indices calculated from the Sellmeier coefficients in Table 2.1. Therefore, the optical constants, cited in the Tables 2.1 and 3.1 are applicable to assess any other nonlinear interactions for using this crystal.

Potassium titanyl phosphate, KTP, is an important nonlinear crystal. We have computed [26] both the critical and noncritical temperature phase-matching bandwidths for various three-wave parametric interactions including SHG by using the Sellmeier coefficients, cited in Tables 2.1 and 3.1. The phase-matching temperature bandwidths at NCPM are given by

$$\Delta TL_c = \frac{2\lambda_1}{2.25} \left[ \text{Abs} \left( \frac{dn_1}{dT} + \frac{dn_1}{dT} + \frac{\lambda_1}{\lambda_2} \frac{dn_2}{dT} - \frac{\lambda_1}{\lambda_3} \frac{dn_3}{dT} \right) \right]^{-1}, \quad (4.23)$$

where  $\Delta TL_c$  denotes the temperature bandwidth,  $L_c$  is the crystal length, and  $\lambda_1$ ,  $\lambda_2$ , and  $\lambda_3$  are the fundamental (indices 1, 2) and second-harmonic

**Table 4.3: Comparison of NCPM Temperatures and Temperature-Bandwidths  $\Delta TL_c$  for several SHGs in LBO crystal (after Ref. 24 with permission from AIP)**

Fundamental wavelength ( $\mu\text{m}$ )	(Type)	Experiment		Calculated [24]		[Calculated] <sup>a</sup>		Refs. for expt.
		$T$ ( $^{\circ}\text{C}$ )	$\Delta TL_c$	$T$ ( $^{\circ}\text{C}$ )	$\Delta TL_c$	$T$ ( $^{\circ}\text{C}$ )	$\Delta TL_c$	
1.025	(I)	190.3	3.2	205.9	4.6	196.6	4.8	[17]
1.064	(I)	148.1	3.9	148.7	4.8	136.9	4.9	[17]
1.11	(I)	108.2	5.2	98.8	5.3	83.4	5.1	[17]
1.15	(I)	61.1	7.2	65.3	6.0	48.7	5.2	[17]
1.21	(I)	24.3	9.1	25.3	7.8	15.3	5.4	[17]
1.253	(I)	-2.9	10.0	-1.3	10.6	2.8	5.6	[17]
0.95	(I)	320.0	--	317.5	4.3	355.9	4.5	[18]
1.026	(I)	200.0	--	204.3	4.6	194.9	5.2	[18]
1.181	(I)	40.0	--	43.7	4.6	29.1	5.3	[18]
1.4742	(I)	60.0	--	59.7	13.9	46.2	6.2	[18]
1.6	(I)	160.0	--	158.4	10.2	128.8	6.3	[18]
1.75	(I)	320.0	--	319.1	10.0	264.0	7.1	[18]
1.21	(I)	25.0	--	25.3	10.7	15.3	5.4	[19]
1.295	(I)	-21.4	--	-16.9	11.6	-1.9	5.7	[19]
1.495	(I)	75.0	--	75.3	12.8	57.5	6.3	[19]
1.155	(II)	-12.5	--	-15.0	8.5	-24.3	9.2	[18]
1.2625	(II)	39.1	--	32.0	9.3	27.0	8.6	[19]
1.48	(I)	50.0	8.0	47.5	9.5	49.4	6.2	[24]
1.135	(I)	77.4	4.7	77.2	5.7	60.6	5.2	[23]

$\Delta TL_c$  is in  $^{\circ}\text{C cm}$ .

<sup>a</sup> Calculated data from Sellmeier equation of Mao *et al.* [Ref. 21] and thermo-optic coefficients of Velsko *et al.* [Ref. 14]

**Table 4.4: Calculated and Reported Temperature Phase-Matching Bandwidths for SHG, SFG, and DFG in KTP (after Ref. 26 with permission from IEEE)**

Wavelength ( $\mu\text{m}$ ) [ $1/\lambda_1 + 1/\lambda_2 = 1/\lambda_3$ ]			PM Angle ( $\theta, \phi$ )	$\Delta TL_c$ ( $^{\circ}\text{C cm}$ )			Refs. for Expt.
$\lambda_1$	$\lambda_2$	$\lambda_3$		Calculated Set I	Observed Set II		
0.994 <sup>x</sup>	0.994 <sup>z</sup>	0.497 <sup>x</sup>	(90°, 90°)	173	146	175	[27]
1.0642 <sup>x</sup>	0.8068 <sup>z</sup>	0.4589 <sup>x</sup>	(90°, 90°)	139	112	122	[28]
1.0642 <sup>xy</sup>	1.0642 <sup>z</sup>	0.5321 <sup>xy</sup>	(90°, 23°)	24	26	24	[29], [30]
1.0642 <sup>x</sup>	1.0642 <sup>yz</sup>	0.5321 <sup>x</sup>	(68.6°, 90°)	100	98	100	[30]
1.0796 <sup>y</sup>	1.0796 <sup>z</sup>	0.5398 <sup>y</sup>	(90°, 0°)	20	18	20	[31]
1.3188 <sup>y</sup>	0.6594 <sup>z</sup>	0.4396 <sup>y</sup>	(90°, 0°)	9	8	$8.5 \pm 0.5$	[32]
1.3382 <sup>y</sup>	0.6691 <sup>z</sup>	0.4461 <sup>y</sup>	(90°, 0°)	10	9	$8.5 \pm 0.5$	[32]
1.5791 <sup>zx</sup>	1.0642 <sup>y</sup>	0.6358 <sup>y</sup>	(75.5°, 0°)	30	30	$29.5 \pm 0.5$	[33]
1.6 <sup>zx</sup>	1.54 <sup>y</sup>	0.78 <sup>y</sup>	(52.1°, 0°)	70	43	insensitive	[34]
1.54 <sup>y</sup>	0.78 <sup>zx</sup>	0.52 <sup>y</sup>	(59°, 0°)	52	46	to temp .	[34]

or sum-frequency (index 3) wavelengths. The terms  $dn_1/dT$ ,  $dn_2/dT$ , and  $dn_3/dT$  represent the thermo-optic coefficients for the fundamental and second-harmonic or sum-frequency light components with the crystal orientation taken into consideration. The computed and the experimental values are shown in Table 4.4, which speak for themselves. Wang and Ohtsu [34] have reported a frequency tunable SFG at  $0.52 \mu\text{m}$  and DFG at  $1.6 \mu\text{m}$  by using diode lasers at  $0.78$  and  $1.54 \mu\text{m}$ . An excellent stability against slight deviation from both the PM angle and temperature fluctuation was clearly observed in a series of experiments. This observation is also clearly indicated in this calculation. However, there is no possibility of having a NCPM configuration for this interaction, and ultimately the walk-off effect degrades the conversion efficiency. Since the optical constants explain the existing NLODs, these can be applied to assess any other possible future NLODs.

Potassium niobate, KNO, is well suited for temperature-tuned NCPM Type-I SHG, due to its large temperature dependence [35] of the refractive indices, in particular for  $n_z$  values. These thermo-optic coefficients have recently been analyzed [16]. The fundamental wavelength can be tuned over a large spectral range. Two NCPM Type-I configurations are possi-

**Table 4.5: Calculated and Reported NCPM SHG  
(Type I) Temperatures in KNO Crystal**

$\lambda_p$ ( $\mu\text{m}$ )	Temperatures [ °C ]		
	Measured	Calculated	Refs. for expt.
$\phi = 0^\circ$ [ $n_y/\lambda_p = n_z/\lambda_s$ ]			
0.8385	-34.15	-30.0	[38]
0.8406	-28.3	-26.0	[39]
0.842	-22.75	-20.0	[40]
0.856	15	14	[41]
0.856	15	14	[37]
0.860	20	21	[42]
0.8612	30	29	[37]
0.866	42	40	[37]
0.871	57	55	[43]
0.946	180	177	[42]
0.950	185	180	[44]
$\phi = 90^\circ$ [ $n_x/\lambda_p = n_z/\lambda_s$ ]			
0.982	20	20	[42]
0.986	25	25	[36]
1.064	180/188	188	[45]

ble for SHG. In one scheme, the optical waves are propagating along the X-axis ( $\phi = 0^\circ$ ,  $\theta = 90^\circ$ ) and in another scheme, the optical waves are propagating along the Y-axis ( $\phi = 90^\circ$ ,  $\theta = 0^\circ$ ). In the first case, the fundamental wave is polarized along the Y-axis, and in the second case, the fundamental wave is polarized along the X-axis. Some experimental parameters of temperature-tuned NCPM SHG are reviewed by Biaggio *et al.* [36]. These values agree with very recent experimental values [37] of a frequency doubling of tunable Ti:sapphire laser with KNO crystal in an external cavity and are shown in Table 4.5. The room-temperature Sellmeier coefficients in Table 2.1, the Sellmeier coefficients for thermo-optic coefficients in Table 3.1, and Eqs. (2.16), (3.29) and Eq. (4.1) are used to calculate the PM wavelength as a function of temperature. Because of the uncertainty in the refractive indices of  $\Delta n = \pm 0.00025$ , an error of 1 nm is estimated in fundamental wavelength and 2°C in temperature values. However, the discrepancy between the calculated and experimental values for fundamental wavelengths are noticeably larger than the predicted error. It is difficult to analyze these variations, since in most experimental data,

there is no accuracy in the determination of the crystal temperature. On the other hand, there are different measured fundamental wavelengths in the first scheme at room temperature. By considering this uncertainty in the experiment, the present calculation is sufficient to explain the NCPM wavelengths and temperatures for this crystal. We have also noticed in analyzing the thermo-optic coefficients along the Y-axis, that there is some abnormal behavior of refractive indices at higher temperatures. Therefore, a precise measurement of refractive indexes along the Y-axis can be used to overcome this problem.

Poulin *et al.* [46] reported a travelling wave SHG of a semiconductor distributed-feedback laser of  $1.56\text{ }\mu\text{m}$  at room temperature in a KNO crystal. An output power of  $2.2\text{ nW}$  at  $0.78\text{ }\mu\text{m}$  was obtained by using  $11.3\text{ mW}$  of fundamental power. Since KNO crystal has been used in the autocorrelator to measure the very short pulse width, we [47] have also measured the travelling-wave SHG of a semiconductor laser with fiber pig-tail, having variable output power of maximum  $100\text{ mW}$  and wavelength of  $1.48\text{ }\mu\text{m}$  at room temperature in this crystal. The variation of fundamental laser power versus SHG power is shown in Fig. 4.6 for KNO and LIO crystal. It is clearly observed that the KNO is better than LIO crystal in this region. The inset is the CCD photograph of SHG.

$\text{ZnGeP}_2$  is a suitable nonlinear chalcopyrite crystal for SHG of  $\text{CO}_2$  laser and its harmonic. We found [48] that only Type-I SHG is allowed in the range of  $3.17\text{-}10.32\text{ }\mu\text{m}$  with NCPM at either end at room temperature. The PM angle is insensitive to changes in temperature due to less  $dB/dT$  values. One of the interesting outcomes of temperature-dependence studies is the onset of Type-II SHG at a higher temperature. While the birefringence is not enough for this interaction to occur at room temperature, the positive  $dB/dT$  increases the birefringence at higher temperatures to a value sufficient to compensate for the crystal dispersion. At a temperature of  $275^\circ\text{C}$ , the Type-II SHG appears at a wavelength of  $6.2\text{ }\mu\text{m}$  and continues through to the higher temperatures with a wider range around this wavelength. It is noticed that the PM angles are close to noncritical, which provides, apart from ease of device operation, realization of the maximum effective nonlinear coefficient for this particular case. The possibility of Type-II NCPM SHG near  $5.5\text{ }\mu\text{m}$  is of particular interest for SHG of the CO-laser and the SH of the  $\text{CO}_2$  laser.

Figure 4.7 shows the coherence length versus wavelength-characteristic

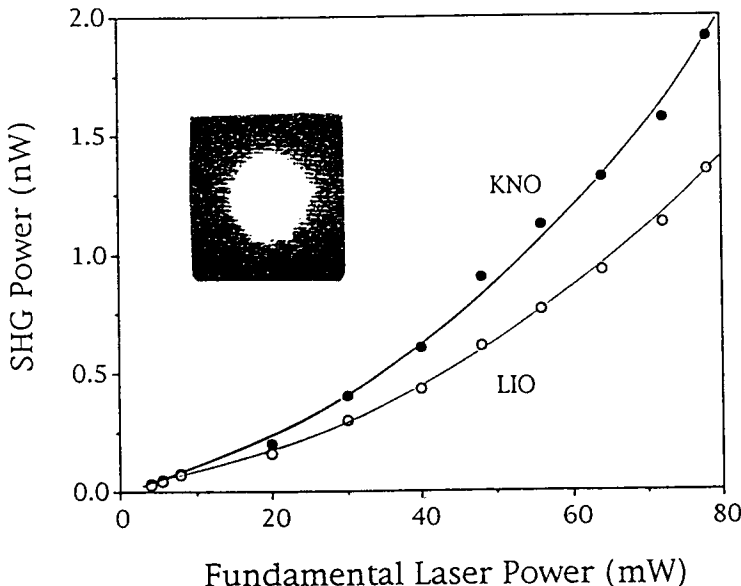


Figure 4.6: Second harmonic power at  $0.74 \mu\text{m}$  as a function of the fundamental power at  $1.48 \mu\text{m}$  in KNO and LIO crystals. Inset is the CCD photograph of SHG in KNO crystal.

curve for extraordinary refractive indices of  $\text{ZnGeP}_2$  at room temperature. It exhibits a maximum near  $7.5 \mu\text{m}$ , whereas similar coherence-length curves show a maximum near  $8 \mu\text{m}$  for  $\text{CdGeP}_2$  and  $6 \mu\text{m}$  for  $\text{CuGaS}_2$ . The maximum coherence length in these chalcopyrite crystals is of the order of  $80 \mu\text{m}$ , whereas for  $\text{CdTe}$ , this value is  $200 \mu\text{m}$  [64]. This large value for  $\text{CdTe}$  is due to a wide transmission range and consequently low dispersion. The experimental values [65-67] of coherence lengths were reported to be  $(66.1 \pm 1)$ ,  $(48.5 \pm 1)$  and  $57.7 \mu\text{m}$  for  $\text{ZnGeP}_2$ ,  $\text{CdGeP}_2$ , and  $\text{CuGaS}_2$ , respectively. We have calculated these values as  $64.3$ ,  $48.3$ , and  $55.7 \mu\text{m}$  from our Sellmeier equations, and therefore, this agrees well with the experimental values. The variation of coherence length with temperature, i.e.,  $dL_{\text{coh}}/dT$ , is an important parameter. Barnes and Piltch [64] calculated the  $dL_{\text{coh}}/dT$  for  $\text{CdTe}$ . The variation of coherence length with temperature is very small in  $\text{ZnGeP}_2$ ,  $\text{CdGeP}_2$ , and  $\text{CuGaS}_2$ , and is almost of the same order of magnitude as that of  $\text{CdTe}$ .  $dL_{\text{coh}}/dT$  is determined by two factors;

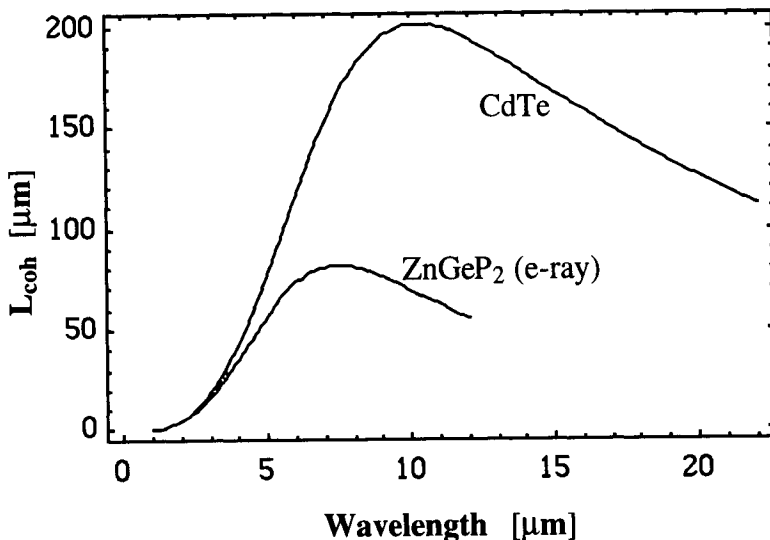


Figure 4.7: Coherence length for SHG in ZnGeP<sub>2</sub> (extraordinary refractive index) and CdTe crystals at room temperature.

dispersion ( $n_2 - n_1$ ) and ( $dn_2/dT - dn_1/dT$ ). Both these factors change independently from a large to a lower value as one passes from band edge to the region of transmission cut-off. A similar nature of exhibiting a maximum and a minimum as in ZnGeP<sub>2</sub> and CuGaS<sub>2</sub> is shown in CdTe. On the other hand, there is a broad maximum in CdGeP<sub>2</sub> at 9  $\mu\text{m}$ . The characteristic behavior of  $dL_{coh}/dT$  in ZnGeP<sub>2</sub> for ordinary refractive indices is shown in Fig. 4.8.

#### 4.1.2 Noncritical Optical Parametric Oscillators

Optical parametric oscillators (OPOs) are suitable devices in NLODs to generate tunable, coherent lasers by using a high pump-power laser and a novel nonlinear material of high optical quality. That means a pump photon of frequency  $\omega_p$  is incident on a nonlinear medium and spontaneously divided into two lower-energy photons. These are called the signal photon of frequency  $\omega_s$  and idler photon of frequency  $\omega_i$ . The energy and momentum must be conserved and are governed by the equations

$$\omega_p = \omega_s + \omega_i, \quad (4.24)$$

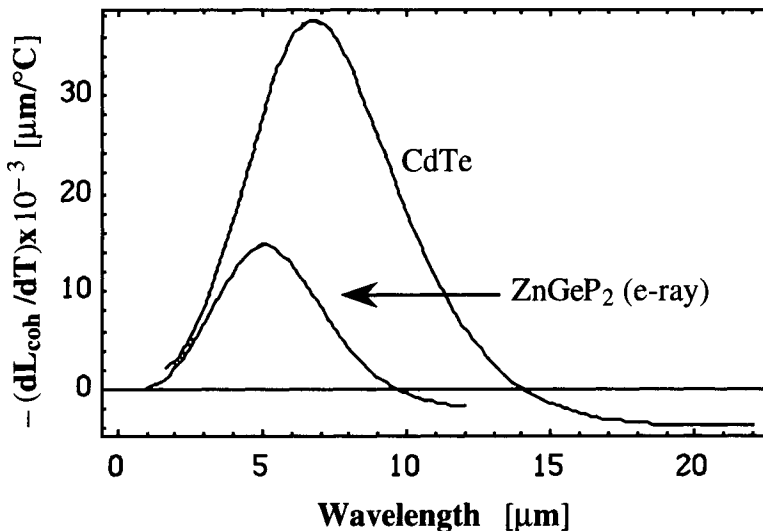


Figure 4.8: Derivative of coherence length with respect to temperature ( $dL_{coh}/dT$ ) versus wavelength for  $ZnGeP_2$  (extraordinary refractive index) and  $CdTe$  crystals.

$$\mathbf{K}_p = \mathbf{K}_s + \mathbf{K}_i. \quad (4.25)$$

A convenient way of achieving OPO is to place the nonlinear crystal inside a resonator. When the optical parametric gain of the resonator exceeds its optical loss, oscillation occurs. The signal and idler waves continue to grow dramatically above the threshold of oscillation, and the characteristic of the output (either a signal or an idler) is similar to that of a laser. At a temperature  $T$ , the momentum mismatch factor  $\Delta K$  for collinear interactions of all three waves can be written as

$$\Delta K(\theta, \lambda, T) = 2\pi \left[ \frac{n_p}{\lambda_p}(\theta, \lambda_p, T) - \frac{n_s}{\lambda_s}(\theta, \lambda_s, T) - \frac{n_i}{\lambda_i}(\theta, \lambda_i, T) \right], \quad (4.26)$$

where  $n_p$ ,  $n_s$ , and  $n_i$  are the refractive indices for the pump, signal, and idler waves, respectively. From the energy conservation Eq. (4.24), the following equation can be rewritten to have the wavelength relation between the pump, signal, and idler

$$\lambda_s = \frac{\lambda_i \lambda_p}{(\lambda_i - \lambda_p)}. \quad (4.27)$$

Tuning is achieved by controlling the refractive index, which is a function of angle and temperature. To compute the tuning curves, the refractive index as a function of temperature as well as wavelength must be known with sufficient accuracy.

A temperature-tuned noncritically PM is possible by using some nonlinear crystals which possess strong temperature dependence on refractive indices with different values along the different optical axes. Here, some temperature-tuned optical devices using the nonlinear crystals, such as ADP, CDA, CD\*A, KD\*P, LBO, LNO, and KNO, have been summarized. ADP is used for a temperature-tuned OPO by pumping with 0.266  $\mu\text{m}$  and varying the crystal temperature from 50 to 110°C. Some experimental results are shown in Table 4.6. CD\*A is a very useful material [11] for OPO in the near-IR, because temperature PM can be achieved at 90° to the optical axis. It can be temperature-tuned [50] from 0.85  $\mu\text{m}$  to 1.45  $\mu\text{m}$ . A temperature-tuning curve is shown in Fig. 4.9. The damage threshold is greater than 300 MW/cm<sup>2</sup>. The calculated values of NCPM temperatures differ with the experimental values. A small change in the measured wavelength and the deuterated level of the crystal effect the calculated values. There is no accuracy of the experimental values. On the other hand, because of the extreme sensitivity of  $d\theta_{\text{pm}}/dT$  to small changes in the  $dn/dT$  values for NCPM Type-I OPO in these ferroelectric crystals, this large discrepancy could be accounted for by relatively small errors in the estimated thermo-optic data. However, the characteristic behaviors agree well with the experimental values.

On the other hand, the LBO crystal is characterized by a high optical damage threshold, wide transmission range, small double refraction angles, and moderate nonlinear coefficients. It has major advantages over BBO for parametric generations, since it possesses a NCPM capability and is temperature-tuned. As a biaxial crystal, LBO also offers several more PM possibilities than BBO. For parametric generations, a phase-matched interaction can be pursued in any of the three principal planes XY, YZ, and XZ, with nonvanishing nonlinear coefficients, where X, Y, and Z refer to the principal axes of the optical indicatrix with  $n_z > n_y > n_x$ .

In the XY plane, the broad temperature-tuning potential is extremely important for Type-I NCPM OPO, ( $e \Rightarrow oo$ ,  $\theta = 90^\circ$ ,  $\phi = 0^\circ$ ). In this configuration, all fields propagate along the crystal X-axis and the polarization of the pump field is parallel to the Y-axis, whereas the polarization of the

**Table 4.6: Comparison of the NCPM Temperatures for Several OPOs in KDP Isomorphs and Other Crystals**

Pump laser ( $\mu\text{m}$ )	Nonlinear crystal	Type of Inter- actions	Expt. Tuning range ( $\mu\text{m}$ )	Conv. eff. (%)	Temp. Variations		Refs. for Expt.
					Expt. ( $^{\circ}\text{C}$ )	Calculated ( $^{\circ}\text{C}$ )	
0.266	ADP	I (eoo)	0.440 – 0.68	10	50 - 110	60 - 104	[49]
0.532	CDA	I (eoo)	0.854 – 1.41	30/60	50 - 70	32 - 100	[50]
0.532	CD*A	I (eoo)	0.850 – 1.45	---	50 - 70	80 - 130	[50]
0.266	KD*P	I (eoo)	0.470 – 0.61	40	40 - 100	44 - 100	[51]
0.266	KD*P	I (eoo)	0.370 – 0.60	20	40 - 100	44 - 150	[52]
0.532	LNO	I (eoo)	0.630 – 3.60	---	50 - 450	50 - 430	[53]
0.532	LNO:MgO	I (eoo)	1.010 – 1.13	7	107 - 110	----	[54]
0.532	LNO	I (eoo)	0.966 – 1.185	---	114 - 127	110 - 122	[55]
0.532	KNO	I ( $x$ axis)	0.860 – 1.40	32	180 - 200	180 - 200	[36]

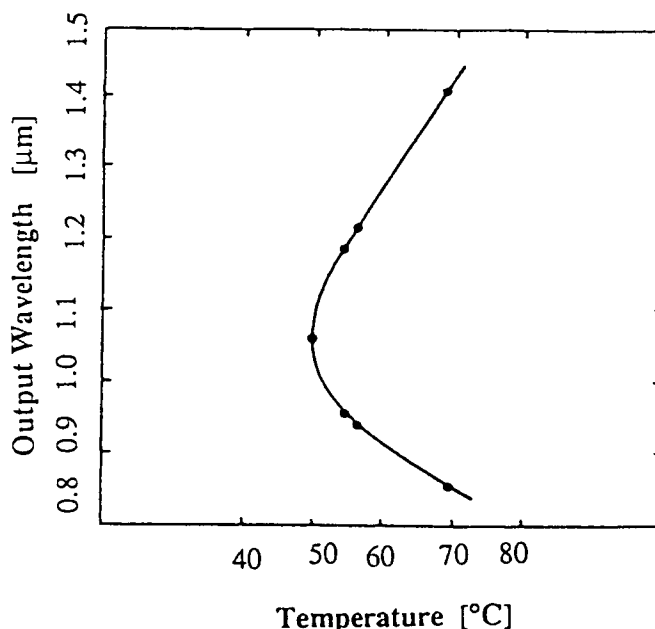


Figure 4.9: Temperature-tuning curve in CD\*A for a pump wavelength of  $0.532\mu\text{m}$ .

signal and idler are parallel to the Z-axis. The signal and idler are generated at the two frequencies  $\omega_s$  and  $\omega_i$  ( $\omega_s + \omega_i = \omega_p$ ) by the pump frequency  $\omega_p$ . Fig. 4.10 shows a temperature-tuning curve for a pump laser having wavelength  $0.605\text{ }\mu\text{m}$  (190 fs pulsed dye laser). Banfi *et al.* [56] tried to explain the experimental data by an empirical  $T$  dependence of  $[n_y(\lambda_p) - n_z(2\lambda_p)]$ , which has no physical significance to verify all other OPOs. The experimental tuning range was  $0.85\text{-}0.97\text{ }\mu\text{m}$  of the signal and  $1.6\text{-}2.1\text{ }\mu\text{m}$  of the idler for a temperature change from 32 to  $85^\circ\text{C}$ . The calculated solid curve based on this model is tunable from  $0.76$  to  $1.21\text{ }\mu\text{m}$  of the signal and from  $1.21$  to  $2.97\text{ }\mu\text{m}$  of the idler, for a temperature change from  $25.3$  to  $248^\circ\text{C}$ . The bold solid curve is based on this model. The dashed curve is based on the Sellmeier coefficients of Mao *et al.* [21], and a dispersionless  $dn/dT$  along X- and Y-axes and a wavelength dependent  $dn/dT$  along the Z-axis [14]. Their calculated values are  $8^\circ\text{C}$  lower at the room temperature and  $26^\circ\text{C}$  higher at the high temperature region in comparison to the present work. Some data are shown in Table 4.7. By considering the experimental accuracy of  $dn_y/dT$  as  $1.0 \times 10^{-6}/^\circ\text{C}$ , the uncertainty of NCPM temperatures are  $\pm 1.0$  to  $\pm 20.0^\circ\text{C}$  at the degenerate point to the other wavelength region.

Ebrahimzadeh *et al.* [57] generated a continuously tunable OPO from  $0.652$  to  $2.65\text{ }\mu\text{m}$  by using a  $0.5235\text{-}\mu\text{m}$  laser as a pump (frequency-doubled, FM mode-locked, Q-switched diode-laser-pumped Nd:YLF laser) for a temperature variation of  $124$  to  $191^\circ\text{C}$ . They calculated a theoretical temperature-tuning curve by using Sellmeier [58] and temperature-dependent index data [14]. There was a discrepancy between the experimental data and the calculated curve, and this was possibly clarified due to the conflicting values of  $dn/dT$ . We have calculated the same tuning curve by using Tables 2.1, 3.1, and Eqs. (2.16), (4.1), (4.20), (4.21), (4.26), and (4.27). The calculated tuning curve is shown as the plus signs, and the experimental points [57] are shown as the open circles in Fig. 4.10. The degenerate NCPM temperature is  $171.9^\circ\text{C}$ . By considering the experimental accuracy of  $dn_y/dT$  to be  $\pm 1.0 \times 10^{-6}/^\circ\text{C}$ , the uncertainty of the NCPM temperature is  $\pm 20.0^\circ\text{C}$  throughout the generated wavelength region. It explains the observed NCPM temperatures. Some computed values are cited in Table 4.8 for comparison.

Lin *et al.* [58] also investigated a Type-I NCPM temperature-tuned OPO by using a pump laser at  $0.532\text{ }\mu\text{m}$ . It was tuned from  $0.65$  to  $2.9\text{ }\mu\text{m}$

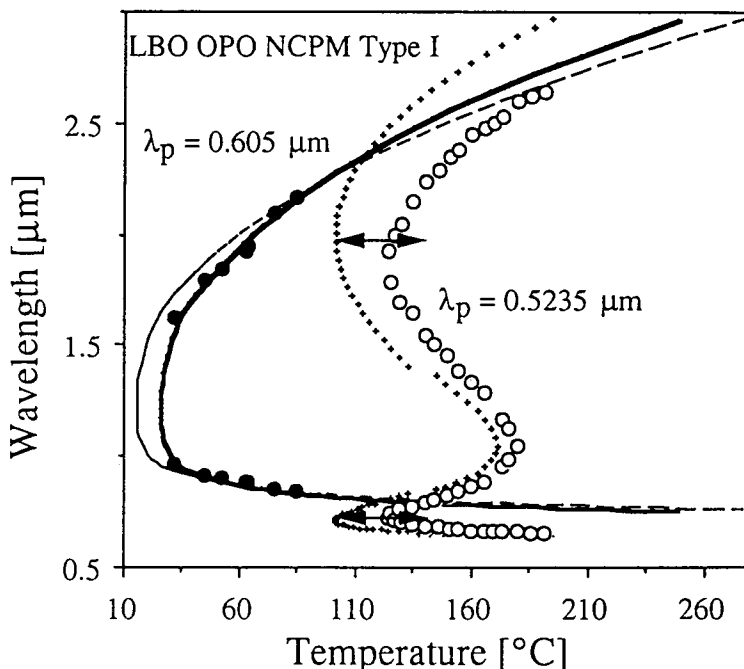


Figure 4.10: The NCPM temperature-tuning characteristics of the LBO OPO, pumped at  $0.605 \mu\text{m}$  and  $0.5235 \mu\text{m}$  in Type-I interaction along the X-axis ( $e \rightarrow oo$ ,  $\theta=90^\circ$ ,  $\phi=0^\circ$ ): Solid and open circles are the data of Banfi *et al.* [Ref. 56] and Ebrahimzadeh *et al.* [Ref. 57], respectively. The calculated dashed tuning curve is plotted using the room temperature Sellmeier equation of Mao *et al.* [Ref. 21] and thermo-optic coefficients of Velsko *et al.* [Ref. 14] for a  $0.605\text{-}\mu\text{m}$  pump. The bold solid and plus curves are calculated tuning ranges using optical constants from Tables 2.1 and 3.1 and Eqs. (2.16), (3.29), (4.1), (4.20), (4.21), (4.26), and (4.27) for  $0.605$  and  $0.5235 \mu\text{m}$ s, respectively, (after Ref. 24 with permission from AIP).

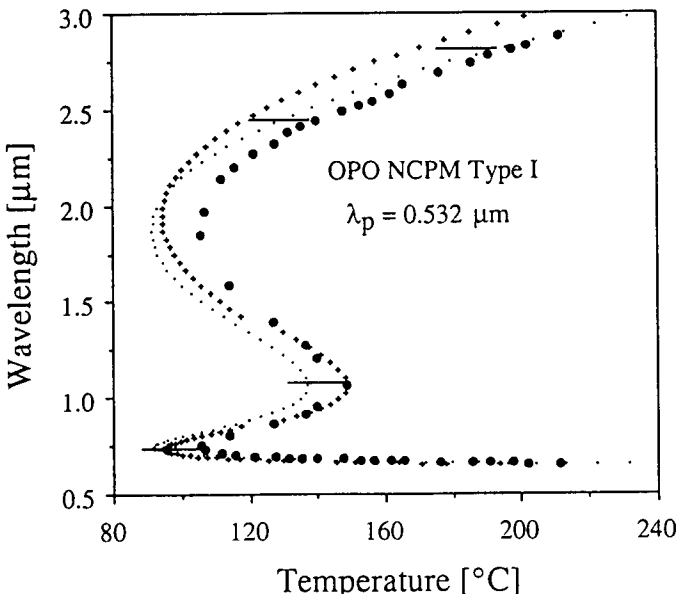


Figure 4.11: The NCPM temperature-tuning range of a LBO OPO, pumped at  $0.532\text{ }\mu\text{m}$  in a Type-I interaction along the X-axis ( $e \rightarrow oo$ ,  $\theta=90^\circ$ ,  $\phi=0^\circ$ ): Dotted and solid plus curves are calculated tuning ranges using the Sellmeier equation of Mao *et al.* [Ref. 21], thermo-optic coefficients of Velsko *et al.* [Ref. 14], and optical constants from Tables 2.1 and 3.1 and Eqs. (2.16), (3.29), (4.1), (4.20), (4.21), (4.26) and (4.27), respectively. The solid circles are the data of Lin *et al.* [Ref. 58] (after Ref. 24 with permission from AIP).

for a temperature variation of 105 to 211°C. The double-valued retracing behavior was observed in the temperature range between 105 and 140°C. A temperature-dependent relation was formulated for  $[n_y(\lambda, T) - n_z(\lambda, T)]$  to verify the experimental tuning range. But this equation is not capable of verifying the other NLODs. Figure 4.11 shows the temperature-tuning behavior from 0.65 to 2.98  $\mu\text{m}$  for this device. The calculated plus curve is based on the optical constants in Tables 2.1, and 3.1, and Eqs. (2.16), (3.29), (4.1), (4.20), (4.21), and (4.26) and (4.27); and it agrees with the experimental data [58] as the solid circles. When considering the experimental accuracy of  $dn_y/dT$  to be  $\pm 1.0 \times 10^{-6}/^\circ\text{C}$ , the uncertainty of the NCPM temperatures are  $\pm 15.0$  to  $\pm 20.0^\circ\text{C}$  at the degenerate point to the other

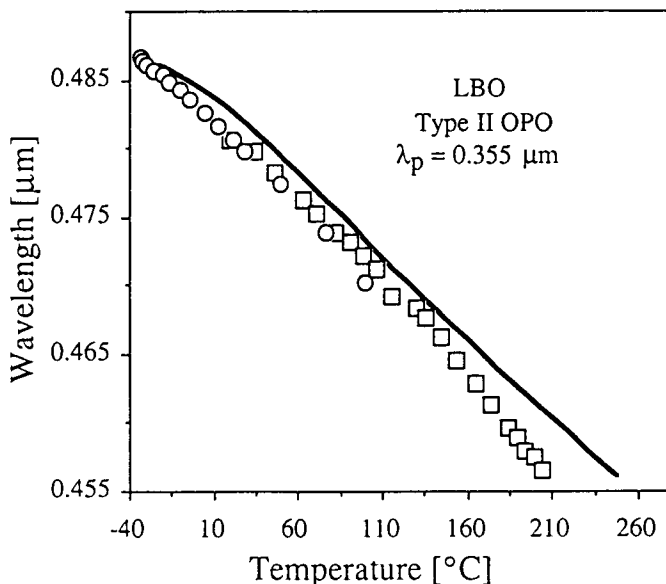


Figure 4.12: The NCPM temperature-tuning range of a signal wave for a LBO OPO, pumped at  $0.355 \mu\text{m}$  in a Type-II interaction along the Z-axis ( $e \rightarrow oe$ ,  $\theta=0^\circ$ ,  $\phi=90^\circ$ ): The solid curve represents the calculated tuning range using constants from Tables 2.1 and 3.1 and Eqs. (2.16), (3.29), (4.1), (4.20), (4.21), (4.26), and (4.27); open circles and squares are the data of Hanson and Dick [Ref. 59], and Cui *et al.* [Ref. 60], respectively, (after Ref. 24 with permission from AIP).

wavelength region. The calculated dotted curve is based on the Sellmeier equation of Mao *et al.* [21] and  $dn/dT$  of Velsko *et al.* [14]. Their calculated temperatures are 6–15°C lower than the experimental values throughout the tuning range.

A Type-II NCPM OPO ( $e \Rightarrow oe$ ,  $\theta = 0^\circ$ ,  $\phi = 90^\circ$ ) was investigated by Hanson and Dick [59] using a  $0.355\text{-}\mu\text{m}$  pump laser and a LBO crystal. In this process, the signal wave is polarized along the Y-axis, the pump and idler waves are polarized along the X-axis, and all waves propagate along the Z-axis of the crystal without walk-off. A tuning was reported for a signal from  $0.470$  to  $0.487 \mu\text{m}$  over the temperature range from  $-35$  to  $100^\circ\text{C}$ . Cui *et al.* [60] obtained a tuning range from  $0.481$  to  $0.457 \mu\text{m}$  for the signal wave, and from  $1.355$  to  $1.59 \mu\text{m}$  for the idler wave for a temper-

**Table 4.7: Comparison of the NCPM Temperatures and Temperature-Bandwidths  $\Delta TL_c$  for SFG and OPOs in LBO Crystal (after Ref. 24 with permission from AIP)**

Fundamental wavelength ( $\mu\text{m}$ )	(Type)	Experiment		Calculated [24]		(Calculated) <sup>a</sup>		Refs. for expt.
		$T$ ( $^\circ\text{C}$ )	$\Delta TL_c$	$T$ ( $^\circ\text{C}$ )	$\Delta TL_c$	$T$ ( $^\circ\text{C}$ )	$\Delta TL_c$	
<b>SFG (1.064 +1.135) (I)</b>								
OPO $\lambda_p=0.532$	(I)	112.0	5.0	109.4	5.3	95.0	4.9	[23]
$\lambda_s = 0.7474$		105.6	---	95.5	4.9	91.3	4.9	[58]
$\lambda_s = 0.6855$		131.3	---	115.0	4.6	120.0	4.9	
$\lambda_s = 0.6525$		211.5	---	185.0	4.5	205.2	4.9	
OPO $\lambda_p=0.5235$	(I)							[57]
$\lambda_s = 1.047$		180.0	---	171.9	4.8	161.3	4.9	
$\lambda_s = 0.7244$		124.0	---	101.6	4.8	101.2	4.9	
$\lambda_s = 0.671$		154.4	---	117.0	4.7	128.4	4.9	
OPO $\lambda_p=0.605$	(I)							[56]
$\lambda_i = 1.62$		31.7	---	32.6	7.8	24.6	5.4	
$\lambda_i = 1.95$		64.2	---	60.2	6.4	52.6	5.4	
$\lambda_i = 2.17$		85.0	---	84.1	5.8	83.7	5.4	
OPO $\lambda_p=0.355$	(II)							[59]
$\lambda_s = 0.4806$		19.5	---	39.1	2.7	17.0	3.6	[60]
$\lambda_s = 0.4711$		106.5	---	121.2	2.4	136.2	3.5	
$\lambda_s = 0.4574$		200.0	---	235.0	2.2	312.0	3.4	
OPO $\lambda_p=0.308$	(II)							[24]
$\lambda_s = 0.386$		---	---	20.9	2.2	3.1	2.9	
$\lambda_s = 0.381$		---	---	96.9	1.9	117.8	2.9	
OPO $\lambda_p=0.266$	(II)							[61]
$\lambda_s = 0.3138$		20.0	--	9.7	1.8	6.5	2.3	
$\lambda_s = 0.3130$		38.0	--	34.4	1.6	40.6	2.3	
$\lambda_s = 0.3116$		68.9	--	72.5	1.5	100.9	2.3	
OPO $\lambda_p=0.5145$	(II)							[62]
$\lambda_s = 0.946$		20.0	---	27.2	5.9	7.5	7.1	
$\lambda_s = 0.938$		31.0	---	45.0	5.5	30.0	7.1	
$\lambda_s = 0.932$		40.0	---	57.5	5.3	46.9	7.1	

<sup>a</sup> Calculated from the Sellmeier equation of Mao *et al.* [Ref. 21] and thermo-optic coefficients of Velsko *et al.* [Ref. 14].  $\Delta TL_c$  is in  $^\circ\text{C cm}$ .

ature change from 20 to 200°C. There was no theoretical analysis of this device. We have calculated the same by using the above-mentioned optical constants in Tables 2.1 and 3.1, and Eqs. (2.16), (3.29), (4.1), (4.20), (4.21), (4.26), and (4.27). It is shown in Fig. 4.12 as the solid curve. The experimental data are shown as the open circles [59] and the open squares [60]. The calculated values are approximately 20°C higher than the experimental values throughout the tuning range, even at room temperature. This discrepancy may be due to the crystal quality or may be due to the accuracy of the actual measurement of the crystal temperature. By considering the experimental accuracy of  $dn_y/dT$  to be  $\pm 1.0 \times 10^{-6}/^\circ\text{C}$ , the uncertainty of the NCPM temperature is  $\pm 6.0 - \pm 12.0^\circ\text{C}$  at the low temperature to the higher temperature region. This explains the experimental values. On the other hand, it is not possible to analyze these experimental data satisfactorily by using the other Sellmeier equations [21] and dispersionless  $dn/dT$  of Velsko *et al.* [14].

Tang *et al.* [61] reported a Type-II NCPM temperature-tuned OPO by using a 0.266- $\mu\text{m}$  pump in a LBO crystal. The temperature tuning was accomplished by changing the temperature from 20 to 70°C to achieve a signal from 0.3138 to 0.3116  $\mu\text{m}$ . There was no theoretical analysis to verify the experimental results. By using the optical constants in Tables 2.1 and 3.1 and Eqs. (2.16), (3.29), (4.1), (4.20), (4.21), (4.26), and (4.27), We have calculated the temperature-tuning behavior which is shown in Fig. 4.13 as the solid curve. The experimental points are marked as the solid circles [61]. All the experimental points are within 10°C of the calculated values. A predicted temperature-tuning curve is also shown in Fig. 4.13 for a 0.308- $\mu\text{m}$  pump. A temperature tuning is possible for a signal from 0.3870 to 0.3802  $\mu\text{m}$  by changing the temperature from 2 to 108°C. The other Sellmeier equation [21] and dispersionless  $dn/dT$  [14] are unable to verify the experimental values as shown in Table 4.7.

Robertson *et al.* [62] observed another Type-II NCPM temperature-tuned OPO by using a single-frequency argon-ion laser as a pump having a wavelength of 0.5145  $\mu\text{m}$ . A tuning range of 14 nm has been observed from 0.946  $\mu\text{m}$  by increasing the temperature from 20 to 40°C. We have calculated the same tuning behavior from optical constants, but the temperature change is required from 27.1 to 57.5°C. If the refractive index of the idler wavelength is decreased by 0.00012 at room temperature, which is within the experimental accuracy, the calculated temperature change is

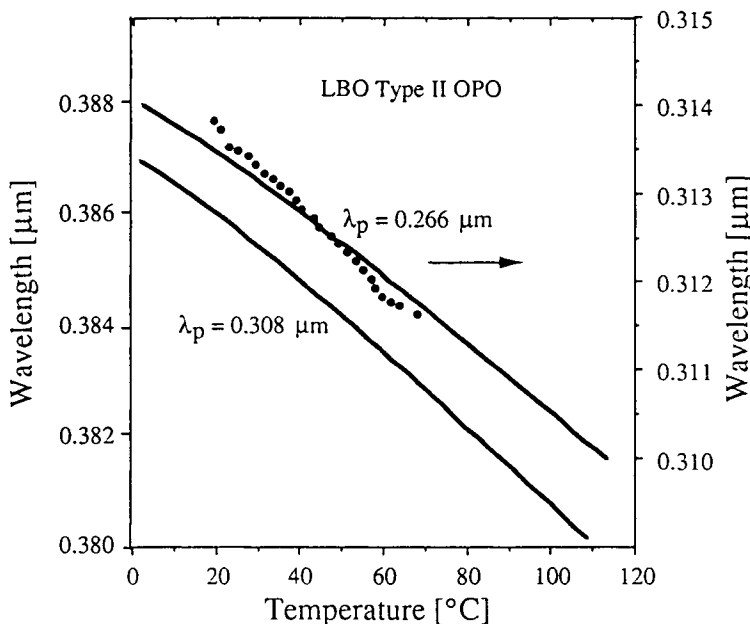


Figure 4.13: The NCPM temperature-tuning characteristics of a signal wave for a LBO OPO, pumped at  $0.266$  and  $0.308\text{ }\mu\text{ms}$  in Type-II interaction along the Z-axis ( $e \rightarrow oe$ ,  $\theta=0^\circ$ ,  $\phi=90^\circ$ ): The solid curves represent the calculated tuning ranges; solid circles are data of Tang *et al.* [Ref. 61] (after Ref. 24 with permission from AIP).

from  $20.3$  to  $46.5^\circ\text{C}$ . Therefore, the presently formulated optical constants satisfactorily agree with the experimental values.

Potassium niobate, KNO crystal, has an excellent chemical stability and is non-hygroscopic. It possesses large thermo-optic coefficients along the X- and Z-axes. Therefore, a temperature-tuned optical parametric oscillator was constructed by Biaggio *et al.* [36], which was similar to that described by Kato [63]. A singularly resonant configuration of the oscillator cavity of  $5\text{ cm}$  long with two flat mirrors has been used. A high quality KNO crystal of dimensions  $X \times Y \times Z = 5.4\text{ mm} \times 13.4\text{ mm} \times 8.3\text{ mm}$  was placed into a temperature-controlled copper oven. The Y faces of the crystal were polished and antireflection coated. The input mirror had a reflectivity  $Rr > 99.5\%$  in the spectral range between  $1.050$  and  $1.150\text{ }\mu\text{m}$ ,

and a transmission higher than 90% at  $0.532\text{ }\mu\text{m}$ . The output mirror had a reflectivity  $Rr = 80\%$  in the spectral range between  $1.050$  and  $1.150\text{ }\mu\text{m}$  with a transmission  $Ts > 90\%$  at  $0.532\text{ }\mu\text{m}$ . A frequency-doubled Q-switched Nd:YAG laser was used as a pump ( $\lambda_p = 0.532\text{ }\mu\text{m}$ ) with a repetition rate of 5 Hz and pulse width of 25 ns. The pump was propagating along Y-axis with polarization parallel to the Z-axis. The generated signal and idler waves were propagated along the same direction with polarizations parallel to the X-axis. The nonlinear-optical coefficient  $d_{113}$  was used for the NCPM interaction. Stable oscillations of both signal and idler waves were observed for a pump-beam intensity of  $10\text{ MW/cm}^2$ . The OPO was tunable in the spectral range from  $0.960\text{ }\mu\text{m}$  for the signal wave to  $1.2\text{ }\mu\text{m}$  for the idler wave by changing the temperature of the crystal from  $188.2$  to  $195.5^\circ\text{C}$ . The schematic temperature-tuning curve based on this model of thermo-optic coefficients for this OPO with the experimental data as open circle [36], is shown in Fig. 4.14. A conversion efficiency of 10% was reported and an intensity ratio of 0.5 between idler and signal waves were measured in the spectral range  $1.13\text{--}0.997\text{ }\mu\text{m}$ .

### 4.1.3 Sum Frequency Generation

Sum frequency generation (SFG) is used for effective conversion of IR-radiation to the visible- or UV-region, where highly sensitive detectors are available. This scheme is used to convert the  $\text{CO}_2$  laser ( $\lambda = 10.6\text{ }\mu\text{m}$ ) into the visible- or near-IR region with a conversion efficiency of 30 to 40% by mixing with dye or Nd:YAG laser as a pump in a nonlinear crystal. Here only the temperature-tuned SFG will be discussed. ADP is useful for a temperature-tuned SFG. The analyses of thermo-optic coefficients are useful to verify the temperature-dependent optical devices, even at the room temperature, to get the information about the temperature stability. Table 4.8 shows some SFG schemes by using ADP and some other nonlinear crystals.

Stickel and Dunning [68] demonstrated a NCPM Type-I SFG of  $0.240\text{--}0.242\text{ }\mu\text{m}$  by mixing the SH of ruby laser and IR-dye laser in a temperature-tuned  $-20$  to  $80^\circ\text{C}$  KDP crystal. Similarly, a NCPM Type-I SFG [69] is obtained by mixing the stimulated Raman Scattering (SRS) of  $1.064\text{ }\mu\text{m}$  with radiation at  $0.220\text{ }\mu\text{m}$ , which is generated by mixing the OPO radiation with SRS Stokes wavelengths produced by the fourth harmonic of Nd:YAG laser in nitrogen atmosphere, i.e., the wavelength of  $0.283\text{ }\mu\text{m}$  in

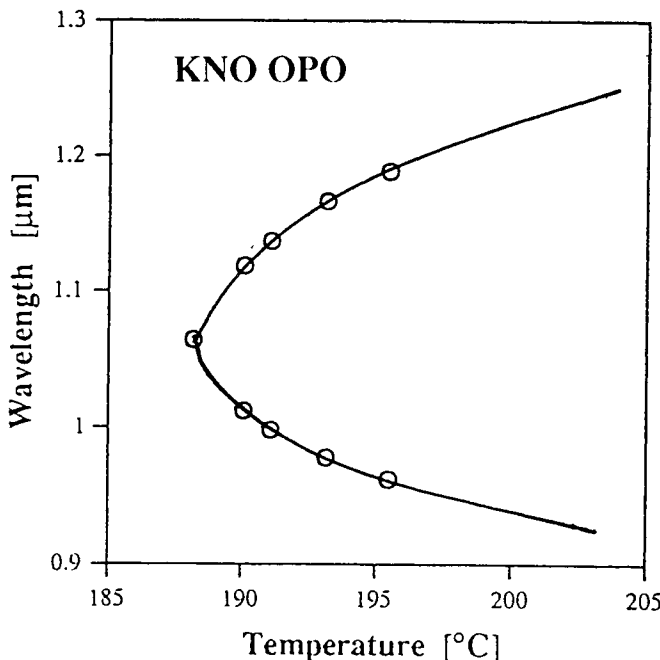


Figure 4.14: The NCPM temperature-tuning range for a KNO OPO, pumped at  $0.532 \mu\text{m}$  in a Type-I interaction along the X-axis ( $e \rightarrow \infty$ ,  $\theta=0^\circ$ ,  $\phi=90^\circ$ ): The solid curve represents a calculated tuning range using constants from Tables 2.1 and 3.1 and Eqs. (2.16), (3.29), (3.38) - (3.40), (4.1), (4.26), and (4.27); open circles are the data of Biaggio *et al.* [Ref. 36].

this crystal. An output energy of  $40 \mu\text{J}$  was generated. ADP crystals have been widely used to make a NCPM temperature-tuned Type-I SFG device. There are various schemes [70-76] for NCPM mixing as shown in Table 4.8. Normally, argon, ruby, and Nd:YAG lasers have been used to mix with various dye lasers to generate high power UV radiation. Massey and Johnson [76] used Nd:YAG laser to mix with the SH of dye laser ( $0.246$ - $0.302 \mu\text{m}$ ) and generated the shortest wavelength of  $0.208 \mu\text{m}$  in ADP crystal. In this scheme, a NCPM Type-I SFG was achieved by keeping the ADP crystal at  $-120^\circ\text{C}$ . The experimental and calculated temperature changes for the same tuning are shown in Table 4.8. It is noticed that the calculated temperatures differ with the experimental values. The calculated values vary sensitively with the generated wavelengths, and there is no experimental

**Table 4.8: Comparison of the NCPM Tuning Ranges for Several SFGs in KDP Isomorphs and Other Crystals**

Interacting lasers $\lambda_p, \lambda_i$ ( $\mu\text{m}$ )	NL crystal	Type of Interactions	Expt. Tuning range ( $\mu\text{m}$ )	Power, energy, CE (%)	Temp. Variations Expt. Calculated for expt.	Refs.
0.3471, dye	KDP I (ooe)		0.240-0.242	1 MW	-20 to 80	-56 to 70 [68]
0.220, 1.39	KDP I (ooe)		0.190	20 $\mu\text{J}$	20	0 [69]
0.477-, dye	ADP I (ooe)		0.252-0.268	8 mW	20	15 [70]
0.3638, dye	ADP I (ooe)		0.243-0.247	4 mW	20	14 [71]
0.351, dye	ADP I (ooe)		0.243	0.3 mW	8	5 [72]
0.4131, dye	ADP I (ooe)		0.2475	---	-103	-58 [73]
0.3471, dye	ADP I (ooe)		0.240-0.248	1 MW	-20 to 80	-21 to 74 [68]
0.532, dye	ADP I (ooe)		0.246-0.249	3 $\mu\text{J}$	-120 to 0	-103 to -78 [74]
1.064, SH dye	ADP I (ooe)		0.222-0.235	10%	-120 to 0	24 to 94.5 [75]
1.064, SH dye	ADP I (ooe)		0.208-0.214	1.7 $\mu\text{J}$	-120 to 0	-61 to -24 [76]
THG of 0.586	BBO I (ooe)		0.1953	5%	-178	-183.5 [77]
0.5145, 2.7-4.5	LNO I (ooe)		0.43-0.46	---	180-400	175-380 [78]
0.6764, 1.064	KNO I (ooe)		0.4136	0.1 mW	-4	-6 [79]
0.6943, 1.064	KNO I (ooe)		0.4201	7.9 W	27.2	28.0 [79]
0.19, 1.9	LBO I(CPM)		0.1727	~50 nJ	200	190 [80]

accuracy on the measured wavelengths. Due to the extreme sensitivity of  $d\theta_{\text{pm}}/dT$  to small changes in the  $dn/dT$  values, particularly at the band edge region for NCPM Type-I SFG, this large discrepancy could be accounted for by relatively small errors in the extrapolated thermo-optic coefficients.

A SFG Type-I scheme has been used by Lokai *et al.* [77] to generate the shortest wavelength of  $0.1953 \mu\text{m}$  in a BBO crystal at  $-178^\circ\text{C}$  by mixing the unpolarized output of an excimer laser-pumped dye laser,  $0.586 \mu\text{m}$  with its second harmonic. The calculated temperature is  $-183.5^\circ\text{C}$  and agrees well with the experimental value. Similarly, a temperature-tuned, NCPM Type-I SFG was demonstrated by Abbas *et al.* [78] by using a LNO crystal. They used an intense cw argon-ion laser as a pump to mix with the IR-radiation from  $2.7$  to  $4.5 \mu\text{m}$  in a phase-matched condition by varying the crystal temperature from  $180$  to  $400^\circ\text{C}$ . The generated signal is

tuned from 0.43 to 0.46  $\mu\text{m}$ . The present theoretical model on thermo-optic coefficients explains these experimental parameters with the consideration of the uncertainties in measuring refractive indices.

Baumert and Gunter [79] used a KNO crystal for NCPM Type-I SFG of a cw Nd:YAG laser (1.064  $\mu\text{m}$ ) of power 2.1 W with the pump radiation of krypton laser (0.6764  $\mu\text{m}$ ) of power 26.2 mW at a temperature of  $-4^\circ\text{C}$ . The generated signal wavelength is 0.4136  $\mu\text{m}$  and the power was over 0.1 mW. They also used a Q-switched ruby laser having peak power of 20 kW to mix with the Nd:YAG laser to generate a signal of wavelength 0.4201  $\mu\text{m}$  at  $27.2^\circ\text{C}$ . The present model is capable of explaining the NCPM temperatures.

Recently, Seifert *et al.* [80] have demonstrated the generation of tunable femtosecond pulses as low as 0.1727  $\mu\text{m}$  by a phase-matched ( $\theta = 90^\circ$ ,  $\phi = 73^\circ$ ) SFG in a LBO crystal. They used a commercial tunable fs Ti:sapphire laser having wavelength 0.760 to 0.815  $\mu\text{m}$  as a pump. The idler pulse (1.9  $\mu\text{m}$ ) is mixed with the fourth harmonic of 0.760- $\mu\text{m}$  pump in a LBO crystal which was kept at  $200^\circ\text{C}$  to produce a VUV pulse at 0.1727  $\mu\text{m}$ . Our calculated phase-matched temperature agrees well with this experiment.

## 4.2 Optical-Fiber Communication Systems

Silica glass (  $\text{SiO}_2$  ) is the basic optical-fiber material, and it has been extensively used to make various kinds of optical fibers [81], amplifiers [82], and fiber lasers [83] with suitable doping materials since the late 1960s. Fiber lasers and amplifiers are the first step to replace the older electronic regenerators/repeaters and to lead into the all-optical, complete photonics age in the future.

The refractive index, its dispersion, chromatic dispersion, and its variation as a function of temperature are important characteristics of the silica-based glasses, which are necessary for the evaluation of optical fiber transmission system designs using such glasses made with optical fibers. In general, they are measured at discrete wavelengths in the transmission range of the glasses, and their interpolation/extrapolation technique is state-of-the-art. A knowledge of the refractive index as a function of temperature is necessary to evaluate chromatic dispersion at different temperatures because it plays a vital role in the optical fiber communication system.

In Chapter Two, the room temperature refractive indices are fitted in a

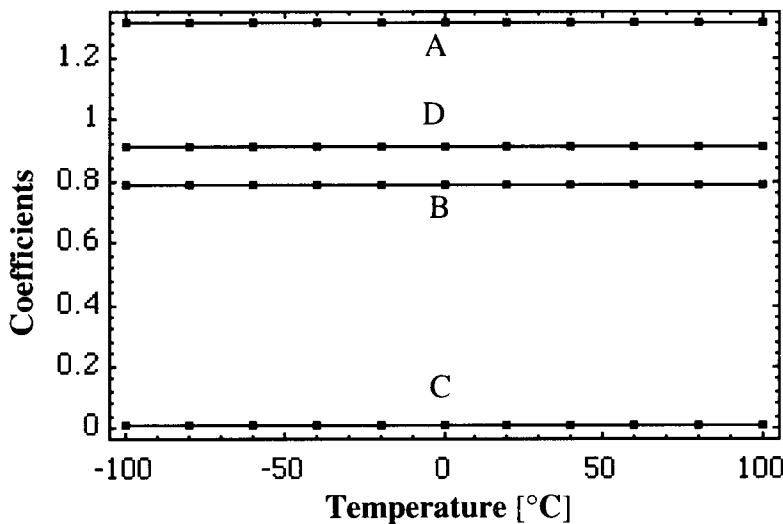


Figure 4.15: A typical plot of the temperature-dependent Sellmeier coefficients (*A*, *B*, *C*, *D*) for SiO<sub>2</sub> glass (after Ref. 85 with permission from IEEE).

two-pole Sellmeier formula for three kinds of silica glasses-SiO<sub>2</sub>, aluminosilicate, and Vycor glasses [84]. Here, we arrive at relations of Sellmeier coefficients using temperature and smoothed thermo-optic coefficients, which are evaluated in Chapter Three. Two other aspects are also considered from the temperature-dependent Sellmeier coefficients [85] viz. chromatic dispersion and zero dispersion wavelengths at different temperatures, and are compared with the experimental values.

The Sellmeier coefficients at any temperature *T* are computed from the room temperature Sellmeier equation and the smoothed  $dn/dT$  values by calculating refractive indices from Eq. [4.1]. We have evaluated the Sellmeier coefficients from the calculated refractive indices of SiO<sub>2</sub>, aluminosilicate, and Vycor glasses from -100°C to 100°C at 20°C intervals. All these Sellmeier constants (*S*) are then separately plotted against temperature. Strangely enough, all are found to fit nicely into straight lines. A typical plot of the coefficients for the fused silica is shown in Fig. 4.15. Constants of the straight lines are obtained by least-square analysis of the data and are shown in Table 4.9. These optical constants are used to calculate refractive indices at any operating temperature.

**Table 4.9: The Linear Fitted Constants ( $m$  = Slope,  $c_1$  = Intercept), of the Least Squares Analyses of the Temperature-Dependent Sellmeier Coefficients ( $S$ ) of FS, AS, and V Glasses (after Ref. 85 with permission from IEEE)**

Sellmeier ( $S$ ) Coefficients	Fitted Constants	Fused Silica (FS) $\text{SiO}_2$	Alumino Silicate (AS)	Vycor Glass (V)
$A$	$m \times 10^6$	6.90754	24.95380	45.70720
	$c_1$	1.31552	1.41294	1.27409
$B$	$m \times 10^5$	2.35835	-0.11466	-1.47194
	$c_1 \times 10$	7.88404	9.50465	8.27657
$C$	$m \times 10^7$	5.84758	12.24700	12.35900
	$c_1 \times 100$	1.10199	1.32143	1.06179
$D$	$m \times 10^7$	5.48368	11.60740	12.58560
	$c_1$	0.91316	0.90443	0.93839
$E$	--	100.0	100.0	100.0

( $S = mT + c_1$ ,  $T$  is the temperature in degree centigrade)

#### 4.2.1 Chromatic Dispersion and Zero-Dispersion Wavelength

Chromatic dispersion plays an important role in an optical fiber communication system, manifested through the wavelength dependence of the refractive index  $n(\lambda)$  as in Eq. (2.16) by the following relation

$$V(\lambda) = -\frac{\lambda}{c} \frac{d^2 n(\lambda)}{d\lambda^2}, \quad (4.28)$$

and

$$\begin{aligned} V(\lambda) &= 1/(cn)[-4/\lambda^5 \{BC^2/(1-C/\lambda^2)^3 + DE^2/(1-E/\lambda^2)^3\} \\ &\quad + \lambda(dn/d\lambda)^2 + 3n(dn/d\lambda)], \end{aligned} \quad (4.29)$$

where

$$dn/d\lambda = -1/(n\lambda^3)[BC/(1-C/\lambda^2)^2 + DE/(1-E/\lambda^2)^2], \quad (4.30)$$

and  $c$  is the speed of light.

Chromatic dispersions are computed for these glasses at different temperatures by using the temperature-dependent Sellmeier coefficients and

are shown in Fig.4.16 for  $\text{SiO}_2$  and alumino-silicate glasses at 26°C. The dispersion characteristics are not linear for the whole spectral region. The temperature dependence of chromatic dispersion at 1.53  $\mu\text{m}$  is computed for  $\text{SiO}_2$  glass and it is  $-1.5 \times 10^{-3} \text{ ps}/(\text{nm}\cdot\text{km}\cdot\text{K})$ . This value is exactly the same as that of experimental one [86]. The wavelength at which the chromatic dispersion is zero is called the zero-dispersion wavelength and is denoted as  $\lambda_0$ . The dispersion behavior near the zero dispersion wavelength is shown in Fig. 4.17 for Vycor glass at -100°C and 100°C, respectively. The dependency is almost linear as shown. The zero-dispersion wavelengths are also computed for these glasses at different temperatures. The zero-dispersion wavelengths are 1.273, 1.393, and 1.265  $\mu\text{m}$  at 26°C for  $\text{SiO}_2$ , aluminosilicate, and Vycor glasses, respectively. Interestingly, the temperature dependency of zero-dispersion wavelength is linear and  $d\lambda_0/dT$  is 0.025 nm/K for  $\text{SiO}_2$ . This study agrees well with the experimental [86] values of  $0.029 \pm 0.004 \text{ nm/K}$  and  $0.031 \pm 0.004 \text{ nm/K}$  for two dispersion-shifted optical fibers within the experimental accuracy.  $d\lambda_0/dT$  is 0.03 nm/K for both aluminosilicate and Vycor glasses. Zero-dispersion wavelength as a function of temperature  $T$  is shown in Fig. 4.18 for  $\text{SiO}_2$  glass. This analysis implies that  $d\lambda_0/dT$  is dominated by the material of the core-glass of the optical fiber instead of the optical fiber design. This is one of the fundamental optical properties of the glass itself.

The Ohara and Schott optical glasses [87-88] are useful in many optical and opto-electronic studies. The room-temperature Sellmeier coefficients [89] as cited in Table 2.2 can be used to faithfully interpolate and extrapolate the refractive indices beyond the measured wavelength region. The Abbé number ( $\nu_d$ ) is calculated from

$$\nu_d = (n_d - 1)/(n_f - n_c), \quad (4.31)$$

where  $n_f$ ,  $n_d$  and  $n_c$  represent refractive indices at wavelengths 0.4861, 0.5876, and 0.6563  $\mu\text{m}$ , respectively. The Abbé numbers of these optical glasses lie between 50 to 70 as shown in Table 4.10 for some selected Schott and Ohara optical glasses. The material chromatic dispersions ( $V$ ) of these glasses also play a vital role in the optical communication systems, femtosecond technology, and other optical devices. They are shown through the wavelength dependence of the refractive index as shown in Eq. (4.28). Chromatic dispersions [89] are calculated for these glasses by using Sellmeier coefficients of Table 2.2 and are shown in Fig. 4.19 from the 0.7

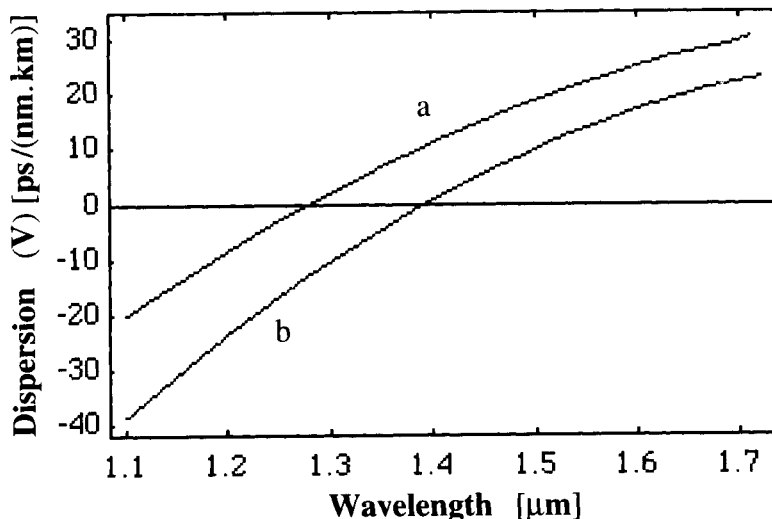


Figure 4.16: The characteristic behavior of dispersion for  $\text{SiO}_2$  (a) and aluminosilicate (b) glasses at  $26^\circ\text{C}$  from  $1.1$  to  $1.7 \mu\text{m}$  (after Ref. 85 with permission from IEEE).

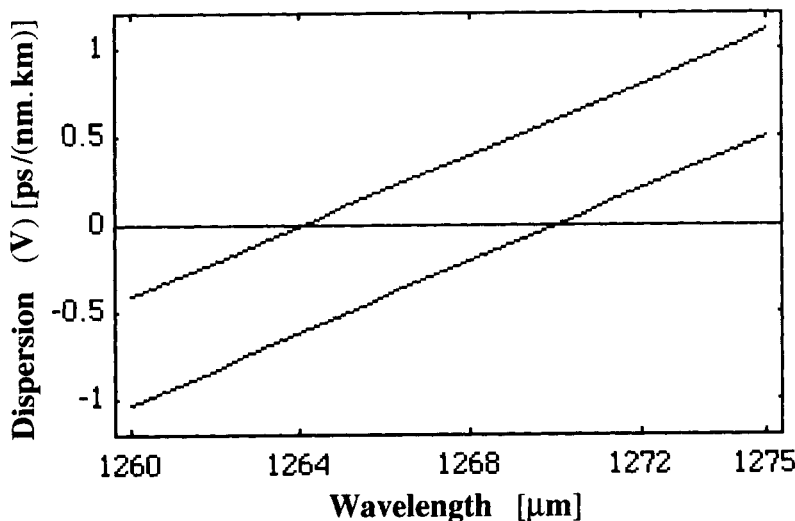


Figure 4.17: The characteristic behavior of dispersions for Vycor glass at  $-100^\circ\text{C}$  and  $+100^\circ\text{C}$  (the upper and lower lines, respectively), (after Ref. 85 with permission from IEEE).

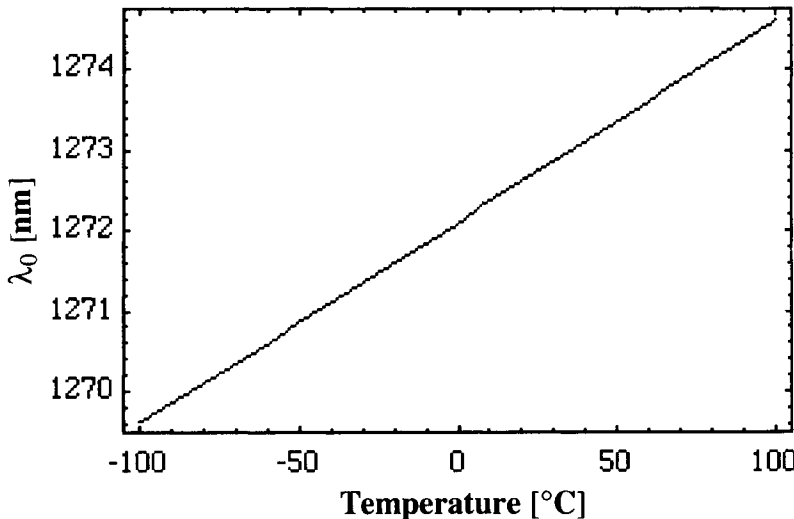


Figure 4.18: Zero dispersion wavelength  $\lambda_0$  as a function of temperature  $T$  for  $\text{SiO}_2$  glass, (after Ref. 85 with permission from IEEE).

to  $1.8 \mu\text{m}$  wavelength region. The dispersion characteristics are not linear and increase from high negative values to small positive ones for these glasses. These values are calculated for three optical windows i.e., at  $0.85$ ,  $1.33$ , and  $1.55 \mu\text{m}$  and are shown in Table 4.10 for some Schott glasses and SSL6 Ohara glass at  $20^\circ\text{C}$ . The zero-dispersion wavelength is varied from  $1.28$  to  $1.58 \mu\text{m}$  for these optical glasses. Since the zero-dispersion wavelength lies at  $1.884 \mu\text{m}$  for SF6 glass, it is useful for compressing laser pulses in the femtosecond region.

Similarly, the dispersion characteristics are calculated for the high-index tellurite glasses [90] by using Sellmeier coefficients [91] of Table 2.3 and are shown in Fig. 4.20. The dispersion characteristics are not linear and are increasing from high negative values to small positive ones as the wavelength increases. This nonlinear behavior is due to the variation of dispersion of refractive indices. Since the  $\text{SiO}_2$  glass possesses less dispersion in the visible region, the zero-dispersion wavelength lies at  $1.273 \mu\text{m}$ . The pure  $\text{TeO}_2$  glass has zero dispersion at  $1.688 \mu\text{m}$ , whereas, by using a modifier, this value shifts toward the longer wavelength side, i.e., at around  $2 \mu\text{m}$  as shown in Table 4.10. Therefore, the chromatic dispersions are neg-

**Table 4.10: Optical Properties of Some Selected Schott, Ohara, Binary Tellurite  $pM_mO_n-(100-p)TeO_2$  and  $SiO_2$  Glasses at Room Temperature**

Glasses	Abbe number ( $v_d$ )	Chromatic dispersions [ps/(nm.km)] at			$\lambda_0$ (μm)
		0.86 μm	1.33 μm	1.55 μm	
BaLF4	53.69	-151.9	-14.80	6.28	1.474
BaK1	57.59	-140.2	-13.35	6.36	1.468
PSK3	63.51	-114.2	-1.87	17.10	1.348
SK4	58.58	-145.5	-10.90	10.90	1.429
SSK4A	55.12	-159.4	-16.65	5.36	1.487
SK5	59.52	-119.9	-7.37	10.73	1.409
Laf2	44.67	-242.2	-33.46	-3.28	1.581
BK7	64.15	-104.3	1.00	19.53	1.320
FK5	70.41	-86.6	4.67	21.34	1.281
LaK10	50.37	-196.3	-12.62	17.33	1.412
KzFS6	48.43	-162.7	-4.40	22.72	1.361
ZK1	57.99	-126.2	-8.21	10.85	1.414
SSL6	51.19	-138.1	-5.96	15.78	1.382
SF6	25.35	-471.1	-88.60	-40.30	1.884
$pM_mO_n$					
20Na <sub>2</sub> O	18.5	-805.1	-166.90	-91.20	2.221
10Al <sub>2</sub> O <sub>3</sub>	20.0	-781.6	-159.30	-84.20	2.121
25ZnO	18.7	-864.0	-174.60	-93.10	2.149
20BaO	18.3	-890.7	-183.70	-100.10	2.214
15BaO	18.1	-899.1	-182.00	-97.70	2.169
10Sb <sub>2</sub> O <sub>3</sub>	17.5	-972.8	-198.30	-106.90	2.179
20MoO <sub>3</sub>	15.4	-1123.2	-230.20	-127.10	2.274
20WO <sub>3</sub>	16.4	-1070.2	-216.10	-116.00	2.170
10Nb <sub>2</sub> O <sub>5</sub>	16.4	-1062.8	-208.60	-108.30	2.086
20Tl <sub>2</sub> O	14.5	-1196.3	-244.10	-136.00	2.324
TeO <sub>2</sub>	17.7	-864.5	-122.20	-35.70	1.688
SiO <sub>2</sub>	69.0	-83.8	5.30	21.70	1.273

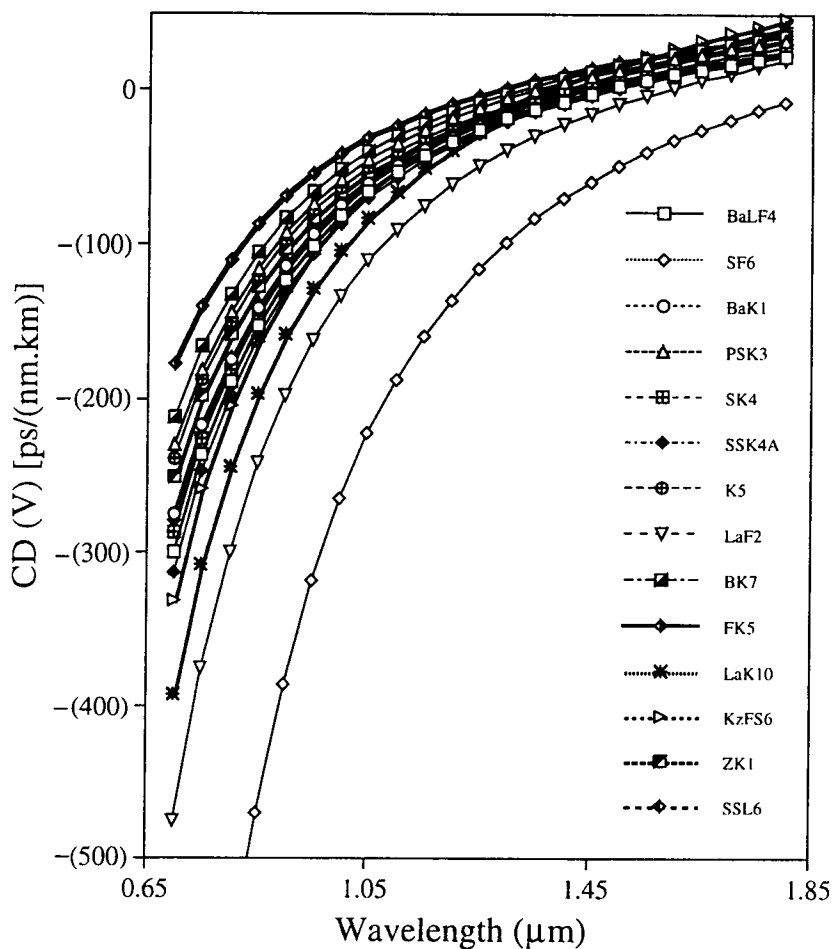


Figure 4.19: The characteristic behavior of chromatic dispersion for some selected Schott and Ohara optical glasses at 20°C (after Ref. 89 with permission from OSA).

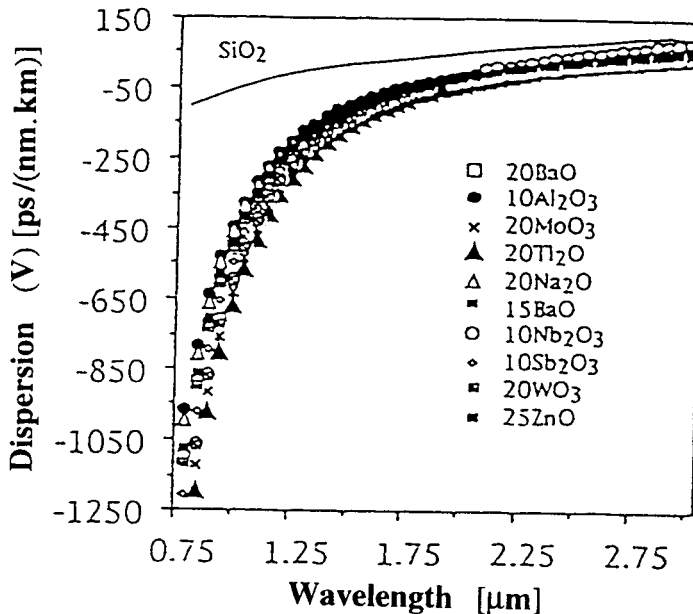


Figure 4.20: The characteristic behavior of chromatic dispersion for binary tellurite glasses  $pM_mO_n(100-p)TeO_2$  at 23°C (after Ref. 91 with permission from ACS).

ative at the three optic windows for binary tellurite glasses. We believe this demonstrates that binary tellurite glass prisms are better than SF6 glass prisms for compressing laser pulses in the femtosecond region.

### 4.3 Thermo-Optic Switch

Thermo-Optic (TO) switches based on optical waveguides are efficient to reroute transmitted laser from one port to other by changing the refractive index of the waveguide only by means of varying the ambient temperature surrounding the waveguide. As we have seen, there are many optical materials which possess thermo-optic coefficients of different values within the range of  $5 \times 10^{-3}$  to  $1.0 \times 10^{-6}$ . Therefore, by a judicious choice of the optical materials and by making a waveguide, an efficient TO switch can be made. TO switches have some beneficial characteristics such as low trans-

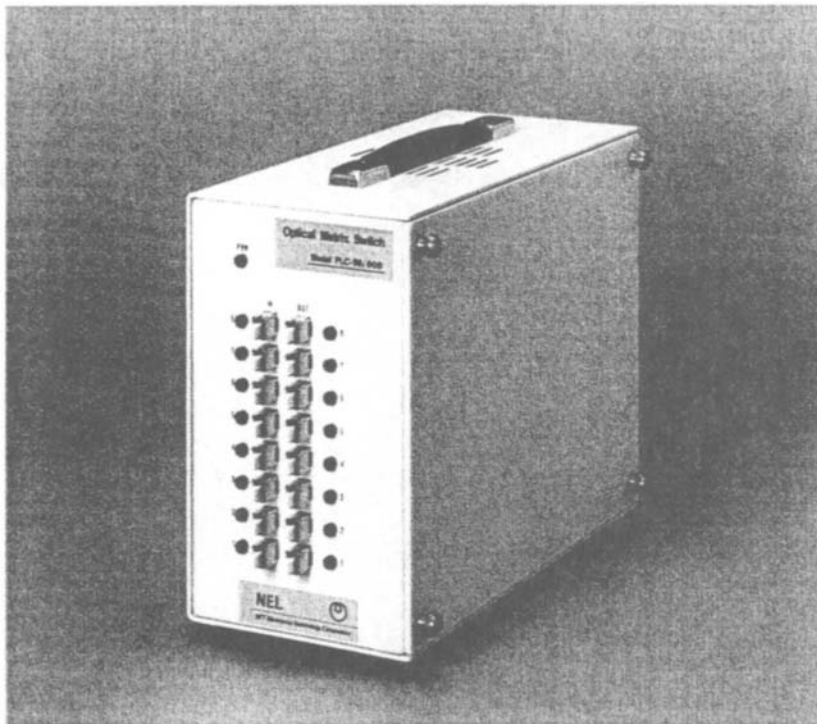


Figure 4.21: A thermo-optic switch ( $8 \times 8$  optical matrix), based on thermo-optic effect (after Ref. 92).

mission loss, low fiber-coupling loss, high stability, high producibility, and they are suitable for large scale integration. This switch will lead to the all-optical age of an OFCS's switching system.

Recently, NTT [92] of Japan has developed a  $8 \times 8$  Optical Matrix Switch (OMS) based on a silica-based waveguide on a silicon substrate. This waveguide operates as an active device by using the phase-control technique that is based on the thermo-optic effect of the waveguide material and a Mach-Zehnder interferometer (MZI). A product of this switch is shown in Fig. 4.21. The basic principle of it is explained by the initial investigation of the  $2 \times 2$  TO switch [93]. Figure 4.22 shows (a) a top view (b) a cross-sectional view along a line Q – U of a  $2 \times 2$  TO switch. This switch has a MZI configuration with two 3-dB directional couplers (DC) with a 50% coupling ratio and two waveguide arms of the same length. TO phase shifts are accomplished by using thin film heaters at both arms of

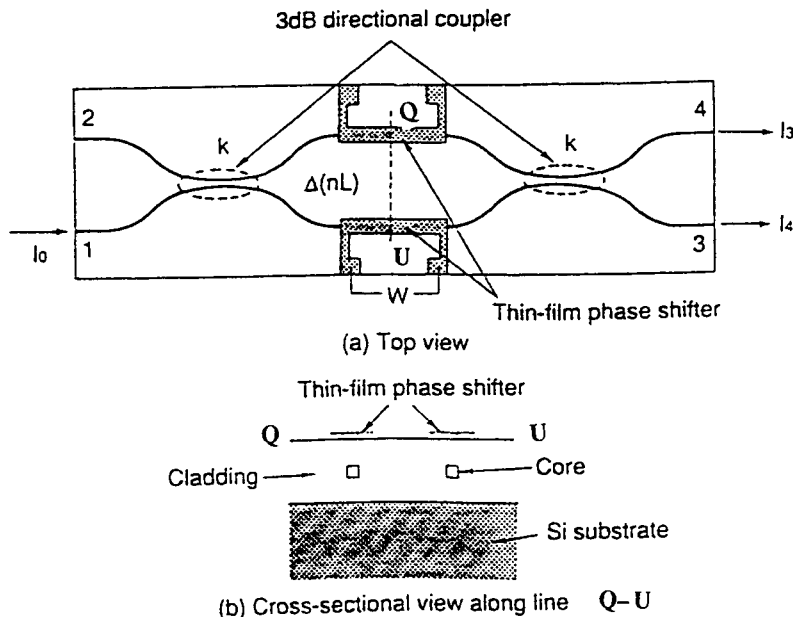


Figure 4.22: Configuration of a  $2 \times 2$  Mach-Zender interferometer (MZI) switch (after Ref. 93).

the waveguide. The normalized optical output power of the MZI are

$$I_3/I_0 = (1 - 2k)^2 \cos^2(\Delta\phi/2) + \sin^2(\Delta\phi/2), \quad (4.32)$$

$$I_4/I_0 = 4k(1 - k) \cos^2(\Delta\phi/2), \quad (4.33)$$

where  $\Delta\phi$  is the phase difference between the waveguide arms of the MZI and is expressed by the following equation.

$$\Delta\phi = 2\pi L_{ht} \Delta n / \lambda, \quad (4.34)$$

$\lambda$  is the wavelength and  $k$  is the DC coupling ratio. Here the coupling ratios are assumed to be the same at both arms.  $L_{ht}$  is the heater length and  $\Delta n$  the effective refractive index difference between the waveguide arms. In the off-state ( $\Delta n = 0$ ), Eqs. (4.32) and (4.33) are reduced to

$$I_3/I_0 = (1 - 2k)^2, \quad (4.35)$$

$$I_4/I_0 = 4k(1 - k). \quad (4.36)$$

The optical signal light passes through the cross path. However, some part of the optical signal remains in the through-path except when  $k = 0.5$ . The switching action from the cross-state (path 1-4 or 2-3) to the bar-state (path 1-3 or 2-4) is achieved by using a half wavelength optical path-length difference between the two waveguide arms, which is obtained by tuning the TO phase-shifter. In the on-state ( $L_{ht}\Delta n = \lambda/2$ , the Eqs. (4.35) and (4.36) are

$$I_3/I_0 = 0, \quad (4.37)$$

$$I_4/I_0 = 1. \quad (4.38)$$

These equations do not depend on  $k$ . The temperature change for switching at the waveguide core is about  $13^\circ$  for  $L_{ht} = 5$  mm at  $\lambda = 1.31 \mu\text{m}$  for  $dn/dT = 10.0 \times 10^{-6}/^\circ\text{C}$ .

A combination of flame hydrolysis deposition (FHD) and reaction ion etching (RIE) techniques are used to fabricate this switch on a Si substrate. A waveguide with a low  $\Delta$  (relative refractive index difference between the core and cladding  $\Delta = 0.3\%$ ) is normally used for the switch. The core size is  $8 \mu\text{m} \times 8 \mu\text{m}$  and the cladding thickness is  $50 \mu\text{m}$ . A Cr thin-film heater is used for the TO phase-shifter. Its size is almost 5 mm long and  $50 \mu\text{m}$  wide. The switch is approximately 30 mm long and 3 mm wide. The output optical characteristics of this  $2 \times 2$  TO switch are shown in Fig. 4.23 as a function of the phase-shifting driving power. The insertion loss is 0.5 dB and the switching electric power is about 0.4 W. The switching response time is 1 to 2 msec.

## 4.4 Optical-Fiber Temperature Sensor

The thermo-optic coefficients of the optical glasses made into optical fibers are used as a sensing element for measuring temperatures and other sensing devices. The phase of the guided laser will change as the ambient temperature of the sensing fiber varies. A polarimetric fiber sensor using a frequency stabilized semiconductor laser has been demonstrated [94] for remote temperature measurement. They measured the temperature change from the phase delay in between two orthogonally polarized modes in a polarization maintaining fiber. The measurement accuracy was less than  $0.005^\circ\text{C}$ . The construction of this sensor is simple. A leading fiber (long length) and a sensing fiber (short length) are both polarization maintaining

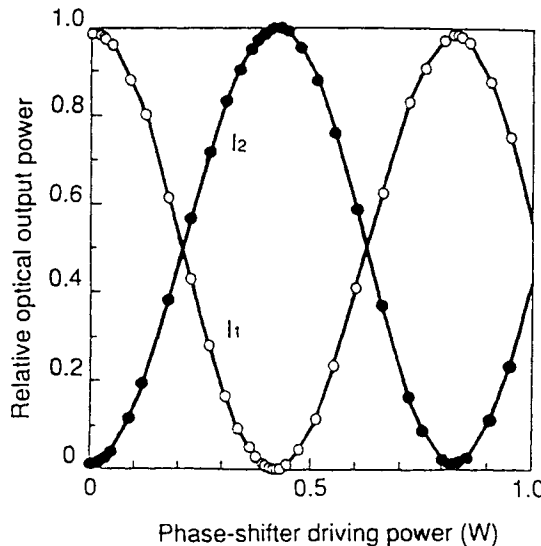


Figure 4.23: A characteristic response of the thermo-optic  $2 \times 2$  MZI switch, (after Ref. 93).

fibers, and are connected together by a polarization rotating coupler. This coupler is used to rotate the polarization axes of the sensing fiber by  $45^\circ$  with respect to the axes of the leading fiber. The endface of the sensing fiber is polished and some metallic alloy is used to make an in-built mirror.

A semiconductor laser was used to launch a linearly polarized light into the leading fiber; and there is only one polarization mode. Two polarization modes are equally excited at the coupler, i.e., at the input end of the sensing fiber. A phase delay occurs after reflection from the mirror. This phase delay is due to the modal birefringence of the fiber. The phase delay  $\phi$  is related to the modal birefringence,  $B_f$  as

$$\phi = 2\pi B_f \nu L_f / c, \quad (4.39)$$

where  $\nu$  is the laser frequency,  $L_f$  is the length of sensing fiber, and  $c$  is the velocity of light. The effective optical-path difference between two modes is  $B_f L_f$ . The phase delay in the sensing fiber is measured by the interference between the two modes with an analyzer and a photodiode. The sensing fiber induces a phase delay between two modes by changing the temperature.

Ball *et al.* [95] have used an active fiber sensor to measure temperature. In this sensor, a rare-earth doped fiber is used as a fiber laser instead of using the fiber grating. This fiber laser acts as an active Bragg-grating sensor. The effective refractive index of the fiber controls the Bragg wavelength. A laser diode is used to pump the fiber laser. The response of the active sensor was measured by a grating spectrum and a Fabry-Perot optical spectrum analyzer. In measuring temperature, the fiber laser was wound onto a thin copper cylinder, which was kept in a hot plate. A calibrated thermocouple was used to measure temperature with a resolution of 1°C. They have correlated their measurements with the fiber expansion and thermo-optic coefficients. The wavelength varies linearly with both the applied strain and temperature and is given by

$$\delta\lambda/\lambda = (0.79 \pm 0.02)\epsilon + 7.1 \times 10^{-6}\Delta T, \quad (4.40)$$

where  $\epsilon$  is the applied strain,  $\delta\lambda$  is the wavelength shift, and  $\Delta T$  is the temperature change in degrees centigrade. At the operating wavelength of an erbium-doped fiber laser (about 1.53 μm), the laser wavelength changes at a rate of 0.011 nm/°C. This resolution is not sufficient. Therefore, some semiconductor waveguides having large thermo-optic coefficients should be employed to make an efficient high-resolution temperature sensor.

## 4.5 Thermo-Optic Modulators

OFCS will require the realization of low-cost guided-wave active and passive components. Crystalline silicon (c-Si) is a suitable candidate for such applications in the near-infrared wavelength region. Recently, hydrogenated amorphous silicon (a-Si:H) has been used to make a planar waveguide [96] with the crystalline silicon as a substrate by a low-temperature plasma-enhanced chemical vapor deposition (PECVD) technology. A schematic cross section of the planar waveguide is shown in Fig. 4.24. It consists of a ~3 μm-thick undoped a-Si:H core layer, between two undoped a-SiC:H cladding layers. For good ohmic contacts, a heavily B-doped a-Si:H top layer has been deposited on the top. Planar waveguides of various lengths were fabricated by substrate cleaving. Waveguides with lengths of 0.62 and 1.65 μm were realized [96]. A Fabry-Perot-like characteristic was observed when these waveguides were heated and the transmitted intensity versus temperature was plotted. A periodic amplitude modulation of the

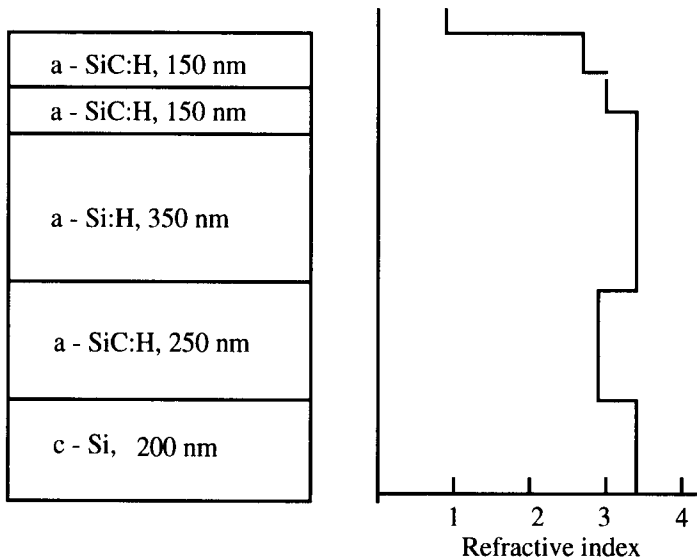


Figure 4.24: A schematic diagram of the thermo-optic modulator based on waveguide structure (after Ref. 96 with permission from the author and IEEE).

transmitted light was due to the thermo-optic effect in an étalon cavity. Thermal transient simulations predict that a modulation rate of 3 MHz is achievable. The thermo-optic effect was already proposed [97, 98] for realizing light modulators in silicon. Thermal phenomena are inherently slow processes. In spite of that, modulators with operation frequencies near 1 MHz were integrated on silicon chips using the standard VLSI technology [97]. This was possible due to the high thermal conductivity of silicon. But the silicon-on-silicon waveguides to date are very lossy. Therefore, some suitable highly thermal conducting and low-loss optical waveguide is to be investigated for realizing a good thermo-optic modulator.

## 4.6 REFERENCES

1. P. A. Franken, A. E. Hill, C. W. Peters, and G. Weinreich, Phys. Rev. Lett. **7**, 118 (1961).
2. J. A. Giordmaine, Phys. Rev. Lett. **8**, 19 (1962).
3. P. D. Maker, R. W. Terhune, M. Nisenoff, and C. M. Savage, Phys. Rev. Lett. **8**, 21 (1962).
4. J. A. Giordmaine and R. C. Miller, Phys. Rev. Lett. **14**, 973 (1965).
5. N. Bloembergen, *Nonlinear Optics* (Benjamin, New York 1965).
6. F. Zernike and J. E. Midwinter, *Applied Nonlinear Optics* (John Wiley, New York, 1973).
7. R. W. Boyd, *Nonlinear Optics* (Academic Press, San Diego, CA, 1992).
8. Y. R. Shen, *The Principles of Nonlinear Optics* (John Wiley, New York, 1984).
9. *Data Sheet 704*, (Quantum Technology Inc., 1990).
10. Y. S. Liu, W. B. Jones, and J. P. Chernoch, Appl. Phys. Lett. **29**, 32 (1976).
11. Quantum Technology, Inc. Data sheet **708**, (1990).
12. D. Eimerl, L. Davis, S. Velsko, E. Graham, and A. Zalkin, J. Appl. Phys. **62**, 1968 (1987).
13. K. Kato, IEEE J. Quantum Electron. **QE-22**, 1013 (1986).
14. S. Velsko, M. Webb, L. Davis, and C. Huang, IEEE J. Quantum Electron. **27**, 2182 (1991).
15. G. Ghosh, Opt. Lett. **19**, 1391 (1994).
16. G. Ghosh, Appl. Phys. Lett. **65**, 3311 (1994).
17. T. Ukachi, R. Lane, W. Bosenberg, and C. L. Tang, J. Opt. Soc. Am. B **9**, 1128 (1992).
18. K. Kato, IEEE J. Quantum Electron. **30**, 2950 (1994).
19. S. Lin, B. Wu, F. Xie, and C. Chen, J. Appl. Phys. **73**, 1029 (1993); Appl. Phys. Lett. **59**, 1541 (1991); **60**, 2032 (1992).
20. L. Wei, D. Guiqing, H. Qingzhen, Z. An, and L. Jingkui, J. Phys. D. Appl. Phys. B **2**, 1073 (1990).
21. H. Mao, B. Wu, C. Chen, D. Zhang, and P. Wang, Appl. Phys. Lett. **62**, 1866 (1993).
22. I. Gontijo, Opt. Commun. **108**, 324 (1994).
23. J. T. Lin, J. L. Montgomery, and K. Kato, Opt. Commun. **80**, 159 (1990).
24. G. Ghosh, J. Appl. Phys. **78**, 6752 (1995).
25. M. S. Webb and S. P. Velsko, IEEE J. Quantum Electron. **26**, 1394 (1990).
26. G. Ghosh, IEEE Photon. Technol. Lett. **7**, 68 (1995).

27. W. P. Risk, R. N. Payne, W. Lenth, C. Harder, and H. Meier, *Appl. Phys. Lett.* **55**, 1179 (1989).
28. J. C. Baumert, F. M. Schellenberg, W. Lenth, W. P. Risk, and G. C. Bjorklund, *Appl. Phys. Lett.* **51**, 2192 (1987).
29. T. Y. Fan, C. E. Huang, B. Q. Hu, R. C. Eckhardt, Y. X. Fan, R. L. Byer, and R. S. Feigelson, *Appl. Opt.* **26**, 2390 (1987).
30. T. Kishimoto, K. Imamura, and M. Itoh, in *Digest of Annual Meeting* (Japan Society of Applied Physics, Tokyo, 1991), paper 29p-PB-11.
31. V. M. Garmash, G. A. Ermanov, N. J. Pavlova, and A. V. Tarasov, *Sov. Tech. Phys. Lett.* **12**, 505 (1986).
32. R. A. Stolzenberger, C. C. Hau, N. Payghambarian, J. J. E. Reid, and R. A. Morgan, *IEEE Photon. Technol. Lett.* **1**, 446 (1989).
33. K. Kato, *IEEE J. Quantum Electron.* **27**, 2043 (1991).
34. W. Wang and M. Ohtsu, *Opt. Commun.* **102**, 304 (1993).
35. B. Zysset, I. Biaggio, and P. Gunter, *J. Opt. Soc. Am. B* **9**, 380 (1992).
36. I. Biaggio, P. Kerkoc, L.-S. Wu, and P. Gunter, *J. Opt. Soc. Am. B* **9**, 507 (1992).
37. H. Tsuchida, *Opt. Rev.* **3**, 309 (1996).
38. J. C. Baumert, P. Gunter, and H. Melchior, *Opt. Commun.* **48**, 215 (1983).
39. A. Hammerich, D. H. McIntyre, C. Zimmermann, and T. W. Hansch, *Opt. Lett.* **15**, 372 (1990).
40. M. K. Chun, L. Goldberg, and J. F. Weller, *Appl. Phys. Lett.* **53**, 1170 (1988).
41. W. J. Kozlovsky, W. Lenth, E. E. Latta, A. Moser, and G. L. Buna, *Appl. Phys. Lett.* **56**, 2291 (1990).
42. P. Gunter, *Appl. Phys. Lett.* **34**, 650 (1979).
43. L. S. Wu, H. Looser, and P. Gunter, *Appl. Phys. Lett.* **56**, 2163 (1990).
44. G. J. Dixon, Z. M. Zhang, R. S. F. Chang, and N. Djeu, *Opt. Lett.* **13**, 137 (1988).
45. I. Biaggio, H. Looser, and P. Gunter, *Ferroelectrics* **94**, 157 (1989).
46. M. Poulin, C. Latrasse, M. Tetu, and M. Breton, *Opt. Lett.* **19**, 1183 (1994).
47. G. Ghosh, M. Endo, and H. Yajima, in *Digest of Annual Meeting* (Japanese Soc. Appl. Phys. Kyushu, 1996), paper 29p-PB-11.
48. G. C. Bhar and G. Ghosh, *IEEE J. Quantum Electron.* **QE-16**, 838 (1980).
49. G. A. Massey, J. C. Johnson, and R. A. Elliott, *IEEE J. Quantum Electron.* **QE-12**, 143 (1976).
50. G. A. Massey and R. A. Elliott, *IEEE J. Quantum Electron.* **QE-10**, 899 (1974).

51. G. A. Massey and J. C. Johnson, IEEE J. Quantum Electron. **QE-15**, 201 (1979).
52. G. Ghosh and G. C. Bhar, IEEE J. Quantum Electron. **QE-18**, 143 (1982).
53. Y. Tanaka, T. Koshida, and S. Shionoya, Opt. Commun. **25**, 273 (1978).
54. W. J. Kozlovsky, C. D. Nabors, R. C. Eckardt, and R. L. Byer, Opt. Lett. **14**, 66 (1989).
55. D. C. Gerstenberger and R. W. Wallace, J. Opt. Soc. Am. B **10**, 1681 (1993).
56. G. Banfi, R. Danielius, A. Piskarskas, P. Trapani, P. Foggi, and R. Righini, Opt. Lett. **18**, 1633 (1993).
57. M. Ebrahimzadeh, G. J. Hall, and A. I. Ferguson, Opt. Lett. **18**, 278 (1993).
58. S. Lin, J. Huang, J. Ling, C. Chen, and Y. R. Shen, Appl. Phys. Lett. **59**, 2805 (1991).
59. F. Hanson and D. Dick, Opt. Lett. **16**, 205 (1991).
60. Y. Cui, M. H. Dunn, C. J. Norrie, W. Sibbett, B. D. Sinclair, Y. Fang, and J. A. C. Terry, Opt. Lett. **17**, 646 (1992).
61. Y. Tang, Y. Cui, and M. Dunn, Opt. Lett. **17**, 192 (1992).
62. G. Robertson, M. J. Padgett, and M. H. Dunn, Opt. Lett. **19**, 1735 (1994).
63. K. Kato, IEEE J. Quantum Electron. **18**, 451 (1982).
64. N. P. Barnes and M. S. Piltch, J. Opt. Soc. Am. **67**, 628 (1977).
65. G. D. Boyd, E. Buehler, and F. G. Storz, Appl. Phys. Lett. **18**, 301 (1971).
66. G. D. Boyd, H. M. Kasper, and J. H. McFee, IEEE J. Quantum Electron. **QE-7**, 563 (1971).
67. G. D. Boyd, E. Buehler, F. G. Storz, and J. H. Wernick, IEEE J. Quantum Electron. **QE-8**, 419 (1972).
68. R. E. Stickel, Jr. and F. B. Dunning, Appl. Opt. **17**, 1313 (1978).
69. Y. Takagi, M. Sumitani, N. Nakashima, and K. Yoshihara, IEEE J. Quantum Electron. **QE-21**, 193 (1985).
70. E. Liu, F. B. Dunning, and F. K. Tittel, Appl. Opt. **21**, 3415 (1982).
71. B. Couillaud, T. W. Hansh, and S. G. Mac Lean, Opt. Commun. **50**, 127 (1984).
72. H. Hemmati and J. C. Bergquist, Opt. Commun. **47**, 157 (1983).
73. R. P. Mariella, Jr., Opt. Commun. **29**, 100 (1979).
74. G. A. Massey, M. D. Jones, and J. C. Johnson, IEEE J. Quantum Electron. **QE-14**, 527 (1978).
75. M. D. Jones and G. A. Massey, IEEE J. Quantum Electron. **QE-15**, 204 (1979).
76. G. A. Massey and J. C. Johnson, IEEE J. Quantum Electron. **QE-12**, 721 (1976).

77. P. Lokai, B. Burghardt, and W. Muckenheim, *Appl. Phys. B* **45**, 245 (1988).
78. M. M. Abbas, T. Kostiuk, and K. W. Ogilvie, *Appl. Opt.* **15**, 961 (1976).
79. J. C. Baumert and P. Gunter, *Appl. Phys. Lett.* **50**, 554 (1987).
80. F. Seifert, J. Ringling, F. Noack, V. Petrov, and O. Kittelmann, *Opt. Lett.* **19**, 1538 (1994).
81. B. Bendow and S. S. Mitra, *Fiber Optics: Advances in Research and Developments* (Plenum, New York, 1979).
82. E. Desurvire, *Erbium-Doped Fiber Amplifiers* (Wiley, New York, 1994).
83. M. J. F. Digonnet, Ed., *Rare-Earth Doped Fiber Lasers and Amplifiers* (Dekker, New York, 1993).
84. J. H. Wray and J. T. Neu, *J. Opt. Soc. Am.* **59**, 774 (1969).
85. G. Ghosh, M. Endo, and T. Iwasaki, *IEEE J. Lightwave Technol.* **LT-12**, 1338 (1994).
86. K. S. Kim and M. E. Lines, *J. Appl. Phys.* **73**, 2069 (1993).
87. *Schott Optical Glass Catalog* (Schott Glass Technologies Inc., Duryea, Pa, 1992).
88. *Ohara Optical Glass Catalog* (OHARA Inc., Kanagawa, 1990; 1995).
89. G. Ghosh, *Appl. Opt.* **36**, 1540 (1997).
90. H. Takebe, S. Fujino, K. Morinaga, *J. Am. Ceram. Soc.* **77**, 2455 (1994); and private communication.
91. G. Ghosh, *J. Am. Ceram. Soc.* **78**, 2828 (1995).
92. *Technical Data Sheet* (NTT Elec. Tech. Corp., Ibaraki, 1996).
93. M. Okuno, N. Takato, T. Kitoh, and A. Sugita, *NTT Review* **7**, 57 (1995).
94. H. Tsuchida, Y. Mitsuhashi, and S. Ishihara, *IEEE J. Lightwave Technol.* **LT-7**, 799 (1989).
95. G. A. Ball, W. W. Morey, and P. K. Cheo, *IEEE Photon. Technol. Lett.* **5**, 267 (1993).
96. G. Cocorullo, F. G. Della Corte, I. Rendina, A. Rubino, and E. Terzini, *IEEE Photon. Technol. Lett.* **8**, 900 (1996).
97. G. Cocorullo, M. Iodice, and I. Rendina, *Opt. Lett.* **19**, 420 (1994).
98. G. Cocorullo, M. Iodice, I. Rendina, and P. M. Sarro, *IEEE Photon. Technol. Lett.* **7**, 363 (1995).

This page intentionally left blank

## Chapter 5

# Future Technology

The refractive index of any optical material at an ambient temperature  $T$  for any electromagnetic wave within the transmission region of the material, having wavelength  $\lambda$  and intensity  $I$ , can be expressed by the following equation:

$$n(\lambda, T) = n(\lambda, rt) + \frac{dn}{dT}(T - rt) + n_2 I \quad (5.1)$$

where  $rt$  is the room temperature,  $dn/dT$  is the thermo-optic coefficient, and  $n_2$  is the intensity dependent nonlinear coefficient of the optical material. Measured values of  $n_2$  are found to vary in the range of  $2.2\sim3.4\times10^{-20}$  m<sup>2</sup>/W [1] for silica glass/fibers. Suppose a Ti:Sapphire femtosecond laser pulse of average power 2.0 W with a beam diameter of 0.8 mm is focused onto a silica or a BK7 glass. The value of  $I$  is  $4\times10^6$  W/m<sup>2</sup>. Thus, the intensity dependent nonlinear part is of the order of  $8\sim13\times10^{-14}$ . On the other hand, the contribution due to the thermo-optic coefficient is of the order of  $10^{-6}/^\circ\text{C}$ . So, the effect of fluctuation from ambient temperature in micro  $^\circ\text{C}$  is greater than that of the intensity contribution. Therefore, in bulk materials, the contribution of thermo-optic coefficients is not negligible and it is a dominating factor, in particular, for femtosecond pulse transmission. The values of thermo-optic coefficients vary from  $10^{-3}$  to  $10^{-6}$  for semiconductors to optical glasses. In some materials, these values are negative. Several other kinds of optical glasses having large  $n_2$  values have been used to make optical fibers [4-6]. A lead silicate fiber has  $n_2$  value of  $0.2\times10^{-18}$  m<sup>2</sup>/W [4]. Some chalcogenide optical fibers [6] possess large  $n_2$  values, twice that of lead silicate fiber.

Therefore, the future technology based on engineering the refractive indices of the optical materials is exciting. The foregoing analyses will help to design either a highly temperature sensitive or a temperature-immune system/device by a judicious choice of the optical materials. In the case of optical fiber communication systems (OFCS), by utilizing wavelength division multiplexing (WDM), we can transmit many lasers in a single fiber. But the chromatic dispersion and the thermo-optic coefficients are posing problems for the present THz communication systems. Therefore, some suitable systems/devices are to be incorporated within this OFCS to nullify this effect.

On the other hand, some low-cost temperature sensors can be made with some suitable optical materials which possess large thermo-optic coefficients. Although most scientists believe that the temperature effect is slow, we believe this effect will create a new scenario by a prudent choice/investigation of optical materials. Also, the wavelength of the laser propagating through the optical materials is of prime importance since the temperature effect is not at all the same throughout the transmitting wavelength region.

All optical switches based on thermo-optic coefficients and the intensity of the transmitting laser will provide us with the momentum to achieve an all-optical communication age. By combining thermo-optic, electro-optic, and magneto-optic phenomena, new systems or designs can also be made.

## REFERENCES

1. R. H. Stolen, W. A. Reed, K. S. Kim, and K. W. Quoi, Proc. Symp. Opt. Fiber Measurements (NIST, Boulder, Colorado, 1992), p. 71.
2. K. S. Kim, R. H. Stolen, W. A. Reed, and K. W. Quoi, Opt. Lett. **19**, 257 (1994).
3. T. Sato, Y. Suetsugu, M. Takagi, E. Sasaoka, and M. Nishimura, Opto-Electronics Conf., Chiba, Japan, July 12-15, 1994; Symp. Opt. Fiber Measurements, Boulder, Colorado, Sept. 13-15, 1994.
4. M. A. Newhouse, D. L. Weidman, and D. W. Hall, Opt. Lett. **15**, 1185 (1990).
5. M. Asobe, K. Suzuki, T. Kanamori, and K. Kubodera, Appl. Phys. Lett. **60**, 1153 (1992).
6. M. Asobe, T. Kanamori, and K. Kubodera, IEEE Photon. Technol. Lett. **4**, 362 (1992).

# Subject Index

Boldface numerals indicate tables.

Italic numerals indicate figures.

## A

- Abbé number  
definition, 300  
values of  
    BaLF4, **303**  
    BaK1, **303**  
    BK7, **303**  
    FK5, **303**  
    KzFS6, **303**  
    LaF2, **303**  
    LaK10, **303**  
    PSK3, **303**  
    SF6, **303**  
    SiO<sub>2</sub>, **303**  
    SK4, **303**  
    SK5, **303**  
    SSK4A, **303**  
    SSL6, **303**  
    Tellurite glasses, **303**  
    TeO<sub>2</sub>, **303**  
    ZK1, **303**  
Abhisaricas, 1-2

## B

- Band gaps  
absorption, 14, 119-127, **16-**  
    *33, 124*  
excitonic, 123-126, **129-139,**

- 124, 244*  
isentropic, 124-127, **129-139,**  
*124*  
lattice, **129-137, 124**

## C

- Coherence length, 267  
    ADP, *271, 272*  
    CdTe, 283, 284  
    KDP, *271, 272*  
    ZnGeP<sub>2</sub>, 283, 284

## D

- Difference frequency generation  
    KTP, 279  
Dispersions (chromatic and zero)  
    definition, 299  
    values of  
        BaLF4, **303, 304**  
        BaK1, **303, 304**  
        BK7, **303, 304**  
        FK5, **303, 304**  
        fs 7940, *301, 302*  
        KzFS6, **303, 304**  
        LaF2, **303, 304**  
        LaK10, **303, 304**  
        PSK3, **303, 304**

SF6, **303, 304**  
 SiO<sub>2</sub>, **303, 305**  
 SK4, **303, 304**  
 SK5, **303, 304**  
 SSK4A , **303, 304**  
 SSL6, **303, 304**  
 Tellurite glasses, **303, 305**  
 TeO<sub>2</sub>, **303, 305**  
 vc 7913, **301**  
 ZK1, **303, 304**

**O**

Optical-fiber communication systems, 297-305  
 Optical parametric oscillators, 283-294, in  
     ADP, **286**  
     CDA, **286**  
     CD\*A, **286, 286**  
     KD\*P, **286**  
     KNO, **286, 295**  
     LBO, **291, 288-290, 293**  
     LNO, **286**  
     LNO:MgO, **286**

**R**

Refractive Index  
     Cauchy formula, 11  
     Characteristic curves, 13  
     Hartmann formula, 11  
     Herzberger equation, 11  
     Lorentz and Lorentz relation, 118

Measurement, 6-9  
 Schott formula, 10  
 Sellmeier equation, 12-15  
 Sellmeier coefficients and values of  
     as1723, **32, 103**  
     ADA, **16, 34**  
     AD\*A, **16, 35**  
     ADP, **16, 36-37**  
     AD\*P, **16, 38**  
     Ag<sub>3</sub>AsS<sub>3</sub>, **16**  
     AgBr, **16**  
     AgCl, **16, 39**  
     AgGaS<sub>2</sub>, **16**  
     AgGaSe<sub>2</sub>, **17**  
     AgInSe<sub>2</sub>, **17, 40-41**  
     Ag<sub>3</sub>SbS<sub>3</sub>, **17**  
     AlAs, **17, 42**  
     AlN, **17**  
     ALON, **17**  
     AL<sub>2</sub>O<sub>3</sub>, **17**  
     AlPO4, **17, 43**  
     BaF<sub>2</sub>, **18**  
     BAH32, **31**  
     BAL4, **31, 103**  
     BAL11, **31**  
     BAL23, **31, 107**  
     BBO, **17**  
     Ba(COOH)<sub>2</sub>, **17**  
     BaTiO<sub>3</sub>, **18, 45-46**  
     BeO, **18**  
     BeSO(BeSO<sub>4</sub>, 4H2O), **18**  
     BGO, **18**  
     BSO, **18**  
     BGZA(4), **32**

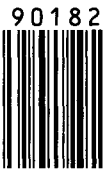
- BK7, **104**  
BNN, **18, 44**  
BP, **18**  
BSM4, **31**  
BSM9, **31, 104-105**  
BSM22, **31**  
BSM24, **31**  
C (diamond), **18**  
CaCO<sub>3</sub>, **18, 47-50**  
CaF<sub>2</sub>, **18, 19, 51**  
CaMoO<sub>4</sub>, **19, 52-53**  
CaWO<sub>4</sub>, **19, 53-54**  
CDA, **19, 55**  
CD\*A, **19, 56**  
CdF<sub>2</sub>, **19**  
CdGeAs<sub>2</sub>, **19**  
CdGeP<sub>2</sub>, **19**  
CdS, **19, 20**  
CdSe, **20**  
CdTe, **20**  
CO(NH<sub>4</sub>)<sub>2</sub>, Urea, **20**  
CsBr, **20**  
CsCl, **20**  
CsI, **20**  
CuAlSe<sub>2</sub>, **20, 57-58**  
CuCl, **20**  
CuGaS<sub>2</sub>, **20**  
CuGaSe<sub>2</sub>, **20, 59-60**  
CuInS<sub>2</sub>, **20, 61-62**  
C<sub>12</sub>H<sub>22</sub>O<sub>11</sub>, **20, 21**  
DLAP, **21**  
fs7940, **32, 105-106**  
GaAs, **21**  
GaN, **21**  
GaP, **21, 63**  
GaSb, **21**  
GaSe, **21**  
Ge, **21**  
HfO<sub>2</sub>; Y<sub>2</sub>O<sub>3</sub>, **22**  
HgGa<sub>2</sub>S<sub>4</sub>, **21**  
HgS, **21**  
 $\alpha$ -HIO<sub>3</sub>, **21, 22, 63-65**  
InAs, **22**  
InP, **22**  
InSb, **22, 66**  
KBO, **22**  
KB\*O, **22**  
KBr, **22**  
KCl, **22, 66-67**  
KCl:Ki, **22, 67-68**  
KDA, **22, 69**  
KDP, **22, 23, 69-71**  
KD\*P, **23, 72-73**  
KDP:Rb, **23, 73**  
KF, **22**  
KI, **23**  
KLN, **23**  
KM, **23**  
KNO, **23, 74-75**  
KRS5, **29**  
KRS6, **29, 92-93**  
KTA, **23, 24**  
KTP, **24**  
KzFs6, **32**  
LaF<sub>3</sub>, **24**  
LAP, **24**  
LBO, **24, 75**  
LFM, **24**  
LiF, **24**  
LIO, **24, 25**

- LNO, **25, 76-79**  
 LNO:MgO, **25**  
 LTO, **25, 79-80**  
 LiYF<sub>4</sub>, **25**  
 MAP, **25**  
 MDB, **25, 26, 81**  
 mNA, **26**  
 MgAl<sub>2</sub>O<sub>3</sub>, **26**  
 MgF<sub>2</sub>, **26**  
 MgO, **26**  
 NaBr, **26**  
 NaCl, **26**  
 NaCOOH, **26**  
 NaF, **26**  
 NaI, **27**  
 NaNO<sub>3</sub>, **27, 82**  
 NSL5, **31**  
 PbF<sub>2</sub>, **27**  
 PBH6, **31, 107-108**  
 PBL26, **31, 106**  
 PBM<sub>3</sub>, **31**  
 PbMoO<sub>4</sub>, **27**  
 PbS, **27**  
 PbSe, **27**  
 PbTe, **27, 82**  
 POM, **27**  
 RDA, **27, 83**  
 RD\*A, **27, 83**  
 RDP, **27, 84**  
 RD\*P, **27, 28, 85**  
 RTP, **28**  
 Ruby, **28, 85-86**  
 Se, **28, 86**  
 Si, **28, 86**  
 β-SiC, **28**  
 α-SiC, **28**  
 Silica, **32**  
 α-SiO<sub>2</sub> (Quartz), **28, 87**  
 S-BSL7, **31, 104**  
 SF6, **31, 107-108**  
 S-FPL51, **31**  
 S-FPL52, **31**  
 S-FPL53, **31, 108-109**  
 S-FSL5, **31**  
 S-LAL10, **32**  
 S-LAM2, **32**  
 S-LAM51, **32**  
 S-NSL36, **32**  
 SrF<sub>2</sub>, **28, 88**  
 SrMoO<sub>4</sub>, **28, 29, 89**  
 SrTiO<sub>3</sub>, **29, 90**  
 SSL6, **32**  
 Te, **29**  
 TeO<sub>2</sub>, **29**  
 Tellurite glasses, **33**  
 TiO<sub>2</sub>, **29, 91**  
 Tl<sub>3</sub>AsSe<sub>3</sub>, **29, 91-92**  
 TiBr, **29**  
 TiCl, **29**  
 vc7913, **32, 109**  
 YAG, **29, 93-94**  
 Y<sub>2</sub>O<sub>3</sub>, **29**  
 ZnO, **30, 95**  
 α-ZnS, **30, 96-97**  
 β-ZnS, **30, 96**  
 ZnS, **30, 94**  
 ZnSe, **30, 98**  
 ZnSiAs<sub>2</sub>, **30**  
 ZnTe, **30**  
 ZnWO<sub>4</sub>, **30, 99-100**

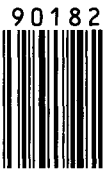
- ZrO<sub>2</sub>:12%Y<sub>2</sub>O<sub>3</sub>, **30, 101-102**
- ZSL1, **32**
- Zernike's formula, **11**
- S**
- Second harmonic generation
- ADA, **270**
  - AD\*A, **270**
  - ADP, **270**
  - AD\*P, **270**
  - BBO, **273**
  - CDA, **269, 270**
  - CD\*A, **270**
  - KDA, **270**
  - KDP, **270**
  - KD\*P, **270**
  - KNO, **280, 282**
  - KTP, **279**
  - LBO, **275, 276-278**
  - RDA, **270**
  - RD\*A, **270**
  - RDP, **270**
- Sum-frequency generation, **294-297**
- ADP, **296**
  - BBO, **296**
  - KDP, **296**
  - KNO, **296**
  - KTP, **279**
  - LBO, **291, 296**
  - LNO, **296**
- T**
- Temperature bandwidth, **266**
- Temperature sensor, **308-310**
- Temperature tuning, **275, 276-294**
- Thermo-optic coefficients
- definition, **115**
  - measurement, **115**
  - expt. equation, **116**
  - dispersion relations
  - Clausius-Mossotti, **117**
  - Prodhommes' model, **119, 125**
  - Schott glass **119**
  - Semiempirical equations, **121**
  - Sellmeier equation, **126**
  - Tsay's model, **120-121**
  - Sellmeier coefficients and values of
    - as1723, **138, 237, 239**
    - ADA, **129, 142, 151**
    - ADP, **129, 147, 151**
    - AgCl, **129, 216**
    - AgGaS<sub>2</sub>, **129, 183**
    - Al<sub>2</sub>O<sub>3</sub>, **129, 192, 198**
    - ALON, **129, 192, 198**
    - BAL4, **138, 250**
    - BAL11, **138, 250**
    - BAL23, **138, 250**
    - BaF<sub>2</sub>, **129-130, 204, 216**
    - BBO, **130, 167, 171**
    - BeO, **130, 193, 198**
    - BGO, **130, 198**

- BGZA(4), **139, 206, 216**  
 BK7, **138, 249, 252**  
 BSM4, **138, 251**  
 BSM24, **138, 251**  
 C (diamond), **130, 234**  
 CaCO<sub>3</sub>, **130, 191, 198**  
 CaF<sub>2</sub>, **130, 205, 217-218**  
 CaMoO<sub>4</sub>, **130, 199**  
 CaO, **246**  
 CaWO<sub>4</sub>, **131, 194, 198**  
 CDA, **131, 143, 151, 152**  
 CD\*A, **131, 144, 152**  
 CdF<sub>2</sub>, **131, 206, 218**  
 CdGeP<sub>2</sub>, **131, 180, 183-185**  
 CdS, **131, 234**  
 CdSe, **131, 234**  
 CdSiP<sub>2</sub>, **131, 182**  
 CdTe, **131, 228, 234, 236**  
 CsBr, **131, 207, 218-219**  
 CsI, **132, 207, 219**  
 CuGaS<sub>2</sub>, **132, 181, 185-187**  
 DLAP, **132, 169, 171**  
 fs7940, **238, 239-241**  
 Ge, **132, 228, 229-231**  
 GaAs, **132, 228, 234**  
 GaN, **132, 234**  
 GaP, **132, 234**  
 GaSe, **132, 171**  
 HfO<sub>2</sub>:Y<sub>2</sub>O<sub>3</sub>, **132, 196, 199**  
 HgS, **132, 171**  
 InAs, **132, 228, 234**  
 InP, **132, 235**  
 KBr, **132, 208, 219-220**  
 KCl, **133, 209, 220**  
 KDA, **133, 145, 152**  
 KDP, **133, 148, 152, 153**  
 KD\*P, **133, 149, 153**  
 KI, **133, 210, 220**  
 KNO, **133, 160, 171-173**  
 KRS5, **137, 216, 224-225**  
 KTP, **133, 173-175**  
 KzFS6, **253**  
 LBO, **134, 166, 175**  
 LiF<sub>2</sub>, **134, 221**  
 LIO, **134, 157, 175**  
 LiYF<sub>4</sub>, **134, 210, 221**  
 LNO, **134, 156, 175-177**  
 LTO, **134, 177-178**  
 MgAl<sub>2</sub>O<sub>4</sub>, **134, 199**  
 MgF<sub>2</sub>, **134, 215, 221-222**  
 MgO, **134, 197, 199**  
 NaCl, **135, 212, 222-223**  
 NaF, **135, 213, 223-224**

- NSL5, **138, 251**  
PBH6, **138, 249, 253**  
PbMoO<sub>4</sub>, **135, 199**  
PbS, **135, 235**  
PbSe, **135, 228, 235**  
PbTe, **135, 228, 235**  
RDA, **135, 146, 154**  
RDP, **135, 150, 154**  
a-Si, **136, 234**  
Si, **136, 228, 231, 233, 235**  
 $\alpha$ -SiO<sub>2</sub>, **136, 191, 199-200**  
SrF<sub>2</sub>, **136, 214, 224**  
S-BSL7, **138, 249, 252**  
SF6, **138, 249, 253**  
S-FSL5, **138, 249, 252**  
S-LAL10, **138, 249, 253**  
S-LAM2, **138, 252**  
Soda-lime-silica, **139**,  
SRM glasses, **139, 242**  
SSL6, **138**  
TeO<sub>2</sub>, **136, 195, 201**  
TiO<sub>2</sub>, **136, 201**  
Tl<sub>3</sub>AsSe<sub>3</sub>, **136, 170, 178**  
vc 7913, **237, 241**  
YAG, **137, 196, 201**  
ZnGeP<sub>2</sub>, **137, 181, 187-189**  
ZnSe, **137, 228, 235**  
ZnSiAs<sub>2</sub>, **137, 182, 189**  
ZnSiP<sub>2</sub>, **137, 182**
- ZrO<sub>2</sub>:12%Y<sub>2</sub>O<sub>3</sub>, **137, 197, 201**
- Thermo-optic modulator, **311**
- Thermo-optic switch  
configuration, **307**  
response, **309**  
schematic diagram, **306**
- W**
- Walk-off angle, **267**



9 780122 818554



6 08628 18555 2

**ISBN 0-12-281855-5**